Invited Speaker

452 Surface microstructural evolution during Rolling Contact Fatigue of Rolling Element Bearing steels
Dr Sophie Cazottes[1], Aurore Goigoux[1,2,3], Dr Christine Sidoroff[3], Pr Fabrice Ville[2], Pr Muriel Veron[4], Thierry Douillard[1], Dr Pierre-Emmanuel Dubois[3], Dr. Nans Biboulet[2]
[1]INSA Lyon, CNRS, MATEIS, UMR 5510, Villeurbanne, France, [2]INSA Lyon, CNRS, LaMCoS, UMR5259, Villeurbanne, France, [3]NTN EUROPE, Research Innovation Development, Annecy, France, [4]Université Grenoble Alpes, CNRS, Grenoble INP, SIMaP, Grenoble, France
786 The nature of diffuse scattering in fcc metal alloys – investigation by 3D-ED and 4D-STEM
Hannah Cole[1], Mr James Miller[1], Mr James Hogg[1], Mr Petr Vacek[1], Mr Owain Houghton[1], Prof Howard Stone[1], Prof Paul Midgley[1]
[1]Department of Materials Science & Metallurgy, University of Cambridge, Cambridge,, United Kingdom

Oral Presentation

52 Differential Phase Contrast Microscopy and Atom Probe Tomography of Ferromagnetism in High-Entropy Alloys
Ms. Shabnam Taheriniya[1], Dr Harald Rösner[1], Mr. Gerhard Wilde[1]
[1]Institute of Materials Physics, University of Münster, 48149 Münster, Germany
79 Solving the controversy of the metal-insulator phase transition in chromium nitride thin films
Magnus Garbrecht[1], Ms Ashalatha Indiradevi Kamalasanan Pillai[1], Mr Bidesh Biswas[2], Mr Bivas Saha[2]
[1]The University of Sydney, Sydney, Australia, [2]Jawaharlal Nehru Centre for Advanced Scientific Research, Bangalore, India
92 TEM Investigations on the Impact of Hydrogen on Phase Transformations in Aluminum Alloys
M. Omar Boukir[1], M. Xavier Sauvage[1], M. Kaveh Edalati[2]
[1]Univ Rouen Normandie, INSA Rouen Normandie, CNRS, Groupe de Physique des Matériaux UMR 6634, F-76000, Rouen, France, [2]2WPI, International Institute for Carbon-Neutral Energy Research (WPI-I2CNER), Kyushu University, Fukuoka 819-0395,, Fukuoka, Japan
99 Silicide precipitation in aged quasi-α Ti alloys
Dr Frédéric Fossard[1], Mr. Thibaut Armanni[2], Mr. Thierry Douillard[3], Mr. Jean-Sébastien Mérot[1], Mr. Benoît Appolaire[4]
[1]Université Paris-Saclay, ONERA, CNRS, LEM, Châtillon, France, [2]Université Paris Saclay, ONERA, Matériaux et Structures, Châtillon, France, [3]INSA Lyon, Université de Lyon, MATEIS, UMR CNRS 5510, Villeurbanne, France, [4]Université de Lorraine, CNRS, Institut Jean Lamour, Nancy, France
111 Exploring novel joining technique of Gas Actuated Bonding by utilizing In-situ Environmental-TEM
Dr. Rahul Bhattacharya[1], Dr. Martin Ek[1], Dr. Filip Lenrick[1]
[1]LTH, Lund University, Lund, Sweden
264 Triggering and tracking grain boundary phase transformation at atomic resolution
Dr Siyuan Zhang[1], Xuyang Zhou[1], Saba Ahmad[1], Prince Mathews[1], Tilmann Hickel[1], Jörg Neugebauer[1], Amel Shamseldeen Ali Alhassan[2], Benjamin Berkels[2], Gerhard Dehm[1], Christina Scheu[1]
[1]Max-Planck-Institut für Eisenforschung, Düsseldorf, Germany, [2]RWTH Aachen University, Aachen, Germany
266 Extending 4D-STEM based strain mapping to polycrystalline materials
Lukas Schretter[1], Mr. Jürgen Eckert[1,2], Mr. Christoph Gammer[1]
[1]Austrian Academy of Sciences, Leoben, Austria, [2]Montanuniversität Leoben, Leoben, Austria
269 Dissolving alloying additions inside precipitates of lightweight alloys to promote phase transformations

Prof. Laure Bourgeois[1,2], Shenghan Su[2], Matthew Weyland[1,2], Loreibelle Abian[2], Jiehua Li[3], Philip Nakashima[2], Nikhil Medhekar[2]
[1]Monash Centre for Electron Microscopy, Monash University, Australia, [2]Department of Materials Science & Engineering, Monash University, Australia, [3]Department of Metallurgy, Montanuniversität Leoben, Austria

349 Grain evolution during annealing of a semisolid Al-Cu alloy studied with lab-based diffraction contrast tomography
Jun Sun[1], Jette Oddershede[1], Florian Bachmann[1], Jules Dake[2], Erik Lauridsen[1]
[1]Xnovo Technology ApS, Køge, Denmark, [2]Ulm University, Ulm, Germany

465 Capturing the diffusion of individual atoms in 3D: heat-induced alloying in Au@Ag nanoparticles
Dr Mikhail Mychinko[1], Dr. Ajinkya Kadu[1], Dr. Annick De Backer[1], Ana Sánchez Iglesias[2], Prof. Dr. Luis Liz-Marzán[2], Prof. Dr. Sara Bals[1]
[1]EMAT and NANOlab Center of Excellence, University of Antwerp, Antwerp, Belgium, [2]Bionanoplasmonics laboratory, CIC BiomaGUNE, San Sebastián, Spain

537 Segregation to Creep-induced Planar Faults in Ni-base Single Crystal Superalloys
Zhongmin Long[1], Dr. David Bürger[2], Dr. Christian Dolle[1], Yuting Dai[3], Prof. K. V. Vamsi[4], Prof. Yolita M. Eggeler[1]
[1]Microscopy of Nanoscale Structures & Mechanisms,Laboratory for Electron Microscopy, Karlsruhe Institute of Technology, Karlsruhe, Germany, [2]Institute for Materials, Ruhr-Universität Bochum, Bochum, Germany, [3]Institute of Nanotechnology, Karlsruhe Institute of Technology, Karlsruhe, , Germany, [4]Metallurgical Engineering and Materials Science, Indian Institute of Technology Indore, Indore, India

577 Formation of MgSi grain boundary precipitates with core-shell structure in fcc-Al
Dr Ali Ahmadian[1,2,3], Vahid Tavakkolisaiej[2,4], Dr. Torsten Scherer[2], Dr. Andrey Mazilkin[2], Dr. Yulia Ivanisenko[2], Prof. Dr. Christian Kübel[2,3,4]
[1]Helmholtz Institute Ulm, Ulm, Germany, [2]Institute of Nanotechnology, Karlsruhe Institute of Technology, Eggenstein-Leopoldshafen, Germany, [3]Karlsruhe Nano Micro Facility, Karlsruhe Institute of Technology, Karlsruhe, Germany, [4]Department of Materials and Earth Sciences, Technical University of Darmstadt , Darmstadt, Germany

601 Uncovering microscopic details of shearing mechanisms in the $L1_2$ structure by unambiguous stacking fault analysis
Nicolas Karpstein[1], Malte Lenz[1], Andreas Bezold[2], Rico Zehl[3], Mingjian Wu[1], Alfred Ludwig[3], Guillaume Laplanche[3], Steffen Neumeier[2], Erdmann Spiecker[1]
[1]Friedrich-Alexander-Universität Erlangen-Nürnberg, Department of Materials Science & Engineering, Institute of Micro- and Nanostructure Research, and Center for Nanoanalysis and Electron Microscopy (CENEM), Erlangen, Germany, [2]Friedrich-Alexander-Universität Erlangen-Nürnberg, Department of Materials Science & Engineering, Institute I: General Materials Properties, Erlangen, Germany, [3]Ruhr-Universität Bochum, Institut für Werkstoffe, Bochum, Germany

618 ACOM-TEM Investigation of the white etching layer formation in rail track
Pr Muriel Véron[1], Matteo Russo[2]
[1]Université Grenoble Alpes, CNRS, Grenoble INP, SIMaP, F-38000 Grenoble, France, [2]Univ. de Lyon, INSA Lyon, CNRS UMR 5510, MATEIS, F-69621 Villeurbanne, France, [3]Univ. de Lyon, INSA Lyon, CNRS UMR 5259 LaMCoS, F-69621 Villeurbanne, France

632 Elemental segregation at substrate/metal interface to manipulate heterogeneous nucleation
Dr Shihao Wang[1,2,3], Dr Yun Wang[3], Dr Zhongyun Fan[3], Dr Quentin Ramasse[1,2]
[1]SuperSTEM Laboratory, STFC Daresbury Campus, Daresbury WA4 4AD, United Kingdom, [2]School of Chemical and Process Engineering, University of Leeds, Leeds LS2 9J, United Kingdom, [3]BCAST, Brunel University London, Uxbridge, Middlesex UB8 3PH, United Kingdom

636 Enhanced nanoscale phase characterisation in modern steels using precession electron diffraction and energy filtering

Aleksander Brozyniak[1], Matthias Wallner[2], Philipp Kürnsteiner[1], Peter Oberhumer[1], Katharina Steineder[2], Heiko Groiss[1]
[1]Christian Doppler Laboratory for Nanoscale Phase Transformations, Center for Surface and Nanoanalytics, Johannes Kepler University Linz, Altenberger Str. 69, 4040 Linz, Austria, [2]voestalpine Stahl GmbH, voestalpine-Straße 3, 4020 Linz, Austria

657 Elucidating the effect of silicon on Fe-Zn phase formation in galvanized steel via advanced TEM

Dr. Alexey Minenkov[1], Johannes Knapp[2], Thomas Mörtlbauer[2], Heiko Groiss[1]
[1]Christian Doppler Laboratory for Nanoscale Phase Transformations, Center for Surface and Nanoanalytics, Johannes Kepler University Linz, Linz, Austria, [2]voestalpine Stahl GmbH, Linz, Austria

689 In situ insights into the thermal stability of high-entropy nanoalloys

Syrine Krouna[1], Anissa Acheche[2], Jaysen Nelayah[1], Christian Ricolleau[1], Guillaume Wang[1], Hakim Amara[2], Damien Alloyeau[1]
[1]Université Paris Cité, Paris, France, [2]ONERA, Châtillon , France

710 Direct imaging of deformation in metallic glasses using precession nanodiffraction mapping

Dipl.-Ing. Simon Fellner[1], Dipl. Ing. Lukas Schretter[1], Univ. Prof. Dr.-Ing. Habil. Dr. h.c. Jürgen Eckert[1,2], Dr. Christoph Gammer[1]
[1]Erich Schmid Institute of Materials Science, Austrian Academy of Sciences, Leoben, Austria, [2]Department of Materials Science, Montanuniversität Leoben, Leoben, Austria

747 Supersilent AlCoFeNiCux (x = 0.6 – 3.0) high-entropy alloys

Dr. Andreja Jelen[1]
[1]J. Stefan Institute, Ljubljana, Slovenia

Poster Presentation

21 Local mobility and atomic structure in Pd- and Zr-based bulk metallic glasses

Olivia Vaerst[1], Dr Harald Rösner[1], Dr Martin Peterlechner[2], Prof Dr Gerhard Wilde[1]
[1]University of Münster, Institute of Materials Physics, Münster, Germany, [2]Karlsruhe Institute of Technology, Laboratory for Electron Microscopy , Karlsruhe, Germany

26 XRD and TEM study of the quasicrystalline phase in pellets consolidated using spark plasma sintering

Dr Ruitao Li[1,2], Dr Khiam Aik Khor[3], Dr Zaoli Zhang[4], Dr Chris B Boothroyd[2], Associate Professor Zhili Dong[2]
[1]School of Mechanical Engineering, Jiangsu University, Zhenjiang, China, [2]School of Materials Science and Engineering, Nanyang Technological University, Singapore, Singapore, [3]School of Mechanical & Aerospace Engineering, Nanyang Technological University, Singapore, Singapore, [4]Erich Schmid Institute of Materials Science Austrian Academy of Sciences, Leoben, Austria

46 Interdiffusion-controlled phase formation at an interconnect interface during soldering

Sandra Gaertner[1], Dr. Harald Rösner[1], Apl. Prof Dr. Sergiy Divinskiy[1], Prof. Dr. Gerhard Wilde[1]
[1]Institute of Materials Physics, University Münster, Münster, Germany

112 3D Investigation of Lath Martensite in a Low-Carbon Stainless Steel Using PFIB-EBSD Tomography

Mehdi Mosayebi[1], Mr Daniel Paquet[2], Mr Pierre-Antony Deschênes[2,3], Mr Laurent Tôn-Thât[2], Dr Nabil Bassim[1,4]
[1]Materials Science and Engineering Department, Hamilton, Canada, [2]Hydro-Québec, Hydro-Québec Research Institute, Varennes, Canada, [3]Mechanical Engineering Department, École de technologie supérieure, Montreal, Canada, [4]Canadian Centre for Electron Microscopy, McMaster University, Hamilton, Canada

132 Developing alloys presenting nanograins and spinodal decomposition: structural and compositional characterization

Juan Macchi[1], Olha Nakonechna[2], Ronan Henry[1], Celia Castro[1], Kaveh Edalati[2], Frederic De Geuser[3], Xavier Sauvage[1], Williams Lefebvre[1]

[1]Univ Rouen Normandie, INSA Rouen Normandie, CNRS, Normandie Univ, GPM UMR 6634, Rouen, France, [2]WPI, International Institute for Carbon-Neutral Energy Research (WPI-I2CNER), Kyushu University,, Fukuoka, Japan, [3]University Grenoble Alpes, CNRS, Grenoble INP, SIMaP, Grenoble , France

205 Correlative TEM and APT studies of metallic Mg specimens prepared and analyzed under controlled environments

Cecile Bonifacio[1], Daniel Perea[2], Pawel Nowakowski[1], Mary Louise Ray[1], Paul Fischione[1]
[1]E.A. Fischione Instruments Inc., Export, USA, [2]Pacific Northwest National Laboratory, Richland, USA

214 Strain mapping using high-resolution electron backscatter diffraction technique: The influence of sample preparation

Dr Pawel Nowakowski[1], Mrs Mary Ray[1], Mr Paul Fischione[1]
[1]Fischione Instruments, Export, USA

283 Creep-induced microstructural evolution of the eutectic Mo-Si-Ti alloy by correlative electron microscopy

Hemanth Thota[1], Herr Dr.-Ing. Daniel Schliephake[2], Herr Dr.-Ing. Alexander Kauffmann[2], Herr Huichao Wu[3], Frau Prof. Dr. rer.nat. Astrid Pundt[2], Herr Prof. Dr.-Ing. Martin Heilmaier[2], Frau TT-Prof. Dr.-Ing. Yolita M. Eggeler[1]
[1]Microscopy of Nanoscale Structures & Mechanisms, Laboratory for Electron Microscopy (LEM), Karlsruhe Institute of Technology (KIT), Karlsruhe, Germany, [2]Institute for Applied Materials (IAM-WK), Karlsruhe Institute of Technology (KIT), Karlsruhe, Germany, [3]Institute of Energy and Climate Research (IEK), Forschungszentrum Jülich GmbH, Jülich, Germany

284 Investigating Impact-Induced Deformation in Cold-Sprayed Aluminum-Quasicrystals Composite Coatings

Reza Jafari[1], Dr. Mari Honkanen[2], Dr. Renato Pero[3], Dr. Turkka Salminen[2], Assoc. Prof. Heli Koivuluoto[1], Prof. Minnamari Vippola[1,2]
[1]Materials Science and Environmental Engineering, Faculty of Engineering and Natural Sciences, Tampere University, Tampere, Finland, [2]Tampere Microscopy Center, Tampere, Finland, [3]Alemnis AG, Gwatt (Thun), Switzerland

358 Microstructure and Phase Analysis of an Al-Mg-Si Alloy Produced by Laser Power-Bed Fusion

Dr.-ing Hongcai Wang[1,4], Mohammad Alhakim[1], Dr. Temesgen Yallew[1], Dr. rer. nat. Yilmaz Sakali[2], Keyur Solanki[3], Dr.-Ing. Julian Müller[1], Prof. Dr. Benjamin Butz[1], Dr.-Ing. Carolin Zinn[3], Prof. Dr.-Ing. Axel von Hehl[3]
[1]Lehrstuhl für Mikro- und Nanoanalytik, Universität Siegen, Siegen, Germany, [2]Gerätezentrum für Mikro- und Nanoanalytik MNaF, Universität Siegen, Siegen, Germany, [3]Lehrstuhl für Materialkunde und Werkstoffprüfung, Universität Siegen, Siegen, Germany, [4]Lehrstuhl Werkstoffwissenschaft, Ruhr-Universität Bochum, Bochum, Germany

400 In-situ beam driven experiments by Electron time-correlation microscopy of amorphous structures

Dr. Martin Peterlechner[1], Olivia Vaerst[2], Prof. Gerhard Wilde[2]
[1]Karlsruhe Institute of Technology, Laboratory for Electron Microscopy (LEM), Karlsruhe, Germany, [2]University of Münster, Institute of Materials Physics, Muenster, Germany

453 Strain mapping of a Σ5(310) grain boundary in Cu bi-crystal using scanning transmission electron microscopy

Anoosheh Akbari[1], Dr. Hui Ding[2], Dr. Harald Rösner[1], Dr. Esakkiraja Neelamegan[1], Dr. Christian. H. Liebscher[2], apl. Prof. Dr. Sergiy Divinski[1], Prof. Dr. Gerhard Wilde[1]
[1]University of Münster, Institute of Materials Physics, Münster, Germany, [2]Max-Planck-Institut für Eisenforschung GmbH, Düsseldorf, Germany

545 Enhancing tool performance with complex microscopy investigation of additively manufactured M2 steel and composites

Ing. Ph.d. Martina Koukolíková[1], Mr. Pavel Podaný[1], Mr. Miroslav Urbánek[1], Mr. Michal Brázda[1], Mrs. Ivana Poláková[1], Mr. Josef Hodek[1]

[1]COMTES FHT a.s., Dobrany, Czech Republic

548 ACOM characterization of phase transitions during overageing of aluminium alloys using a direct electron detector

Dr Arthur Després[1], Thomas Perrin[1], Dr Pierre Heugue[2], Pr Alexis Deschamps[1], Dr Fréderic de Geuser[1]
[1]Univ. Grenoble Alpes, CNRS, Grenoble INP, SIMaP, F-38000 Grenoble, France, [2]Safran Transmission Systems, Colombes, France

559 Study of metal powders oxidation by means of Energy Dispersion Spectroscopy (EDS)

Dr. Matteo Giardino[1,2], Dr. Federico Simone Gobber[1,2], Mr. Antonio Pennacchio[1], Prof. Marco Actis Grande[1,2]
[1]Department of Applied Science and Technology (DISAT), Politecnico di Torino, Alessandria, Italy, [2]RU Torino Politecnico, Consorzio INSTM, Firenze, Italy

678 Investigating microstructural phenomena in Additive Manufactured metals through high temporal thermal cycles in-situ heating

Dr. Alice Bastos da Silva Fanta[1], Yi-Chieh Yang[1], Christina Koenig[1], Prof. Joerg Ralf Jinschek[1]
[1]DTU Nanolab, Kgs. Lyngby, Denmark

701 TEM study of neutron radiation damage in tungsten

Dr. Michael Klimenkov[1], Ute Jäntsch[1], Michael Rieth[1], Hans-Christian Schneider[1], Wouter Van Renterghem[2], Dmitry Terentyev[2]
[1]Karlsruhe Institute of Technology, 76344 Eggenstein-Leopoldshafen, Germany, [2]SCK CEN, Nuclear Materials Science Institute, Boeretang 200, 2400 Mol, Belgium

739 The fatigue response of the IN939 superalloy prepared by additive manufacturing

Ivo Kuběna[1], Markéta Gálíková[1], Ivo Šulák[1]
[1]Institute of Physics of Materials, Czech Academy of Sciences, Brno, Czech Republic

760 Gallium liquid bridge evolution on varied substrates

Le Shu[1], Ningyan Cheng[1], Long Ren[2], Binghui Ge[1]
[1]Institutes of Physical Science and Information Technology, Anhui University, Hefei, China, [2]International School of Materials Science and Engineering, Wuhan University of Technology, Wuhan, China

771 Microstructure and thermal stability of ultrafine-grained CuZn5 processed by HPT

Yuting Dai[1,2], M.Sc. Marcel Sos[2], Prof. Christian Kübel[1,2]
[1]Institute of Nanotechnology, Karlsruhe Institute of Technology, Karlsruhe, Germany, [2]Department of Materials and Earth Sciences, Technical University Darmstadt, Darmstadt, Germany

787 Microstructural assessment of mechanically alloyed low activation 9-Cr oxide-dispersion strengthened steels

Dr. Michael Thomas Duerrschnabel[1], Dr. Carsten Bonnekoh[1], Ute Jäntsch[1], Siegfried Baumgärtner[1], Henning Zoz[2], Dr. Michael Rieth[1]
[1]Karlsruhe Institute of Technology (KIT), Institute of Applied Materials, Hermann von Helmholtz Platz 1, Eggenstein-Leopoldshafen, Germany, [2]Zoz Group, Maltozstraße, Wenden, Germany

803 Analysis of fire gilding on medieval jewellery using focused ion beam

Jan Manak[1], Jan Duchon[1], Estelle Ottenwelter[2]
[1]Institute of Physics of the Czech Academy of Sciences, Prague, Czech Republic, [2]Institute of Archaeology of the Czech Academy of Sciences, Prague, Czech Republic

812 Structure of refractory high entropy alloy and high entropy nitride thin films

Doctor Dimitri Litvinov[1], Doctor Michael Stüber, Professor Sven Ulrich[1], Professor Jarir Aktaa[1]
[1]Institute for Applied Materials, Karlsruhe Institute of Technology, Eggenstein-Leopoldshafen, Germany

836 Automated Detection of Material Defects for High-throughput Electron Micrographs Analysis

Andrei Tudor Durnescu[1], Sotero Pedro Romero Morón[1], Christina Nicole König[1], Joerg R. Jinschek[1]
[1]Danish Technical University, Lyngby-Taarbaek, Denmark

848 NiTi shape memory alloy microstructure after high stress at elevated temperatures containing modulated M2 martensite

Jan Duchoň[1], Yuchen Chen[1], Miloslav Klinger[1], Petr Šittner[1]
[1]FZU - Institute of Physics of the Czech Academy of Sciences, Prague, Czech Republic
883 In Situ SEM at Elevated Temperature for Materials Science
Ondřej Ambrož[1], Petr Horodyský[2], Jan Čermák[1], Patrik Jozefovič[1], Kateřina Sixtová[2], Šárka Mikmeková[1], Ondřej Lalinský[1]
[1]Institute of Scientific Instruments of the Czech Academy of Sciences, Brno, Czech Republic, [2]Crytur, Turnov, Czech Republic
885 Characterization of a multiphase nucleus of spheroidal graphite cast irons by transmission electron microscopy techniques
PhD Alessandro Pugliara[1,2], PhD Lydia Laffont[1], PhD Claudie Josse[2], PhD Teresa Hungria[2], PhD Jacques Lacaze[1]
[1]CIRIMAT, Toulouse INP, Université Toulouse 3 Paul Sabatier, CNRS, Université de Toulouse, 4 allée Emile Monso, 31030, Toulouse, France, [2]Centre de microcaractérisation CASTAING, Université Toulouse 3 Paul Sabatier, Toulouse INP, INSA Toulouse, CNRS, Université de Toulouse, Espace Clément Ader, 3 Rue Caroline Aigle, 31400, Toulouse, France
897 Surface tension of Au-catalysed GaAs-nanowires
Mr. Christopher Røhl Yskes Andersen[1,2], Mr. Marcus Tornberg[3,4,5], Mr. Daniel Jacobsson[3,4], Prof. Jonas Johansson[4,5], Prof. Kimberly A. Dick[3,4,5], Prof. Kristian S. Mølhave[2]
[1]Quantum DTU, Tech. Uni. of Denmark, Kgs. Lyngby, Denmark, [2]DTU Nanolab, Tech. Uni. of Denmark, Kgs. Lyngby, Denmark, [3]nCHREM, Lund Uni., Lund, Sweden, [4]NanoLund, Lund Uni., Lund, Sweden, [5]Solid State Physics, Lund Uni., Lund, Sweden
901 Microstructural Characterization of Electron Beam Welded Joints between EHEA and Austenitic Stainless Steel
M.Sc. Patrik Jozefovič[1], M.Sc. Jan Rončák[1], M.Sc. Ondřej Ambrož[1], M.Sc. Jan Čermák[1], Ph.D. Šárka Mikmeková[1]
[1]Institute of Scientific Instruments of the Czech Academy of Sciences, Brno, Czech Republic
923 SEM Insights: Sample Temperature Evolution during EBSD
Christina Koenig[1], Yi-Chieh Yang[1], Senior Researcher Alice Bastos S. Fanta[1], Professor Joerg Jinschek[1]
[1]National Center for Nanofabrication and Characterisation (DTU Nanolab), Kgs. Lyngby, Denmark
971 Atomic-scale structure and defect evolution in Σ5 [001] tilt grain boundaries in copper
Dr. Rer. Nat Hui Ding[1], Anoosheh Akbari[2], Dr Esakkiraja Neelamegan[2], Prof. Sergiy Divinski[2], Prof. Gerhard Wilde[2], Prof. Christian H. Liebscher[1,3]
[1]Structure and Nano- / Micromechanics of Materials, Max-Planck-Institut für Eisenforschung GmbH, Düsseldorf, Germany, [2]Institutre of Materials Physics, University of Münster, Münster, Germany, [3]Faculty of Physics and Astronomy and RC FEMS, Ruhr University Bochum, Bochum, Germany
984 Characterization of casting inclusions in superalloys by BSE and EDS
Prof. Dr. Dragan Rajnović[1]
[1]Faculty of Technical Sciences, University of Novi Sad, Novi Sad, Serbia
988 Deformation of steel chips due to machining
Dr. Sabine Schwarz[1], Univ.Ass. Dipl.-Ing. Christian Baumann[2]
[1]University Service Centre for Transmission Electron Microscopy (USTEM), TU Wien, Vienna, Austria, [2]Institute of Production Engineering and Photonic Technologies, Vienna, Austria
993 HR-EBSD Analysis of High-Entropy Alloys: Understanding the Role of Alloying Elements in Mechanical Performance
Mr Pedro Henrique Fernandes Oliveira[1,2], Mr Julio Spadotto[2,3], Mr Edward Pickering[2,3], Mr Francisco Coury[1], Mr Claudemiro Bolfarini[1]
[1]Federal University of Sao Carlos, Sao Carlos, Brazil, [2]The University of Manchester, Manchester, United Kingdom, [3]Henry Royce Institute, Manchester, United Kingdom
1043 In situ SEM of slip localization and its relation to the onset of ductile fracture
Mr Antoine Ollivier, Dr Antonio Pereira, Dr Nicholas Blanchard, Professor Loic Vanel, Dr Döme Tanguy

[1]Universite Claude Bernard Lyon 1, CNRS, Institut Lumière Matière, Villeurbanne, France

1061 Fast large-area EDS characterization of additive manufactured steels

Dylan Bailey[1], Christina Nicole König[1], Dr. Joerg Jinschek[1]
[1]National Centre for Nano Fabrication and Characterization (DTU Nanolab),Technical University of Denmark(DTU), Kgs. Lyngby, Denmark

1108 Novel In-situ TKD Nano-tensile Testing: Insights into Nanoscale Crystal Plasticity and Grain Boundary Mechanics

Dr. Tijmen Vermeij[1], Dr. Amit Sharma[1], Dr. Xavier Maeder[1], Prof. Johann Michler[1]
[1]Laboratory for Mechanics of Materials and Nanostructures, Swiss Federal Laboratories for Materials Science and Technology (EMPA), Thun, Switzerland

1112 Structure and stability of core-shell AuTiOx nanoparticles for CO oxidation

Stefan Kei Akazawa[1], Rikke Egeberg Tankard[2], Filippo Romeggio[2], Jakob Kibsgaard[2], Ib Chorkendorff[2], Stig Helveg[1], Christian Danvad Damsgaard[1,2,3]
[1]Center for Visualizing Catalytic Processes (VISION), Department of Physics, Technical University of Denmark, Kgs. Lyngby, Denmark, [2]Surface Physics and Catalysis, Department of Physics, Kgs. Lyngby, Denmark, [3]National Center for Nano Fabrication and Characterization, Kgs. Lyngby, Denmark

1136 Utilization of TEM in archaeology to gain in-depth information on historic artifacts

Lennart Voß[1], Lennart Voss[1], Dr. Ulrich Schürmann[1], Lena Grandin[2], Christian Horn[3], Dr. Khurram Saleem[1], Bruno Vindrola-Padrós[4], Prof. Dr. Lorenz Kienle[1]
[1]Kiel University, Department for Materials Science, Kiel , Germany, [2]The Archaeologists, National Historical Museums, Stockholm/Uppsala, Sweden, [3]University of Gothenburg, , Gothenburg, Sweden, [4]Kiel University, Institute of Prehistory and Early History, Kiel, Germany

1142 Correlating microscopy methods: the case of precipitation in lean, bioabsorbable Mg alloys

Dr. Robin Schäublin[1,2], Ms. Tatiana Akhmetshina[1], Dr. Peng Zeng[2], Dr. Stephan Gerstl[1,2], Prof. Jörg Löffler[1]
[1]Department of Materials, ETH Zürich, Zürich, Switzerland, [2]ScopeM, ETH Zürich, Zürich, Switzerland

1151 Multiscale characterization of Al-4Fe alloy grown by additive manufactoring

Dr Frédéric Fossard[1], Pauline Stricot[2], Simon Fritz[2], Eric Grevin[1], Maria Tsoutsouva[2], Nicolas Horezan[2], Quentin Barrès[2], Aidar Zakirov[3], Williams Lefebvre[3], Louise Toualbi[2], Yann Le Bouar[1]
[1]Université Paris-Saclay, ONERA, CNRS, LEM, Châtillon, France, [2]Université Paris Saclay, ONERA, Matériaux et Structures, Châtillon, France, [3]Groupe de Physique des Matériaux, Université et INSA de Rouen, UMR CNRS 6634, Rouen, France

1154 Electron Microscopy of a Gas-Atomized NiSiV Powder

Inga Konow[1], Sigurd Wenner[2], Leander Michels[3], Jan Ove Odden[3], Ursula Ludacka[1], Randi Holmestad[1]
[1]Department of Physics, Norwegian University of Science and Technology (NTNU), Trondheim, Norway, [2]Sintef industry, Department og Materials and Nanotechnology, Trondheim, Norway, [3]Elkem, Kristiansand, Norway

1169

Direct observation of quadrupolar strain fields forming a shear band in metallic glasses

Dr Sangjun Kang[1], Dr Di Wang[2], Prof Xiaoke Mu[3], Prof Christian Kübel[1]
[1]Tu Darmstadt, Darmstadt, Germany, [2]Karlsruhe Institute of Technology , Karlsruhe , Germany, [3]Lanzhou University, Lanzhou , China

Late Poster Presentation

1222 Nanocrystals with dilated interplanar distances in the carburized surface case of Inconel-718 gas-processed at 570°C

Dr Corneliu Sarbu[1], Phd Student Marian Cosmin Istrate
[1]National Institute for Materials Physics, Magurele, Romania

1233 Parent grain reconstruction of martensitic microstructures: a comparison of different methods
Dr. Barbara Šetina Batič[1]
[1]Institute of Metals and Technology, Ljubljana, Slovenia
1250 Comparative Analysis of Sample Preparation and Imaging Methods for Metallographic Examination of Archaeological Silver
Dr Alexandra Suvorova[1], Prof Walter Bloom[2]
[1]The University of Western Australia, Perth, Australia, [2]Western Australia Museum, Fremantle, Australia
1329 Observation of phase transformation of Sn by transmission electron microscopy
Mr. Yamato Kirii[1], Mr. Tetsuya Kubota[1], Mr. Sotatsu Yanagimoto[1], Mr. Takumi Sannomiya[1]
[1]Tokyo Institute of Technology, Yokohama, Japan

452

Surface microstructural evolution during Rolling Contact Fatigue of Rolling Element Bearing steels

Dr Sophie Cazottes[1], Aurore Goigoux[1,2,3], Dr Christine Sidoroff[3], Pr Fabrice Ville[2], Pr Muriel Veron[4], Thierry Douillard[1], Dr Pierre-Emmanuel Dubois[3], Dr. Nans Biboulet[2]
[1]INSA Lyon, CNRS, MATEIS, UMR 5510, Villeurbanne, France, [2]INSA Lyon, CNRS, LaMCoS, UMR5259, Villeurbanne, France, [3]NTN EUROPE, Research Innovation Development, Annecy, France, [4]Université Grenoble Alpes, CNRS, Grenoble INP, SIMaP, Grenoble, France

PS-02 (1), august 28, 2024, 10:30 - 12:30

Background incl. aims
To reduce CO2 emission and comply with European legislation, automotive market implements new electrical powertrain. It implies changes in the operating conditions of its bearings requiring new material development (grades and/or thermochemical treatments) for bearing manufacturers. A typical mode of failure for bearings operating in contaminated lubricant is surface-initiated spalling on a dent[1,2], such as in gearboxes. The denting process creates micrometer-scale shoulders, intensifying localized stress [3] and leading to plastic deformation over the operational lifespan (Figure 1,a). Therefore, cracks are often observed to be initiated at the vicinity of the shoulder. However, the life cycle of the bearing was observed to be dependent of its initial microstructure[4]. To guide the development of new materials, a better understanding of the link between microstructure of the material and its performance in contaminated conditions is needed. Understanding the influence of each microstructural constituent on microstructural evolution, fracture development, and propagation is paramount for the development of more durable materials.

Methods
This study presents a multi-scale characterization of martensitic 100Cr6 bearings before and after RCF under standard test conditions. Samples were collected from bearings before and after the tests. Observations were realized at different locations (outside the dent area, under the dent, under the shoulder) using techniques such as SEM, SEM/FIB, EBSD, TKD and TEM-ASTAR.

Results
Prior to RCF, finishing operations leads to the formation of a 0.5 µm thick surface layer consisting in refined martensite and spread primary carbides. After RCF, away from the dent, no further grain refinement was observed along the raceway; the refined surface layer being resistant enough to plastic deformation during fatigue. Surprisingly, at the bottom of the dent, were large plastic deformation occurred during the indentation phase, no significant additional alteration of the microstructure was observed.
The major microstructural evolutions were observed beneath the dent shoulder where plastic flow occurred during the indentation and running-in, and where the stress is localized during the rolling process. First a fibered region is observed below surface, with a thickness of around 1µm (Figure1b). In this region, martensite grains are refined so that nano-grains are observed, and primary carbides are sheared. Below and down to 3 µm deep, far from finished surface, an ultra-fine grain layer is observed, mixing coarse and fine martensite. The martensite morphology, size and disorientations maps suggest that martensite undergoes refinement through twinning and continuous Dynamic Recrystallisation (Figure 1,b).
Crack initiation was preferentially observed in the nano-grain layer, at carbides/matrix interfaces. Above the crack, another refined grain region is detected that was interpreted to be due to high deformation and stresses through crack propagation.

In all characterized areas, nanosized austenite islands were observed. The initial retained austenite does not completely transform during fatigue in this case while it is known to transform under surface-RCF [5]. The major microstructural evolution observed is related to the refinement/reorientation of martensite grains that occurs through twinning and/ cDRX depending on the initial orientation of the grains.

Conclusion

The multiscale characterization of such localized deformed area, in non homogenous pieces (indentation being a random process) is a complex and tedious task to achieve. However, it gave crucial information about the microstructural deformation mechanisms. We infer that a material producing dents with smaller shoulder and less primary carbides at its surface would improve its lifetime.

Fig. 1: (a) Schematic representation of a dent after RCF, (b) SEM-BSE image of a crack initiated under the dent shoulder, and c) ASTAR-ACOM map of the white square area.

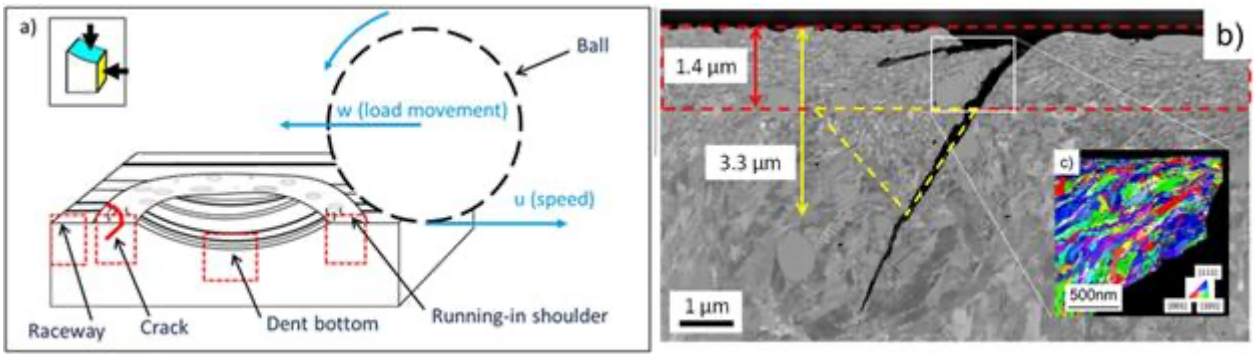

Keywords:

Steel, Rolling Cycle Fatigue, Microstructure,

Reference:

[1] S. H. Loewenthal et D. W. Moyer, vol. 101, pp. 171-176, 1979
[2] F. Ville et D. Nélias, Tribology Transactions, vol. 42, pp. 231-240, 1999.
[3] L. Fourel, J.-P. Noyel, E. Bossy, X. Kleber, P. Sainsot et F. Ville, Tribology International, vol. 164, p. 107224, 2021.
[4] C. Sidoroff, M. Perez, P. Dierickx et D. Girodin, ASTM Special Technical Publication, pp. 312-348, January 2015.
[5] M. Paladugu et R. S. Hyde Wear, Vols. %1 sur %2406-407, pp. 84-91, 2018.

786

The nature of diffuse scattering in fcc metal alloys – investigation by 3D-ED and 4D-STEM

Hannah Cole[1], Mr James Miller[1], Mr James Hogg[1], Mr Petr Vacek[1], Mr Owain Houghton[1], Prof Howard Stone[1], Prof Paul Midgley[1]
[1]Department of Materials Science & Metallurgy, University of Cambridge, Cambridge,, United Kingdom

PS-02 (2), Lecture Theater 5, august 28, 2024, 14:00 - 16:00

Background and aims:
Previous investigations of some fcc metal alloys have shown the presence of diffuse 'spots' between Bragg reflections at <111> and <112> zone axes. These have been attributed to various effects including thermal diffuse scattering, surface steps, stacking faults or nano twins, short range chemical ordering and even relrod spiking from HOLZ [1,2]. Such diffuse scattering may arises from the presence of local crystalline order/disorder in the alloy. Where it occurs, 3D 'shape' and strength of the diffuse scattering can reveal the origin of the disorder. For example, a linear defect in real space would give rise to a 'plane' of diffuse scattering while a planar defect would produce a diffuse 'rod' [3]. We hypotheses that the 1/3 {422} and 1/2 {311} diffuse 'spots' seen previously are in fact where the Ewald sphere intersects with a <111>* reciprocal lattice 'rod'. Here we use a combination of 3D-ED and scanning electron diffraction (SED), a variant of 4D-STEM, to reveal the nature of the diffuse scattering.

Method:
Two fcc alloys were investigated. The first was a single crystal Ni-base superalloy (CMSX-4) which has a γ matrix (A1 structure) and γ' precipitates ($L1_2$ structure). This specimen was taken from a <001> tensile sample and electropolished as a 3 mm disc. The second sample was an age-hardened AuPt24Pd alloy which was homogenised and then cooled at 5 K/min. This second alloy undergoes phase separation into two regions of chemical segregation: one rich in Au and Pd, and another rich in Pt. The alloy specimen was a TEM foil that was prepared by FIB lift out.

A FEI Tecnai Osiris 80-200 TEM was used to acquire selected area diffraction patterns and HR-TEM images of the specimens. A Thermo Fisher Spectra 300 TEM was used for the 3D-ED, SED and complementary STEM-EDX experiments.

3D-ED was performed using the continuous rotation electron diffraction (cRED) method. Here, the sample is rotated continuously so that a 'movie' with many hundreds of frames is acquired across a tilt range, in this case +/- 60 °. By extracting these movie frames, and considering each as a central section through 3D reciprocal space, a full diffraction 'tomogram' can be reconstructed. This technique has been used primarily for structural determination using the 3D distribution of Bragg reflections. However, here we consider the 3D distribution of diffuse intensity between the Bragg reflections.

The 3D reconstruction was achieved using a combination of python scripts (using the open-source packages hyperspy and pyXem) and the program PETS2 [4]; the 3D visualisation was performed in either Vesta or Avizo. Strain maps (using SED) and associated elemental maps (EDX) were determined using hyperspy and pyXem.

Results:
Figure 1(a) shows a zero order Laue zone (ZOLZ) section (Fourier slice) taken from the reconstructed 3D reciprocal space of the Ni-base superalloy sample. The zone axis orientation is <110> and the weak Bragg reflections are from the ordered γ' precipitates. In this section, we can see clear evidence of lines of diffuse scattering in the <111>* direction, which is likely to originate from the γ phase. Moreover, these lines of diffuse scattering do not appear along the <111>* rows that pass through the origin as indicated by the dashed arrows in figure 1(a). Figure 1(b) shows a ZOLZ slice from the <111> zone axis. The diffuse scattering is now present as faint, relatively broad 'spots' of diffuse scattering at the 1/3 {422} position. Similar results were obtained using conventional selected area diffraction and SED. Figure 1(c) shows a FOLZ slice from another <110> axis, 60 degrees from that in (a). This illustrates how information can be obtained with this method that is not readily accessible through conventional 2D diffraction. Again diffuse 'lines' are seen in figure 1(c) between Bragg reflections. It is notable that these lines are shifted with respect to those in figure 1(a) as they were obtained from a higher section in reciprocal space.

Similar diffraction results, shown in Figure 1(d), are seen for the AuPt24Pd alloy. The strain and EDX maps (not shown here) indicate clear phase separation at the 10-20 nm scale in the <110> and <100> directions but these orientations rule out that this is the origin of the <111>* diffuse scattering seen in the diffraction patterns.

The results described above are only consistent with the 3D model of diffuse scattering illustrated in figure 1(e) in which rods of diffuse intensity run parallel to <111>*.

Given the nature of the diffuse scattering seen in these alloys it is likely that it is related to a change of local atomic structure in the {111} planes. The lack of diffuse scattering through the origin indicates that any atomic displacement related to the local structure in the {111} planes is transverse in nature – an analogy would be the 'streaking' seen in <110> patterns from fcc crystals arising from stacking faults with shear vectors 1/6 <112> in the {111} planes. However, here, given the rather broad nature of the diffuse scattering it is speculated that its origin may be highly localised chemical order within the {111} planes, leading to small atomic displacements in the plane because of the change in inter-atomic bonding between atom species. Such small, localised shears in the {111} plane would be expected to give rise to the <111>* diffuse rods seen.

Conclusions:
3D-ED has be used to determine the 3D structure of diffuse scattering in fcc metallic alloys. Through the analysis of Laue zone sections, taken from the 3D reconstruction (tomogram) of the diffraction tilt series, it has been shown that the diffuse scattering can be described using a series of <111>* diffuse rods whose origin is likely to be small transverse displacements (shears) in the {111} planes brought about by changes in local atomic structure [5].

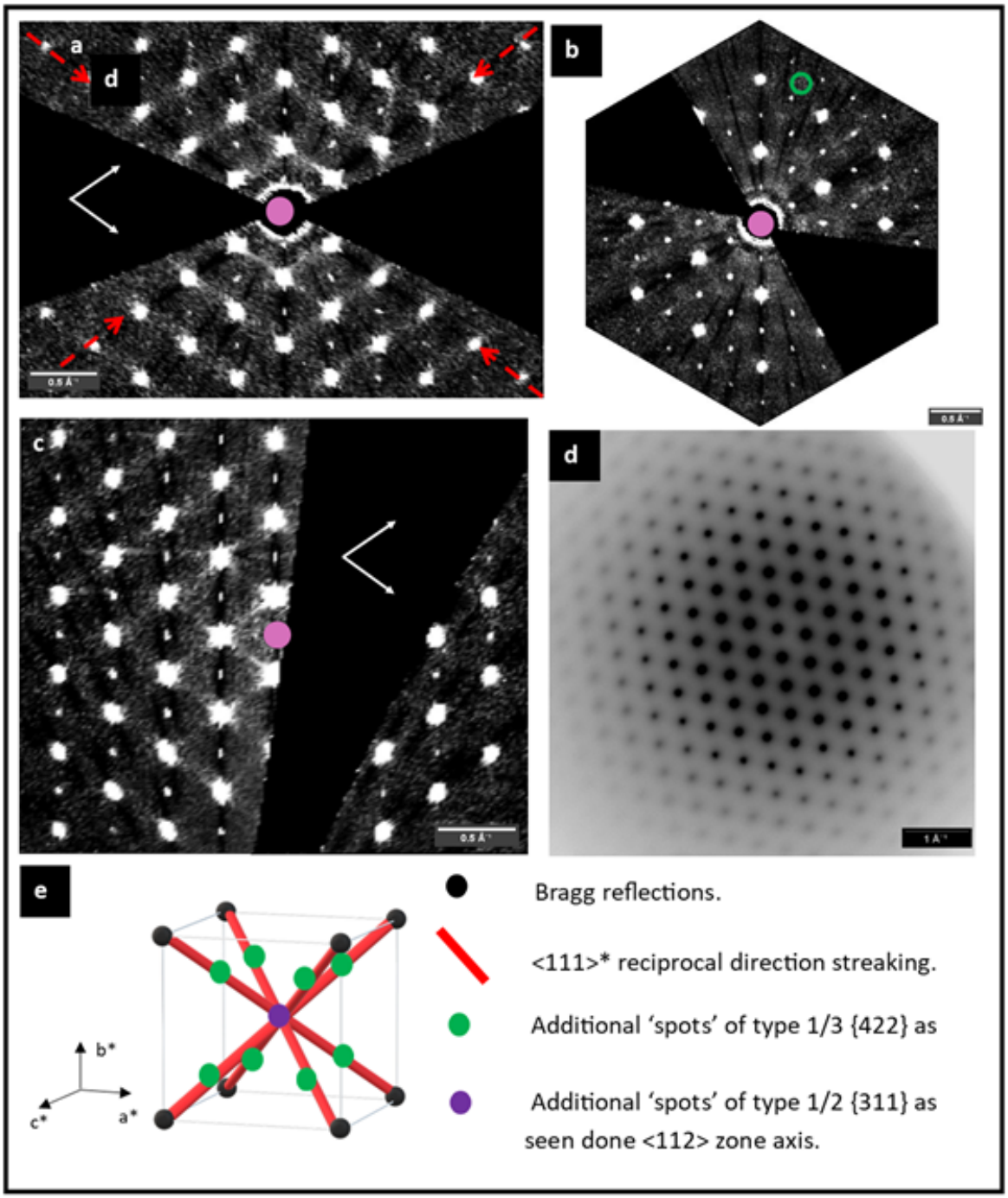

Figure 1) Subfigures a-c are Fourier slices taken from the reconstructed 3D reciprocal space of the Ni-base superalloy sample, with the pink dot showing the position of the origin. a) Zero order Laue zone (ZOLZ) with zone axis orientated in <110> direction, with the white arrows showing the direction of the <111>* streaking and the dashed red arrows indicating the absent streaks through the origin. B) ZOLZ with zone axis orientated in <111> direction, with a green circle to indicate the position of the diffuse 1/3 {422} 'spots'. c) A first order Laue zone (FOLZ) from another <110> direction a) with the white arrows marking the <111>* direction again. d) A conventional 2D diffraction pattern with inverted colours from <110> direction from the AuPt24Pd alloy showing the diffuse <111>* streaking as well. e) 3D model of the proposed diffuse <111>* diffuse rods and their intersection with additional spot positions.

Keywords:

Streaking, Diffuse Scattering, 3D-ED, SED

Reference:

[1] Coury, F.G., Miller, C., Field, R. et al. On the origin of diffuse intensities in fcc electron diffraction patterns. Nature 622, 742–747 (2023).
[2] Zhang, R., Zhao, S., Ding, J. et al. Short-range order and its impact on the CrCoNi medium-entropy alloy. Nature 581, 283–287 (2020).
[3] H.Z. Xiao, A.C. Daykin, Extra diffractions caused by stacking faults in cubic crystals, Ultramicroscopy, Volume 53, Issue 4, 325-331 (1994).
[4] Lukas Palatinus, Jaromíra Hrdá, PETS2 (Version 2.2.20231114.143), http://pets.fzu.cz/ (2023).
[5] Acknowledgement to Rolls-Royce PLC and the EPSRC ICase voucher number (220040) for the funding of this project and the worshipful company of goldsmiths for help with the supply of material for this project. PAM thanks the EPSRC for funding under grant numbers EP/V007785/1 and EP/R008779/1.

52

Differential Phase Contrast Microscopy and Atom Probe Tomography of Ferromagnetism in High-Entropy Alloys

Ms. Shabnam Taheriniya[1], Dr Harald Rösner[1], Mr. Gerhard Wilde[1]
[1]Institute of Materials Physics, University of Münster, 48149 Münster, Germany

PS-02 (1), august 28, 2024, 10:30 - 12:30

Background incl. aims
High-entropy alloys (HEAs) are emerging as promising materials for future applications due to their high configurational entropy and diverse local atomic environments. Among the four core effects in HEAs, the concept of the ‘cocktail effect’, resulting from multi-principal alloy design, is particularly intriguing as it can lead to the emergence of new properties. When elements with different structural, kinetic, and ferromagnetic properties are combined in single-phase or nanocomposite HEAs, unexpected interactions and the emergence of new properties or phases can occur, surpassing predictions based on simple mixtures. Certain equiatomic alloys, initially paramagnetic, have been found to exhibit ferromagnetic properties after undergoing deformation processes like rolling or cold-working. This unexpected behavior has been attributed to changes in the local atomic environment and the creation of defects during deformation, resulting in the formation of ferromagnetic clusters. Understanding the mechanisms behind deformation-induced ferromagnetism in these alloys is the aim of this contribution.
Methods
In this study, single phase (CoCrFeMnNi) and nanocomposite HEAs (CoCrFeMnNi and HfNbTaTiZr) were processed using high-pressure torsion (HPT), subjecting the samples to a constant pressure of 9 GPa either as a single disk or stacked disks, with the top anvil rotating at 1 rpm at ambient temperature for up to 15 revolutions. Vibrating sample magnetometry (VSM) confirmed that HPT processing induces the development of ferromagnetic properties. The distribution and orientation of magnetic domains post-deformation were examined in detail using differential phase contrast scanning transmission electron microscopy (DPC STEM), analytical TEM and atom probe tomography (APT) analysis.
Results
Analytical TEM indicates that while the nanocomposite HEA shows significant phase sep-aration due to co-deformation, its saturation magnetization measured by VSM is lower than that of the HPT-processed Cantor alloy. The pronounced phase separation in the nanocomposite HEA leads to lamellar-like alignments of NiCo-rich ferromagnetic and Cr-rich anti-ferromagnetic domains observed by DPC, reducing the overall magnetic moment. Conversely, the absence of such phase separation in the HPT-processed Cantor alloy results in comparable coercivity. APT analyses reveal that this difference arises from the deformation-induced local enrichment of ferromagnetic elements, particularly Ni, showcasing the 'cocktail effect' in HEAs where inter-element interactions lead to unique magnetic behavior.
Conclusions
Our study demonstrates that HPT processing of HEAs induces a transition from paramagnetic to ferromagnetic states at ambient conditions. Deformation-induced ferromag-netism can be explained by the 'cocktail effect’ in HEAs, where the formation of ferromagnetic particles is linked to deformation-induced element-selective atomic migration and local enrichment of ferromagnetic elements.

Keywords:

high-entropy alloy; ferromagnetism; nanocomposites; deformation

79

Solving the controversy of the metal-insulator phase transition in chromium nitride thin films

Magnus Garbrecht[1], Ms Ashalatha Indiradevi Kamalasanan Pillai[1], Mr Bidesh Biswas[2], Mr Bivas Saha[2]
[1]The University of Sydney, Sydney, Australia, [2]Jawaharlal Nehru Centre for Advanced Scientific Research, Bangalore, India

PS-02 (1), august 28, 2024, 10:30 - 12:30

Background incl. aims
CrN is a hard coating material that has applications in abrasion and wear-resistant cutting tools, bearings, and tribology applications due to its high hardness, high-temperature stability, and corrosion-resistant properties. Recently, CrN has also attracted significant interest due to its high thermoelectric power factor [1]. Much of debate in the literature is around CrN's unique and intriguing metal-insulator phase transition. While CrN bulk single-crystals exhibit the characteristic metal-insulator transition accompanied with structural (orthorhombic-to-rocksalt) and magnetic (antiferromagnetic-to-paramagnetic) transition at ~260 - 280 K, observation of such phase transition in thin-film CrN has been scarce, and the exact cause of the absence of the transition in several thin film studies is not well-understood [2].
Methods
STEM images and EDS maps were recorded with an image- and probe-corrected and monochromated Themis-Z 60-300 kV equipped with a high-brightness XFEG source and Super-X EDS detector system for ultra-high-count rates, operated at 300 kV. The spatial resolution in STEM mode was 0.7 Å. EDS maps used for atomic % quantification have well above 1 M counts, and k-factor analysis and absorption-corrected background subtraction were employed.
Results
Here, we demonstrate that the formation of a secondary metallic Cr2N phase during the growth inhibits the observation of metal-insulator phase transition in CrN thin films, see Figure 1. When the Cr-flux during deposition is reduced below a critical limit, an epitaxial and stoichiometric CrN thin film is obtained that reproducibly exhibits the phase transition. Annealing of the mixed-phase film inside reducing NH3 environment converts the Cr2N into CrN as revealed by HRSTEM imaging and EDS mapping, and a discontinuity in the electrical resistivity at ~277 K appears.
Conclusion
In summary, we show that formation of the secondary metallic Cr2N phase inside CrN during the thin film growth process inhibits the observation of its metal-insulator electronic phase transition. A high Cr-flux during the deposition process results in metallic Cr2N networks inside the CrN matrix. When the Cr-flux is reduced below the critical limit of the growth rate of 1 nm/min, a stoichiometric single-crystalline CrN thin film is obtained that reproducibly exhibits the electronic phase transition. Our results also show that when the Cr2N, inside the high-flux mixed film, is converted to CrN by annealing it inside NH3 environment at high temperature, the electronic phase transition is recovered. This strongly manifests the fact that phase pure and stoichiometric CrN films can show the metal-insulating electronic phase transition. The demonstration of the origin behind the controversy of the metal-insulator transition in CrN thin films marks significant progress for its potential applications in nanoscale devices [3,4,5].
Figure Caption
Figure 1 (a) Low-magnification HAADF-STEM micrograph of the HCF film is presented that shows the presence of both Cr2N and CrN. Inset shows the EDP of the film with cubic [001] and hexagonal patterns. (b) STEM-EDS elemental maps corresponding to (a) show the spatial distribution and morphology of the Cr2N and CrN grains. (c) HAADF-STEM micrograph of the HCF film with bright regions that represent the Cr2N, while the darker parts showing CrN grains. (d) Cr, (e) N and (f) Cr+N

STEM-EDS maps corresponding to the region (c) showing the different grains. (g) HAADF-STEM micrograph of the LCF film showing single-phase epitaxial single-crystalline CrN growth on MgO substrate. (h) Homogeneous and uniform Cr and N atomic distribution in the LCF film is demonstrated by the STEM-EDS map. (i) Atomic-resolution STEM image of the CrN/MgO interface from the LCF film is presented that exhibits cubic epitaxial CrN crystal growth on MgO substrate.

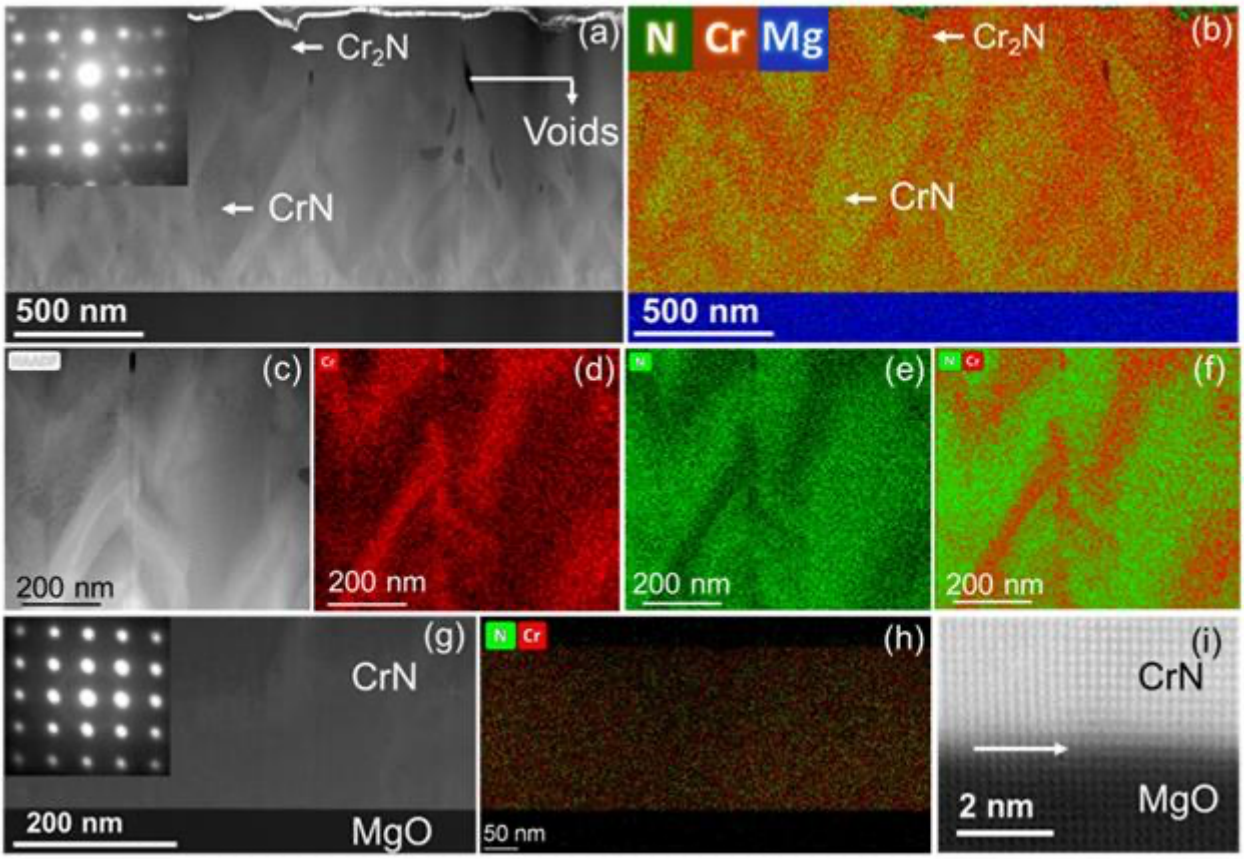

Keywords:

Chromiumnitrate, phase transition, STEM, EDS

Reference:

[1] B.Biswas et al Phys.Rev.Materials 5, (2021) .
[2] X.Y.Zhang et al Phys.Rev. B 84 (2011).
[3] S.Chakraborty et al Acta Mater. 227, (2022).
[4] B.Biswas, et al Phys.Rev.Lett. 131 (12), (2023).
[5] The authors acknowledge the facilities at Sydney Microscopy and Microanalysis at The University of Sydney.

92

TEM Investigations on the Impact of Hydrogen on Phase Transformations in Aluminum Alloys

M. Omar Boukir[1], M. Xavier Sauvage[1], M. Kaveh Edalati[2]
[1]Univ Rouen Normandie, INSA Rouen Normandie, CNRS, Groupe de Physique des Matériaux UMR 6634, F-76000, Rouen, France, [2]2WPI, International Institute for Carbon-Neutral Energy Research (WPI-I2CNER), Kyushu University, Fukuoka 819-0395,, Fukuoka, Japan

PS-02 (1), august 28, 2024, 10:30 - 12:30

Background :
This study investigates the influence of hydrogen on phase transformations in aluminium alloys, materials of critical importance to the transportation industry due to their superior strength-to-weight ratio[1]. Given the potential of hydrogen to induce hydrogen embrittlement (HE) in metals and alloys, this investigation is of paramount importance. The mechanisms behind HE involve the interactions between hydrogen and crystalline defects such as dislocations, vacancies, grain boundaries, and interfaces[2]. However, understanding these mechanisms has been challenging due to difficulties in localizing hydrogen. Phase transformation, including precipitation, is governed by nucleation sites, atomic mobility, and interface energies, all associated with crystalline defects. Utilizing advanced microscopy techniques, this work aims to indirectly gather information on how hydrogen interacts with defects by examining the influence of hydrogen on phase transformation.
Methods :
The materials under investigation were two aluminum alloys: Al-Cu, chosen for its excellent contrast in STEM-HAADF and its well-known precipitation sequence, and Al-Zr, selected for the strong interaction between zirconium and hydrogen[4]. The JEOL ARM-200F microscope, equipped with a STEM corrector, serves as the primary tool for characterizing structural changes under various conditions, complemented by Atom Probe Tomography (APT) and Thermal Desorption Spectroscopy (TDS) for elemental analysis and hydrogen trapping state investigation, respectively. Precipitates were analyzed under different zone axes to assess their shape and diameter, Additionally, Energy Filtering Transmission Electron Microscopy (EFTEM) was employed to produce thickness maps, enabling the calculation of precipitate density. The distribution of dislocations varied with each state, characterized using both bright field and dark field modes in TEM, and more precisely with the LADF detector in STEM, where dislocations predominantly aligned along (111) planes.
Results and Conclusions :
Findings for the Al-Cu alloy indicated a significant slowdown in the initial aging hardening kinetics in hydrogen-charged samples. STEM-HAADF imaging revealed a reduced precipitate density compared to uncharged samples, suggesting that while hydrogen does not alter the precipitation sequence, it does influence the growth and coalescence rates of precipitates. This effect was even more evident under high hydrogen pressure, especially in extensively deformed samples, indicating a slowdown in precipitation processes and defect recovery. In contrast, the Al-Zr alloy's hardness measurements showed no noticeable difference between samples aged in hydrogen and air. However, TEM analysis revealed that under hydrogen, the diameter of zirconium precipitates was twice as large as those aged in air, with a similar nucleation rate for both conditions. This suggests that hydrogen enhances zirconium diffusion, accelerating precipitate growth.

Keywords:

Hydrogen, Precipitation, Microscopy, Aluminium alloy,

Reference:

J.G. Kaufman, E.L. Rooy, Aluminum alloy castings : properties, processes, and applications, ASM Int. (2004).
A. Oudriss, J. Creus, J. Bouhattate, E. Conforto, C. Berziou, C. Savall, Acta Mater. 60 (19) (2012) 6814–6828.
Chunhui Liu, Ziyao Ma, Peipei Ma, Lihua Zhan. Materials Science & Engineering A 733 (2018) 28–38.

99

Silicide precipitation in aged quasi-α Ti alloys

Dr Frédéric Fossard[1], Mr. Thibaut Armanni[2], Mr. Thierry Douillard[3], Mr. Jean-Sébastien Mérot[1], Mr. Benoît Appolaire[4]
[1]Université Paris-Saclay, ONERA, CNRS, LEM, Châtillon, France, [2]Université Paris Saclay, ONERA, Matériaux et Structures, Châtillon, France, [3]INSA Lyon, Université de Lyon, MATEIS, UMR CNRS 5510, Villeurbanne, France, [4]Université de Lorraine, CNRS, Institut Jean Lamour, Nancy, France

PS-02 (1), august 28, 2024, 10:30 - 12:30

Increasing temperature properties of materials is a major strategic challenge for the aviation industry. Titanium alloys like the so-called Ti6242 offer excellent specific mechanical strength and good corrosion resistance up to temperatures of around 550°C. On one hand, molybdenum can be added to reduce creep/fatigue effects known as dwell effect [1] but the associated decrease of alpha phase fraction is detrimental to high temperature performances. On the other hand, addition of silicon improves the mechanical properties at high temperature [2] and compensate molybdenum addition. Still, the strengthening mechanism of silicon is still under discussion.
During aging, silicon leads to the precipitation of silicides [3] which could play a role in the strengthening of the alloy. We have characterized the microstructures by complementary electron microscopies to corroborate the relationship between silicides and macroscopic mechanical properties.
In order to characterize the microstructure at different relevant scales, we used SEM and TEM imaging. Despite a good accuracy, the analysis of the planar or projected images revealed that the strong anisotropies of the lamellae microstructure prevents a good description of the silicide population. Therefore, we also performed 3D reconstructions by FIB/SEM (figure a) on the alloys in the aged state to get reliable statistics on the dimensions, shape and organisation of the silicides in the microstructure (figure b). An additional S/TEM study has been used to determine the precipitate structure and chemistry.
Thanks to FIB/SEM reconstructions, volumes containing 4000 precipitates each have been analysed. Results showed that aged Ti6244 alloys host precipitates with an elongated shape and a mean Feret radius of almost 40 nm. Moreover, when the Si content is doubled, the precipitate density increases (+55 %). The analysis of the precipitate organisation, with respect to the Ti matrix orientation, reveals that the precipitates are mainly located in the beta phase and that their nucleation is likely to occur at the interface between alpha and beta. It also showed that two directions of elongation are favored.
A careful analysis by high resolution S/TEM (figure c) reveals that the S2 silicides are semi-coherent and that their composition is close to (Ti,Zr)6Si3 which is not expected with respect to the thermomechanical treatment used and the CALPHAD calculations. The Burgers relationship between both titanium phases and the S2 silicides are clearly defined and explains the two observed variants. Additional TEM observations after creep at high temperature illustrates the role of the silicide in the dislocation anchoring (figure d).
Thanks to combined microscopy techniques, we show that the silicide precipitation plays a key role in the strengthening of the Ti6244 alloys. The semi-coherent structure and the spatial organization of the precipitates suggest that an Orowan mechanism is favored.

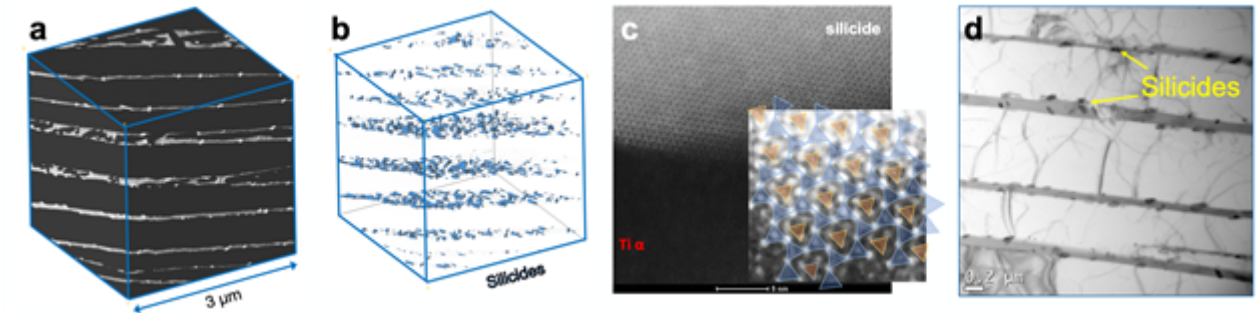

Keywords:

FIB/SEM tomography, titanium, silicides, HRSTEM

Reference:

[1] W. J. Evans et al., Metallurgical Transactions A, 10(12), pp. 1837-1846(1979).
[2] Paton, N.E. et al.(1976), Metallurgical Transactions A, 7(11), pp. 1685–1694.
[3] Banerjee, D. et al. (2013), Acta Materialia, 61(3), pp. 844–879.

111

Exploring novel joining technique of Gas Actuated Bonding by utilizing In-situ Environmental-TEM

Dr. Rahul Bhattacharya[1], Dr. Martin Ek[1], Dr. Filip Lenrick[1]
[1]LTH, Lund University, Lund, Sweden

PS-02 (1), august 28, 2024, 10:30 - 12:30

Background
The reliability of a critical industrial component is decided by the durability of the weakest joint or spot. For applications involving high-temperature operational conditions especially coupled with corrosive environments like fuel cell interconnections, molten metal baths, etc., the joints are the most vulnerable regions for catastrophic failure due to localized material degradation by selective corrosion leading to compromised mechanical behavior. The existing joining techniques lead to a continuous metallic phase with modified microstructural characteristics at the bridging junctures or employ a joining alloy that integrates two parent materials. These bridging phases are proving to be the weakest points of the components because they are prone to corrosion compared to parent materials. This is effectuated by the microstructural transformation as well as local compositional fluctuation incorporated in the bridging phases as a consequence of the joining techniques and procedure currently in use.
On the other hand, the semiconductor industry utilizes emerging brazing technologies built on well-established Chemical Vapor Transfer (CVT) technologies (e.g., CVD, MOVPE, PVD). Even though both oxide removal and metal migration into the gap are crucial in metal bonding, there is only one published concept for delivery of non-metallic MPD [1], and a few studies of utilizing active gases for oxide removal.

Methods
The methodology of GAB requires the joints to be made from the bulk material itself by utilizing both gaseous oxide removers (OXR) and gas phase melting point depressants (MPD). In transient liquid phase (TLP) diffusion bonding, a method that lies between brazing and diffusion bonding, diffusion is sped up by a metal MPD interlayer. The preparation of superalloys or the brazing of Al-alloys has been conducted by the oxide removing technology which is contemporarily in practice. This process resulted in the best possible corrosion resistance and strength because both the joint and the bulk have obtained a similar surface oxide and microstructure. Furthermore, by introducing melting point depressing gases on metal surfaces, GAB induces a transient liquid phase similar to chemical vapor transport (CVT) technology. The two critical rate-determining steps in GAB are the removal of the pre-existing surface oxides of the nanoparticles and metal migration into the gap corresponding to the effect of temperature of exposure and partial pressure of the MPD precursor gas.

Results
GAB of pure Cu has been studied in-situ Environmental Transmission Electron Microscope (E-TEM) from a nanometer-sized AgCu particle. Temperature was held constant at 520°C, where the particle is identified as solid. After gaseous AsH3 is allowed to flow into the chamber, the particle is observed to alloy with As and is then identified as liquid (without any temperature change). Similar trials are attempted on 316L steel nanoparticles in experiments conducted utilizing a similar setup of in-situ E-TEM wherein GAB is obtained by melting point reduction using phosphine (AsH3). Therefore, we have built upon the well-established Chemical Vapor Transport (CVT) technology to induce a transient liquid phase that could form joints with greatly enhanced mechanical and anti-corrosion properties. This leads to a novel metal joining technology called Gas Actuated Bonding (GAB) wherein melting point depressing (MPD) elements are transported as MPD-precursor gas to the joining zones.

This takes place during processing to initiate surface reactions that create a liquid transition phase. This will lead to a profound improvement in the quality and consistency of the bridging phase in terms of microstructural consistency, thermal stability, along with enhanced mechanical properties.

Conclusion

Miniature components can be effectively assembled utilizing GAB by circumventing the need for obstructive fillers through the use of MPD-precursor gases that particularly actuate the outermost surfaces. Thus, heat-affected zones and deformation are subsequently prevented. This further validates GAB as a highly suitable manufacturing technology for such small and complex components. Hence, we can observe a drastic improvement in performance as the joints and bulk will have homogeneous surface oxides and homogeneous microstructure. The GAB mechanism is thus thoroughly investigated and understood by in-situ E-TEM experiments at various partial pressures of the MPD gases and the temperature of in-situ heating.

Graphic description

Preliminary results from GAB of AgCu. a) Schematic illustration. b) Elemental mapping in E-TEM. A nanometer-sized particle of AgCu is observed to be solid at 520°C in a vacuum. When AsH3 is flowed into the chamber the particle alloys with As and melts. c) Isothermal Section of the Ag-As-Cu Ternary Phase Diagram at 500°C. The red line indicates the compositional change of the particle after introducing AsH3.

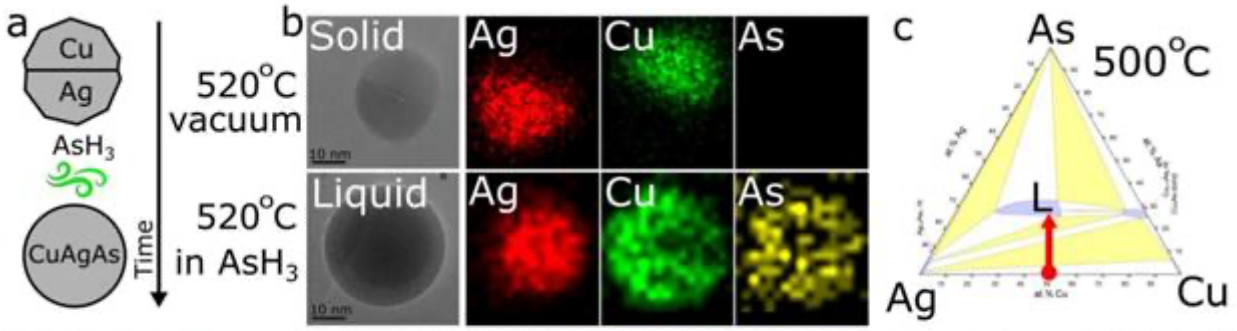

Figure 3. Preliminary results from GAB of AgCu. a) Schematic illustration. b) Elemental mapping in E-TEM. A nanometre sized particle of AgCu is seen to be solid at 520°C in vacuum. When AsH_3 flows into the chamber the particle alloys with As and melts. b) Isothermal section of the Ag-As-Cu ternary phase diagram at 500°C. The red line indicates the compositional change of the particle after introducing AsH_3.

Keywords:

Insitu Environmental-TEM, Gas-actuated bonding, Deoxidation

Reference:

Lenrick, Filip, Martin Ek, Knut Deppert, Lars Samuelson, and L. Reine Wallenberg. "Straight and kinked InAs nanowire growth observed in situ by transmission electron microscopy." Nano Research 7, no. 8 (2014): 1188-1194

264

Triggering and tracking grain boundary phase transformation at atomic resolution

Dr Siyuan Zhang[1], Xuyang Zhou[1], Saba Ahmad[1], Prince Mathews[1], Tilmann Hickel[1], Jörg Neugebauer[1], Amel Shamseldeen Ali Alhassan[2], Benjamin Berkels[2], Gerhard Dehm[1], Christina Scheu[1]
[1]Max-Planck-Institut für Eisenforschung, Düsseldorf, Germany, [2]RWTH Aachen University, Aachen, Germany

PS-02 (1), august 28, 2024, 10:30 - 12:30

Background incl. aims
Phase diagrams and crystallographic defects are essential pillars for modern materials design. In recent years, increasing numbers of defect phases (also known as “complexions”) have been identified, and there are evidences on their phase transformations. Nevertheless, due to the vast variety of defects (for example, grain boundaries have five degrees of freedom), it remains challenging to study their thermodynamics in a systematic way, eventually requiring the construction of defect phase diagrams [1].
Methods
We developed a quasi in situ approach to trigger phase transformations of a single grain boundary. The same defect was monitored by atomic-resolution scanning transmission electron microscopy during various steps of triggers. We also developed automatic pattern recognition to distinguish different grain boundary structural units, and applied ab initio simulations to understand their thermodynamics.
Results
We demonstrate the phase transformation of a Mg grain boundary triggered by local Ga alloying using focused ion beam, as well as the structural evolution with time. As shown in Fig. 1, successive steps of Ga incorporation lead to phase transformations of a Mg [0001] tilt grain boundary [2, 3]. There are two aspects of the phase transformations: 1. Structural transformation from T-type (highlighted in green in Fig. 1a) to A-type (highlighted in red in Fig. 1b) structural units; 2. Formation of chemically ordered grain boundary phases as shown in Fig. 1c, d.
Conclusion
The discovered grain boundary phases and their transformations observed quasi in situ enabled us to construct a phase diagram for this grain boundary. Our developed methodology including atomic resolution imaging, automatic pattern recognition, and ab inito simulations formulates a blueprint to develop defect phase diagrams systematically and propel a new paradigm for materials design.

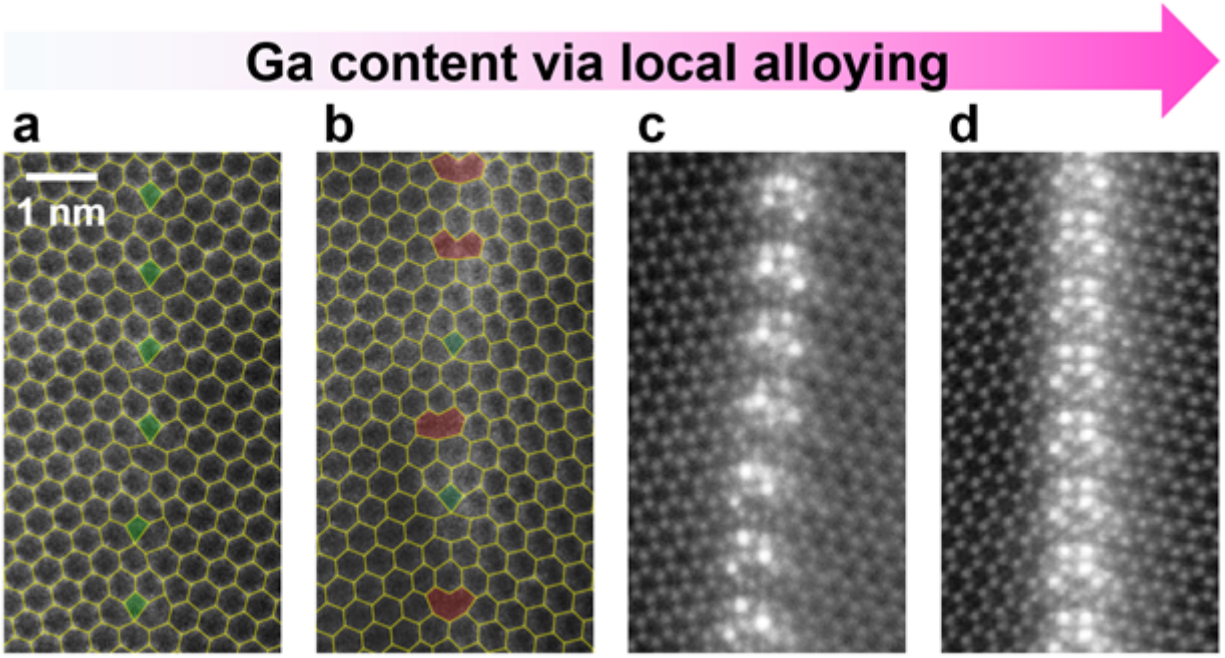

Keywords:

Grain boundary complexion, phase transformation

Reference:

[1] S. Korte-Kerzel, T. Hickel, L. Huber, et al., DOI: https://doi.org/10.1080/09506608.2021.1930734
[2] S. Zhang, Z. Xie, P. Keuter, et al., DOI: https://doi.org/10.1039/D2NR05505H
[3] X. Zhou, P. Mathews, B. Berkels, et al., DOI: https://doi.org/10.48550/arXiv.2303.09465

266

Extending 4D-STEM based strain mapping to polycrystalline materials

Lukas Schretter[1], Mr. Jürgen Eckert[1,2], Mr. Christoph Gammer[1]
[1]Austrian Academy of Sciences, Leoben, Austria, [2]Montanuniversität Leoben, Leoben, Austria
PS-02 (2), Lecture Theater 5, august 28, 2024, 14:00 - 16:00

Background incl. aims
Four-dimensional scanning transmission electron microscopy (4D-STEM)-based techniques for elastic strain mapping have advanced significantly, offering a robust tool to investigate deformation mechanisms in materials at the nanoscale. In single crystalline materials, measurements of the reciprocal lattice vectors allow to accurately determine the full in-plane elastic strain tensor [1]. This technique exhibits high sensitivity, enabling the detection of stress fields associated with individual dislocations. In amorphous materials, like metallic glasses, 4D-STEM based strain mapping techniques have also been successfully utilized to determine nanoscale strain states in materials [2]. In contrast, for polycrystalline microstructures, lying between the two extreme cases of single crystals and amorphous materials, a technique for local nanoscale strain mapping is lacking. Although global strains can be inferred from the ellipticity of diffraction rings in selected area diffraction (SAD) patterns, this method provides only average values across multiple grains, lacking insights into the stress state within individual grains or at grain or phase boundaries. This study aims to close this gap and develop a new routine to map the nanoscale strain in polycrystalline materials, facilitating the measurement of strain fields and grain rotations during in-situ deformation of polycrystalline materials with a resolution of 2 nm.
Methods
To demonstrate the technique a 50 nm thick nanocrystalline gold (Au) thin film is used. The sample was produced by DC magnetron sputtering and subsequently underwent heat treatment at 360 °C to reduce the dislocation density present after deposition. The thin film was mounted on a push-to-pull MEMS device and in-situ tensile testing was conducted using a Hysitron PI 95 nanoindenter holder capable of recording the load-displacement data during deformation. The tensile test was intermittently halted during deformation to acquire full 4DSTEM datasets. Precession electron diffraction was employed to enhance the quality of diffraction patterns. By precessing the electron beam the experiment is shifted towards more kinematical diffraction conditions vastly improving the quality of the diffraction patterns. On the one hand, inner intensity distributions are reduced, making peak detection more precise, and on the other hand, more diffraction disks are revealed thus improving on the crystal orientation determination. The utilization of a direct electron detector and an in-column energy filter further refines the dataset quality.

Results
The resulting strain and orientation maps, obtained during in-situ deformation, affirm the feasibility of this study's objectives. Only small changes in crystal orientation were observed, consistent with the low plasticity exhibited by the nanocrystalline thin film. The limited thickness of the Au film, consisting of a single layer of grains, might also lead to less pronounced grain rotation. Nonetheless, orientation changes within individual grains resulting in subgrain structures could be detected and quantified. At the same time, the precise determination of elastic strain states in polycrystalline materials during in-situ deformation was demonstrated. Under loading, a discernible shift towards higher tensile strains was observed, with a histogram analysis revealing a gradual increase in the tensile strain spread with increasing applied load. This clearly indicates, that even in the elastic regime dislocations are generated. Following fracture, the average strain go back to zero, however an even larger spread is measured. This shows that the increase in dislocation density and thus the

broader strain distribution is not due to a measurement artifact but an actual mechanism in the material that can be quantified.

Conclusions

Atomic-level elastic strains in a nanocrystalline thin film were determined by combining concepts from single crystalline strain mapping and automated crystal orientation mapping techniques. This paves the way for future in-situ deformation experiments on industrially relevant polycrystalline structural materials, thereby enhancing our understanding of their deformation mechanisms.

1. C. Gammer, J. Kacher, C. Czarnik, O. L. Warren, J. Ciston, A. M. Minor. Local and transient nanoscale strain mapping during in situ deformation. Applied Physics Letters 109 (2016) 081906.
2. H. Sheng, D. Şopu, S. Fellner, J. Eckert, C. Gammer. Mapping Shear Bands in Metallic Glasses: From Atomic Structure to Bulk Dynamics. Physical Review Letters 128 (2022) 245501.
We acknowledge support from the Austrian Science Fund (FWF):Y1236-N37

Keywords:

In-situ, strain mapping, 4D-STEM, ACOM-TEM

269

Dissolving alloying additions inside precipitates of lightweight alloys to promote phase transformations

Prof. Laure Bourgeois[1,2], Shenghan Su[2], Matthew Weyland[1,2], Loreibelle Abian[2], Jiehua Li[3], Philip Nakashima[2], Nikhil Medhekar[2]
[1]Monash Centre for Electron Microscopy, Monash University, Australia, [2]Department of Materials Science & Engineering, Monash University, Australia, [3]Department of Metallurgy, Montanuniversität Leoben, Austria

PS-02 (2), Lecture Theater 5, august 28, 2024, 14:00 - 16:00

Background incl. aims
Microalloying elements are commonly added to high-strength aluminium alloys, mainly to promote the formation of key strengthening precipitate phases. Classic examples include Sn, Cd and In at the 100 ppm level [1], which significantly accelerate the nucleation of the strengthening phase θ' in Al-Cu alloys, thereby improving the precipitation hardening response. More dramatic is the effect of Ag additions to Al-Cu-Mg and Al-Cu-Li alloys, where new phases (Ω and T1) form in high number densities, leading to ultra-high-strength alloys typically used in the aerospace industry. In all these cases, the microalloying additions either segregate at the precipitate-matrix interfaces or precipitate first as a well-defined crystalline phase before acting as heterogeneous nucleation sites [1].
An unusual case is that of Au additions to Al-Cu, where the precipitation hardening response is enhanced and accelerated through Au dissolving inside the strengthening precipitate phase θ' [2].
This observation leads to two questions which this work aimed to address:
(1) What is the mechanism by which Au enters the precipitates and promotes their formation?
(2) Can other elements behave in this way?
Answering these questions would be useful not only for improving one's fundamental understanding of phase transformations, but also to provide a potential way of immobilizing contaminants.

Methods
This work employed a combination of aberration-corrected scanning transmission electron microscopy, density functional theory (DFT) simulations and classical nucleation theory (CNT) calculations. The microscopy was performed on a FEI Titan3 FEGTEM and a Thermo Fisher Scientific Spectra-ϕ FEGTEM, both double-aberration corrected and operated at an accelerating voltage of 300 kV in scanning transmission electron microscopy (STEM) mode. Al-1.7at%Cu-0.02at.%Au alloys having undergone different ageing treatments were examined. More details about the experimental and computational procedures can be found in Refs. [3-4].

Results
In order to understand how Au atoms are incorporated into θ' precipitates, the alloy was characterised at the very early stages of ageing. It was found that the overwhelming majority of θ' precipitates at the earliest stages of precipitation were 80-100 nm long and only 1 to 1.5-unit cell high, with ~2nm long θ" precipitate regions at the semi-coherent interfaces (see Fig. 1). The 1c-high configuration has never been observed in pure Al-Cu alloys. Chemical analysis indicated the presence of Au atoms within the structure. An atomic-scale mechanism is proposed that involves the transformation of the plentiful coherent θ" precipitates into 1c-high θ' through the incorporation of Au solute and vacancies. This mechanism is supported by DFT and CNT calculations [3,5].
The intriguing possibility that other solute elements may dissolve into the θ' phase was also examined through DFT simulations.

Conclusion

An unusual mechanism through which a microalloying element (here Au) promotes the formation of a strengthening precipitate phase (here θ') by dissolving inside it, was investigated at the atomic scale. This was found to lead to sub-nanoscale thick precipitates of aspect ratio >100. This direct transformation mechanism may also be at play in other important aluminium alloy systems, such as Al-Cu-Li with Ag additions.

The authors acknowledge the Monash Centre for Electron Microscopy, a Node of Microscopy Australia, and the Australian Research Council.

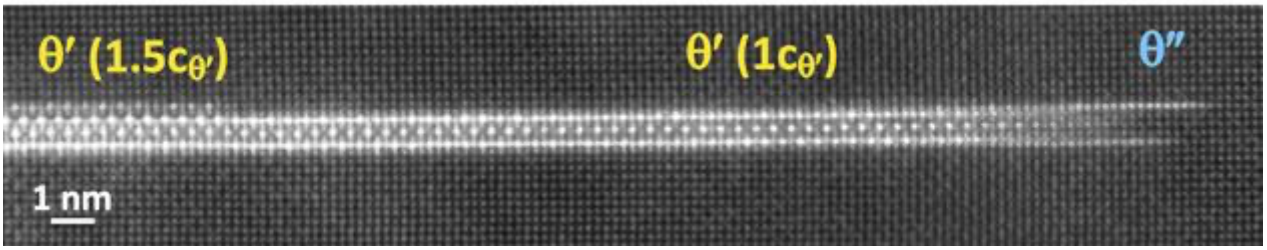

Keywords:

STEM; aluminium; precipitates; phase transformations

Reference:

[1] Polmear, IJ et al., Light Alloys. Metallurgy of the Light Metals, 5th Ed. (Butterworth-Heinemann, 2017).
[2] Chen, Y et al., Acta Materialia 125 (2017) 340.
[3] Bourgeois, L. et al., Nature Communications 11 (2020), 1248.
[4] Su, S, Bourgeois, L and Medhekar, NV, Acta Materialia 255 (2023) 119048.
[5] Su, S et al., in preparation.

349

Grain evolution during annealing of a semisolid Al-Cu alloy studied with lab-based diffraction contrast tomography

Jun Sun[1], Jette Oddershede[1], Florian Bachmann[1], Jules Dake[2], Erik Lauridsen[1]
[1]Xnovo Technology ApS, Køge, Denmark, [2]Ulm University, Ulm, Germany

PS-02 (2), Lecture Theater 5, august 28, 2024, 14:00 - 16:00

Background incl. aims
3D experimental data of simultaneously high temporal and spatial resolution is key to validation of computational modelling of materials phenomena. In this study, we exploit lab-based diffraction contrast tomography (DCT) [1], to capture the evolution of grain structure over a series of interrupted annealing treatments of a semisolid Al-Cu alloy [2,3]. The time resolved response measured on the present Al-Cu model system provides insights into the rearrangement, densification and coarsening of powder compacts at late-stage sintering. The wealth of the experimental data lends itself particularly well to investigations of both grain size and orientation (rotation) evolution.

Methods
The semisolid Al-Cu alloy specimen was subjected to ten sequential isothermal heat treatments, each 15 min at 630°C, and we used lab-based DCT to non-destructively track the microstructural evolution of individual grains through the corresponding eleven temporal states of interrupted annealing. The lab environment setting allows us to reconstruct the results and analyze changes to the microstructure before subsequent treatment of the sample. Furthermore, we take advantage of the recently developed DCT advanced acquisition schemes [4] to cover a large sample volume of 10 mm^3.

Results
During the experiment, we observe both grain coarsening (from 1934 grains with a mean grain size of 194 µm at the initial state to 934 grains with a mean grain size of 247 µm after ten annealing steps) and grain rotations. A statistical study of the evolving grain structure reveals that the disappearing grains are generally among the smaller ones at the beginning of the experiment. In addition, the rotations of individual grains are typically small fluctuations irrespective of grain size, but when an abruptly large rotation is observed, it is more likely to occur for a smaller grain at the last annealing step(s) before the grain vanishes. Finally, the experimental data indicates that Σ3 twin boundaries are especially stable, and that grains sharing such a boundary will rotate together in their local environment to keep the boundary intact.

Conclusion
Our investigations show that the crystallography of grain contacts undoubtably plays a pivotal role in the microstructural evolution of semisolid systems during heat treatment and should be included in predictive simulations of coarsening. To help incorporate our experimental observations into the next generation of models, the eleven grain maps have been made publicly available to the scientific community via the Materials Data Facility [5].

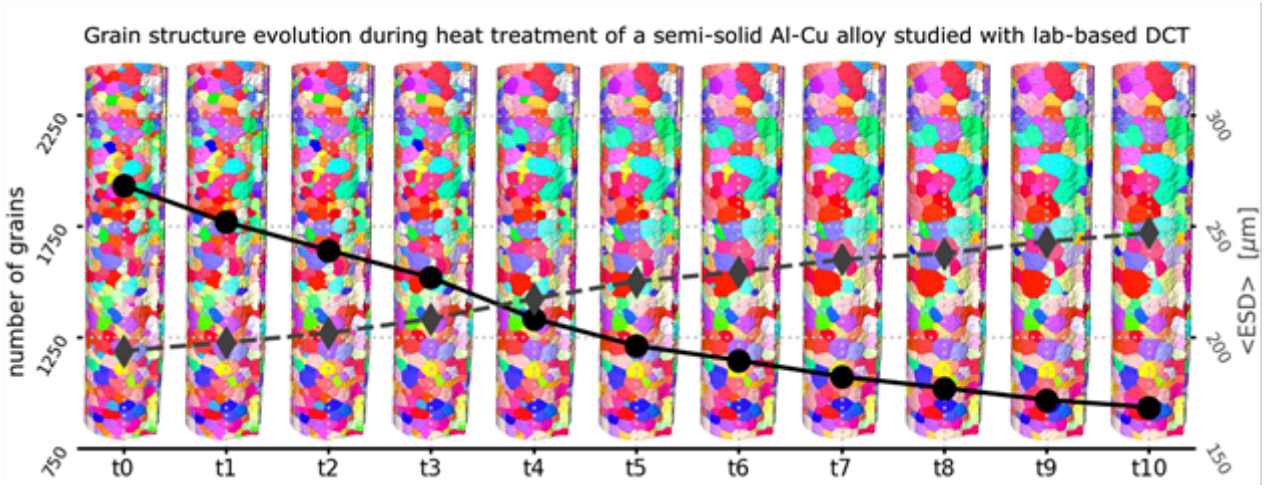

Keywords:

Lab-based DCT, Coarsening, 4D structure

Reference:

[1] Holzner, C., et al., doi:10.1017/S1551929516000584 (2016).
[2] Dake, J., et al., doi:10.1073/pnas.1602293113 (2016).
[3] Sun, J., et al., doi:10.1016/j.tmater.2024.100025 (2024).
[4] Oddershede, J., el al., doi: 10.1007/s40192-021-00249-w (2022).
[5] Sun, J., et al., doi:10.18126/5Q8S–3EF9 (2023).

465

Capturing the diffusion of individual atoms in 3D: heat-induced alloying in Au@Ag nanoparticles

Dr Mikhail Mychinko[1], Dr. Ajinkya Kadu[1], Dr. Annick De Backer[1], Ana Sánchez Iglesias[2], Prof. Dr. Luis Liz-Marzán[2], Prof. Dr. Sara Bals[1]
[1]EMAT and NANOlab Center of Excellence, University of Antwerp, Antwerp, Belgium,
[2]Bionanoplasmonics laboratory, CIC BiomaGUNE, San Sebastián, Spain

PS-02 (2), Lecture Theater 5, august 28, 2024, 14:00 - 16:00

Background incl. aims
In recent decades, bimetallic core-shell nanoparticles (NPs) have attracted great attention in materials science, primarily due to their unique optical properties based on surface plasmon resonances. However, the practical application of these materials, particularly under elevated temperature conditions, often leads to particle reshaping and redistribution of metals between the core and shell of the particle, gradually altering nanoplasmonic properties. Consequently, advancing nanoplasmonic-based technologies necessitates a comprehensive understanding of heat-induced transformations, considering factors like nanoparticle size, shape, and defect presence. Conventional two-dimensional Scanning Transmission Electron Microscopy (2D STEM) imaging falls short in reliably analysing diffusion, especially in asymmetric NPs. Thus, employing three-dimensional (3D) characterization techniques becomes paramount. Herein, electron tomography (ET) emerges as a pivotal tool. Moreover, achieving atomic resolution in the 3D investigation of elemental redistribution is crucial. This enables drawing conclusions regarding the structural parameters influencing diffusion kinetics in bimetallic NPs, such as core-shell Au@Ag NPs.
Methods
To conduct a thorough 3D investigation of heat-induced alloying in individual Au@Ag NPs, ET based on High-Angle Annular Dark Field (HAADF) STEM was combined with in situ heating holders.1 To reach ET reconstructions with atomic resolution, an aberration-corrected Themis Z transmission electron microscope offering a spatial resolution of 60 pm was used. The 3D reconstruction of each studied NP was performed after several heating steps using advanced reconstruction algorithms2 supported by convolutional neural network, allowing for compensation of scanning distortions during the acquisition of HAADF-STEM projections and missing wedge artifacts.3 Mass-thickness contrast (Z-contrast) of HAADF-STEM ET enabled us to distinguish between individual Au and Ag atoms, facilitating the determination of atom positions. Additionally, a set of selected slices through the obtained reconstructions were used as an input for StatSTEM analysis,4 to correlate the kinetics of atomic redistribution with the presence of lattice distortions.
Results
As reported in our previous work, we observed significantly faster alloying kinetics in pentatwinned (PT) Au@Ag NPs compared to their single-crystalline (SC) counterparts, which we attributed to lattice distortions near the twin boundaries, facilitating faster atomic transport.5 To support this hypothesis, heat-induced alloying in SC and PT Au@Ag nanorods (NRs) with similar sizes and compositions was studied using atomic resolution ET. To induce alloying, all particles were heated to 450°C using the specialized heating tomography holder until complete and uniform alloying was achieved. To investigate intermediate states of alloying, the heating process was interrupted, and atomic resolution ET series were acquired after several heating time intervals. The obtained tomography datasets were further utilized as input for advanced ET reconstruction algorithms, where prior knowledge is typically used to enhance the outcome of the reconstructed 3D volumes. Specifically, the Sparse Spheres Reconstruction (SSR) algorithm2 was implemented, where parameters such as the sizes and intensity values of atoms within an NP can be parameterized, leading to the improved distinction between individual Au and Ag atoms. In this manner, we were able to study the atomic

transport in different NPs in 3D and assess the diffusion kinetics in the SC regions of the studied NPs or in the vicinity of twin boundaries, where lattice distortions can be carefully determined from the positions of all atoms obtained from atomic resolution ET reconstructions.

Conclusion

In this work, we demonstrate the capability of advanced ET techniques to conduct in situ investigations and quantitative analyses of heat-induced processes in complex NPs, such as core-shell Au@Ag NRs, with atomic resolution in 3D. By employing these techniques, which involve the combination of state-of-the-art TEM instruments with dedicated heating tomography holders and specialized reconstruction algorithms, we show that diffusion kinetics are faster in regions where twin boundaries cause higher interatomic distances compared to the "perfect" crystal lattice of Au and Ag.

The project has received funding from European Research Council (ERC Consolidator Grant 815128, REALNANO) and European Commission (grant 731019, EUSMI).

Keywords:

Electron tomography, in-situ, bimetallic nanoparticles

Reference:

1. Vanrompay, H. et al. Nanoscale 10, 22792–22801 (2018).
2. Zanaga, D, et al. Nanoscale 8, 292-299 (2016).
3. Lobato, I. et al. npj Comput Mater 10, 10 (2024).
4. De Backer, A. et al. Ultramicroscopy 171, 104-116 (2016).
5. Mychinko, M. et al. Small 17, 1–11 (2021).

537

Segregation to Creep-induced Planar Faults in Ni-base Single Crystal Superalloys

Zhongmin Long[1], Dr. David Bürger[2], Dr. Christian Dolle[1], Yuting Dai[3], Prof. K. V. Vamsi[4], Prof. Yolita M. Eggeler[1]
[1]Microscopy of Nanoscale Structures & Mechanisms,Laboratory for Electron Microscopy, Karlsruhe Institute of Technology, Karlsruhe, Germany, [2]Institute for Materials, Ruhr-Universität Bochum, Bochum, Germany, [3]Institute of Nanotechnology, Karlsruhe Institute of Technology, Karlsruhe, , Germany, [4]Metallurgical Engineering and Materials Science, Indian Institute of Technology Indore, Indore, India

PS-02 (2), Lecture Theater 5, august 28, 2024, 14:00 - 16:00

Nickel-base single crystal (SX) superalloys have long been served as indispensable materials for turbine blades in aerospace gas engines, owing to their outstanding creep properties. The unique mechanical resistance is attributed to the coherent γ/γ' microstructure in which the cuboidal γ' precipitates exhibit an ordered L12 crystal structure embedded in γ matrix channels, which is a solid solution with a face-centered cubic (FCC) structure. In severely harsh operation environments, the mechanical properties of superalloys are primarily controlled by the precipitate shearing events associated with elemental segregation to and away from dislocations and planar faults within the γ' phases [1].

The present work focuses on understanding the alloying segregation to dislocations and planar defects. Some key aspects under investigation are: a) Do the nano defect phases, formed through elemental segregation, contribute to the stabilizing defect phases within the γ' precipitate? b) Does the elemental segregation to defects result in a reduction of defect energy, thereby facilitating the cutting of the γ' precipitate by the defects? To address these aspects, we designed double creep shear specimens such that deformation takes place along a specific loading direction [11-2] to activate the slip system [11-2](111) with Schmid factor of 1. Local high-resolution energy dispersive X-ray (EDX) is used in scanning transmission electron microscopy (STEM) mode to measure the elemental segregation to planar defects as a function of creep strains (1% and 2%). Both creep-deformed sample states allow us to differentiate whether a compositional steady state, and consequently a nanophase, has formed in the vicinity of the crystal defects[2], or if transient states are measured. Transient states would indicate ongoing diffusion processes that potentially control the kinetics of shear processes [3].

Microstructural characterization post creep deformation with the low magnification high-angle annular dark-field (HAADF) STEM micrograph of the 1% crept sample in Figure 1(A), and the conventional dark field two-beam condition image of the 2% crept sample in Figure 1(C) both depict the termination of planar fault motion inside the precipitate, indicating a leading partial dislocation shearing segment within the γ' phase. High-resolution HAADF images in Figure 1(B) and (D), elucidate that along these leading segments, the nature of the largest stacking fault is a superlattice extrinsic stacking fault (SESF), while at the very tip, in front of SESF we observe a short complex intrinsic stacking fault (CISF). Both faults show the same defect configuration: a closely spaced pair of Shockley partial dislocations with identical Burgers vector1/6[11-2] glide on adjacent (111) planes. This process creates two energetically unfavourable CISFs, which are known to subsequently reshuffle Al-Al atom positions to convert the high-energy fault structure into a stable SESF with low planar fault energy [4].

The chemical distributions across the SESFs in Figure 2 illustrate almost identical segregation tendencies for 1% and 2% crept samples. The γ forming elements such as Cr, Co, W, or Re are enriched in the vicinity of the SESF, while γ' alloying elements Ni and Al are depleted. Quantitatively comparing the local alloying element concentration magnitudes at the SESFs show

that the 1% crept sample exhibits the same local composition as the 2% crept sample, even though it experienced a longer creep time. This observation concludes that the segregation to the SESF has reached a steady state and establishes a stabilized nano-defect phase within the SESF after 1% creep strain. This result suggests that with a longer creep time, alloying elements do not further diffuse to the SESF.

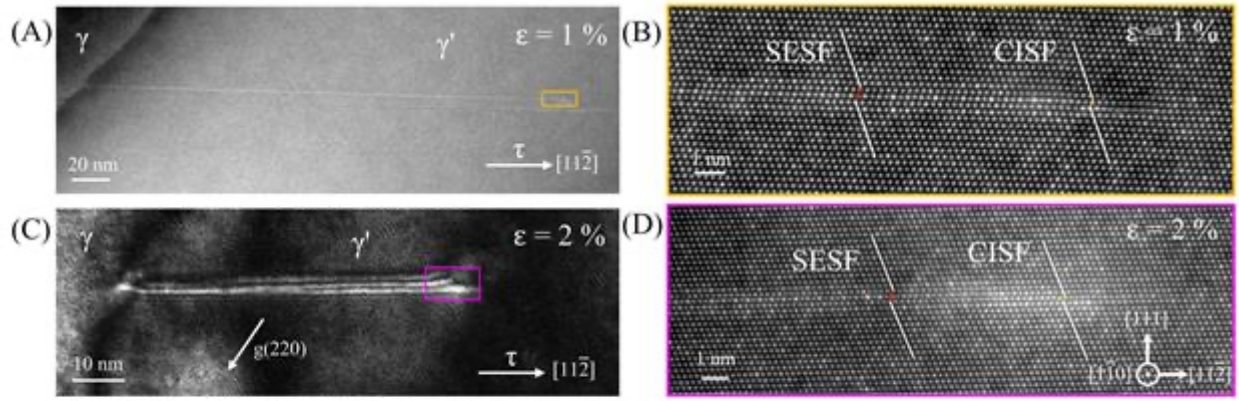

Fig. 1. Analysis of creep-induced SESFs after ε = 1% and ε = 2% creep samples at 750°C and 250 MPa: (A) and (C) show lower magnification HAADF image and two-beam condition conventional dark field image; (B) and (D) high-resolution HAADF images.

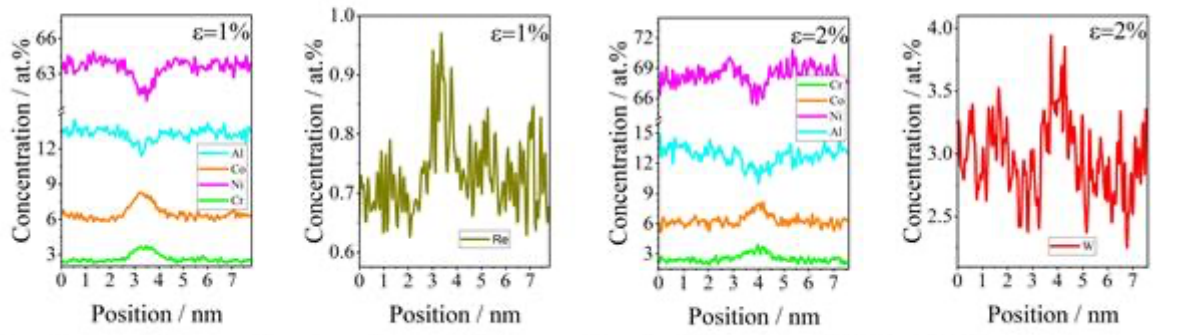

Fig. 2. Corresponding concentration line profiles across SESFs after ε = 1% and ε = 2% creep strains at 750°C and 250 MPa in superalloy samples.

Keywords:

superalloys, stacking fault, reshuffling, segregation

Reference:

References:
[1] Y.M. Eggeler, et al., Annual Review of Materials Research 51(1) (2021), p. 209-240.
[2] T.M. Smith, et al., Nature Communications 7(1) (2016), p.13434.
[3] D. Barba, et al., Metallurgical and Materials Transactions A 49(9) (2018), p. 4173-4185.
[4] M. Kolbe, Materials Science and Engineering A 319–321 (2001), p 383 –387
[5] Authors gratefully acknowledge financial support by the German Research Foundation (Deutsche Forschungsgemeinschaft, DFG), the Research Training Group GRK 2561 MatCom – ComMat, and Karlsruhe Nano Micro Facility (KNMFi) at Karlsruhe Institute of Technology for the access to probe-corrected Titan Themis Z. K. V. Vamsi gratefully acknowledges IIT Indore for providing the Young Faculty Research Seed Grant (YFRSG).

577

Formation of MgSi grain boundary precipitates with core-shell structure in fcc-Al

Dr Ali Ahmadian[1,2,3], Vahid Tavakkolisaiej[2,4], Dr. Torsten Scherer[2], Dr. Andrey Mazilkin[2], Dr. Yulia Ivanisenko[2], Prof. Dr. Christian Kübel[2,3,4]
[1]Helmholtz Institute Ulm, Ulm, Germany, [2]Institute of Nanotechnology, Karlsruhe Institute of Technology, Eggenstein-Leopoldshafen, Germany, [3]Karlsruhe Nano Micro Facility, Karlsruhe Institute of Technology, Karlsruhe, Germany, [4]Department of Materials and Earth Sciences, Technical University of Darmstadt , Darmstadt, Germany

PS-02 (2), Lecture Theater 5, august 28, 2024, 14:00 - 16:00

Background incl. aims
Aluminum (Al) shows promise as an excellent conductor, but its usefulness in electrical and electronic industries is often limited by its relatively low strength. Alloying pure Al with other metals like Mg, Cu, or Ag can increase its strength, but this also results in a decrease in its electrical conductivity [1]. Another method to strengthen Al is by reducing the grain size through severe plastic deformation such as high pressure torsion extrusion. However, grain growth can occur at elevated temperatures [2]. Adding small amounts of Mg and Si can stabilize grain growth by forming MgSi precipitates, which hinder grain boundary migration. This phenomenon is known as the solute-drag effect [3]. The impact of these precipitates on electrical conductivity is primarily influenced by their size, shape, atomic structure, and composition. All these parameters depend on the thermomechanical treatment and this work aims to bridge between structural and physical properties including the influence of individual mechanism during the thermomechanical preparation of the material.
Methods
In this study, Al - 0.94 at.%Mg-1 at.%Si solid solution were plastically deformed at 100°C using high pressure torsion extrusion (HPTE) and subsequently aged at temperature between 130°C and 160°C for up to 48 hours to generate MgSi precipitates. Tensile tests and Vickers hardness measurments were carried out to get information about the mechanical strength at different areas of the sample. Electrical conductivitz was measured on the sample surface by the Eddy current method using a Sigmascope device.
To investigate the overall microstructure, scanning electron microscopy (SEM) in combination with electron backscatter diffraction (EBSD) was performed using a Yeiss Auriga 60 equipped with EDAX Digiview EBSD camera. Information about dislocation density and crystal size was recorded bz X-ray diffraction experiments.
The nanometer sized precipitates were studied using high resolution transmission electron microscopy (HRTEM) including geometric phase analysis (GPA) as well as advanced scanning transmission electron microscopy (STEM) techniques such as energy dispersive X-ray spectroscopy (EDS), electron energy loss spectroscopy (EELS) and 4D-STEM were conducted on a double corrected Titan Themis Z operated at 300 kV. Atom probe tomography was conducted correlatively for accurate quantification of the composition of the precipitates.

Results
The initial polycrystalline Al - 0.94 at.%Mg - 1 at.%Si was about 100 um. Following high-pressure torsion extrusion (HPTE), the grain size reduced by a factor of 20. Subsequent aging processes did not result in significant grain growth but rather induced texturing, as illustrated in the SEM-EBSD inverse pole figure (Figure 1a). STEM-EDS measurements detected the formation of magnesium silicide (MgSi) precipitates at both grain boundaries (GBs) and within the grain interiors. It is noteworthy that the morphology of GB precipitates differs from those within the grains. Within the grains, precipitates primarily exhibit an elongated rod-like morphology, while at the GBs, precipitates appear

as symmetrical spherical caps (see Figure 1b). This difference in morphology can be attributed to the higher energy of the GB, which attracts solute magnesium and silicon atoms more strongly. As an illustration, Figure 1c depicts a low-angle boundary with a misorientation angle of approximately 4° between adjacent grains. Such a low-angle GB would be composed of a series of dislocations with spacings typically falling within the range of 11nm. Notably, GB precipitates were observed to preferentially form at the initial positions of these edge dislocations. Atomic-resolution imaging of a single precipitate revealed a core-shell structure with a partially disordered shell. 4D-STEM was utilized to determine the phase of the precipitate core, elucidating the presence of a complex U2-$MgSi_2$ phase.

Conclusion

The formation of MgSi-precipitates by HPTE is responsible for a higher strength and better electrical conductivity. Our electron microscopy studies reveal that the morphology, crystal structure and composition of GB precipitates differs from precipitates formed within the grains. The GB precipitate shows a core-shell structure with higher concentration of Si in the outer shell. This can be attributed to the higher segregation energy of Mg in Al than Si. Finally, the GB precipitate could mainly attribute to the better performance during conductivity measurements. HPTE can be used to increase the fraction of GB precipitates and this may open the path to engineer fcc-Al for better performance as electrical conductor.

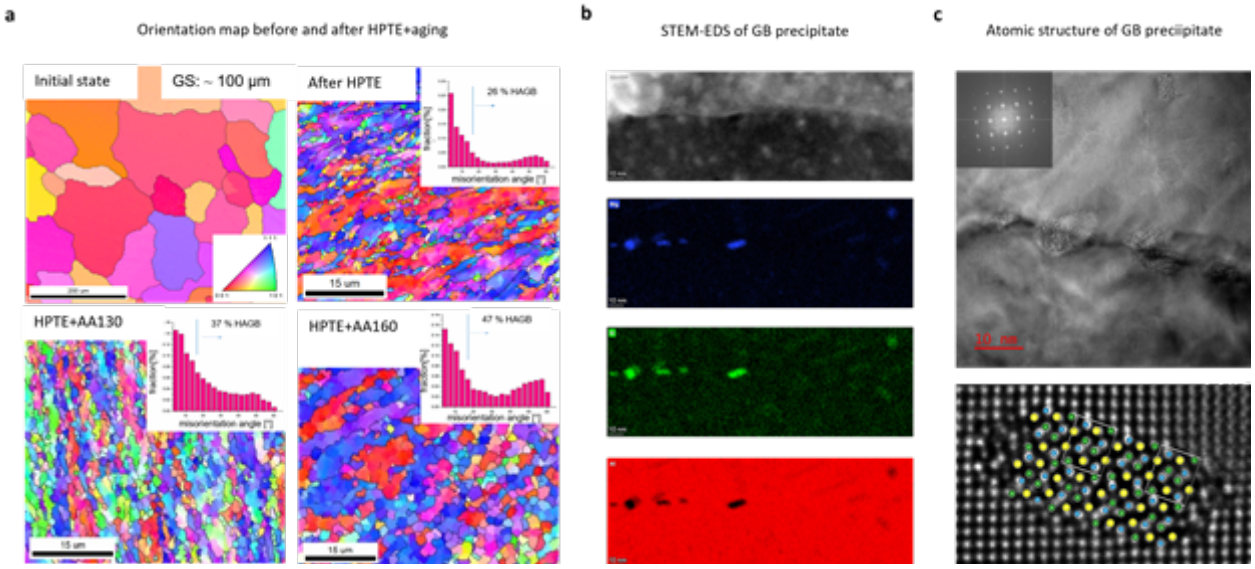

Keywords:

Grain boundary, precipitation, STEM, APT

Reference:

[1] Orlova, T.S.; Latynina, T.A.; Mavlyutov, A.M.; Murashkin, M.Y.; Valiev, R.Z.; “Effect of annealing on microstructure, strength and electrical conductivity of the pre-aged and HPT-processed Al-0.4Zr alloy”, J. Alloys Compd., 784, 2019, 41-48.

[2] Ivanisenko, Y., Kulagin, R., Fedorov, V., Mazilkin, A., Scherer, T., Baretzky, B., & Hahn, H.; “High pressure torsion extrusion as a new severe plastic deformation process”, Mater. Sci. Eng. A., 664, 2016, 247-256.

[3] U.F. Kocks; “Laws for Work-Hardening and Low-Temperature Creep”; J. Eng. Mater. Technol., 98, 1976, 76-85.

601

Uncovering microscopic details of shearing mechanisms in the $L1_2$ structure by unambiguous stacking fault analysis

Nicolas Karpstein[1], Malte Lenz[1], Andreas Bezold[2], Rico Zehl[3], Mingjian Wu[1], Alfred Ludwig[3], Guillaume Laplanche[3], Steffen Neumeier[2], Erdmann Spiecker[1]
[1]Friedrich-Alexander-Universität Erlangen-Nürnberg, Department of Materials Science & Engineering, Institute of Micro- and Nanostructure Research, and Center for Nanoanalysis and Electron Microscopy (CENEM), Erlangen, Germany, [2]Friedrich-Alexander-Universität Erlangen-Nürnberg, Department of Materials Science & Engineering, Institute I: General Materials Properties, Erlangen, Germany, [3]Ruhr-Universität Bochum, Institut für Werkstoffe, Bochum, Germany

PS-02 (3), Lecture Theater 4, august 30, 2024, 14:00 - 16:00

Background incl. aims
γ/γ'-strengthened Ni- and Co-base superalloys for applications at high temperatures rely on the precipitation-strengthening effect of the $L1_2$-ordered γ' phase embedded into the face-centered cubic γ matrix phase. Therefore, the microscopic mechanisms by which the γ' phase can be sheared crucially influence the mechanical properties of the alloy, and their understanding is of key importance. In this context, an established method to discriminate between intrinsic and extrinsic stacking faults (SFs) is their edge-on imaging in high-resolution scanning transmission electron microscopy (HRSTEM) in ⟨110⟩ projection. The superlattice ordering within the $L1_2$ phase gives rise to a larger variety of fault structures – namely, complex and superlattice variants of both intrinsic and extrinsic stacking faults. Notably, whether a given SF is complex or not may not be reliably revealed by studying one ⟨110⟩ projection alone [1, 2]. We present an experimentally feasible approach that enables this differentiation in a reliable and unambiguous way. This approach entails examining the fault structure not only in ⟨110⟩ projection, but also in a neighboring ⟨211⟩ projection, which is achieved by tilting the specimen by 30° in the TEM. Two applications of this analysis technique are discussed in this contribution: the first is the experimental validation of microscopic details of a well-known formation mechanism for superlattice extrinsic stacking faults, and the second concerns the shear-based γ'-to-χ phase transformation often observed in superalloys based on the Co-Al-W system, in which χ is an equilibrium phase [3].

Methods
Fault structures in the single crystalline Co-base superalloys ERBOCo-4 (composition in at.%: Co43.2-Ni32.0-Al8.0-Cr6.0-Ti2.8-Si0.4-Hf0.1-Ta1.8-W5.7) and ERBOCo-VF60 (composition in at.%: Co79.8-Al8.9-Ta2.3-W9.0) are analyzed. HRSTEM imaging was performed at a double Cs-corrected FEI Titan³ Themis at 300 kV as well as a probe-corrected Thermo Fisher Scientific Spectra 200 C-FEG at 200 kV. On the latter, spatially resolved energy-dispersive X-ray spectroscopy (EDXS) was conducted using the Super-X G2 detector.

Results
The first example concerns a high-temperature deformation mechanism of the γ' phase which involves the formation of SFs. Details of this study can be found in Ref. [2] and are briefly summarized in the following. Under [001] compression, a common deformation mode resulting in the formation of superlattice extrinsic SFs (SESFs) is the well-known Kolbe mechanism [4]. Here, two identical a/6⟨112⟩ Shockley partial dislocations shear into γ' on neighboring planes, leaving behind two neighboring complex intrinsic SFs (CISFs) which together constitute a complex extrinsic SF (CESF). Complex variants of SFs typically possess high SF energies due to nearest-neighbor violations in the superlattice ordering; therefore, the central fault plane of the CESF undergoes a diffusion-mediated reordering step which effectively translates that plane by a/2⟨110⟩ and transforms the fault into a

lower-energy SESF. While numerous observations of this mechanism have been made in Ni- and Co-base superalloys since its model description in 2001, two key aspects have previously eluded experimental verification: firstly, a direct observation of the complex nature of the intrinsic segment between the two leading partials, and secondly, the occurrence of reordering. By imaging the fault structure and leading partials in a compressively deformed sample of Co-base superalloy ERBOCo-4 not only in ⟨110⟩ projection (which may be ambiguous regarding the complex or superlattice character of a fault), but also in ⟨211⟩ projection, we were able to reveal the intrinsic and extrinsic segments as CISF and SESF, respectively, directly confirming both aforementioned aspects [2].

In the second example, microscopic details of the γ′($L1_2$)-to-χ($D0_{19}$) phase transformation were elucidated in the Co-base superalloy ERBOCo-VF60 (see figure). The accelerated formation of the χ phase during annealing (850 °C, 20 h) was prompted by the diffusion of Cr into the superalloy, destabilizing the γ/γ′ microstructure. Coherent, plate-shaped χ precipitates have formed on {111} planes. Based on the fcc-to-hcp transformation, the transformation of the $L1_2$ structure (ABC stacking) to the $D0_{19}$ structure (AB stacking) is shear-based and can be achieved by the introduction of an SISF after every other plane of the $L1_2$ structure. By studying the leading partials driving the transformation at the tip of a precipitate in HRSTEM, details of the transformation process were uncovered [5]. In [110] projection (bordered in red), the formation of SFs is evident, causing a change in stacking. Furthermore, a change in the alternating bright/dark contrast of atomic columns on the planes marked by dashed red circles implies the involvement of a diffusion-mediated reordering process. By additionally imaging the fault structure in [211] projection (bordered in black), the Burgers vectors of the leading partials were determined unambiguously (from superlattice shifts made visible by Fourier filtering in this projection) as noted in the schematic drawing. Notably, the transformation does not progress directly through shearing by a/3⟨112⟩ partials necessary to form SISFs, but rather by a/6⟨112⟩ partials which leave behind CISFs. The smaller Burgers vectors facilitate shearing and reduce elastic strains at the transformation front. At the same time, the high-energy CISFs are transformed into lower-energy SISFs by reordering processes. As illustrated in the schematic drawing, this fault configuration can serve to transform the ABC stacking of γ into the AB stacking of χ. The sum of all translation vectors in this configuration, and therefore the net strain introduced into the microstructure, is zero. Fault configurations following this pattern of three a/6⟨112⟩ partials creating CISFs followed by reordering to SISFs were observed repeatedly at the transformation fronts, indicating that this may be the preferred transformation mechanism. Besides the change in crystal structure, the formation of the χ phase also involves a significant enrichment of W and Ta supplied by diffusion from the surrounding microstructure. An in-depth characterization and discussion of elemental distributions associated with this phase transformation was conducted based on EDXS measurements down to the atomic scale.

Conclusion

We have presented two experimental applications of a novel HRSTEM-based method to reliably and unambiguously identify the complex or superlattice nature of both intrinsic and extrinsic SFs in the $L1_2$ structure. In both cases, microscopic details of shearing mechanisms in the γ′ phase of high-temperature superalloys were elucidated. In the future, this method may help uncover the details behind other $L1_2$ shearing processes.

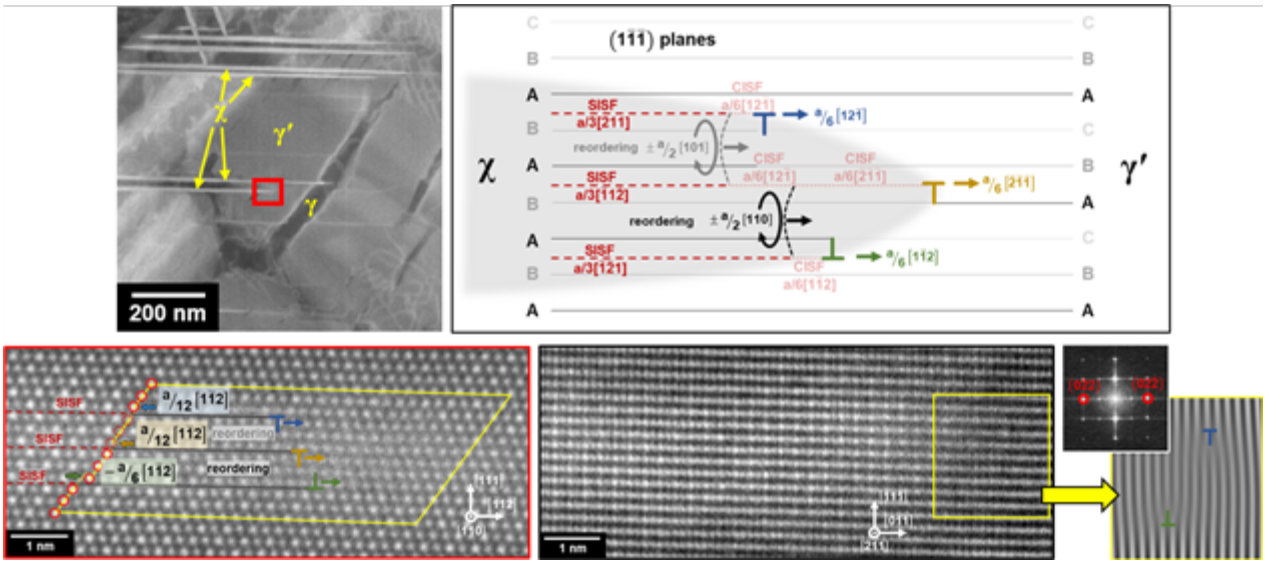

Keywords:

Scanning-transmission-electron-microscopy, superalloys, stacking-faults, deformation-mechanisms, phase-transformations

Reference:

[1] P.M. Sarosi, G.B. Viswanathan, M.J. Mills, Scripta Mater 55(8) (2006) 727-730.
[2] N. Karpstein, M. Lenz, A. Bezold, M. Wu, S. Neumeier, E. Spiecker, Acta Mater 260 (2023) 119284.
[3] Y.Z. Li, F. Pyczak, M. Oehring, L. Wang, J. Paul, U. Lorenz, Z. Yao, J Alloy Compd 729 (2017) 266-276.
[4] M. Kolbe, Mat Sci Eng a-Struct 319 (2001) 383-387.
[5] N. Karpstein, A. Saksena, R. Zehl, A. Bezold, O.M. Horst, D. Bürger, A. Kostka, C. Zenk, S. Neumeier, B. Gault, A. Ludwig, S.G. Fries, G. Laplanche, E. Spiecker, Manuscript in preparation.

618

ACOM-TEM Investigation of the white etching layer formation in rail track

Pr Muriel Véron[1], Matteo Russo[2]
[1]Université Grenoble Alpes, CNRS, Grenoble INP, SIMaP, F-38000 Grenoble, France, [2]Univ. de Lyon, INSA Lyon, CNRS UMR 5510, MATEIS, F-69621 Villeurbanne, France, [3]Univ. de Lyon, INSA Lyon, CNRS UMR 5259 LaMCoS, F-69621 Villeurbanne, France

PS-02 (3), Lecture Theater 4, august 30, 2024, 14:00 - 16:00

The growing concern to reduce the environmental impact of freight and passenger transport has increased the importance of rail as an energy-efficient mode of transport. Rail track maintenance has often been carried out on a preventive basis. In order to control costs and primary-source and primary consumption, while taking into account the increase in traffic, a more optimized approach to maintenance is necessary. This involves better anticipating the appearance of rail defects and modeling their evolution. The aim of the OPTIMRAIL(*) Project is to make maintenance predictive, by determining behavioral laws for the evolution of rail microstructure leading to the formation of defects, such as "squat", which accounts for 70% of rail defects following the survey conducted by SNCF in 2021 [1]. The squat defect is characterized by a collapse of the rail tread and a more or less pronounced network of cracks. [Figure 1 (a)]. It is linked to a surface tribological transformation (STT) leading to crack initiation. The latter is called the white etching layer (WEL) because of its appearance under the optical microscope after chemical etching [Figure 1 (b)]. The mechanisms by which the initial perlitic microstructure of railway steels evolves into the white phase are still debated in the literature. Two mechanisms are generally proposed. The first involves a thermally activated mechanism leading to martensite formation following austenitization followed by rapid quenching. The second mechanism is driven by an accumulation of plastic deformation that ultimately leads to nanograins of ferritic structure supersaturated with carbon atoms.

In the aim to clarify the mechanisms, samples of rails that had been in service under real traffic conditions were collected, and metallurgical analysis of the rolling band and the near surface layer was performed [2]. In particular, thin foils have been prepared by FIB at the near surface, allowing to study detailed microstructures from the surface up to 30 microns bellow. Automated crystal orientation and phase maps were produced using ASTAR technique [3] to investigate microstructure evolution (phases, orientation and disorientation). Perlitic structure remains fine and well organized 30 micron below the surface [Figure 1 (c)]. 20 microns below the surface, optical microscopy revealed a transformation in white phase, and ACOM-TEM maps start to show disorganization of perlitic structure, and only Fe3C and ferrite phases. At the surface, the organized perlitic structure is totally lost [Figure 1 (d)]. In some area, richer in carbides, ferrite quality of indexation is poor. Austenite phase seems to have a better reliability in this area, still with some discrepancy between modeled and real diffraction pattern, probably due to strain field induced by the many carbides. To verify the presence of austenite, orientation and phases maps were conducted at two different tilt (0° and 15°) along X axis. Austenite was still better recognize in similar region for the two maps, and coherency of orientation between the two maps was verified. We can then conclude that retained austenite was formed during rail track service, meaning that the mechanism at the origin of the WEL involves austenitization followed by rapid quenching. This information also provide clues of the temperature reached during friction. Martensite and carbide formations are currently under investigation.
(*)The work carried out as part of the OPTIMRAIL project is supported by the Carnot Institute Ingénierie@Lyon.

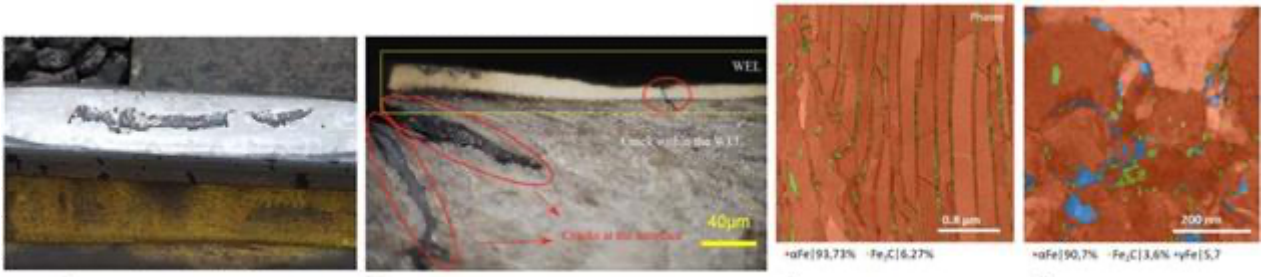

a) b) c) d)

Keywords:

Steel; ACOM, Phase transformation

Reference:

[1] SNCF Réseau, « Rapport Annuel Sécurité », 2021.
[2] S. Simon et al. (2012) International Conference on Contact Mechanics and Wear of Rail/Wheel Systems (CM2012), Chengdu, China, August 27-30.
[3] EF. Rauch, M. Veron (2014) Materials Characterization, v9, 98.

632

Elemental segregation at substrate/metal interface to manipulate heterogeneous nucleation

Dr Shihao Wang[1,2,3], Dr Yun Wang[3], Dr Zhongyun Fan[3], Dr Quentin Ramasse[1,2]
[1]SuperSTEM Laboratory, STFC Daresbury Campus, Daresbury WA4 4AD, United Kingdom, [2]School of Chemical and Process Engineering, University of Leeds, Leeds LS2 9J, United Kingdom, [3]BCAST, Brunel University London, Uxbridge, Middlesex UB8 3PH, United Kingdom

PS-02 (3), Lecture Theater 4, august 30, 2024, 14:00 - 16:00

Background incl. aims
Heterogeneous nucleation on a substrate in a metallic melt is a fundamental step in tailoring the microstructure of engineering materials with desired properties, and therefore it is a research topic of critical scientific and technological importance to meet the goals of the 'circular economy' [1]. The structural and chemical compatibility at a substrate/metal-liquid interface dictates the heterogeneous nucleation process. This can be altered by elemental interfacial segregation, affecting the nucleation behaviour accordingly [2]. Atomic-scale interfacial segregation has been linked to the successful application of TiB2-based grain refiners for aluminium casting, also explaining some of their limitations depending on the nature of segregation structure [2,3]. Interfacial segregation has also been applied as a strategy to modify native oxides in aluminium and magnesium alloys, whereby naturally occurring oxides can then be harnessed for grain refinement [2,4]. Studies of the microstructure and composition across the substrate/metal interface, down to the atomic scale, are thus essential in determining nucleation potency.
Advances in aberration-corrected scanning transmission electron microscopy (STEM) and electron energy-loss spectroscopy (EELS) now routinely allow for both atomic-resolution imaging and compositional analysis of materials. In this work, we use advanced STEM-EELS to investigate different substrate/metal interfaces including TiB2/Al, MgO/Mg, and γ-Al2O3/Al in the corresponding casting alloy ingots of different grain refinement performances, aiming to provide an overview of our atomic-level understanding of the behaviour of interfacial segregation and its resultant effect on heterogeneous nucleation and grain refinement.
Methods
Casting experiments were used to evaluate the grain refinement. Pressurized melt filtration was applied to different alloy melts to collect the inoculant particles, by which the possibility of substrate/metal interface appearing in a TEM foil specimen is greatly increased for characterization. STEM imaging and EELS acquisition were performed on a Nion UltraSTEM100 scanning transmission electron microscope, equipped with a Gatan Enfina EELS spectrometer retrofitted with a MerlinEELS direct electron detector. The microscope was operated at an accelerating voltage of either 100 or 60kV, depending on the beam sensitivity of the observed structures, with the probe-forming optics configured for a 31mrad convergence semi-angle and a probe size of 1Å or smaller.
Results
High-precision high-angle annular dark field (HAADF) STEM imaging and EELS mapping offer an atomic-level view of how interfacial segregation affects the grain refining performance in model alloy systems, with an example of the TiB2/Al system shown in Figure 1. Rigid- or non-rigid registration were applied to series of (spectrum) images, taken with short dwell times and along different zone axes, to reveal the precise structure and chemistry of an atomically thin, so-called Al3Ti 2-dimensional compound (2DC) segregation layer at the interface between inoculant TiB2 particles and Al matrix: figure 1d. This structure was shown to account for the grain refinement achieved in an Al-0.2Al5Ti1B alloy. Similarly, a Zr-segregation-induced Ti2Zr 2DC (figure 1e) is atomically resolved at the interface, which poisons the grain-refining effect of TiB2: a coarse and columnar grain structure forms in Al-0.1Zr-0.2Al5Ti1B. Interestingly, the grain refinement behaviour is rejuvenated after the

addition of Mg (Al-0.1Zr-0.2Al5Ti1B-1Mg), which results in the dissolution of the poisoning Ti2Zr 2DC and the formation of hitherto never-observed Mg-rich layers adopting a local structure similar to bulk Al, and thus termed Al-like layers (figure 1f-h). Analysis of the electron energy loss near-edge fine structure (ELNES) provides additional information regarding the valence state and/or electronic structure of these interfacial structures, for instance confirming the nature of the 'Y-O' bonding within a Y-rich segregation layer at the MgO/Mg interface [4].

Conclusion

Atomic-resolution STEM-EELS has provided conclusive evidence to clarify the role of interfacial 2DCs in determining the nucleation potency of TiB2 and thus the grain refining performance. With the high spatial resolution and single-electron-sensitive EELS detector, advanced STEM-EELS is expected to be a powerful tool in understanding heterogeneous nucleation, designing grain refiners, and controlling solidification structures and mechanical properties across a wide range of metallic materials.

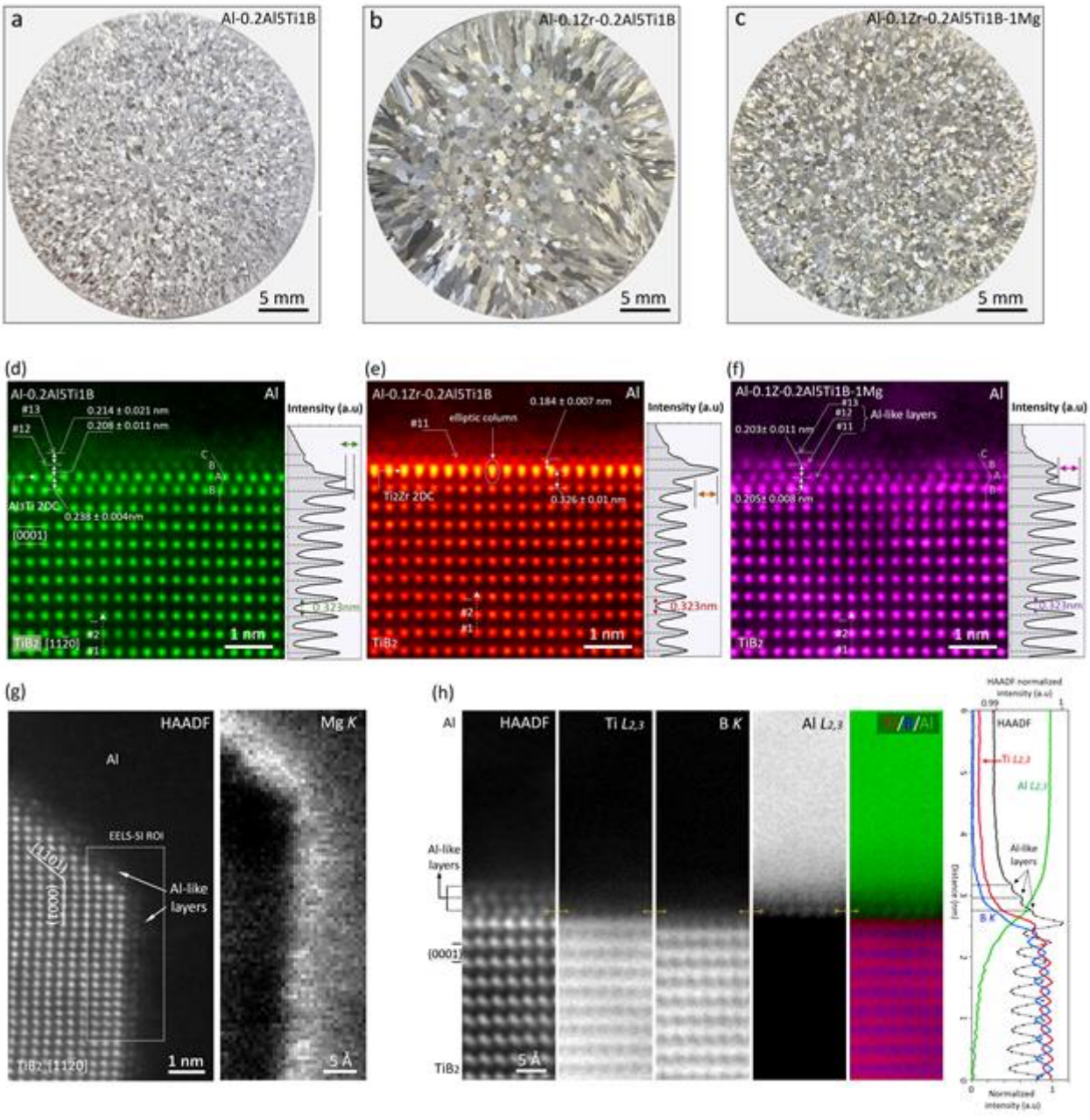

Keywords:

Interfacial segregation, STEM/EELS, Solidification

Reference:

[1] J.A. Dantzig, M. Rappaz, Solidification, EPFL Press, Lausanne, Switzerland, 2009.
[2] Y. Wang, S. Wang, Z. Que, C. Fang, T. Hashimoto, X. Zhou, Q.M. Ramasse, Z. Fan, Manipulating Nucleation Potency of Substrates by Interfacial Segregation: An Overview, Metals. 12 (2022) 1636.
[3] K.F. Kelton, A.L. Greer, Nucleation in Condensed Matter Applications in condensed matter: applications in materials and biology, Elsevier, 2010.
[4] S. Wang, Y. Wang, Q.M. Ramasse, R. Schmid-Fetzer, Z. Fan, Segregation of Yttrium at the Mg/MgO interface in an Mg-0.5Y Alloy, Acta Mater. 257 (2023) 119147.

636

Enhanced nanoscale phase characterisation in modern steels using precession electron diffraction and energy filtering

Aleksander Brozyniak[1], Matthias Wallner[2], Philipp Kürnsteiner[1], Peter Oberhumer[1], Katharina Steineder[2], Heiko Groiss[1]
[1]Christian Doppler Laboratory for Nanoscale Phase Transformations, Center for Surface and Nanoanalytics, Johannes Kepler University Linz, Altenberger Str. 69, 4040 Linz, Austria, [2]voestalpine Stahl GmbH, voestalpine-Straße 3, 4020 Linz, Austria

PS-02 (3), Lecture Theater 4, august 30, 2024, 14:00 - 16:00

Background incl. aims
The development of lightweight and ductile Advanced High-Strength Steel hinges upon a comprehensive understanding of phase change kinetics during production. In addition to various techniques for chemical characterisation, transmission electron microscopy (TEM) is an essential tool for the structural analysis of examined phases. In this work, we showcase a significant enhancement in the acquisition of diffraction patterns (DPs) for nanostructured phases in modern steel systems, such as quenched and partitioned (Q&P) steels. We combined zero-loss energy filtering (EF) with precession electron diffraction (PED) to access crystallographic information of nano-inclusions inaccessible by standard diffraction techniques.

Methods
Selected area electron diffraction (SAED) is usually not suitable for the challenging task of nano-inclusions crystallography, which requires information about different zone axes for unambiguous phase identification. Due to the large aperture size, dynamic diffraction effects and, in particular, the intricate steel matrix containing arbitrarily oriented, strained and ferromagnetic grains, an in-depth analysis of SAED patterns is limited. To address these limitations and achieve a high lateral resolution, we employed site-specific nanobeam diffraction in PED mode with a beam diameter of approximately 1 nm and a precession angle of 1 - 3° around the central axis. Unlike standard DPs, where dynamical effects are unavoidable, PED provides quasi-kinematical results and a larger number of reflections through pattern integration, thus compensating for small variations in sample thickness or misorientation. The influence of inelastic and multiple scattering was mitigated through additional zero-loss filtering, noticeably enhancing the signal-to-noise ratio of our PED patterns. The experiments were performed with a JEOL JEM-2200FS equipped with an in-column Ω-filter and a TVIPS universal scan generator using a TemCam-XF416 CMOS camera.

Results
One application example is the investigation of iron carbides embedded in Q&P steels with varying Si or Al content, annealed at 320°C and 420°C. Our site-specific PED patterns provided enhanced clarity, revealing a multitude of carbide diffraction spots and enabling a more reliable analysis compared to results obtained via SAED. By conducting sample tilt series towards different crystallographic zone axes (Fig. 1), we achieved unambiguous identification of the carbide phase, its orientation relationship to the martensitic matrix, and the lattice parameters. The presence of orthorhombic θ-Fe_3C [2] was confirmed, in line with prior X-ray diffraction (XRD) measurements in the steel alloys annealed at 420°C. In alloys annealed at 320°C, where XRD results were inconclusive, the tilt series approach revealed the presence of transition carbides ε-Fe_3C (hexagonal) and η-Fe_2C (orthorhombic/quasi-hexagonal) [3][4]. Utilising the tilt series approach alongside the improved accuracy of the PED patterns allowed for a definitive distinction between ε- and η-transition carbides, overcoming previous challenges [1]. Further examples of PED applications are shown.

Conclusions

Our findings underscore the benefits of employing PED together with EF for characterising the crystallography of nanostructured phases in modern steel systems. Through comparison of DP quality, we demonstrate the insights attainable for complex samples by PED. The rising availability of commercial PED solutions and the convenient applicability of the PED method enhanced through EF, demonstrated on our examples, may incentivize the broader scientific community to embrace this method for investigating metals and alloys.

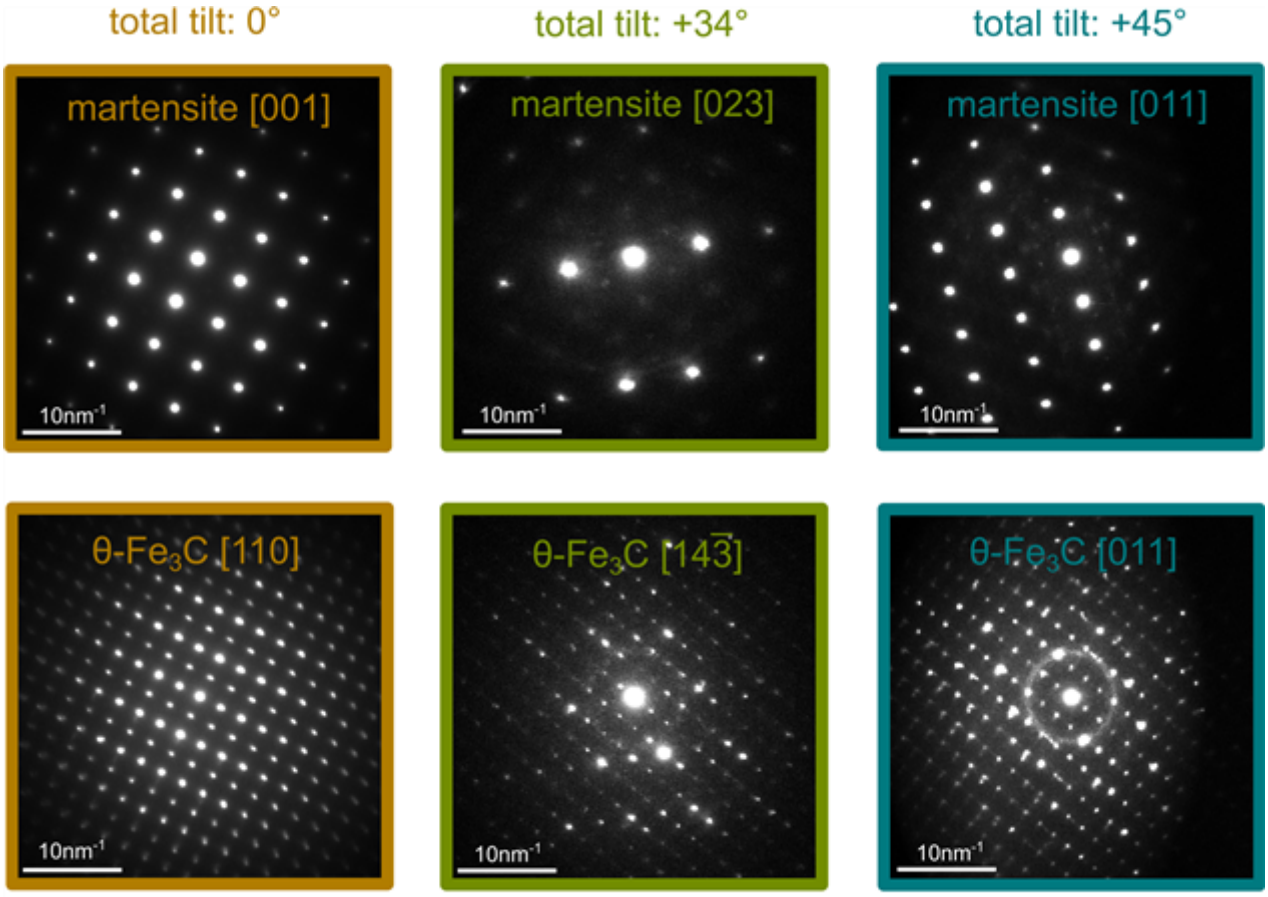

Fig. 1: Tilt series yielding DPs at three corresponding crystallographic zone axes of martensite and a θ-Fe_3C nano-inclusion.

Keywords:

PED, steel, nano-inclusions, phase characterisation

Reference:

[1] Allain, S.Y.P. et al., Materials 11, 1087 (2018).
[2] Fang, C.M.; Van Huis, M.A.; Sluiter, M.H.F.; Zandbergen, H.W., Acta Mater. 58, 2968-2977 (2010).
[3] Nagakura, S., J. Phys. Soc. Jpn. 14, 186-195 (1959).
[4] Lv, Z.Q.; Sun, S.H., Jiang, P.; Wang, B.Z.; Fu, W.T., Comput. Mater. Sci. 42, 692-697 (2008).

657

Elucidating the effect of silicon on Fe-Zn phase formation in galvanized steel via advanced TEM

Dr. Alexey Minenkov[1], Johannes Knapp[2], Thomas Mörtlbauer[2], Heiko Groiss[1]
[1]Christian Doppler Laboratory for Nanoscale Phase Transformations, Center for Surface and Nanoanalytics, Johannes Kepler University Linz, Linz, Austria, [2]voestalpine Stahl GmbH, Linz, Austria
PS-02 (3), Lecture Theater 4, august 30, 2024, 14:00 - 16:00

Introduction

Raising the bar for weight reduction, safety, and environmental protection in modern automotive and construction materials can be barely achieved without new types of Advanced High-Strength Steel (AHSS) [1] and must be guided by in-detail structural and chemical characterization. To meet safety and durability requirements, modern AHSS products additionally need effective corrosion protection, and the galvannealing process, which involves hot-dip galvanizing in a Zn bath followed by annealing, is considered to be one of the most efficient methods for achieving this goal. Such a well-balanced but complex process of interfacial interactions can be significantly affected by alloying elements, which are added in AHSS to augment its mechanical properties and achieve a superior combination of high tensile strength and good formability [1,2]. For instance, silicon affects the steel bulk properties enhancing the Fe-liquid-Zn interfacial reaction by solute Si in the α-Fe phase. An additional effect is attributed to the formation of surface oxides on the steel sheet during annealing before immersion in the Zn bath [3,4]. One can conclude that the structural and chemical peculiarities of the steel/coating interface region including the so-called inhibition layer, e.g. [3], must be considered as a key factor governing the phase formation kinetics. Advanced transmission electron microscopy (TEM) can help us collect morphological, structural, and elemental information at the nanoscale. For a deeper understanding of phase evolution, it is necessary to study not only fully galvanized samples processed at different annealing times but also steel sheets at the outlet of the bath, coated with almost pure Zn.

Methods

We optimized various TEM sample preparation techniques and showed that low-temperature FIB is a method of choice for dependable Zn-coated steel preparation [3], which can be further enhanced utilizing a plasma P-FIB operated with, for instance, Xe ions. Cross-sectional TEM lamellae were prepared using a CrossBeam 1540 XB SEM (Zeiss, Germany) Ga-FIB using W to form a protection capping layer. The final thinning was performed at -60°C applying a Micro Heating Cooling Stage (MHCS) (Kleindiek Nanotechnik GmbH, Germany) based on the thermoelectric effect and 5 kV acceleration voltage to minimize the invasive influence of the Zn-Ga eutectic formation. The investigation was carried out in a JEOL JEM-2200FS (JEOL, Japan) operated at an acceleration voltage of 200 kV. The TEM is equipped with an in-column Ω-filter and a TemCam-XF416 (TVIPS, Germany) CMOS-based camera. HRTEM data processing was done with Gatan Microscopy Suite. Crystal structure simulations were performed via JEMS software. STEM EDX analysis was fulfilled in a scanning (S)TEM mode for qualitative elemental characterization of the specimens with an X-MaxN 80 T detector from Oxford Instruments (United Kingdom).

Results

Employing complementary TEM techniques (HRTEM, SAED, STEM EDX), we traced the formation of Zn-Fe phases in AHSS with high Si content at different stages of galvannealling process along with as-galvanized reference specimen [4]. In particular, it has been disclosed that the Si-based surface oxide layer, formed on steel during the recrystallization annealing step before dipping into the Zn bath (460°C) remains stable, separating the coating from the reaction zone (Figure I). This efficiently

hinders the desired reaction of Fe with Al in a Zn bath at the early stage of hot-dip galvanizing and complicates the formation of the Fe2Al5-xZnx inhibition layer. One can reveal that liquid Zn can penetrate local disruptions in this film forming a δ phase layer below, while Fe diffusion into the coating is suppressed. The δ layer supersaturates with Fe and Si from the steel during long-term annealing at 480°C and decomposes forming a δ phase [5] matrix with Fe-Si-Al-based nanoprecipitates with a cubic structure (Figure II). The phases were identified via HRTEM and STEM EDX. Based on experimental STEM EDX data, the achieved phase configuration was refined via Thermo-Calc Fe–Zn–Si–Al system simulation. It must be emphasized again that the observed Si-based oxide layer remains stable even after long-term annealing, thus Si, which constitutes this membrane, was not actively involved in the Fe-Zn reaction.

Conclusion

Our results indicate the following evolution of phases at the steel/coating interface of AHSS subjected to an industrial continuous hot-dip galvannealing process. During dipping in a liquid Zn bath, Zn penetrates the gaps in an existing oxide film and forms a layer below directly reacting with the Fe. This layer was identified as the δ phase. Thus, the desired Fe2A5-based inhibition layer cannot be formed as intended. Mentioned δ phase layer can grow during subsequent annealing being, however, efficiently constrained by the mixed oxide membrane. While long-term annealing, Si dissolved in the steel destabilizes the δ phase supersaturated with Fe and Al, triggering its decomposition into the δ phase and Fe-Si-Al-based nanoprecipitates. The challenges and solutions on the way toward a fruitful and dependable TEM analysis of galvanized industrial steels will be also discussed in detail.

Acknowledgments: We would like to gratefully acknowledge the financial support by the Austrian Federal Ministry of Labour and Economy, the National Foundation for Research, Technology and Development and the Christian Doppler Research Association.

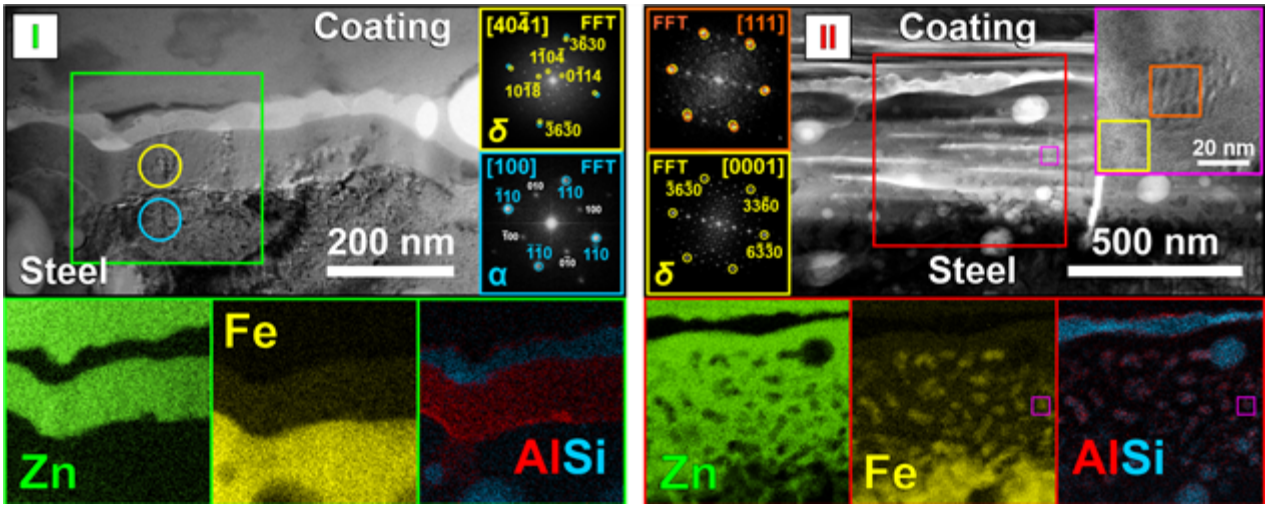

Keywords:

Fe-Zn, phase formation, galvanized steel

Reference:

[1] O. Bouaziz, et al., Driving Force and Logic of Development of Advanced High Strength Steels for Automotive Applications, Steel Res. Int., 84(10), 2013, 937–947, https://doi.org/10.1002/srin.201200288.

[2] Advanced High Strength Steel: Processing and Applications, edited by Tapas Kumar Roy, Basudev Bhattacharya, Chiradeep Ghosh, S. K. Ajmani. Springer Singapore (2018), 216p, https://doi.org/10.1007/978-981-10-7892-7.

[3] Alexey Minenkov, et al., Towards a dependable TEM characterization of hot-dip galvanized steels with low and high Si content, Materials & Design, 227, 2023, 111684, https://doi.org/10.1016/j.matdes.2023.111684.
[4] Alexey Minenkov, et al., Interaction and evolution of phases at the coating/substrate interface in galvannealed 3rd Gen AHSS with high Si content, Materials & Design, 237, 2024, 112597, https://doi.org/10.1016/j.matdes.2023.112597.
[5] Norihiko L. Okamoto, et al., Structure refinement of the δ1p phase in the Fe–Zn system by single-crystal X-ray diffraction combined with scanning transmission electron microscopy, Acta Cryst., B70 (2014), 275-282, https://doi.org/10.1107/S2052520613034410.

689

In situ insights into the thermal stability of high-entropy nanoalloys

Syrine Krouna[1], Anissa Acheche[2], Jaysen Nelayah[1], Christian Ricolleau[1], Guillaume Wang[1], Hakim Amara[2], Damien Alloyeau[1]
[1]Université Paris Cité, Paris, France, [2]ONERA, Châtillon , France

PS-02 (3), Lecture Theater 4, august 30, 2024, 14:00 - 16:00

The structural stability of high entropy nanoalloys (HENA) brings hope to developing more stable nanomaterials for high-temperature applications in different fields such as catalysis or mechanics. Nevertheless, the enhanced thermal stability of nearly equiatomic nanoalloys containing at least 5 metals is nothing more than a theoretical speculation about the impact of thermodynamic contributions and sluggish diffusion kinetics on their structural properties and remains to be proven. In this context, studying the thermal behavior of HENA is a necessary first step to understand their stuctural properties and evalutate their structural stability with the view to better target their potential high-temperature applications.

In the present work, FCC AuCoCuNiPt NPs were directly synthesized on the silicon nitride (SiN) membrane of a MEMS-based heating chip, using pulsed laser deposition, allowing control of both particle composition and size [1]. Then, we used in situ scanning transmission electron microscopy (STEM), corroborated with atomistic simulations, to study in real time and at the atomic scale the structural and compositional evolution of from 298 K to 973 K. We combined atomic-scale STEM imaging with chemical analysis performed by STEM-EDS in an aberration-corrected JEOL ARM 200F TEM, using a Protochips heating holder. Molecular Dynamic (MD) simulations are performed using the open source Large-scale Atomic/Molecular Massively Parallel Simulators (LAMMPS) package. In order to investigate Cu-Au-Co-Ni-Pt NPs, the Embedded Atom Method (EAM) potential derived by Zhou et al. is used to describe the interaction between different atomic pairs [2].

The growth of FCC AuCoCuNiPt NPs is mainly driven by coalescence observable from 623 K (Fig. 1a). Furthermore, both in situ STEM and MD simulations reveal strong structural and chemical evolutions in the NPs with the formation and melting of an AuCu layer at the surface of NPs at high temperature (figure 1b and 1c). This phase separation that appears progressively with temperature is driven by surface effects and pronounced atomic diffusion that is surprisingly more active in these quinary nanoalloys than in monometallic and bimetallic subsystems. Besides ruling out the existence of sluggish diffusion in AuCoCuNiPt nanoalloys, our study allows distinguishing kinetic and thermodynamic effects on their structural properties, which is an essential prerequisite to better control the synthesis of complex nanomaterials. From a practical point of view, this study calls into question the use of AuCoCuNiPt HENA for high-temperature applications and more generally reveals the necessity to investigate the thermal behavior of HENA to determine if and how surface effects govern their structural properties, to evaluate their stability and adapt their potential applications.

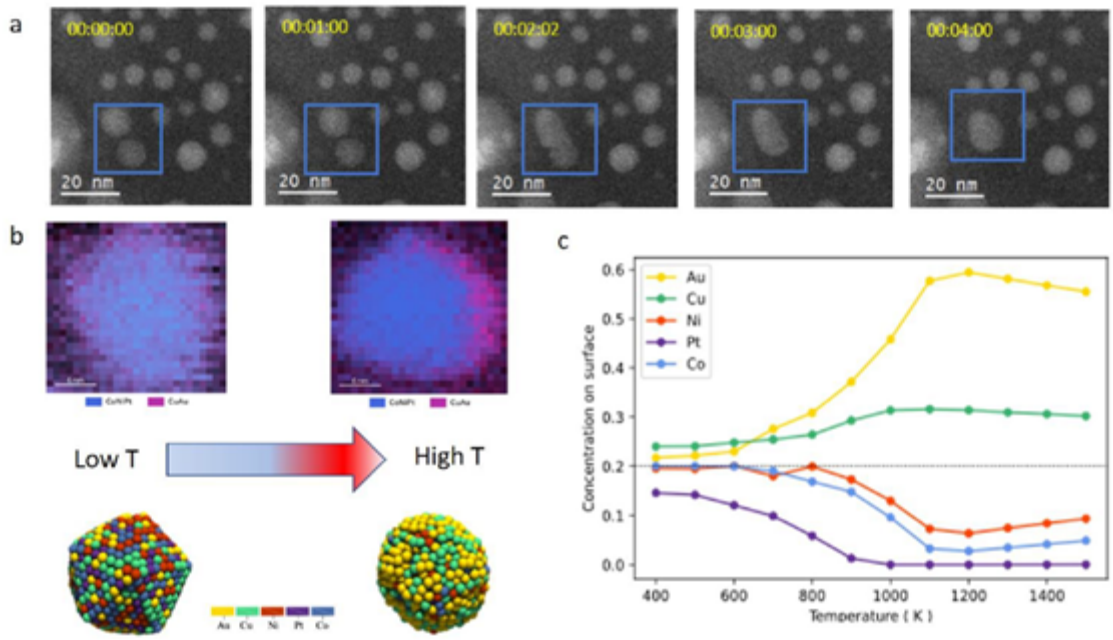

Figure 1: (a) Growth of CoNiCuPtAu HENA driven by coalescence recorded in real time by STEM HAADF at 973 K. The acquisition time is indicated in the top left corner of each image. (b) EDS mappings (top) and MD simulations (bottom) showing the formation of CuAu layer at the surface of CoNiCuPtAu NP at high temperature. (c) Quantitative analysis of MD simulations showing the evolution of the surface concentration as a function of the temperature. The dotted line represents the equiatomic concentration.

Keywords:

In-situ microscopy, atomistic simulations, thermodynamics

Reference:

1. A. Barbero, C. Moreira Da Silva, N. O. Peña, N. Kefane, A. Jaffar, M. Thorey, H. Bouaia, J. Nelayah, G. Wang, H. Amara, C. Ricolleau, V. Huc and D. Alloyeau, Faraday Discuss. 242, 129–143 (2023)
2. Zhou, X. W., Johnson, R. A. & Wadley, H. N. G. Phys. Rev. B 69, 144113 (2004)

710

Direct imaging of deformation in metallic glasses using precession nanodiffraction mapping

Dipl.-Ing. Simon Fellner[1], Dipl. Ing. Lukas Schretter[1], Univ. Prof. Dr.-Ing. Habil. Dr. h.c. Jürgen Eckert[1,2], Dr. Christoph Gammer[1]
[1]Erich Schmid Institute of Materials Science, Austrian Academy of Sciences, Leoben, Austria,
[2]Department of Materials Science, Montanuniversität Leoben, Leoben, Austria

PS-02 (3), Lecture Theater 4, august 30, 2024, 14:00 - 16:00

Background:
Despite having unique attractive properties, non-crystalline/amorphous materials suffer from catastrophic failure after reaching their yield strength. The ability to improve the mechanical and functional properties of metallic glasses depends on understanding their inherent strain state. Recently, nanoscale strain mapping was used to unravel shear band formation in a monolithic metallic glass [1]. The effect of structural changes induced by the introduction of secondary crystalline phases, highly rejuvenated regions or other defects renders transformation mechanisms in metallic glasses even more complex. Due to the emergence of novel dedicated specimen holders, in-situ transmission electron microscopic measurements are a powerful tool allowing to directly measure the deformation behavior of these tailored nanocomposites [2].

Aim:
In this work, we want to directly image the local elastic strain fields at heterogeneities in metallic glasses using precession nanodiffraction mapping.

Methods:
The study was carried out on a CuZr-based metal alloy, which is a well-known glass former. The introduction of heterogeneities included thermal processing techniques and solid state amorphization. Nanosized specimens with an electron transparent window were fabricated through focused ion beam milling. A unique push-to-pull device, which is a micro-electromechanical systems-fabricated flexure device from Bruker was used for in-situ tensile testing in the transmission electron microscope. Precession nanodiffraction mapping was integrated with an in-column energy filter and a direct electron detector from QuantumDetectors. This combinatorial approach enabled rapid acquisition of high quality diffraction patterns. It also allowed us to follow the structural response during in-situ deformation on the nanoscale.

Results:
The results of precession nanodiffraction mapping were able to describe local events of cooperative shear in metallic glasses. From acquired in-plane atomic level strain maps the interaction between heterogeneities could be described quantitatively. Different enthalpy states of the metallic glass showed different shear band mechanisms, which contradicts the model of a uniform disordered material after processing. It was shown, that high interfacial stresses between heterogeneities cause complex strain concentrations preventing strain localization in a single shear band. We were also able to show that crystalline phases strongly influence the stress field in the amorphous phase. Recorded strain maps from elastostatic loaded samples and during in-situ tensile deformation revealed early stages of shear nucleation and propagation on the nanoscale. As a result, a direct link could be established between the structure and properties of these tailored metallic glass composites.

Conclusions:
We demonstrated the experimental measurement of local quantitative strains on the nanoscale. For this purpose, structurally altered metallic glasses were investigated. It could be shown how heterogeneities influence the deformation behavior and mechanical properties. These new findings will improve the understanding of the interplay between structural heterogeneities and carriers of plastic deformation. With these conclusions, our work contributes significantly to the development of new high-performance materials.
Acknowledgments:
The authors gratefully acknowledge the financial support from the Austrian Science Fund (FWF): Y1236-N37.

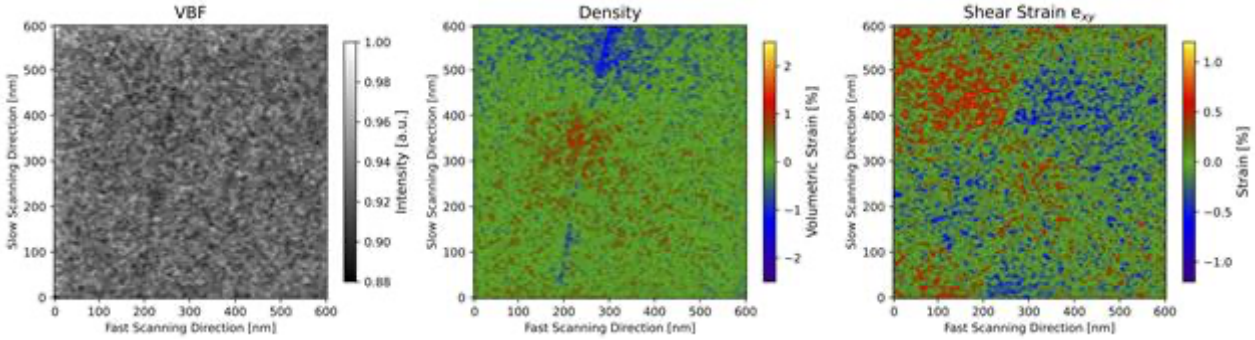

Keywords:

nanodiffraction mapping, metallic glass, deformation

Reference:

[1] H. Sheng, D. Şopu, S. Fellner, J. Eckert, C. Gammer PHYSICAL REVIEW LETTERS 128 (2022) 245501;
[2] H. Sheng, et al. Materials Research Letters, 9 (2021) 190-195.

747

Supersilent AlCoFeNiCux (x = 0.6 – 3.0) high-entropy alloys

Dr. Andreja Jelen[1]
[1]J. Stefan Institute, Ljubljana, Slovenia

PS-02 (3), Lecture Theater 4, august 30, 2024, 14:00 - 16:00

BACKGROUND INCL. AIMS
In the search for the materials that possess a combination of excellent magnetic softness and vanishing magnetostriction, the ferromagnetic high-entropy alloy (HEA) system AlCoFeNiCux (x = 0.6–3.0) was investigated.

HEAs are expected to find applications as supersilent (inaudible to a human ear) materials for transformers, magnetocaloric coolers, and other “humming” electromagnetic machinery.

METHODS
The AlCoFeNiCux HEAs with the Cu content x = 0.6–3.0 were prepared from high purity elements (>99.99 wt.%) by arc melting under an argon atmosphere. Altogether, there were seven samples fabricated.

An evolution of the crystal structure and chemical composition was observed with increasing Cu content by XRD and SEM EDS characterization. The phases constitutions and their domain sizes were characterized by correlative SEM and TEM techniques, as HEAs usually have highly complex structures on different spatial scales that contribute to specific physical properties such as magnetic softness and magnetostriction.

The magnetic properties were investigated by a Quantum Design Magnetic Property Measurement System MPMS3 magnetometer. The magnetometer uses a superconducting magnet with variable magnetic field of ± 7 tesla and the temperature range of the measurements is from 1.8 K to 400 K.

Electrical resistivity was measured by a Quantum Design Physical Property Measurement System PPMS 9T by. The apparatus uses a superconducting magnet with a variable magnetic field of ±9 tesla and the temperature range of the measurements is between 1.9 K and 400 K.

RESULTS
XRD revealed the evolution of the samples’ crystal structure. At low Cu contents, x = 0.6 and 0.8, the predominant phase is bcc (≈85 wt.%) with the unit cell parameter a = 2.869 Å, and the second phase is fcc (≈15 wt.%) with a = 3.612 Å. On increasing the Cu content, the fraction of the fcc phase increases, while the bcc phase fraction decreases. Detailed observation of the fcc-phase diffraction peaks reveals that there are actually two fcc-phases with slightly different unit cell sizes, denoted as fcc(L)-large and fcc(S)-small.
For the two highest Cu contents (x = 2.5 and 3.0), the bcc phase is no longer visible in the XRD patterns and the structure is two-phase, composed of the fcc(L) and fcc(S) phases.

The development of the microstructure of all alloys was made visual by SEM BSE imaging. All alloys show inhomogeneous microstructure, where the brighter parts are enriched in the heaviest element Cu.

The TEM analysis of the AlCoFeNiCu2.5 alloy reveals that the three constituent phases are nanostructured on the 10 nm scale due to fine dispersion of the Guinier-Preston (GP) zones that are

enriched in Cu. The GP zones were observed in all three phases except at the locations of the highest Cu enrichment. The concentrations of the chemical elements also show nanometer-scale variations. It is straightforward to anticipate this result to the entire series of the investigated AlCoFeNiCux (x = 0.6–3.0) HEAs, so that the alloys can be considered as nanostructured composite materials with a multiphase (up to three phases) microstructure.

Magnetic softness characterization was performed by determining the magnetization versus the magnetic field, M(H), hysteresis loops in the magnetic field sweep $\mu_0 H = \pm 7$ T. Rapid change of the M(H) curves in the close vicinity of $H = 0$ and small coercive fields Hc are evident for all samples, revealing magnetic softness.

Magnetostriction experiments were performed at RT in a static magnetic field range $-0.2\ \text{T} < \mu_0 H < 0.2\ \text{T}$ by measuring the samples' elongation (or contraction) with a strain gage. The magnetostriction curves λ(H) at RT show the largest (positive) value $\lambda_s = 21\ \mu\text{m m}^{-1}$ for the lowest Cu content x = 0.6. The positive saturation magnetostriction decreases with increasing x and vanishes ($\lambda_s = 0$) at x = 2.0. For the two alloys with the highest Cu contents, x = 2.5 and 3.0, λs remains very close to zero. In practical terms, all AlCoFeNiCux alloys in the Cu content range $2.0 \le x \le 3.0$ can be considered as vanishing-magnetostriction HEAs, so that the precise Cu concentration within this range is unimportant.

Superior parameters were obtained for the composition AlCoFeNiCu2.0, which shows precisely zero magnetostriction, $\lambda_s = 0$, reasonably low coercivity $H_c \approx 650\ \text{A m}^{-1}$ and substantial saturation magnetic polarization of $J_s \approx 0.55$ T, which is about the same as that of the mumetal, a widely used commercial soft magnet.

CONCLUSIONS

Magnetic softness and vanishing magnetostriction originate from the choice of constituent elements (magnetic Co, Fe, and Ni and nonmagnetic Al and Cu) and the multiphase composite microstructure is nanostructured on the 10 nm scale.

Magnetic softness originates from the nanostructured character of the alloys that are random mixtures of the ferromagnetic Al–Co–Fe–Ni domains and nonmagnetic or weakly magnetic Cu-rich domains on the 10 nm scale, which makes the mechanism of exchange-averaging of magnetic anisotropy efficient.

Since vanishing magnetostriction is a prerequisite for the supersilence of the material in audio-frequency AC applications, such HEAs are expected to find application as supersilent magnetically soft materials in transformers, electromotors, generators, magnetocaloric coolers, and other "humming" electromagnetic machinery.

We found that the alloys in the high Cu content range x = 2.0–3.0 indeed possess the targeted combination.

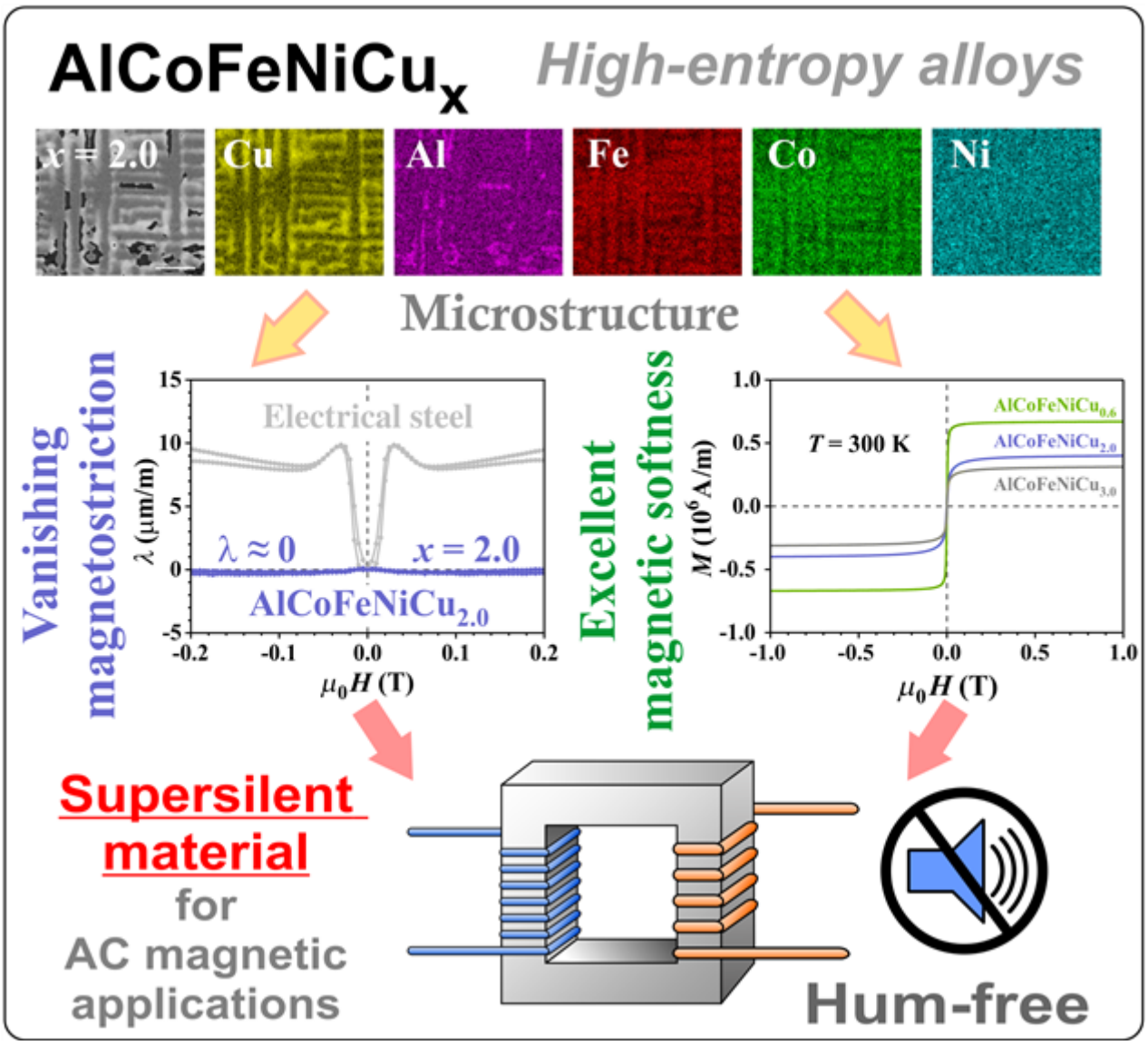

Keywords:

High-entropy alloys, magnetostriction, supersilence

Reference:

[1] J. Luzar, P. Priputen, M. Drienovsky, S. Vrtnik, P. Koželj, A. Jelen, et al., Adv. Mater. Interfaces, 2022, 9, 2201535.

21

Local mobility and atomic structure in Pd- and Zr-based bulk metallic glasses

Olivia Vaerst[1], Dr Harald Rösner[1], Dr Martin Peterlechner[2], Prof Dr Gerhard Wilde[1]
[1]University of Münster, Institute of Materials Physics, Münster, Germany, [2]Karlsruhe Institute of Technology, Laboratory for Electron Microscopy , Karlsruhe, Germany

Poster Group 2

Background incl. aims
Metallic glasses are a category of materials not completely understood yet. Especially the glass transition mechanisms and the origin of structure-property relations are unclear and gaining deeper insights is of great interest. With a detailed analysis of the local structure and atomic mobility in two model systems of bulk metallic glasses, the possibility of observing atomic processes that govern basic glassy mechanisms can be sought after.
Methods
The here investigated Pd- and Zr-based materials are model glass systems with high kinetic stability and superior mechanical properties, respectively. They are prepared by copper mould casting and verified for their amorphous phase by X-ray diffraction. Further characterisation in terms of thermal properties is done by differential scanning calorimetry. Microstructural investigations are based on electron microscopy techniques: In TEM mode, the method of Electron Correlation Microscopy (ECM) is used to probe the local dynamics and structural relaxation times of Pd- and Zr-based metallic glasses. ECM gives further insights into the underlying mechanisms of amorphous phases with nanometer spatial resolution. Experiments are performed both at room temperature and elevated temperatures using FIB-prepared lamella with a Protochips Fusion AX in situ heating holder. Complementary structural investigations concerning the medium range order (MRO) in glassy metals are performed by 4D-STEM fluctuation electron microscopy (FEM), evaluating the normalized variance of speckles in nanobeam diffraction patterns.
Results
ECM yields a structural relaxation time and a stretching exponent from fits to intensity correlations of dark-field images over time. The structural relaxation time is a measure of local mobility in the material and was found to be different for the two investigated material systems, attributed to their different compositions. In addition, the two material systems react differently to the electron beam during the ECM measurements, where the determined stretching exponent might help to understand the underlying dynamics mechanisms in more detail. Comparisons of ECM-determined parameters from room temperature experiments and measurements at elevated temperatures also show a difference between the two material systems, which are connected to the thermal stabilities of each metallic glass. Moreover, the MRO investigated by fluctuation electron microscopy shows different MRO sizes and volume fractions for the two material systems. A comparison of these findings with thermal parameters resulting from macroscopic measurements is performed.
Conclusion
The conducted investigations show clear differences between the two material systems in the local dynamics as well as the atomic structure. These deeper microstructural insights from electron microscopy measurements at various, also elevated temperatures complement the results of macroscopically averaging methods of thermal and mechanical investigations. Combining the findings allows to better understand the glassy state and beam-induced dynamics including underlying mechanisms.

Keywords:

Metallic Glass, Structural Relaxation, ECM

26

XRD and TEM study of the quasicrystalline phase in pellets consolidated using spark plasma sintering

Dr Ruitao Li[1,2], Dr Khiam Aik Khor[3], Dr Zaoli Zhang[4], Dr Chris B Boothroyd[2], Associate Professor Zhili Dong[2]
[1]School of Mechanical Engineering, Jiangsu University, Zhenjiang, China, [2]School of Materials Science and Engineering, Nanyang Technological University, Singapore, Singapore, [3]School of Mechanical & Aerospace Engineering, Nanyang Technological University, Singapore, Singapore, [4]Erich Schmid Institute of Materials Science Austrian Academy of Sciences, Leoben, Austria

Poster Group 2

The production of quasicrystal powders by gas atomization has been commercialized. Among various quasicrystals synthesized, Al-Cr-Fe and Al-Cu-Cr-Fe quasicrystals are very promising materials for coatings and reinforcements in composites due to their high hardness, good wear and corrosion resistance and the relatively low cost of their constituent metals [1]. As these quasicrystals are metal based, the behavior of bonding between the quasicrystalline reinforcement phase and the metal matrix is superior to that for ceramic phase reinforced metal-matrix composites. However, long duration sintering can result in phase changes and decrease the beneficial properties of the quasicrystals in the composites.
In our study, we employed spark plasma sintering to shorten the heating duration for the Al-Cr-Fe and Al-Cu-Cr-Fe quasicrystal powders and thus minimize the chance of phase changes when fabricating quasicrystalline reinforced composites. The phases of the sintered compacts were analyzed using x-ray diffraction. The microstructure of the quasicrystalline phases was further studied using high resolution transmission electron microscopy.
Experimental results showed that even when the heating duration was as short as 30mins during spark plasma sintering at 650ºC, phase changes could still occur. X-ray diffraction patterns showed peaks from the decagonal Al-Cr-Fe phase while HRTEM images revealed that in decagonal Al-Cr-Fe quasiperiodic planes were periodically stacked along the 10-fold axis with a periodicity of about 1.2nm. Spark plasma sintering of icosahedral Al-Cu-Cr-Fe and pure Al blended powders was conducted at 450ºC for 10mins and no phase change was detected using X-ray diffraction or high resolution electron microscopy. This implies that spark plasma sintering is effective in fabricating quasicrystal reinforced Al-based composites.

[1] V. Demange, J. Anderegg, J. Ghanbaja, F. Machizaud, D. Sordelet, M. Besser, P. Thiel, J. Dubois, Applied Surface Science 173, p 327-338 (2001).

Acknowledgement: The author would like to thank the Ministry of Education, Singapore for supporting our Tier 1 projects RG141/22 “Upcycling of steel pipeline structures through functional grading for hydrogen fuel transport and storage” and RG93/16 “Novel metal matrix quasicrystal composites with strong interface chemical bonding for advanced applications”.

Keywords:

quasicrystal, spark plasma sintering

46

Interdiffusion-controlled phase formation at an interconnect interface during soldering

Sandra Gaertner[1], Dr. Harald Rösner[1], Apl. Prof Dr. Sergiy Divinskiy[1], Prof. Dr. Gerhard Wilde[1]
[1]Institute of Materials Physics, University Münster, Münster, Germany

Poster Group 2

Background incl. aims:
Soldering is a well-established method for creating permanent bonds between metal parts, often resulting in the formation of intermetallic compounds. For the purpose of soldering, various elements like Sn, Pb, Bi, Sb, Ag and Cu, or their alloys, are utilized in different compositions based on the respective field of application. The shift towards lead-free solder, driven by environmental regulations, has increased interest in Sn-based solder alloys. However, soldering interconnects involves complex processes related to material transport, phase stability, and phase transformation kinetics.
Methods:
In the present work, the interdiffusion and diffusion-controlled phase formation processes in a Sn-Sb solder alloy between a Ni-based layer with a minor Si amount and a Cu substrate were investigated using various electron microscopy techniques. Initial scanning electron microscopy analysis of cross-section samples provided an overview of the interface, including the Sn-Sb solder alloy. For detailed examination, focused ion beam techniques were employed to create electron-transparent samples for analysis using analytical transmission electron microscopy.
Results:
Examination of the untreated states of the Ni-based layer and the solder alloy allowed differentiation between the initial microstructure and changes post-soldering. The Ni-based layer exhibited a lamellar-type structure with a uniform elemental distribution perpendicular to the soldered interface, while the raw solder alloy consisted of a tetragonal β-Sn phase as a matrix and a trigonal SbSn phase. After the soldering procedure, CuSnNi and SnCu intermetallic compounds formed with various shapes, surrounded by the β-Sn matrix. The SbSn phase persisted as small inclusions. Additionally, the Ni-based layer initially shrank due to diffusive interactions with Cu and Sn, resulting in a thin film with increased Si content compared to the untreated layer, eventually leading to complete consumption of the Ni-based layer.
Conclusions:
This study highlights the intricate processes involved in Cu transport from the substrate through the solder material, emphasizing the significant role of Cu in forming intermetallic compounds. Together with Sn, Cu drives the transformation of the Ni-based layer towards complete consumption. In addition to elemental influences, microstructures play a crucial role in the Ni consumption process.

Keywords:

soldering; electron microscopy; intermetallic compounds

112

3D Investigation of Lath Martensite in a Low-Carbon Stainless Steel Using PFIB-EBSD Tomography

Mehdi Mosayebi[1], Mr Daniel Paquet[2], Mr Pierre-Antony Deschênes[2,3], Mr Laurent Tôn-Thât[2], Dr Nabil Bassim[1,4]
[1]Materials Science and Engineering Department, Hamilton, Canada, [2]Hydro-Québec, Hydro-Québec Research Institute, Varennes, Canada, [3]Mechanical Engineering Department, École de technologie supérieure, Montreal, Canada, [4]Canadian Centre for Electron Microscopy, McMaster University, Hamilton, Canada

Poster Group 2

Background
Lath martensite in steel is well known to be tremendously complex due to a hierarchical microstructure consisting of packets, blocks, sub-blocks, and laths [1]. The complexities arising from this spatially varying and multi-scale microstructure, have effectively hindered the analysis associated with lath martensite. 3D characterization techniques have demonstrated great potential to provide important insights into the 3D morphology of complicated microstructures [2]. In this regard, serial section tomography with Xe+ plasma focused ion beam (PFIB) offers the ability to collect data from sufficiently large volumes to be statistically representative of the bulk material while maintaining sufficient spatial resolution to observe all relevant features of a complex microstructure [3]. Accordingly, this study aimed to employ electron backscatter diffraction (EBSD) technique in conjunction with high-precision and large field-of-view PFIB serial sectioning tomography in order to enable a full identification of the microstructural elements in a lath martensitic structure.
Methods
The material used in this study was an as-quenched low-carbon 13Cr-4Ni martensitic stainless steel. Block-lift-out and U-shaped trench techniques were used to prepare large cross-sectional volumes using TFS Helios G5 PFIB and ZEISS Crossbeam 350 laserFIB, respectively (Figure 1). An automated routine of serial slicing and subsequent EBSD data acquisition were then performed using the Auto-Slice-and-View 4.0 software. Reconstruction steps including the importation of the raw data, thresholding, alignment, clean-up, and segmentation were all carried out in DREAM.3D software. Following reconstruction and segmentation, the final 3D dataset was visualised using ParaView software.
Results
Figure 2(a and b), display the reconstructed 3D volume of the martensitic microstructure in the form of Euler angle and band contrast maps. Martensitic blocks were segmented manually (i.e., using the specific FeatureIDs assigned by DREAM.3D), and then reconstructed in 3D as shown in Figure 2(c-j). Crystallographic analyses revealed that each prior austenite grain (PAG) can be decomposed into clusters of martensitic blocks, namely packets, such that blocks with specific variants can adopt unique morphological arrangements in 3D. Figure 2(c-f) showcase examples of these morphological arrangements including: (i) parallel arrangement of three distinct variants sharing 60°@[011] orientation relationship, (ii) T-shape arrangement of two distinct variants sharing 10.5°@[011] orientation relationship, and (iii) Triangular arrangement of three distinct blocks sharing 10.5°@[011], 49.5°@[011], and 60°@[011] orientation relationships.
The presence of numerous blocks/platelets with various crystallographic and spatial orientations, leads to many opportunities for the martensitic features to meet at different locations and thereby forming complicated networks in 3D. Here we used the acquired morphological information to confirm the physical contact between the martensitic blocks within the volume of the PAGs (Figure 2(g and h)). This was further combined with the crystallographic information (e.g. crystallographic misorientations between the blocks in Figure 2 (d)), to reconstruct the boundary networks in 3D. As

an example, Figure 2(i and j) illustrate 3D perspectives of the boundaries corresponding to 2 different packets and their blocks delineated by a black rectangle in Figure 2(g). 3D observations suggested a significant morphological difference between the packet boundaries (strip-like morphology) and block boundaries (flat surface morphology) within the lath structure of the martensitic stainless steels (Figure 2(i and j)).

Conclusions

Martensitic features including blocks, packets, and their boundaries were analyzed in 3D. Three distinct configurations, including (i) parallel arrangement, (ii) T-shape arrangement, and (iii) Triangular arrangement, were identified for the martensitic blocks depending on their crystallographic variants. Two different morphologies, (1) strip-like morphology, and (2) flat-surface morphology, were also observed for the packet boundaries and block boundaries, respectively.

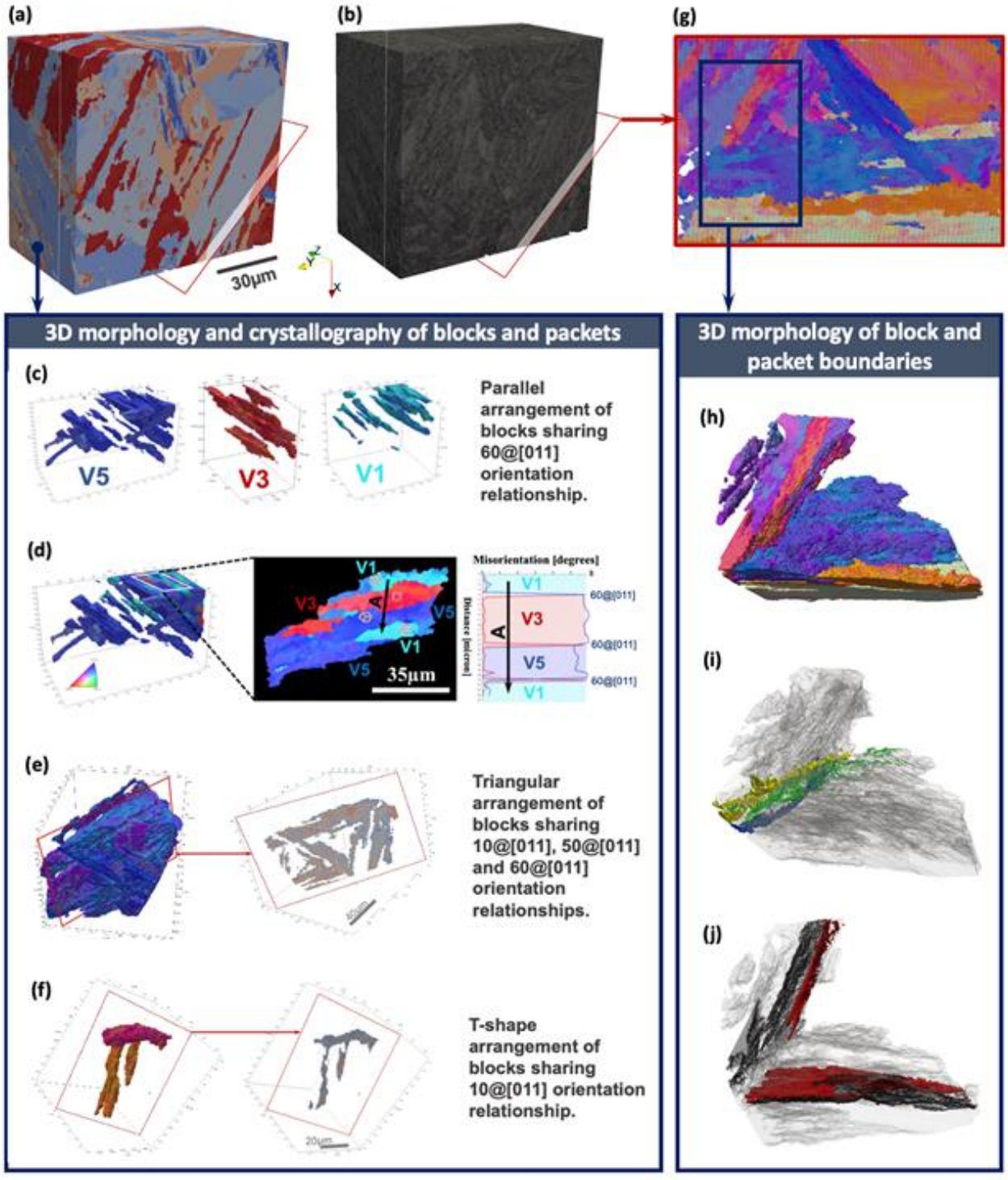

Keywords:

3D-EBSD), PFIB tomography, Lath martensite

Reference:

[1] Kitahara, Hiromoto, et al."Crystallographic features of lath martensite in low-carbon steel."Acta materialia 54.5(2006): 1279-1288.
[2] Morito, Shigekazu,et al."Quantitative analysis of three-dimensional morphology of martensite packets and blocks in iron-carbon-manganese steels."Journal of Alloys and Compounds 577(2013):S587-S592.
[3] Burnett, T.L., et al. "Large-volume serial-section tomography by Xe Plasma FIB dual-beam microscopy."Ultramicroscopy161(2016):119-129.

132

Developing alloys presenting nanograins and spinodal decomposition: structural and compositional characterization

Juan Macchi[1], Olha Nakonechna[2], Ronan Henry[1], Celia Castro[1], Kaveh Edalati[2], Frederic De Geuser[3], Xavier Sauvage[1], Williams Lefebvre[1]
[1]Univ Rouen Normandie, INSA Rouen Normandie, CNRS, Normandie Univ, GPM UMR 6634, Rouen, France, [2]WPI, International Institute for Carbon-Neutral Energy Research (WPI-I2CNER), Kyushu University,, Fukuoka, Japan, [3]University Grenoble Alpes, CNRS, Grenoble INP, SIMaP, Grenoble , France

Poster Group 2

Background incl. aims
The demand for reducing the emissions of CO2 in the transportation industries has, as a direct consequence, increased the need for alloys with enhanced performances. For this purpose, enabling the combination of multiple hardening mechanisms via microstructural design is a key tool. In the present study, in addition to a high Hall-Petch hardening, a different “second phase” hardening of spinodal decomposition is introduced in nanostructured materials.
Methods
Binary systems with a miscibility gap are selected (Fe-Cr and Al-Ag) [1,2]. The nanograins were produce by Severe Plastic Deformation (SPD) using High Pression Torsion (HPT). The resulting nanostructures (characterized by TKD and ACOM-TEM [3]) were aged during different holding times, allowing to establish the kinetics of the spinodal decomposition. The latter was characterized by APT applying the Radial Distribution Function in order to determine the evolution of both the wavelength and amplitude of the 3D concentration fields [4]. Micromechanical testing including micro-bending was applied to evaluate the mechanical properties evolution.
Results
Nanograins were obtained for both studied alloys after 10 revolutions of HPT, with average grain size diameter of 51 nm for the Fe-Cr alloy and about 100 nm for the Al-Ag system repectively. After ageing for 100h at 525 °C, the Fe-Cr average grain size attained 159 nm, showing relatively stable grain size.
The Fe-Cr spinodal decomposition kinetics of the deformed samples were measured to be 10 times faster compared to the non-deformed state. As for the Al-Ag alloy, it presents a non-homogenous composition even in the quenched state (cryo set-up used).
The microhardness evolution of the Fe-Cr alloy after 100h ageing shows that the decrease expected due to the Hall-Petch effect is mostly compensated by the hardening due to the spinodal decomposition. However, the bending torsion values after ageing showed an embrittment of the material.
Conclusion
Binary alloys with nanosized grains were produced by SPD. The miscibility gap in the phases diagrams was exploited to produce spinodal decomposed systems. Therefore, alloy-design considering both hardening effects is proven to be possible. The spinodal decomposition showed to be faster in the deformed nanograin conditions. With the goal of obtaining harder and tougher alloys, optimizing the process parameter is required.

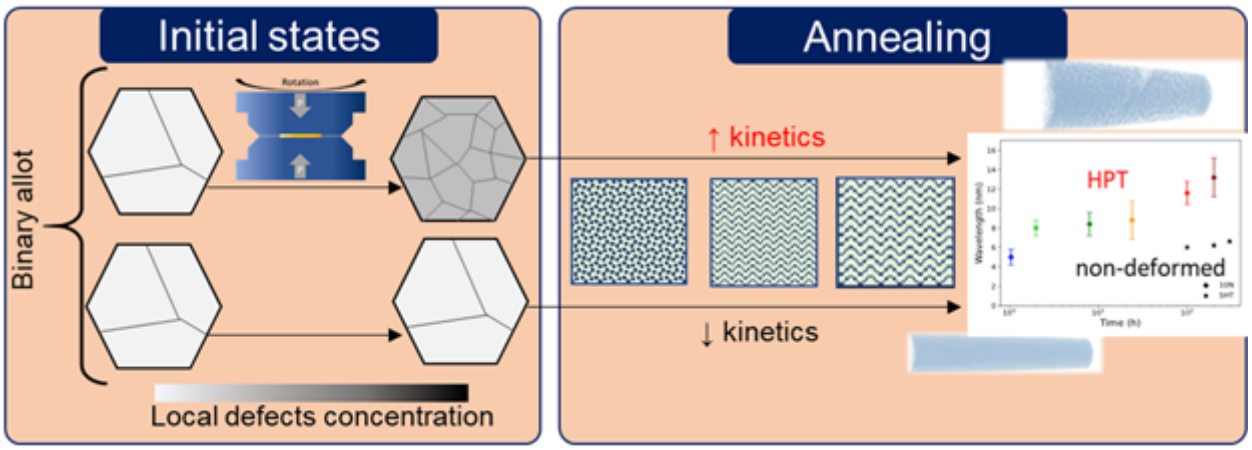

Keywords:

spinodal decomposition, HPT, APT, TKD

Reference:

[1] A. Dahlström, Influence of a mechanical load on the ageing of Fe-Cr alloys, Normandie Université, 2019. https://theses.hal.science/tel-02316065.
[2] K.T. Moore, W.C. Johnson, J.M. Howe, H.I. Aaronson, D.R. Veblen, On the interaction between Ag-depleted zones surrounding γ plates and spinodal decomposition in an Al-22 at.% Ag alloy, 2002. www.actamat-journals.com.
[3] E.F. Rauch, M. Véron, Automated crystal orientation and phase mapping in TEM, Mater Charact 98 (2014) 1–9. https://doi.org/10.1016/J.MATCHAR.2014.08.010.
[4] L. Couturier, F. De Geuser, A. Deschamps, Direct comparison of Fe-Cr unmixing characterization by atom probe tomography and small angle scattering, Mater Charact 121 (2016) 61–67. https://doi.org/10.1016/j.matchar.2016.09.028.

205

Correlative TEM and APT studies of metallic Mg specimens prepared and analyzed under controlled environments

Cecile Bonifacio[1], Daniel Perea[2], Pawel Nowakowski[1], Mary Louise Ray[1], Paul Fischione[1]
[1]E.A. Fischione Instruments Inc., Export, USA, [2]Pacific Northwest National Laboratory, Richland, USA

Poster Group 2

Background

Successful correlative transmission electron microscopy (TEM) and atom probe tomography (APT) studies on metals require a surface and subsurface with minimal defects. The potential of these powerful analytical techniques can be hindered by surface damage during material processing, implanted Ga during focused ion beam (FIB) specimen preparation, or environmental degradation during specimen transfer in an ambient environment. Therefore, specimen preparation is a critical component of successful correlative analyses. We present a sample preparation and analysis workflow under controlled environments using broad Ar ion beam milling of the bulk sample and post-FIB condensed Ar ion beam milling of APT specimens. The aim is to differentiate the sub-surface properties of a metallic sample related to Ga diffusion by FIB preparation and by post-FIB condensed Ar ion beam milling using a controlled environment workflow; APT specimen yield from ambient versus controlled environment sample preparation also will be compared.

Methods

Under controlled environments, bulk Mg foil ribbons (hot rolled and deformed) were prepared using a broad Ar ion beam milling system [TrionMill, Fischione Instruments] to remove surface artifacts. The bulk sample was then transferred in a protected environment to a FIB system for imaging and electron backscattered diffraction (EBSD) analysis. Specific regions on the Ar ion beam milled sample were selected (Fig.1, areas 1 and 2); from these regions, APT specimens were prepared. Areas with multiple grain boundaries were selected to elucidate the distribution of Ga in the Mg specimen during specimen preparation [1]. FIB specimen preparation of the APT specimens followed by post-FIB condensed Ar ion beam milling [NanoMill® TEM specimen preparation system, Fischione Instruments] and subsequent TEM and APT characterization were performed in protected environments. APT characterization involved the use of an environmental transfer hub (ETH) station [2] to transfer the APT specimen to a local electrode atom probe system [LEAP®, CAMECA].

Results

Surface damage and oxides on the bulk were successfully removed by broad Ar ion beam milling based on the resulting pristine surface (Fig. 1a), which is polycrystalline with sub-micron grain sizes that average 600 nm. EBSD analysis of an area near the crack region (Fig. 1a, pink region) found smaller grains; multiple grain boundaries (marked in Fig. 1b) were identified on the band contrast image and inverse pole figure (IPF) map. The acquired TEM image (Fig. 1c) showed the presence of the FIB Pt cap layer (Fig. 1a, area 1), while the post-FIB condensed Ar ion beam milled specimen (Fig. 1a, area 2) showed the removal of the Pt layer from the TEM image (Fig. 1e). The Ga APT reconstructions displayed a significant amount of Ga at 18.7 atomic %, especially on the specimen's surface following Ga FIB milling (Fig. 1d), which is reduced to 3.9 atomic % following post-FIB Ar ion beam milling (Fig. 1f). The dark contrast on the bright field TEM image of the post-FIB condensed Ar ion beam milled specimen (Fig. 1e) correlates to the Ga-rich area marked on the Ga APT reconstructions. Using this feature, the position of the grain boundary decorated with Ga along the vertical axis of the APT specimen was identified (Fig. 1f). For both APT specimens after Ga FIB and Ar ion beam milling, low amounts of O and H (Fig. 1g,h) within the Mg-rich region were observed. At the interface of the Mg and Ga-implanted region, parallel trends of increasing amounts of O and Ga from

the Ga FIB specimen (Fig. 1g) were detected. In contrast, the post-FIB condensed Ar ion beam milled specimen showed a constant amount of O at 0.50 atomic % across the specimen. Additionally, diffusion of Ga via the grain boundaries of the polycrystalline specimen occurred during FIB preparation as evidenced by the Ga-rich line along the APT specimen (Fig. 1h, inset).

Conclusion

The broad Ar ion beam milling, Ga FIB, and condensed Ar ion beam milling workflow – all under controlled environments – removed specimen surface damage, oxidation, and Ga implantation from the specimens. Consequently, the metallic nature of the Mg sample was conserved. Ga diffused to the grain boundary of the post-FIB Ar ion beam milled specimen, which correlates to previous study [3]. The formation of Mg oxide on the FIB-prepared specimen possibly occurred due to FIB-induced thermal effects [4]. APT compositional analysis showed that surface oxidation was suppressed by controlled environment transfers.

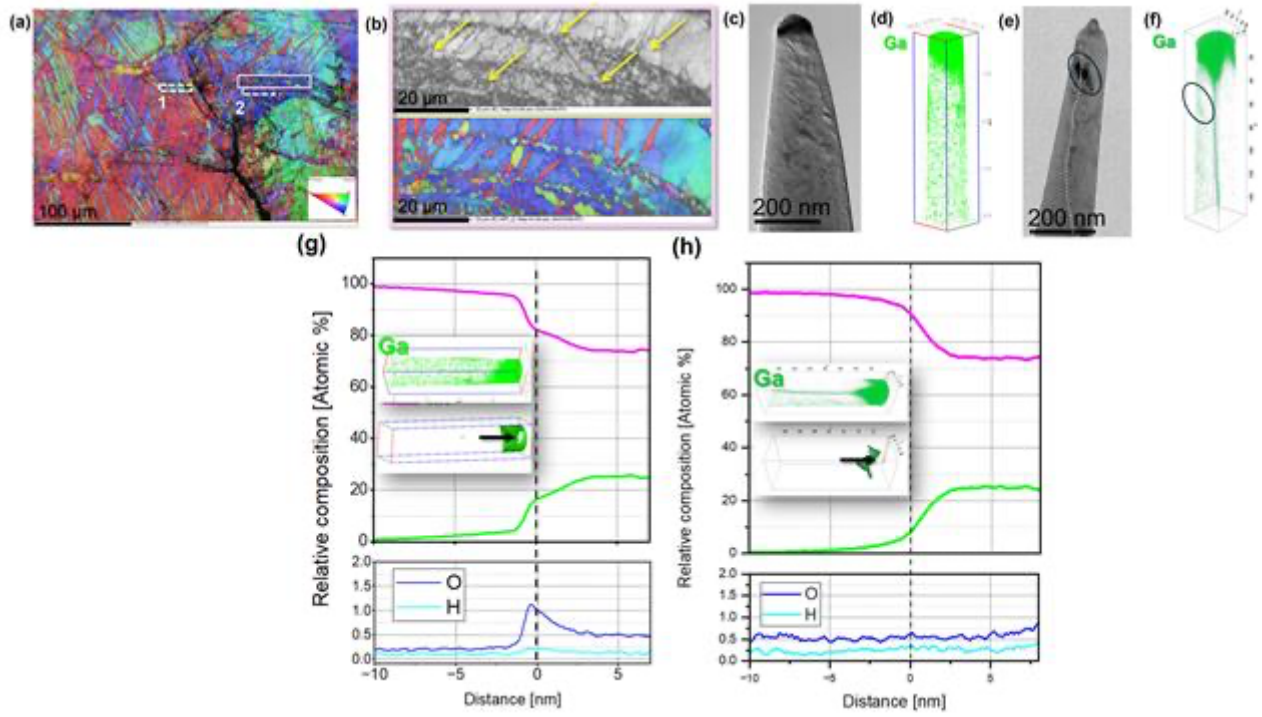

Keywords:

magnesium, controlled environments, specimen preparation

Reference:

References

[1] CS Bonifacio et al., Microsc. Microanal. 28(S1), (2022), pp. 3176-3178.

[2] DE Perea et al., Adv. Struc. Chem. 3(1), (2017), Article ID 12.

[3] I Stloukal & J Cermak, Scr. Mater., 49(6), (2003), pp. 557–562.

[4] D Neuß et al., Cor. Sci., 227, (2024), pp. 111776.

214

Strain mapping using high-resolution electron backscatter diffraction technique: The influence of sample preparation

Dr Pawel Nowakowski[1], Mrs Mary Ray[1], Mr Paul Fischione[1]
[1]Fischione Instruments, Export, USA

Poster Group 2

Background

When developing a new metallic alloy, one of the critical parameters is how it will resist expected loads without failure. Understanding how materials deform is important when doing research and development in fields such as aerospace, where public safety is the top priority. An emerging strain distribution measurement technique is based on cross-correlation analysis of high-resolution electron backscatter diffraction (HR-EBSD) patterns. The technique measures lattice distortion-related differences between EBSD patterns obtained within the same grain. The HR-EBSD technique was applied to elastic strain, evidence of plastic strain, and geometrically necessary dislocations (GND) measurements [1]. However, aside from intrinsic instrumentation limitations, HR-EBSD is very sensitive to diffraction pattern quality. Therefore, sample preparation factors prominently into the accuracy and precision attained in HR-EBSD strain analyses.
However, it is not easy to distinguish between the residual real strain present in a material and the strain induced by sample preparation. To be able to persistently illustrate the effect of stress on the microstructure during sample preparation, we have chosen the phenomenon of dynamic strain-induced transformation (DSIT) of austenite to surface martensite [2, 3]. The DSIT can occur during sample preparation by mechanical polishing (MP) or while using ion beam-based sample preparation techniques: focused ion beam (FIB) or broad ion beam (BIB) [4, 5]. We prepared a series of austenitic precipitation hardening grade steel samples using MP, BIB, and FIB techniques and exposed an austenitic precipitation hardening grade steel to Ga ions at a variety of beam energies and sample geometries. Energy-dispersive X-ray spectroscopy (EDS), electron backscatter diffraction (EBSD) and high resolution (HR)-EBSD techniques were used to assess structural damage induced by sample preparation.

Methods

The samples were mechanically polished by colloidal silica on a grinder/polisher tool [MultiPrep™ system, Allied High Tech Products]. Then the samples were prepared by broad ion beam milling [TrionMill, Fischione Instruments]. Finally, the samples were exposed to Ga ions at a variety of beam energies and milling geometries in a FIB system [Scios DualBeam Ga FIB system, Thermo Fisher Scientific].
After each sample preparation technique, the samples were analyzed using:

- a Ga FIB system equipped with an EDS detector [X-Max 150 mm2 EDS detector with Aztec software, Oxford Instruments] and an EBSD detector [e-FlashFS EBSD detector with Esprt software, Bruker Nano Analytics], and
- a scanning transmission microscope [S-4700 SEM, Hitachi] equipped with an EBSD detector [NordlysNano EBSD detector with Aztec software, Oxford Instruments].

EBSD data were processed using HKL Channel 5 software [Oxford instruments]. High HR-EBSD measurements were done using Open X-Y software [Brigham Young University].

Results and conclusions

Figure 1 shows HR-EBSD average strain measurements and geometrically necessary dislocations (GND) of steel samples after mechanical polishing (Fig. 1a, 1c) and BIB milling at 5 keV, 2 keV, 1 keV, and 3° milling angle (Fig. 1b, 1d). No DIST phase transformation of austenite to martensite is

observed in the sample prepared by BIB milling. In the sample prepared by MP, 20 % strain-induced martensite is observed. Figure 1a shows an HR-EBSD average strain map of partially transformed martensite to austenite grains. Strain accumulation of up to 10-2 of austenite grains around martensite can be observed. This strain gradient can be correlated with the high GND densities shown in Fig. 1c. Compared to the sample prepared by a BIB mill, the GND density is higher – up to two orders of magnitude. No strain is observed in the BIB milled sample. The BIB milled sample with no presence of DIST of austenite to martensite was exposed to Ga FIB at different ion beam energies. The area affected by the Ga ion beam had a very poor quality EBSD pattern (Kikuchi bands shift and overlap). The EDS analyses demonstrate strong Ga ion implantation. Figure 2a shows the HR-EBSD average strain map of regions both exposed and not exposed to a 1 keV Ga FIB. In contrast to the MP sample, no strain gradient correlated with GND density is found. Figure 2b shows {100} crystal plane orientation facing the Ga ions bombardment. The part of the grain exposed to the Ga FIB shows high strain accumulation. This suggests that structural damage is dependent on grain crystallographic orientation. Structural damage and strain accumulation result from FIB-induced atom displacement and vacancies, which leads to strain-induced austenite deformation to martensite.

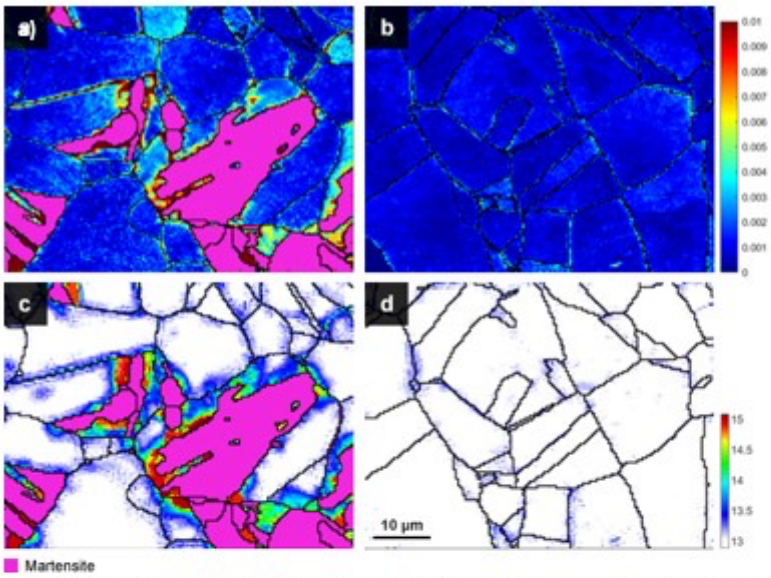

Figure 1: HR-EBSD maps showing average strain for mechanically polished sample (a), after argon broad ion beam milling (b), geometrically necessary dislocation density maps for sample after mechanical polishing (c), and broad ion beam milling (d).

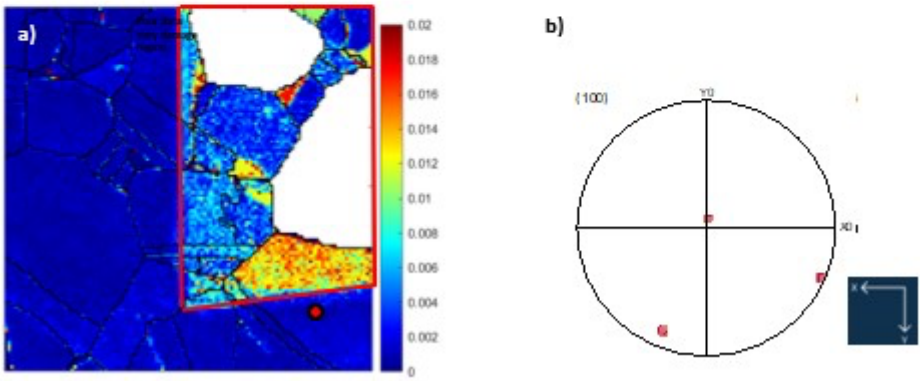

Figure 2: HR-EBSD average strain map (a) of regions both exposed and not exposed to a 1 keV Ga FIB (indicated by the red dot). Pole figure (b) showing {100} crystallographic oriented grain (marked with red dot) that was partially exposed to Ga ion bombardment.

Keywords:

HR-EBSD, GND, strain, BIB, FIB

Reference:

[1] A. Wilkinson, et al., Ultramicroscopy, 62 (1996).
[2] J. Rodríguez-Martínez, et al., EPJ Web of Conferences, 26, (2012).
[3] J. Klostermann, et al., Acta Metallurgica, 12, 4 (1964).
[4] J.R. Michael, et al., Microsc. Microanal. 28, 1 (2021).
[5] R.P. Babu, et al., Acta Materialia, 120 (2016).

283

Creep-induced microstructural evolution of the eutectic Mo-Si-Ti alloy by correlative electron microscopy

Hemanth Thota[1], Herr Dr.-Ing. Daniel Schliephake[2], Herr Dr.-Ing. Alexander Kauffmann[2], Herr Huichao Wu[3], Frau Prof. Dr. rer.nat. Astrid Pundt[2], Herr Prof. Dr.-Ing. Martin Heilmaier[2], Frau TT-Prof. Dr.-Ing. Yolita M. Eggeler[1]
[1]Microscopy of Nanoscale Structures & Mechanisms, Laboratory for Electron Microscopy (LEM), Karlsruhe Institute of Technology (KIT), Karlsruhe, Germany, [2]Institute for Applied Materials (IAM-WK), Karlsruhe Institute of Technology (KIT), Karlsruhe, Germany, [3]Institute of Energy and Climate Research (IEK), Forschungszentrum Jülich GmbH, Jülich, Germany

Poster Group 2

Turbine blades are critical parts of turbine engines because they experience the highest temperature in the combustion zone. The thermodynamic efficiency of the turbine engine directly depends on the turbine entry temperature (TET) of hot gases; the material's temperature capability dictates the operable temperature. The current state-of-the-art, single-crystal nickel-based superalloys operate close to 80 to 90 % of their melting temperatures. There is a continuous need to design newer high-temperature materials that can withstand higher operating temperatures above 1100 °C to improve efficiency and thus reduce CO2 emissions [1].
The Mo-Si-Ti system has been explored as a potential alternative to the existing high-temperature materials because of their lower density and high melting temperatures. The eutectic Mo-Si-Ti alloy showed pesting resistance and optimal creep behavior. It has a two-phase microstructure: a body-centered cubic (bcc), solid solution consisting of Mo, Ti and Si (Mo,Ti,Si)ss and hexagonal silicide (Ti,Mo)5Si3 [2]. The creep mechanism of this alloy is yet unknown and needs further investigation to understand how the creep strain accumulates in response to the applied stress and subsequent microstructural evolution at meso- and nano-scales in the two phases.
Compressive creep tests were performed under vacuum at 1200 °C and true stress of 100 MPa to understand the creep curve with characteristic minimum and creep rate acceleration after that. To understand the microstructural evolution, the samples were crept to true strains of 1.3, 10, 20, and 40 %. Electron backscatter diffraction (EBSD) was performed to study strain distribution in two phases and identify the region of interest for transmission electron microscopy (TEM) specimen preparation by focused ion beam (FIB). The dislocations were imaged using the diffraction contrast of the selected two-beam conditions in scanning transmission electron microscopy (STEM) mode. The invisibility criterion was used to determine the acting slip planes and the character of dislocations in both phases.
The deformation of silicide was observed in 0.2 % crept samples from EBSD-kernel average misorientation (KAM) maps. Both phases undergo deformation by dislocation plasticity. The following slip systems were identified: {110}, {-121} and {-213} planes with Burgers vector b = 1/2 <1-11> in the solid solution and basal slip {0001} or prismatic slip {1-1 00} both with Burgers vector b=1/3<-1-120> in the silicide [3]. During creep deformation, the growth and coarsening of (Ti,Mo)5Si3 precipitates in the solid solution, and the nucleation and growth of solid solution precipitates in the silicide occur [3]. STEM-energy dispersive spectroscopy (EDXS) was performed to determine the local chemical composition of the precipitates in the crept samples. Figure 1a shows numerous dislocations originating from the interface in the solid solution and the interaction of gliding dislocations with (Ti,Mo)5Si3 precipitates. Whereas Fig.1b shows the formation of low-angle grain boundaries in the silicide phase, confirming dynamic recovery. The microstructural findings were correlated with the creep curve, and the dominant creep deformation mechanisms (dislocation climb controlled creep and diffusional creep) were identified in the alloy.

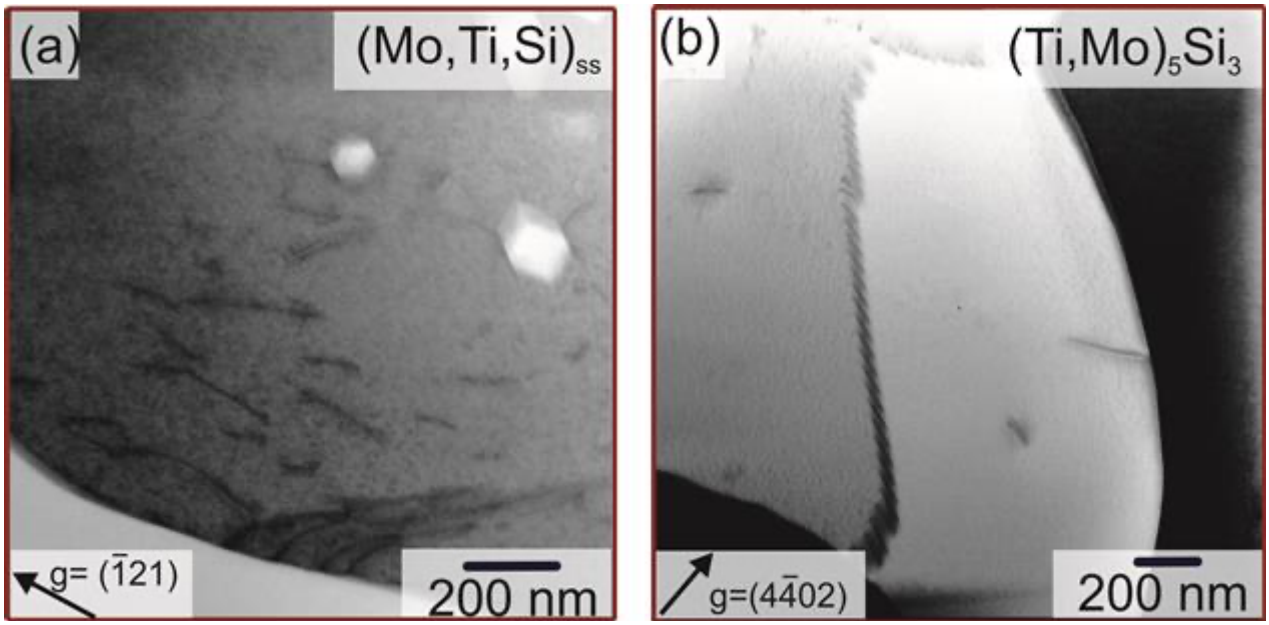

Keywords:

Creep, dislocations, Mo-Si-Ti, (Ti,Mo)5Si3, precipitates

Reference:

[1]J.H.Perepezko, Science 326 (2009) 1068 1069.https://doi.org/10.1126/science.1179327.
[2]D. Schliephake, A. Kauffmann, X. Cong, C. Gombola, M. Azim, B. Gorr, H.J.Christ, M.Heilmaier,Intermetallics.104(2019)133–142.https://doi.org/10.1016/j.intermet.2018.10.028.
[3]H.Thota, D.Schliephake, A.Kauffmann, H.Wu, A.Pundt, M.Heilmaier, Y.M.Eggeler, Adv.Eng.Mater.(2024)Accepted Author Manuscript.https://doi.org/10.1002/adem.202301909
The authors gratefully acknowledge the financial support from the DeutscheForschungsgemeinschaft (DFG) within the framework of GRK 2561 MatCom –ComMat and the grant numbers HE 1872/33-2 and HE 1872/38-1.

284

Investigating Impact-Induced Deformation in Cold-Sprayed Aluminum-Quasicrystals Composite Coatings

Reza Jafari[1], Dr. Mari Honkanen[2], Dr. Renato Pero[3], Dr. Turkka Salminen[2], Assoc. Prof. Heli Koivuluoto[1], Prof. Minnamari Vippola[1,2]
[1]Materials Science and Environmental Engineering, Faculty of Engineering and Natural Sciences, Tampere University, Tampere, Finland, [2]Tampere Microscopy Center, Tampere, Finland, [3]Alemnis AG, Gwatt (Thun), Switzerland

Poster Group 2

Introduction

From the perspective of engineering metallic coatings, it is typically challenging to meet diverse requirements using single-phase coating materials, which often fall short in satisfying industrial needs. With metal matrix composite coatings, however, it becomes feasible to meet these diverse needs effectively. Cold spraying (CS) is a solid-state coating deposition and additive manufacturing technology that is promising for several industrial applications. It is effective in the deposition of a variety of materials, including metals, alloys, polymers, and ceramics, but also it stands out because of its compatibility with heat and oxygen-sensitive materials and capacity to create composite deposits. The CS process in general involves accelerating solid feedstock particles using pressurized and preheated gas, resulting in supersonic particle impact on a substrate. This impact leads to coating formation from deformed particles. During coating processing, impacted metal particles undergo high strain rate deformation, triggering phenomena such as grain refinement and phase transformation. These microstructural changes within CS deposits significantly influence their local mechanical properties. At the micron and submicron scale, these alterations can either enhance or compromise coating performance. Notably, phenomenon such as dynamic recrystallization occurs at interfaces—between particles and between particles and substrates—due to significant plastic deformations and adiabatic shear instability conditions during solid-state deformation. Consequently, heterogeneous microstructures might emerge at these critical locations, accompanied by localized variations in mechanical properties. However, despite numerous efforts to have a clear understanding of such featured developed in CS alloys, the precise relationship between local microstructure and mechanical behavior remains elusive for cold-sprayed composite coatings containing multiple ingredients. To engineer coatings with specific mechanical characteristics, a comprehensive understanding of microstructural features is essential. Investigating how variations in grain size, phase distribution, texture, and defects influence mechanical properties is crucial. Bridging this knowledge gap can optimize cold-sprayed coatings for diverse applications, ensuring reliability and advancing materials science.
Aluminum alloys are in high demand in light-weight structures; however, it has the potential short fall of tribological and mechanical properties. Our research team has made significant strides using cold spraying (CS) to produce compact and well-incorporated aluminum alloy (AA6061)-quasicrystal composite coatings (referred to as Al-QC). The coatings have shown superior tribological characteristics and increased hydrophobicity compared with conventional Al-based coatings and bulk metallurgical counterparts.

Materials and methods

Expanding on our previous works, our current research explores the detailed microstructural intricacies of CS Al-QC composite coatings, particularly emphasizing bonding states and particle-particle interfaces and micromechanical properties. To achieve this, we sprayed the composite coatings using a high-pressure CS system with optimized parameters, utilizing pressurized nitrogen (N2) as the propellant gas. Additionally, we fine-tuned process settings to accelerate a limited

number of particles, facilitating particles impacts on the substrates to study the deposition mechanism. Analytical scanning and [scanning] transmission electron microscopy (SEM) and (S)TEM) played a pivotal role in evaluating the microstructure of our specimens and forming scenarios regarding deposition behavior. Electron backscatter diffraction (EBSD) technique (by conventional and transmission Kikuchi diffraction TKD) was also used to collect crystallographic data from cross-sections of cold-sprayed coatings and to narrate the state of deformation. In-situ nanoindentation mapping (+1600 indents) was performed on the top surface of composite Al-QC coating, embracing both Al and QC phases, to provide detailed micromechanical insight completing the production/microstructure/properties chain.

Results and Conclusions

While QC particles mostly underwent brittle fracture and shattering upon impact, their contribution to in-situ hammering of the coating structure significantly contributed to densification and elimination of pores in the structure. Impact-induced grain refinement close to the exterior of impacted particles and alternation of texture and pattern quality due to high degree of deformation in Al-based matrix was found to be significant. Evidently, these features can endow a reliable bonding between dissimilar constituents in the composite coating structure. Presence of QC fragments turned out to provide enhanced bonding to Al particles within the composites. In addition, hardness and elastic modulus variations were found to be consistent with the heterogeneity of the microstructure induced by particle impacts and their deformation. However, intimate bonding at the interface of Al-QC and formation of interlayer enhanced the coating integrity. The findings regarding the bonding state can potentially justify the enhanced mechanical and tribological properties of composite coatings, and extended retention of the reinforcing phase in the structure under load, as observed in our previous works.

Acknowledgement

Authors would like to thank Mr. Jarkko Lehti and Anssi Metsähonkala, of Tampere University, for spraying the coating samples. This work made use of Tampere Microscopy Center facilities at Tampere University, Finland. Tampere University, the Faculty of Engineering and Natural Sciences is acknowledged by R.J. for the funding.

Keywords:

Electron Microscopy, Aluminum-Alloys, Quasicrystals, Microstructure

Reference:

1. Jafari R et al., J Therm Spray Tech. 2023;32:609–26.
2. Jafari R et al., ITSC 2023. Quebec: ASM International; 2023.
3. Assadi Het al., Acta Materialia. 2016;116:382–407.
4. Zou Y et al., Scripta Materialia. 2009;61:899–902.
5. Raabe D. et al., Physical Metallurgy. Elsevier; 2014. p. 2291–397.

358

Microstructure and Phase Analysis of an Al-Mg-Si Alloy Produced by Laser Power-Bed Fusion

Dr.-ing Hongcai Wang[1,4], Mohammad Alhakim[1], Dr. Temesgen Yallew[1], Dr. rer. nat. Yilmaz Sakali[2], Keyur Solanki[3], Dr.-Ing. Julian Müller[1], Prof. Dr. Benjamin Butz[1], Dr.-Ing. Carolin Zinn[3], Prof. Dr.-Ing. Axel von Hehl[3]
[1]Lehrstuhl für Mikro- und Nanoanalytik, Universität Siegen, Siegen, Germany, [2]Gerätezentrum für Mikro- und Nanoanalytik MNaF, Universität Siegen, Siegen, Germany, [3]Lehrstuhl für Materialkunde und Werkstoffprüfung, Universität Siegen, Siegen, Germany, [4]Lehrstuhl Werkstoffwissenschaft, Ruhr-Universität Bochum, Bochum, Germany

Poster Group 2

Background incl. aims
Aluminum (Al) alloy additive manufacturing (AM) offers a groundbreaking approach to metal fabrication, providing unmatched design flexibility and material efficiency. However, achieving optimal performance hinges upon understanding and controlling microstructures. Microstructure analysis is critical for evaluating properties like grain morphology, size distribution, and phase constitution, which directly influence mechanical properties. By tailoring AM parameters and post-processing techniques based on microstructural insights, engineers can elevate the integrity and performance of Al alloy components. Careful microstructure analysis ensures AM-produced parts meet the stringent quality standards and reliability demanded by diverse industries, from aerospace, automotive, and beyond. Nevertheless, the rapid solidification and intricate thermal histories inherent in AM-produced Al alloys result in microstructures significantly different from conventional processes (e.g., casting), posing substantial challenges in accounting for microstructural elements across various length scales [1]. In this study, a scale-bridging approach [2] combining multiple techniques in scanning electron microscopy (SEM) and transmission electron microscopy (TEM) was employed for obtaining a clear microscopical picture of an Al-Si-Mg alloy [3] produced by Laser Power-Bed Fusion (LPBF).
Methods
Samples are prepared using electropolishing in combination with ion milling from the AM Al alloy. Conventional imaging and diffraction techniques as well as energy-dispersive X-ray spectroscopy (EDS) in both SEM and TEM are used to characterize the as-built microstructure (Figure 1). To reveal the underlying effect of additive manufacturing on the grain structure and phase distribution, a correlative approach for orientation imaging and phase mapping is then employed by using EBSD in SEM and ASTAR in TEM.
Results
Detailed microstructural features such as melting pools, grain structure and distribution/morphology of eutectic phases in the investigated AM alloy will be revealed and analyzed (to be continued).
Conclusion
This comprehensive approach will provide valuable insights into the microstructural evolution of AM-produced Al alloys, facilitating further advancements in material design and process optimization.

The authors acknowledge Dr. Daniel Knoop from Leibniz-IWT in Bremen for providing the specimens and extend the gratitude to the support and resources provided by ZGH at Ruhr-University Bochum. Part of this work was performed at the DFG-funded Micro- and Nanoanalytics Facility (MNaF) of the University of Siegen (INST 221/131-1).

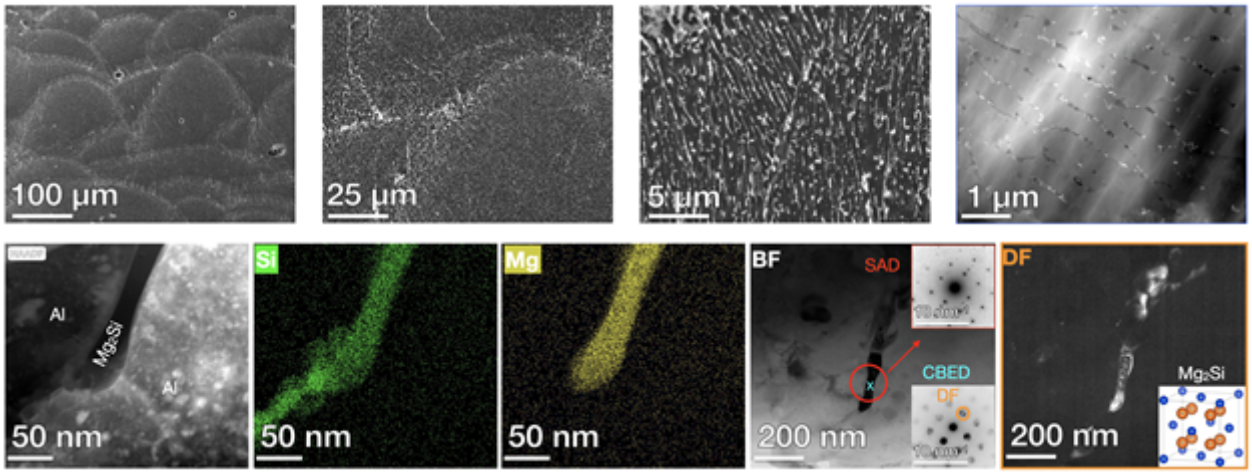

Keywords:

Additive-manufacturing; LPBF; AlMgSi; EBSD; ASTAR

Reference:

[1] Z. Chaghazardi and R. Wüthrich Journal of The Electrochemical Society, 2022, 169, 043510.
[2] H. Wang, C. Somsen, G. Eggeler, E. Detemple Materwissenschaft und Werksttechnik, 2018, 49, 726–740.
[3] D. Knoop, A. Lutz, B. Mais, and A. von Hehl Metals 2020, 10, 514.

400

In-situ beam driven experiments by Electron time-correlation microscopy of amorphous structures

Dr. Martin Peterlechner[1], Olivia Vaerst[2], Prof. Gerhard Wilde[2]
[1]Karlsruhe Institute of Technology, Laboratory for Electron Microscopy (LEM), Karlsruhe, Germany,
[2]University of Münster, Institute of Materials Physics, Muenster, Germany

Poster Group 2

Background & Aims

Amorphous materials are widely present and not straight-forward to study. However, similar to X-ray photon correlation spectroscopy (XPCS) the method of electron correlation microscopy (ECM) was introduced [1]. This approach using the time correlation of diffracted or dark-field intensities was applied at elevated temperatures. However, it was shown that this way of data analysis gives also proper materials parameters at room temperature (RT) [2]. Besides that, also pure materials made amorphous by ion implantation were recently studied [3]. To understand the influence of the beam and the measured signals, results from different materials are compared and discussed. In this work, the imaging and analysis conditions are examined to understand the arising quantitative signals, and to be able to compare ECM data obtained at elevated temperatures to that of electron time-correlation microscopy (EtCM) obtained at any temperature, even at RT where the thermal activation is small.

Methods

The analyzed materials are on the one hand metallic glasses as FeNiP or PdNiP, and on the other hand pure elements as Si or Ge. The metallic glasses were processed by rapid quenching techniques, and the pure elements were synthesized by ion implantation. EtCM is used to probe the dynamics and relaxation times from RT up to the glass transition temperature. The samples for the heating experiments were prepared using a focused-ion beam (FIB) and the lamellae were mounted onto a in-situ heating chip. Additionally, all samples were also structurally characterized using diffraction including fluctuation electron microscopy (FEM). Besides a basically disordered structure, also a preferred length-scale for ordering within the amorphous phase can be given. This number should typically not change during the EtCM experiments.

Results

The analysis of time series of dark-field images enables to measure the intensity variation over time, related to a structural relaxation time. The function of the intensity correlation can be given for every image pixel, thus also a relaxation time constant and a stretching exponent can be deduced. The measurement needs a certain amount of time and dose to achieve reliable numerical values. Different materials show different numbers, however, all materials show that the electron beam and its dose-rate or cumulative-dose are relevant for the achieved numerical values. The dose-rate can be even too high, to induce crystallization at RT. Thus, the dose-rate is measured and given for all experiments.

Conclusion

The imaging conditions during EtCM matter for the numerical values and further treatment of the result. Best results are obtained using low-dose settings and long measurement times. However, it must be noted that amorphous structures show relaxation times on basically all time scales, from atomic jumps on the pico-second scale up to bulk relaxation in terms of (millions of) years. Experimentally, the maximum measurable time scale is less than half of the overall experimental time, and the minimal measurable time scale depends on the frame time for two frames. It can be

concluded, that EtCM experiments at RT are beam driven relaxation studies, helpful to understand the intrinsic time scale for relaxation in any amorphous matter.

Keywords:

amorphous, metallic glass, in-situ, time-correlations

Reference:

References
[1] L. He, P. Zhang, M.F. Besser, M.J. Kramer, P.M. Voyles, Electron Correlation Microscopy: A New Technique for Studying Local Atom Dynamics Applied to a Supercooled Liquid, Microscopy and Microanalysis (2015), 21, 4, 1026-1033.
[2] K.Spangenberg, G. Wilde, M. Peterlechner, Direct View on Non-Equilibrium Heterogeneous Dynamics in Glassy Nanorods, Advanced Functional Materials (2021), 31 (38), 2103742.
[3] D. Radić, M. Peterlechner, K. Spangenberg, M. Posselt, H. Bracht, Challenges of Electron Correlation Microscopy on Amorphous Silicon and Amorphous Germanium, Microscopy and Microanalysis (2023) 29 (5), 1579-1594.

453

Strain mapping of a Σ5(310) grain boundary in Cu bi-crystal using scanning transmission electron microscopy

Anoosheh Akbari[1], Dr. Hui Ding[2], Dr. Harald Rösner[1], Dr. Esakkiraja Neelamegan[1], Dr. Christian. H. Liebscher[2], apl. Prof. Dr. Sergiy Divinski[1], Prof. Dr. Gerhard Wilde[1]
[1]University of Münster, Institute of Materials Physics, Münster, Germany, [2]Max-Planck-Institut für Eisenforschung GmbH, Düsseldorf, Germany

Poster Group 2

Background incl. aims
Grain boundaries (GBs) are pivotal in determining the physical characteristics of materials. The presence of extended strain fields localized at GBs can significantly impact atomic transport within these boundaries. Our research focuses on understanding the atomic structure of GBs and its correlation with the strain state along these boundaries. To delve deeper into the influence of strain on GB diffusion, we are investigating the evolution of strain along GBs under mechanical treatment using two distinct methods across varying length scales to establish a connection between microstructure and atomic transport properties.
Methods
A Cu bi-crystal containing a Σ5(310) GB was fabricated using a modified Bridgman technique, followed by annealing at 800 °C. An electron-transparent sample was prepared using FIB lamella target preparation to observe the GB in a cross-sectional view. The elastic strain along and across the GB was measured at the nanometer scale using a stack of nano-beam diffraction patterns (NBDPs) acquired in STEM mode with a 1 nm probe size, while ensuring grains were oriented in zone axis conditions. A custom-written code was utilized to extract the strain maps [1]. On an atomic scale, strain was characterized using the geometrical phase analysis (GPA) applied to high-resolution STEM images, based on measuring small displacements of lattice fringes relative to a reference lattice in the HR(S)TEM images [2].
Results
In the reference state of the pure Cu GB structure, shear strain, dilation, and rotation were measured along and across the GB using the NBDP method. The strain in the vicinity of the GB was found to be negligible (<0.1%). The results were consistent with the GPA method, showing almost constant small values of strain (<0.5%) in both halves of the crystal. These measurements were compared with strain mapping on cobalt-deposited samples.
Conclusion
Strain analysis of the GB in the Cu bi-crystal was conducted using two methods, GPA and NBDP, both of which yielded consistent results for strain across and along the Gb. GPA provided localized information at the nanometer scale, while NBDP offered strain information over a larger area. The strain analysis using GPA was correlated with the high-resolution structure of the GB. The high-resolution image of the GB provided insights into the variation of motifs within the boundary, potentially influencing strain distribution across both crystal halves.

Keywords:

Grain boundary, Strain, GPA, NBDP.

Reference:

[1] Gammer, C., Mangler, C., Rentenberger, C., & Karnthaler, H. P. (2010). Quantitative local profile analysis of nanomaterials by electron diffraction. Scripta Materialia, 63(3), 312-315.

[2] Hÿtch, M. J.; Putaux, J.-L.; Thibault, J. (2006). Stress and strain around grain-boundary dislocations measured by high-resolution electron microscopy. Philosophical Magazine, 86(29-31), 4641–4656. doi:10.1080/14786430600743876

545

Enhancing tool performance with complex microscopy investigation of additively manufactured M2 steel and composites

Ing. Ph.d. Martina Koukolíková[1], Mr. Pavel Podaný[1], Mr. Miroslav Urbánek[1], Mr. Michal Brázda[1], Mrs. Ivana Poláková[1], Mr. Josef Hodek[1]
[1]COMTES FHT a.s., Dobrany, Czech Republic

Poster Group 2

Background incl. aims
The study explores the application of complex microscopy and imaging techniques to investigate the microstructure of M2 steel and carbide-reinforced composites additively manufactured (AM) using powder-based Directed Energy Deposition (DED). Aiming to understand the material's properties and behaviour under various conditions, the research emphasizes the role of microscopic analysis in enhancing tool and material performance. The emergence of additive manufacturing techniques, such as DED using powder feedstock, has opened new avenues for fabricating components with intricate geometries, complex material variations, and tailored properties. M2 steel is renowned for its exceptional mechanical properties, making it a preferred choice for high-speed steels. Carbide-reinforced composites investigate the impact of incorporating different concentrations of tungsten carbide (WC) particles into a high-temperature nickel-based superalloy Nimonic 80A for applications requiring improved wear resistance, such as forming tools. The role of microscopic analyses in the enhancement of manufacturing processes and material performance is emphasized by the research. These insights will serve as a basis for the digitalization of material testing and the development of material models using finite element methods.
Materials and Methods
The materials were fabricated by DED using a INSSTEK MX-600 system, which is equipped with a 2-kW yttrium fibre laser, under a protective atmosphere of argon 5.0 in a direct metal tooling (DMT) mode. By continuously monitoring and adjusting the laser power multiple times per second, the DMT system ensures a consistent layer by automatically reducing or increasing the laser power. The 800 and 1600 modules (laser-beam spot size: 800 µm and 1600µm) were applied. The powders were fed from separate feeders to the nozzle. The average particle size of the powders was declared by the producer to be 50-150 µm. Nevertheless, powder analyses were conducted adhering to the ISO 13320 standard. This methodology facilitated the precise quantification of particle size and particle fraction across designated particle size ranges through the utilization of laser scattering techniques. The metallographic analyses involved a detailed examination and comprehensive evaluation of the microstructural characteristics inherent in the as-built condition. The study delves into the utilization of advanced microscopy and imaging techniques, encompassing both light and electron microscopy techniques coupled with Energy Dispersive X-ray Spectroscopy (EDX) and Electron Backscatter Diffraction (EBSD). These sophisticated techniques were employed to scrutinize the intricate microstructure of additively manufactured tools, particularly with M2 steel and carbide-reinforced composites, enabling detailed analysis of microstructure, potential defects and phase distribution. The evaluation of the WC phase was conducted in accordance with ASTM E562 (2019) standard. Furthermore, confocal laser microscopy was applied to meticulously assess the wear rate.
Results
The microscopic and imaging analyses revealed significant insights into the correlation between the DED fabrication parameters and the resulting material microstructure. Key findings include the identification of optimal processing conditions for achieving desired mechanical properties and the detection of critical microstructural features that influence the material's performance in engineering applications. The incorporation of M2 steel onto the operational surfaces of tools manifests a notable enhancement in tool longevity, predominantly ascribed to its exceptional hardness, resistance to

wear, and capacity to endure mechanical stresses encountered during cold working cutting tools activities. Microstructural examination unveils a martensitic matrix with the presence of complex carbide particles containing Mo, V, Cr and W. Remarkably, these particles faithfully replicate the characteristic cellular structure inherent in additively manufactured materials in as-built states, i.e. after deposition. The resultant hardness attains a formidable 63 HRC.
The research also demonstrates a substantial improvement in tool life, wear resistance, mechanical properties, and microstructural stability with additively manufactured carbide-reinforced Nimonic 80A layer as a functional coating onto the tool steel. The gradual addition of particles (5%, 10%, 15%, and 20%) highlights the potential for WC-doped Nimonic 80A in multimaterial components, particularly in challenging environments of hot forming operations where wear resistance and mechanical strength are critical. The integration of WC into the Nimonic 80A matrix proved successful, yielding significant advantages for the material, while no defects were detected. Additionally, it was observed that the WC particles were uniformly dispersed within the matrix, contributing to the overall homogeneity of the material.
Conclusion
Microscopy and imaging techniques have proven to be pivotal in advancing the understanding of the microstructural characteristics of M2 high-speed steel and WC-doped Nimonic 80A produced via DED. This study not only highlights the importance of these techniques in material science but also sets the groundwork for future research aimed at optimizing metallic materials for various engineering applications. The investigation into the additively manufactured materials highlights its potential for high-performance applications. The findings not only contribute to the digitalization of material testing and the development of predictive material models but also pave the way for optimizing the manufacturing processes of high-performance tools, showcasing the role of microscopy in advancing materials design and application.

Keywords:

additive manufacturing,M2 steel,composites,complex microscopy

548

ACOM characterization of phase transitions during overageing of aluminium alloys using a direct electron detector

Dr Arthur Després[1], Thomas Perrin[1], Dr Pierre Heugue[2], Pr Alexis Deschamps[1], Dr Fréderic de Geuser[1]
[1]Univ. Grenoble Alpes, CNRS, Grenoble INP, SIMaP, F-38000 Grenoble, France, [2]Safran Transmission Systems, Colombes, France

Poster Group 2

Aluminum alloys are notorious for the many phase transitions that can occur during precipitation heat treatment. Distinguishing these phases is challenging because many of them have only slight variations of their composition and lattice parameters. In this work, we characterized by TEM the evolution of the precipitation state during overageing (>1000h) of 2xxx series aluminium alloys. To identify the phases, a combination of automated crystal orientation mapping (ACOM) and energy dispersive X-ray spectroscopy (EDX) is implemented. Using standard ACOM setting (external CCD camera filming the phosphorescent screen) only one phase is identified in the heat-treated samples (the S phase), while using a direct electron detector, two phases are identified (the S and Q). The identification with the direct electron detector is consistent with the EDX observation. The potential benefit of direct electron detector cameras for phase recognition is discussed. We finally discuss how these observations improve the interpretation of complementary characterizations performed on this material, such as small angle X-ray scattering and hardness measurements.

Keywords:

direct electron camera; aluminium alloys

559

Study of metal powders oxidation by means of Energy Dispersion Spectroscopy (EDS)

Dr. Matteo Giardino[1,2], Dr. Federico Simone Gobber[1,2], Mr. Antonio Pennacchio[1], Prof. Marco Actis Grande[1,2]
[1]Department of Applied Science and Technology (DISAT), Politecnico di Torino, Alessandria, Italy, [2]RU Torino Politecnico, Consorzio INSTM, Firenze, Italy

Poster Group 2

Background incl. aims
Energy Dispersion Spectroscopy (EDS) is a very common technique for elemental composition characterization based on the capacity of specimens to produce characteristic X-rays when illuminated by an electron beam.
Different works have already described the possibility of using EDS for the determination of the thickness of metal and oxide thin film. Such approaches usually rely on the simulation of EDS spectra by means of Monte Carlo method-based algorithms.
The aim of this work is to apply EDS for the determination of the thickness of the oxide layer formed onto the surface of copper alloy powder during its storage in order to provide a tool to rapidly assess the “goodness” of the powder and its compatibility with the laser-based additive manufacturing processes.

Methods
Powder of CuAg 3.4 alloy was prepared via a gas atomization process (VIGA) and sieved to obtain a size distribution compatible with additive manufacturing processes by laser bed powder fusion (LBPF) technique.
The powder was then divided into two batches and stored for 1 month under different conditions. In particular, the first batch was stored under dry Argon whereas the second was stored at room conditions.
The chemical composition of the surface of a CuAg 3.4 alloy powder was investigated by means of Raman spectroscopy using a Renishaw InVia Raman confocal microscope using an excitation wavelength of 633 nm. The optical response of the powder was recorded in diffuse reflectance mode (incidence at 0°) using a Shimadzu UV-2600 UV-visible spectrophotometer equipped with an ISR2700 plus integration sphere.
EDS spectra were recorded using a Zeiss EVO 15 SEM equipped with a Peltier-cooled Oxford Ultim Max 40 EDS detector.
EDS spectra of CuAg 3.4 particles coated with different thicknesses of cupric oxide (CuO) layer were simulated using the WinMCXRay.

Results
From UV-Vis and Raman spectra, it was concluded that the inert sample developed a mixed Cu2O/CuO oxide layer of 5.4 nm thickness whereas the oxidized sample exhibited a thicker layer (15.3 nm) composed mainly of CuO.
Using the WinMCXRay tool, the EDS spectra of CuAg 3.4 particles coated with an oxide layer of different was simulated, and the γ was defined as the ratio between the x-ray count at 0.525 keV (Cu Kα) and 0.931 keV (Cu Lα).
EDX spectra of the two samples were collected under different beam acceleration tension conditions in the range from 3 kV to 12 kV, using a beam current of 800 pA.

After background removal, the value γ was calculated on the experimental spectra and the obtained value was compared with the simulated data to determine the oxide layer thickness t_CuO. For simplicity, we assumed that the oxide layer is composed of CuO only.
We obtained a value of t_CuO=4.6 nm and t_CuO=16.1 nm for the inert and oxidized samples, respectively.

Conclusion
Energy dispersion spectroscopy was revealed to be a very useful and effective tool for assessing the extent of surface oxidation on metal powder. The oxide layer thickness evaluated by EDS are in good agreement with the estimation obtained from the UV-visible measurements and confirm the validity of the adopted procedure.
The possibility of measuring the oxide thickness without the need for more expensive and complicated instruments is of utmost importance in both academic and industrial contexts.

Keywords:

Metal powders, Energy Dispersion Spectroscopy

Reference:

[1] A. Franquet, T. Conard, M. Gilbert, T. Hantschel, and W. Vandervorst, “Thickness and Composition Measurements of Nanoelectronics Multilayer Thin Films by Energy Dispersive Spectroscopy (EDS),” J. Phys.: Conf. Ser., vol. 417, no. 1, p. 012033, Mar. 2013, doi: 10.1088/1742-6596/417/1/012033.
[2] R. Gauvin, E. Lifshin, H. Demers, P. Horny, and H. Campbell, “Win X-ray: A New Monte Carlo Program that Computes X-ray Spectra Obtained with a Scanning Electron Microscope,” Microscopy and Microanalysis, vol. 12, no. 1, pp. 49–64, Feb. 2006, doi: 10.1017/S1431927606060089.
[3] R. Williams, M. Bilton, N. Harrison, and P. Fox, “The impact of oxidised powder particles on the microstructure and mechanical properties of Ti-6Al-4 V processed by laser powder bed fusion,” Additive Manufacturing, vol. 46, p. 102181, Oct. 2021, doi: 10.1016/j.addma.2021.102181.

678

Investigating microstructural phenomena in Additive Manufactured metals through high temporal thermal cycles in-situ heating

Dr. Alice Bastos da Silva Fanta[1], Yi-Chieh Yang[1], Christina Koenig[1], Prof. Joerg Ralf Jinschek[1]
[1]DTU Nanolab, Kgs. Lyngby, Denmark

Poster Group 2

Background incl. aims:
Additive manufacturing (AM) of metal components holds significant potential for delivering customized design, improved flexibility, and cost-effective production. However, controlling the microstructure-defined properties of AM components is a major challenge due to the inherent complexity of extreme thermal processes that form the AM microstructures. Material solidification and solid-solid phase transformation occur under far-from-equilibrium [1] conditions in cyclic layer-by-layer processes. Accordingly, established phase diagram predictions are not significantly relevant for understanding and predicting the phase formation and their consequences for the component properties. Real-time observation of microstructure evolution during AM thermal cycles at sub-µm resolution is therefore crucial for controlling microstructure related properties of AM components, as well as for exploring “unusual” microstructure formations, leading to new and exciting properties.

Methods:
In-situ electron microscopy studies offer the potential to investigate such microstructure phenomena with resolution ranging from mm down to sub-nm. However, achieving extreme thermal profiles, such as those occurring during AM process inside a microscope are not trivial.
Micro-heating devices, based on microelectromechanical systems (MEMS) combine very fast (10^3 ^{o}C/s) heating and cooling rates with high stability [2] and are potentially able to reproduce the thermal cycles of AM process. However, they were primary developed for studies of electron transparent samples smaller than 20 µm in transmission electron microscopy (TEM).

Results:
In this work we will present our efforts in exploring the high heating rates of MEMS heaters to mimic the thermal cycles of AM process inside the scanning electron microscope (SEM) and in the TEM. Supported by computational modelling (COMSOL) and indirect measurements such as Raman spectroscopy, we investigated the limits and the accuracy of MEMS heaters depending on e.g. sample size, environment, and heating rate and will discuss the prospect and limits of this approach. Furthermore, we will present the first electron backscatter diffraction (EBSD) and transmission Kikuchi diffraction (TKD) results demonstrating the potential of correlating microstructure characteristics with non-equilibrium phase transition during AM process.

Conclusion:
Our findings provide deeper understanding and highlight the potential of simulating AM thermal cycles inside the electron microscope using MEMS heater both in the TEM and in the SEM. Specially for metallic specimens, our results shows the capability of replicating ramping rates and temperature gradients inherent to AM processes within the electron microscope, thereby enabling the correlation of microstructural characteristics with phase transitions with spatial resolution varying from sub-nm to µm. This work contributes to advancing the understanding of simulating AM thermal cycles within the electron microscope, offering opportunities for enhanced characterization and analysis of materials under extreme heating conditions.

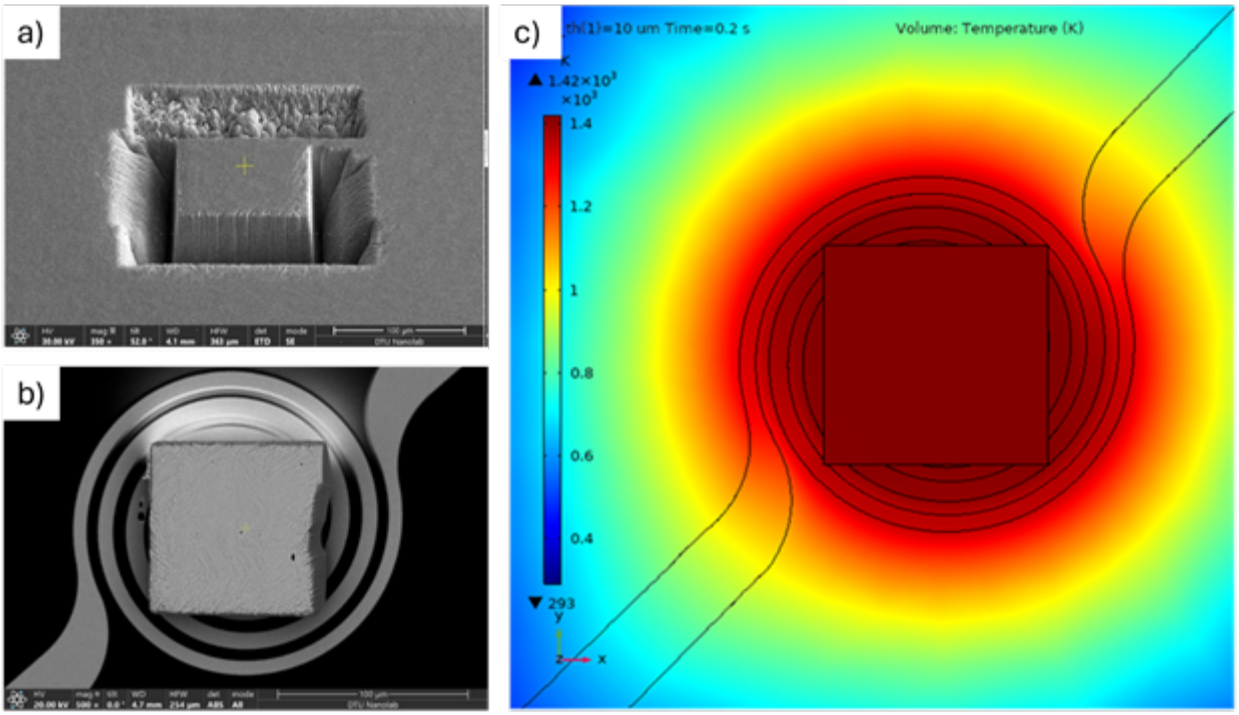

Figure 1: a) Block lift-out sample for mimicking AM-thermal cycles inside the SEM. b) MEMS-heater with stainless steel sample for in-situ thermal cycles in the SEM. c) COMSOL simulations showing fast and homogeneous heat response at the sample surface.

Keywords:

In-situ, MEMS-heater, Additive Manufacturing, SEM

Reference:

Reference

1. Ren, N. et al. Solute trapping and non-equilibrium microstructure during rapid solidification of additive manufacturing. Nat. Commun. 14, 1–13 (2023).
2. Wildffire, D. solution. No Title. https://denssolutions.com/products/wildfire/#brochure.

701

TEM study of neutron radiation damage in tungsten

Dr. Michael Klimenkov[1], Ute Jäntsch[1], Michael Rieth[1], Hans-Christian Schneider[1], Wouter Van Renterghem[2], Dmitry Terentyev[2]
[1]Karlsruhe Institute of Technology, 76344 Eggenstein-Leopoldshafen, Germany, [2]SCK CEN, Nuclear Materials Science Institute, Boeretang 200, 2400 Mol, Belgium

Poster Group 2

Nuclear fusion provides a safe and abundant source of energy for a long period of time and offers several important additional advantages. These include: fusion does not contribute to greenhouse gas emissions or global warming (a), reduction of long-lived radioactive waste compare to the nuclear fission reactors (b) and inherent safety features (c). Tungsten (W) is considered a promising plasma-facing material for future fusion reactors since it has number of advantages such as high melting temperature, excellent thermal conductivity, high strength and low sputtering yield. Its application in the International Thermonuclear Experimental Reactor (ITER), which is being built in Cadarache, France, and in the future Demonstartion Power Plant (DEMO) has significantly increased interest in W behavior under neutron irradiation. Knowledge about the defect formation and their evolution in neutron irradiated W is essential not only for assessing its applicability as a structural material in fusion reactors, but also for understanding numerous irradiation experiments in fission reactors.
ITER grade W was neutron irradiated in the BR2 material test reactor (Mol, Belgium) at 600°C, 800°C, 900°C and 1200°C to a damage dose of 0.1 dpa, 0.2 dpa, 0.5 dpa and 0.8 dpa. The microstructure of the irradiated material was analyzed using the Talos F200X transmission electron microscope (TEM), which is equipped with four energy-dispersive X-ray detectors (Super-X). The precipitates were detected either by high resolution TEM or by EDX elemental mapping, where they are visible in elongated shape.
The detailed TEM characterization of the radiation-induced materials shows the formation of three types of defects, e.g. voids, dislocation loops and nano-sized precipitates. The source of the precipitates are the transmutation-induced elements such as rhenium (Re) and osmium (Os), which accumulate with the damage dose [1]. In addition, a dose-dependent segregation of Re and Os, i.e. the formation of clusters around defects, was observed [2].
The results of the TEM analysis are summarized in Figure 1. The parts (a) and (b) show the voids and dislocation loops formed in W under neutron irradiation. The voids have a round or almost round shape, but in a few cases faceted voids with a size of 3-4 nm have been observed (a). Dislocation loops are typically visible in DF images obtained using a defined g-vector with a “coffee bean” contrast (b). Most loops are between 3 and 10 nm, but individual loops can be up to 20 nm. The number density of dislocation loops at 0.1 dpa and 0.2 dpa is comparable to the number density of voids (about 1022 m-3), while for material irradiated to 0.5 dpa and higher, the number density is reduced by about two orders of magnitude.
Spatial distribution of Re and Os segregation was studied by STEM-EDX element mapping in the TEM, where their local presence was visualized by intensity variations of the different colors. The part (c) demonstrates the distribution of Re (green) in representative areas in the material. The clear segregation was observed at the grain boundaries, line dislocations and radiation-induced voids and loops. At 0.1 dpa and 0.2 dpa, the Re distribution was detected only around the voids, while the Re signal at the dislocation loops was seemingly below the detection limit. There was no Os signal detected in 0.1 dpa damage, while a weak Os signal was detectable in the material with 0.2 dpa. At 0.5 dpa and 0.8 dpa, Re and Os were detected around voids and loops.
The detailed analysis of Re and Os segregation on defects in the sample irradiated to 0.8 dpa is shown in Figure 1d-g. The distribution of Re (green) and Os (blue) are visualized in corresponding

elemental maps (d and e) and shown overlapped in the part (f). The overlapping clearly show that Os tends to form small rich areas inside Re clouds which mostly have a spherical shape. Os-rich areas often have a needle-like shape, indicating the formation of precipitates or their precursor. These Os-rich areas are formed on both voids and dislocation loops.
To provide a detailed visualization of the Os distribution, the intensity profiles were recorded across voids and loops. The example of segregation around a void marked by a yellow arrow is shown in part (d-e). The profile (g) was taken through the void marked with the arrow. It shows the typical reduction in Re-intensity at the void position and the formation of elongated, Os-rich regions adjacent to the void on one side. In the few cases the crystallinity of the precipitate was detected. The atomic spacing of 0.23 nm could correspond to the [111] atomic plane of the ?-WRe2 phase.
The study includes a detailed TEM characterization of the radiation-induced defects, which can be divided into three types, e.g. voids, dislocation loops and precipitates. In addition, a dose-dependent segregation of Re and Os, i.e. the formation of Re rich clusters around defects, was observed.

Figure 1: Extensive TEM analysis of radiation damage in W. TEM images of voids and dislocation loops a shown in parts (a) and (b) correspondingly. Part (c) visualize the Re-segregation on defects, dislocations and grain boundaries. Parts (d-g) demonstrate the analysis of Re- and Os-segregation on defects.

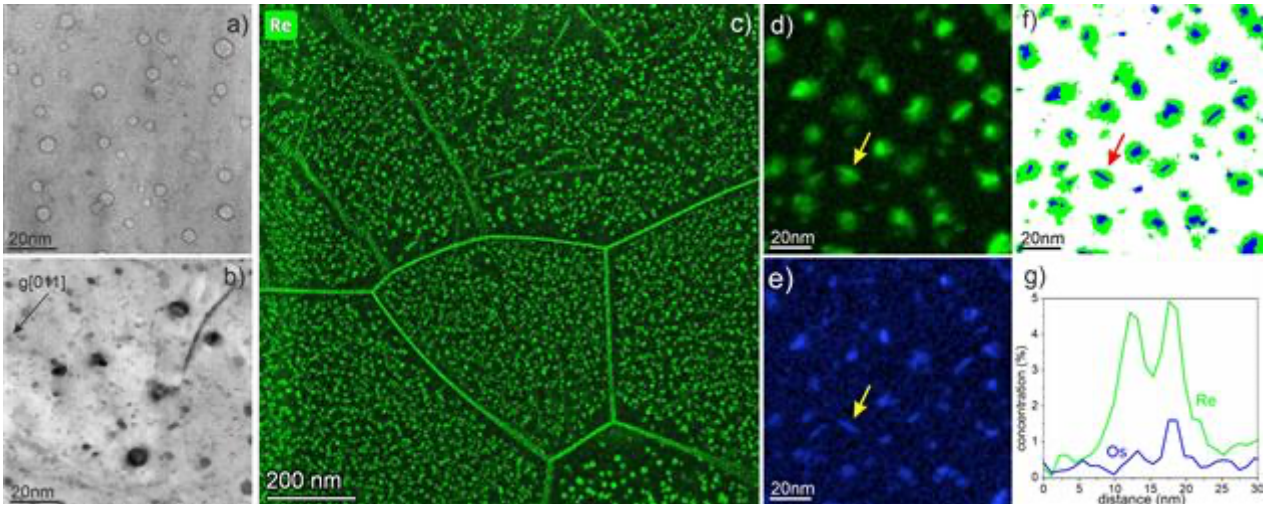

Keywords:

fusion, tungsten, radiation damage, transmutation

Reference:

[1] M. Klimenkov, M. Dürrschnabel, U. Jäntsch, P. Lied, M. Rieth, H.C. Schneider, D. Terentyev, W. van Renterghem, Microstructural analysis of W irradiated at different temperatures, Journal of Nuclear Materials 572 (2022) 154018. https://doi.org/10.1016/j.jnucmat.2022.154018.
[2] M. Klimenkov, U. Jäntsch, M. Rieth, H.C. Schneider, D. Terentyev, W. van Renterghem, Influence of transmutation-induced Re/Os content on defect evolution in neutron-irradiated W, Journal of Nuclear Materials 592 (2024) 154950. https://doi.org/10.1016/j.jnucmat.2024.154950.

739

The fatigue response of the IN939 superalloy prepared by additive manufacturing

Ivo Kuběna[1], Markéta Gálíková[1], Ivo Šulák[1]
[1]Institute of Physics of Materials, Czech Academy of Sciences, Brno, Czech Republic

Poster Group 2

Background incl. aims
Ni-based superalloys have become a time-honored high-temperature material. The first steps in their development were directed towards optimizing the manufacturing processes, chemical composition, and microstructure. The additive manufacturing (AM) technologies, also commonly called 3D printing, emerged and changed some classical approach. AM offers several advantages such as design freedom, very good efficiency of material usage, possibility to create hierarchical structures, crystallographic texture etc. Recently, the parameters of Laser Powder Bed Fusion (L-PBF) were optimized for the nickel based superalloy IN939. The main aim of the contribution is to address fatigue and thermomechanical fatigue (TMF) properties to the specific microstructure of the IN939 prepared by the L-PBF.

Methods
Microstructural analysis was performed by the mean of scanning and transmission electron microscopy. The Tescan Lyra 3 FEG/FIB scanning electron microscope equipped by the energy dispersive spectroscopy and backscattered electron diffraction detector (EBSD) was used the microstructural analysis, texture measurement and grain size evaluation. The Talos 200i transmission electron microscope equipped by the energy dispersive spectroscopy was adopted for the analysis of typical cell structure and strengthening particles.
The material was prepared by AM method. To achieve ideal microstructure, the IN939 was exposed to three-step heat treatment: solution annealing at 1175°C for 45 minutes followed by two step precipitation hardening 1000°C/6h + 800°C/4h.
The isothermal fatigue at 800 °C with symmetrical push-pull cycle was measure. The two modes of TMF, in-phase and out-of-phase loading were used for testing. During in-phase loading, the maximum mechanical loading corresponds to the maximum temperature, while in the out-of-phase mode, the maximum temperature corresponds to the minimum loading.

Results
Microstructural analysis revealed elongated grains with a preferential orientation <001> parallel to building. IN939 incorporates a considerable amount of a reinforced gamma prime phase that is embedded coherently within the matrix.
The fatigue properties at 800 °C and response to the TMF loading were measured. Obviously, the TMF is more detrimental than pure fatigue in very low cycle region, especially the in-phase TMF loading. The differences between particular loading modes decreases with decreasing strain amplitude. The EBSD measurement revealed no grain coarsening or changes in crystallographic texture. The fatigue cracks propagated predominantly along grain boundaries.

Conclusion
Following conclusion based on obtained results can be drawn :
- The typical AM microstructure consist of dislocation cells with crystalographic texture was revealed.
- The In-phase TMF mode seems to be most damaging in very high strain amplitude region, while the diffences in fatigue life in low strain amplitude region are almost negligible.

- The crack propagation path along grain boundaries was documented.

Acknowledgement:
This publication was supported by the project "Mechanical Engineering of Biological and Bio-inspired Systems", funded as project No. CZ.02.01.01/00/22_008/0004634 by Programme Johannes Amos Commenius, call Excellent Research and by the project 23 - 06167S by Czech Science Foundation.

Keywords:

IN939 superalloy, fatigue, additive manufacturing

760

Gallium liquid bridge evolution on varied substrates

Le Shu[1], Ningyan Cheng[1], Long Ren[2], Binghui Ge[1]
[1]Institutes of Physical Science and Information Technology, Anhui University, Hefei, China,
[2]International School of Materials Science and Engineering, Wuhan University of Technology, Wuhan, China

Poster Group 2

Room-temperature liquid metals (LMs) with high conductivity and deformability have received considerable attention in soft and stretchable electronics [1]. In recent years, there has been extraordinary progress in the fabrication of LM-based elastic circuits such as embedding LM particles in an elastomer, mixing LMPs with a solid conductive filler composite, doping LMPs in a polymer matrix, etc. [2]. The formation and separation of liquid bridges between LM particles correspond directly to the connection and disconnection processes of these components, respectively. Hence, unveiling the kinetics of liquid bridge formation and evolution is crucial for achieving controllable design of stretchable LM-based conductors in the assembly of electronic components, thus propelling the development of electronics with enhanced flexibility and adaptability.
Herein, we employed in-situ transmission electron microscopy (TEM) techniques to systematically investigate the wetting behavior between Gallium (Ga), a typical liquid metal, and various substrates, as well as the influence of surface Ga oxide layer thickness on the evolution of Ga liquid bridge formation. As a demonstration, Figure 1 illustrates the dynamic evolution process of Ga liquid bridges on Mo substrates. Our findings indicate that the presence of a thin oxide layer promotes the fluidity of gallium, thereby facilitating the formation of liquid bridges, with their evolution being influenced by interfacial wettability dynamics. Moreover, a delicate equilibrium between viscoelasticity and surface tension emerges with a slight increase in the thickness of the surface oxide layer, resulting in the formation of super-stretched liquid bridges. In contrast, an excessive thickness of the oxide layer constrains the formation of liquid bridges due to its high viscoelasticity.

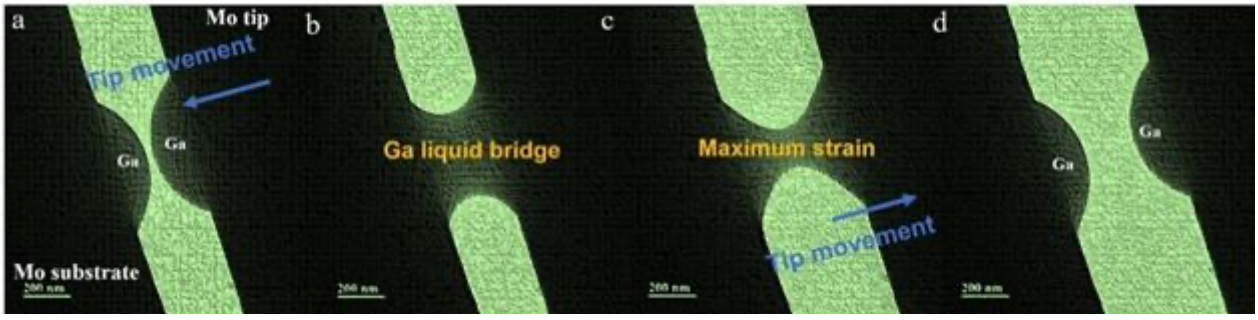

Keywords:

Liquid metal, liquid bridge, Wettability

Reference:

[1]. Y. Lin, J. Genzer, M. D. Dickey, Adv. Sci. 2020, 7, 2000192.
[2]. W. Lee, H. Kim, I. Yang, H. Park, J. Jung, H. Lee, J. S. Park, J. M. Yuk, S. Ryu, J. -W. Jeong, J. Kang, Science 2022, 378, 637.

771

Microstructure and thermal stability of ultrafine-grained CuZn5 processed by HPT

Yuting Dai[1,2], M.Sc. Marcel Sos[2], Prof. Christian Kübel[1,2]
[1]Institute of Nanotechnology, Karlsruhe Institute of Technology, Karlsruhe, Germany, [2]Department of Materials and Earth Sciences, Technical University Darmstadt, Darmstadt, Germany

Poster Group 2

Background and aims:
High-pressure torsion (HPT) is widely known as an effective method for severe plastic deformation (SPD). This intense shear strain, combined with high pressure, not only results in notable grain refinement but also introduces a substantial density of dislocations, thereby enhancing mechanical strength [1].
Concurrently, ensuring the stability of ultrafine-grained (UFG) microstructures is crucial for their reliable performance in practical applications. Grain growth can compromise the enhanced strength of UFG materials, highlighting the importance of investigating microstructural stability for their commercial feasibility [2].
This concern is particularly notable in certain pure metals with low stacking fault energy such as fcc metals. In order to avoid grain growth, the grain boundary (GB) migration has to be limited. This can be done through the segregation of solute elements, which depends on the GB character. In this work, we use copper (Cu) as bulk material and add different amounts of Zn to examine the impact of varying Zn content on microstructural changes and thermal stability of GBs after HPT processing at room temperature.

Methods:
CuZn5 solid solutions were processed using HPT with a pressure of 4.5 GPa. The thermal behaviors of these materials were studied using differential scanning calorimetry (DSC). Scanning transmission electron microscopy (TEM) in combination with energy dispersive X-ray spectroscopy (EDX) was used to investigate the microstructure and composition of Cu-5at.%Zn (CuZn5), with a focus on GB segregation before and after annealing at different temperatures. Additionally, 4D-STEM (ACOM) was utilized to extract information on grain size distribution, grain orientation, and grain boundary types.

Results:
Annealing of CuZn5 up to 300°C by DSC shows a single exothermic peak at about 275°C. it should be mentioned that no grain growth or changes in the grain orientations occurred up to 200°C. High-angle annular dark-field (HAADF)-STEM imaging helps to understand the effect of Zn on the microstructure and GBs. From the 4D-STEM orientation mapping, the GBs can be classified into low-angle GBs, special coincidence site lattice (CSL) boundaries as well as high-angle general GBs. Together with STEM-EDX, it was found out that low energy boundaries such as Σ3 twin boundary is not enriched by Zn. On the other hand, Zn general GBs are segregated with Zn. This observation agrees well with the theory that solute segregation depends strongly on the GB energy. While special Σ-boundaries have low energy, they are less affected by solute segregation.
Conclusion:
CuZn5 maintains a single-phase structure even after annealing, suggesting that the improved thermal stability of the alloys compared to pure Cu is attributed to the presence of solute content. This is due to the solute-drag effect [3], hindering the diffusion of GBs and contributing to the enhanced thermal stability of the alloys

Keywords:

Cu alloys; HPT; DSC; ACOM

Reference:

[1] Mohamed F.A., et al., On the minimum grain size obtainable by high-pressure torsion. Materials Science and Engineering: A, 2012. 558. p. 59-63
[2] Bruder, E., et al., Influence of solute effects on the saturation grain size and rate sensitivity in Cu-X alloys. Scripta Materialia, 2018. 144. p. 5-8
[3] Ayush S., et al., Solute drag assessment of grain boundary migration in Au. Acta Materialia, 2022. 224. 117473

787

Microstructural assessment of mechanically alloyed low activation 9-Cr oxide-dispersion strengthened steels

Dr. Michael Thomas Duerrschnabel[1], Dr. Carsten Bonnekoh[1], Ute Jäntsch[1], Siegfried Baumgärtner[1], Henning Zoz[2], Dr. Michael Rieth[1]
[1]Karlsruhe Institute of Technology (KIT), Institute of Applied Materials, Hermann von Helmholtz Platz 1, Eggenstein-Leopoldshafen, Germany, [2]Zoz Group, Maltozstraße, Wenden, Germany

Poster Group 2

Background incl. aims
In the foreseeable future, it will become more and more necessary to boost energy efficiency to tackle challenges imposed by climate change. Therefore, higher process temperatures are fundamental. Oxide dispersion strengthened (ODS) steels can meet these requirements since they were developed as structural materials in extreme environments such as for example gas turbines, aerospace applications, and nuclear fusion reactors [1]. The latter application limits the use of acceptable elements to those exhibiting low activation [2].
ODS steels represent a class of advanced structural materials that possess compared to conventional type steels superior high-temperature strength and stability. The origin of these exceptional performance lies in their micro and nanostructure, which is characterized by a fine dispersion of nanoscale oxide particles in the steel matrix. These oxide nanoparticles hamper the motion of dislocations and grain boundaries by pinning. Typical oxide nanoparticles consist of Y_2O_3, Y-Ti oxides, Al_2O_3 or similar stable oxides [3].
Electron microscopy is used to characterize grain sizes as well as the size, number densities, structure and chemistry of oxide nanoparticles [3]. Additionally, unwanted nanoscale process remnants need to be monitored.
The aim was to study the mechanical performance as well as microstructure of the ODS steel to reduce the time required for mechanical alloying. When scaling to industrial-scale quantities this helps to reduce production costs.

Methods
Several kilograms of ODS material (Fe-9Cr-1W-0.2Ti+Y_2O_3) was processed by mechanical alloying of the powder under Ar atmosphere in a Simoloyer CM20 and after 5 h, 15 h, and 25 h milling time material was extracted. Afterwards, the material was HIPed at 1150°C and 100 MPa. Each material was tested for hardness and yield strength. Finally, the samples were analyzed by scanning and transmission electron microscopy using a Zeiss Merlin and a Thermofisher Talos F200X. Mainly, electron-backscatter diffraction (EBSD), energy-dispersive X-ray analysis (EDX) and electron energy-loss spectroscopy (EELS) were used.

Results
EBSD maps were employed to determine the grain sizes across different milling times using OIM Analysis. It was found that there is no significant variation in the grain sizes with milling time. In numbers, the average grain size evolved just slightly between 4.6 µm (5 h) and 4.8 µm (25 h) if evaluation with respect to number fraction was chosen.
Thus, TEM experiments were carried out to investigate the nanostructure of the materials and to look for trends depending on the milling time. STEM-EDX elemental mapping revealed that a trend that ODS particles split into two types at short milling times: Y-rich and Ti-rich, whereas at longer milling times (> 15 h) Y-Ti oxides are observed. Average ODS particle sizes and particle number densities extracted from STEM-EDX elemental mappings are between 25 nm and 50 nm and in the

order of 10^{20} particles per m^3 for all samples. The ODS particle size increases from 25 nm at 15 h to 50 nm at 25 h milling time whereas the number densities seem not to depend on the milling time. However, it was also found for all analyzed samples that the distribution of ODS particles is not homogeneous in all grains. In some sample regions, fine ODS particles are present inside grains whereas coarser particles are observed at grain boundaries. A meticulous analysis by EDX and EELS of single ODS particles at higher magnification revealed that some can have a complex chemical structure.
Additionally, the presence of Al-containing nanoparticles was noted, likely stemming from unintentional introduction during the production process. Moreover, nanometer-sized Ar bubbles, attributed to milling in an Ar atmosphere, were observed adhering to ODS particles. These bubbles exhibited an increasing number density with milling time, while maintaining a consistent average size.
Further analysis revealed a few micrometer-sized $M_{23}C_6$-type precipitates in some areas on the sample that can be attributed to excess carbon.
Tensile tests were conducted within the temperature range of 500°C and 800°C. The obtained yield strengths were about 350 MPa and 160 MPa for 500°C and 800°C, respectively. Hardness measurements exhibited no discernible correlation with milling time.

Conclusion
Electron microscopy revealed that a milling time between 5 h and 25 h does not change the microstructure significantly. ODS particle distribution varied, with finer particles within grains and coarser ones at boundaries. TEM revealed Y-rich and Ti-rich particles initially, transitioning to Y-Ti oxides with longer milling. ODS particle number densities showed no significant change with milling time. Some ODS particles had complex chemical structures. However, unintentionally introduced elements like Al or process-related elements like Ar must be closely monitored to ensure material quality and performance of the ODS steel.
Mechanical performance of the ODS material exceeds that of ODS-free material by roughly a factor of 3 at all temperatures.
Thus, the milling time could be reduced in a future industrial ODS steel production process.

Keywords:

ODS, TEM, SEM, mechanical properties

Reference:

[1] Zinkle et al., Nuclear Fusion 57 (2017), 092005.
[2] Möslang et al., International Journal of Materials Research 99 (2008), pp. 1045-1054.
[3] He et al., Journal of Nuclear Materials 501 (2018), pp. 381-387.

803

Analysis of fire gilding on medieval jewellery using focused ion beam

Jan Manak[1], Jan Duchon[1], Estelle Ottenwelter[2]
[1]Institute of Physics of the Czech Academy of Sciences, Prague, Czech Republic, [2]Institute of Archaeology of the Czech Academy of Sciences, Prague, Czech Republic

Poster Group 2

Fire gilding was a frequently used decorative method in the manufacture of medieval jewellery. Standard metallographic preparation of gilded samples often results in deformation of soft gilded layer resulting in an altered microstructure. For that reason, focused ion beam (FIB) milling is particularly well adapted since it allows to obtain damage free cross-section cuts to analyse fragile gilded layer as demonstrated by previous studies on hollow spherical pendants known as gombiky from the 10th century [1]. To compare the skills of the craftsmen in fire gilding in terms of thickness and porosity on other gombiky, more specimens from the same archaeological context were investigated. A characterisation of the gilding layer was also performed to determine the sublayer structure observed in previous studies [1] and to distinguish different metallic phases present in the gilding layer.
Microstructure was examined by scanning electron microscopy (SEM). Energy dispersive spectroscopy (EDS) and electron backscatter diffraction (EBSD) were used to determine chemical composition and crystallographic structure of gilded layers. Samples were then further investigated in more detail by transmission electron microscopy (TEM). Automated crystal orientation mapping (ACOM) was used for thorough examination of the sublayers.
The analysis revealed that gilded layer consists of several Au-Hg-Cu-Ag phases and Cu-Ag precipitates. Amorphous silicon residual from final polishing of gombiky after fire gilding process is also present in the microstructure of gilded layer. Furthermore, it is shown that there is a sublayer gold structure formed on interface between gilded layer and copper substrate. This sublayer is also visible around voids in gilded layer which are created by evaporation of mercury during fire gilding process.
The precise characterisation of gilding layers revealed different quality of the layers; therefore, confirming different level of skill and knowledge of craftsmen in fire gilding. The two-layer structure of the fire gilding layer was observed in all cases. Further information concerning the metallic phases present in the gilding were evidenced.

Keywords:

Fire gilding, Focused ion beam

Reference:

[1] E. Ottenwelter, C. Josse, A. Proietti, L. Robbiola, Fire gilding investigation on early medieval copper-based jewellery by focused ion beam (FIB) on FEG-SEM, Journal of Archaeological Sciences: Reports 46 (2022), 103602

812

Structure of refractory high entropy alloy and high entropy nitride thin films

Doctor Dimitri Litvinov[1], Doctor Michael Stüber, Professor Sven Ulrich[1], Professor Jarir Aktaa[1]
[1]Institute for Applied Materials, Karlsruhe Institute of Technology, Eggenstein-Leopoldshafen, Germany

Poster Group 2

Refractory high entropy alloy and nitride films have attracted attention due to their versatile properties, such as satisfactory mechanical properties, excellent anti-oxidation performance, outstanding corrosion resistance, and vitally important thermostability, indicating high application potentials. In this work, microstructural characterization of VCrNbMoTaW (high entropy alloy - HEA) and (VCrNbMoTaW)N (high entropy nitride - HEN) thin films was carried out by scanning (SEM) and transmission electron microscopy (TEM). The thin films with thicknesses of ca. 5 µm were grown by magnetron sputtering from a multiple-elemental compound target. Cross-section TEM samples were prepared using focus ion beam. For the determination of the thin film composition, energy-dispersive X-ray (EDX) spectroscopy was used. For the crystallographic investigations, conventional TEM with selected area diffraction and high resolution TEM imaging (HRTEM) with fast Fourier transformation (diffractogram) were applied.
SEM-investigation of the surfaces of HEA and HEN thin films shows that the two materials exhibit different surface topographies with significantly different size of the growth features. As further TEM observation shows, they are columns with diameter on the surface much larger for HEA layer (more then 1 µm) than for HEN layer (up to 0.14 µm). The columns in HEA film are not always perpendicular to substrate surface and are elongated in <112> direction. The width of the grains increases in the growth direction and reaches a few hundred nm for the HEA films. EDX measurements on the surface in SEM show almost equal atomic concentrations of all 6 metallic elements in both layers: for HEA thin films, the individual elemental concentrations are around 16-17 %, and for HEN thin films all metal concentrations are between 9 and 11%. The measured N-concentration in HEN is ca. 42-43 at.%. EDX-maps of the surfaces in SEM (on large scale of a few µm) and in cross-section samples in TEM (on small scale of a few nm) of both HEA and HEN thin films show homogeneous distribution of all elements, also of nitrogen in HEN layer. It is found, that HEA thin films exhibit a body-centered cubic (BCC) structure with a lattice parameter of a=0.313 nm.
Incorporating Nitrogen in the 6-component HEA thin film leads to a change of the crystal structure of the HEN thin films. Figure 1 shows HRTEM images of a HEN thin film with evaluated (left hand side) and simulated (right hand side) diffractograms from areas 1-3 of the HRTEM images. The corresponding enlarged filtered point patterns of areas 1-3 are displayed in insertions of the HRTEM images. The evaluations indicate that the HEN thin film has a face-centered cubic (FCC) structure with a lattice parameter of a=0.425 nm. The areas 1-3 in Figure 1 exactly correspond to [111] (area 1), [001] (area 2) and [110] (area 3) zone axes orientations. As for the HEA thin films, we observe for the HEN thin film again a columnar growth, but with a much smaller columnar width of a few tens nm and extension in <110> direction. The length of columns in the HEN thin film is also much smaller (ca. a few hundred nm) in comparison with the HEA thin film (a few µm). As we can see in Figure 1, the width of the columns, which are limited by white dotted lines, increases in the growth direction. Moreover, the existence of 6 forbidden reflections (on the blue dashed circle) in diffractogram of [111]-zone axis orientation from area 1 in Figure 1 can be explained by diffraction from very small and misorientated grains of the HEN thin film. These reflections correspond to ¼ {422} of the first Laue zone. Due to the existence of very small and strained grains, we observe for the HEN thin film a misorientation of sub-grains inside columns of up to 18 °. Different defects observed in both HEA and HEN thin films, such as dislocations and stacking faults were also analysed in this work. For the HEN thin film, we detect (111) stacking faults, which are typical for FCC structure.

Thus, incorporating of Nitrogen in high entropy alloy film leads to a change in the crystal structure from BCC to FCC, a decrease in grain the size with large misorientations and the introduction of many different defects.

Figure 1. HRTEM images of HEN thin films with evaluated (left) and simulated (right) diffractograms from areas 1-3 and corresponding enlarged filtered point patterns of areas 1-3 (insertions).

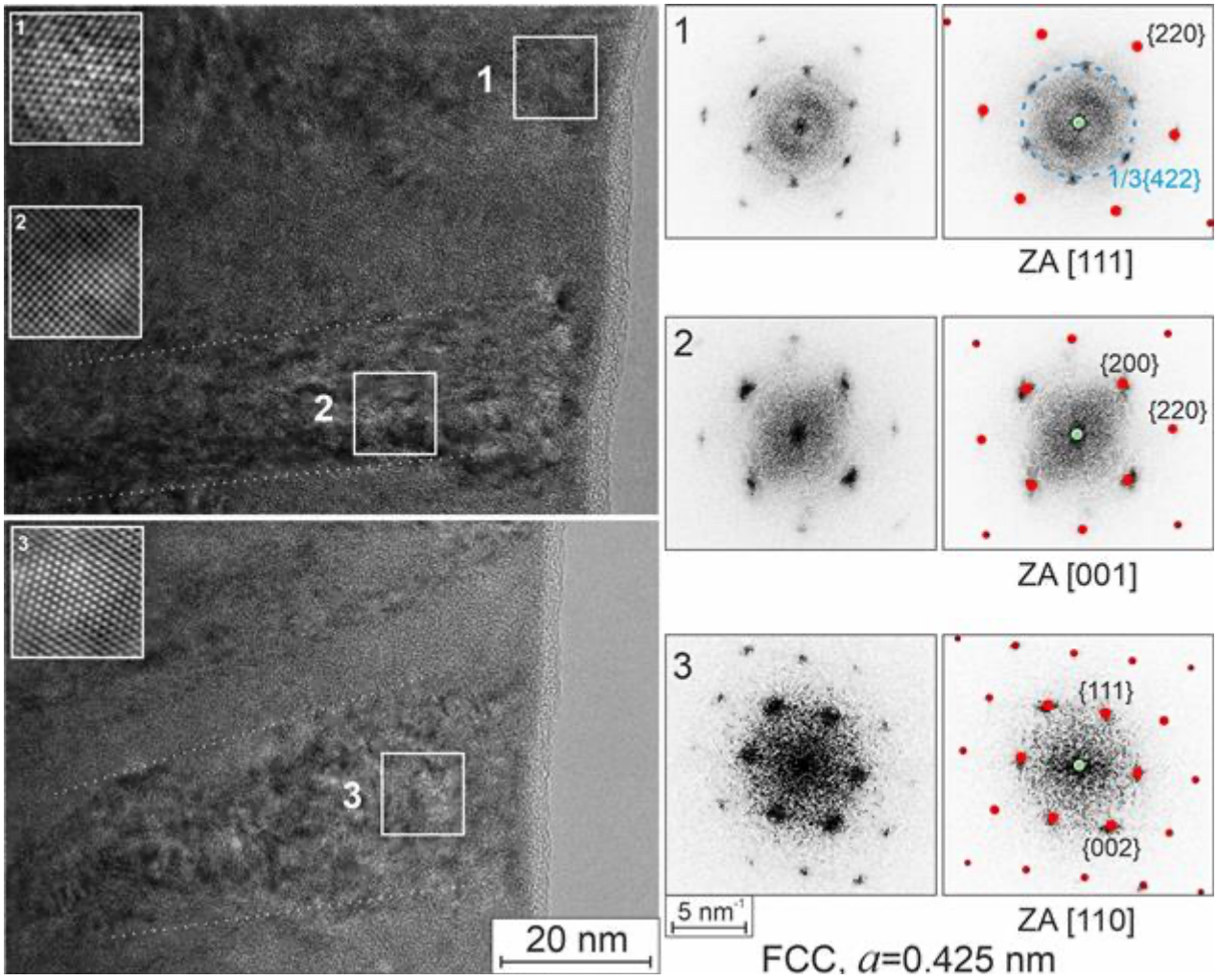

Keywords:

High entropy alloy

836

Automated Detection of Material Defects for High-throughput Electron Micrographs Analysis

Andrei Tudor Durnescu[1], Sotero Pedro Romero Morón[1], Christina Nicole König[1], Joerg R. Jinschek[1]
[1]Danish Technical University, Lyngby-Taarbaek, Denmark

Poster Group 2

Background

Detailed analysis of material's microstructure is required for predicting material properties and fine-tuning manufacturing parameters to achieve the desired characteristics. This feedback process is particularly important when it comes to developing new production techniques such as metal additive manufacturing (AM).
Our goal is to provide a holistic solution that enables reliable materials characterization using a high - throughput approach in a scanning electron microscope (SEM) with automatic detection of characteristic microstructural features, especially defects such as cracks and pores. The scope of the detection framework that we cover includes all aspects of pre-processing the raw images from the microscope, defect identification and visualization of statistical results. In this way, it serves to overcome the current need for automation, providing researchers with a transparent and customizable process for their structural analysis. The customizable definitions of the parameters used in our algorithm also enable optimizations for applications in other fields of imaging, such as optical microscopy in biomedical research.

Methods

We acquired large-area secondary electron (SE) and backscattered electron (BSE) SEM images of an additively manufactured metal sample (316L steel) thereby varying dwell times from 10 microseconds to 100 nanoseconds and pixel size (i.e. magnification) from 391 to 49 nm. This allowed us to develop our image analysis algorithm to identify structural defects across a wide range of imaging conditions and systematically investigate the loss of precision in detection as image acquisition time was lowered (i.e. lower dwell time, larger pixel size). Once the micrographs were acquired, they were passed through a boundary detection procedure which isolates the relevant sample area. Filtering was then performed using multiple thresholding and convolution layers.

Results

Preliminary results have shown great promise in comparison to the manually labelled sections and flexibility to different imaging conditions. Performance metrics have also been compared with the most widely used classical tools in the field as well as with AI tools with which our software overlaps in scope.
The defects were characterized and selected according to user specifications in order to output statistical results and sample descriptors directly from the software interface. The robustness of the detection process has been verified using methods including comparisons with manually labelled sections and results obtained at highest dwell time and magnification. In this way, the development focuses on optimizing result consistency with shorter SEM image acquisition time, focusing on high-throughput analysis.

Conclusion

We have demonstrated in a systematic study the effect of SEM image acquisition parameters, such as dwell time and magnification, on the robustness of automatically detecting defects in AM 316L. This now enables the selection of optimised image acquisition parameters and a minimised data acquisition time (high throughput).

The scope of our developed approach is more comprehensive than any currently available tool can offer. The aim of this development is to make defect analysis more transparent and reliable by providing a unifying platform.

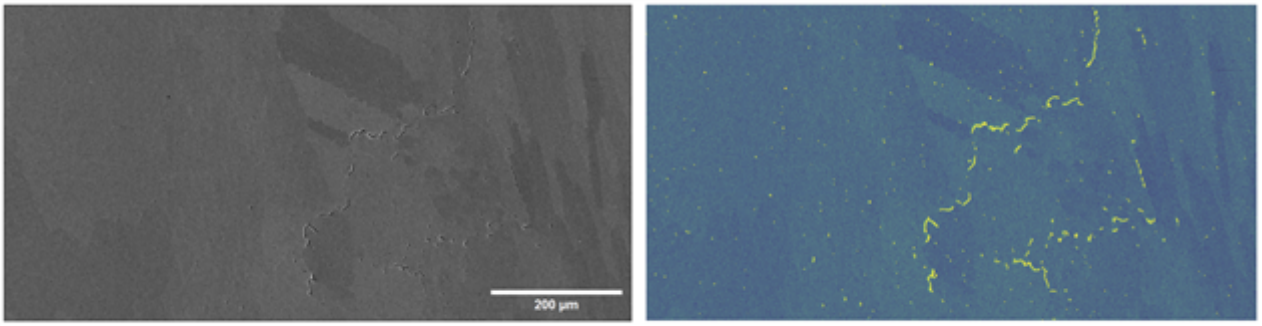

Figure 1: Example of Defect Detection for Dwell Time of 1 μs and Pixel Size of 200 nm with the Identified Features Highlighted in Yellow

Keywords:

Electron Microscopy, High-throughput Defect Analysis

848

NiTi shape memory alloy microstructure after high stress at elevated temperatures containing modulated M2 martensite

Jan Duchoň[1], Yuchen Chen[1], Miloslav Klinger[1], Petr Šittner[1]
[1]FZU - Institute of Physics of the Czech Academy of Sciences, Prague, Czech Republic

Poster Group 2

NiTi shape memory alloy microstructure after high stress at elevated temperatures containing modulated M2 martensite
J. Duchon, Y. Chen, M. Klinger, P. Šittner
Institute of Physics of the Czech Academy of Sciences, Na Slovance 2, Prague, Czech Republic

Background

Nanocrystalline wires with shape memory NiTi were deformed in the martensitic state at low temperatures of -125 °C up to a stress of ~750 MPa. In the next step, the wires were heated well above the temperature Af while maintaining a constant stress of ~750 MPa. The wire was driven towards its thermomechanical stability limits under such a specific condition and finally transformed into plastically deformed austenite. Microstructure of nanocrystalline NiTi shape memory wire was analyzed in Transmission Electron Microscope (TEM) with the aim to reveal the microstructures of martensite variants and lattice defects evolving in the heated wire, and at the same time to reveal the mechanism of plastic deformation and highly constrained reverse martensitic transformation. Although the constrained NiTi martensite wire should transform back to austenite at elevated temperatures, the applied stress prevents this reverse transformation and plastic deformation of martensite occurs instead. However, the mechanism of plastic deformation of martensite under such elevated temperature and high stress conditions remains unclear.

Materials and Methods

The NiTi shape memory wire was commercially prepared by Fort Wayne Metals in cold work state with the following parameters FWM #5 Ti-50.5 at.% Ni, 42% CW, diameter 0.1 mm. Such wire was heat treated by the electric power pulse method with power density 160 W/mm3 and pulse time 15 ms. Final wire has a fully recrystallized microstructure with a mean grain size d = 250 nm and showing transformation temperatures Ms = 63 °C, Af = 93 °C.
Wire microstructure was investigated using TEM specifically FEI Tecnai TF20 X-twin equipped with a field emission gun operating at 200 keV. TEM lamellae were extract from the deformed NiTi wires by Focused Ion Beam (FIB) lift-out technique using a FEI Quanta 3D FIB-SEM microscope. TEM, HRTEM, SAED and nanobeam electron diffraction micrographs were acquired for a detailed understanding of the resulting martensitic microstructure. TEM diffraction patterns and HRTEM images were indexed using the CrysTBox [1] software. HRTEM images have been also processed by Geometric Phase Analysis (GPA), which is part of the software, and it was developed to analyze local strain fields by HRTEM, for example strain fields around dislocation cores. Nanobeam diffraction analysis of modulated martensite was also performed, to have local diffraction information.

Results

TEM analysis of the wires revealed that, when the martensite is heated under the stress towards its stability limits, so the microstructure contains mixed regular B19' and modulated M2 martensitic lattices with a high density of lattice defects, e.g., dislocations. Such a complex microstructure could not be characterized by conventional TEM, therefore HRTEM and nanobeam electron diffraction were used.

TEM analysis showed deformation bands in the microstructure of the martensitic variants were found everywhere in the martensite microstructure. The microstructures of martensitic variants produced by kwinking consist of deformation bands in which the martensitic lattices are rotated with respect to the martensitic matrix sharing a common [010] zone axis. A large number of dislocations in the martensite microstructure were also found here. More detailed TEM analyzes showed that in addition to these commonly observed findings, abnormal diffraction patterns were also observed. Diffraction patterns (SAED, FFT of HRTEM and nanobeam diffraction) from various regions could not be indexed using the lattice parameters of the B19' monoclinic lattice, because of the additional diffraction points appeared halfway between the 000 and 001 points. The occurrence of such additional diffraction spots indicates that the martensite has a modulated lattice with a unit cell twice as long in the c-direction.
During heat treatment the oriented martensite heated at constant applied stress undergoes a B19' => M2 structure change and moreover the martensite plastically deforms before and during the transformation to austenite. The study revealed that the plastic deformation of martensite variants takes place via kwinking deformation involving coordinated dislocation slip, twinning and simultaneously created a long period modulated crystal structure. It is assumed that the modulated martensite structure arises from the B19' martensite structure through coordinated slip of partial dislocations with Burger's vector b = a/2 [100] on the (001) crystal planes. Coordinated slip was forced by kwinking deformation. The partial dislocations began to slide as the martensite was exposed to elevated temperatures.

Conclusions
To find out the deformation process of the martensitic wire, which was exposed to high stress under high temperature conditions and forced to its stability limit, we analyzed the microstructure of the wires annealed to different maximum temperatures by TEM. During this research we found that locally within the grain in some wires the diffraction patterns exhibit a modulated structure. From the diffraction patterns, it was found that the modulated structure has a unit cell twice as long in the c-direction. The formation of these areas within the grains will be due to the plastic deformation occurring in the wire under constant stress and elevated temperature, above the temperature Af.
It was revealed that the heated martensite wire plastically deformed by kwinking deformation and simultaneously transformed into a long-term modulated monoclinic structure with a high density of dislocation defects, before and while undergoing reverse martensitic transformation into plastically deformed austenite. Based on the results, it is suggested that the modulated martensite structure is formed through the coordinated slip of partial dislocations with Burger's vector b = a/2 [100] on (001) crystal planes, thereby achieving a large shear deformation of the crystal lattice, which is forced by kwinking deformation. The modulated structure will be considered as a local and temporary martensite structure that appears before it transforms to austenite under forced heating. During transformation martensite to austenite the modulated martensite generates high density of dislocation defects and a corresponding lattice strain in austenite microstructure.

Keywords:

TEM, NiTi, Martensitic transformation, Shape memory alloys, Modulated martensite

Reference:

[1] M. Klinger. More features, more tools, more CrysTBox. Journal of Applied Crystallography, 50(4), 2017. doi:10.1107/S1600576717006793

883

In Situ SEM at Elevated Temperature for Materials Science

Ondřej Ambrož[1], Petr Horodyský[2], Jan Čermák[1], Patrik Jozefovič[1], Kateřina Sixtová[2], Šárka Mikmeková[1], Ondřej Lalinský[1]
[1]Institute of Scientific Instruments of the Czech Academy of Sciences, Brno, Czech Republic, [2]Crytur, Turnov, Czech Republic

Poster Group 2

Understanding the relationships between microstructure and properties under various conditions is essential for further material development. SEM is suitable for studying not only microstructure but also changes in these materials under different and variable conditions. In the case of elevated temperatures, phenomena associated with diffusion, phase transformations, grain boundaries and precipitation are particularly significant in materials science [1]. Several limitations of in situ experiments in SEM are related to the vacuum environment, which acts as an electrical and thermal insulator. The thermal insulating property of vacuum reduces the risk of damage to microscope components during heating experiments but also complicates sample heating and cooling and temperature measurement. Vacuum prevents both sample oxidation and equipment oxidation during experiments at high temperatures. The development of specific detectors has been necessary to carry out in situ studies under extreme conditions, such as high pressure and temperature [2]. The aim of these experiments was to verify the possibilities of observing phenomena characteristic of materials science using in situ SEM at elevated temperatures. In addition to the phenomena themselves, the aim was to verify the visualization of structure by thermal etching [3]. Pilot experiments were conducted, including melting of the AlMgSi1 alloy, dissolution of secondary phases and visualization of primary austenite grains of TRIP steel, dissolution of intermetallic phases and melting of the AlSi9Cu3(Fe) alloy, phase transformation of the Ti6Al4V alloy, precipitation of phases during artificial aging of CuBe2 and AlMgSi0.5 alloys, and thermal etching of ZrO_2 ceramic for grain visualization.
The samples underwent a complete conventional metallographic procedure, including cutting on the precision metallographic cutter, followed by mounting in resin, and successive grinding and polishing steps. Grinding was performed using SiC papers with grit sizes of 220, 500, 1200, 2000, and 4000, while polishing utilized diamond pastes with abrasive sizes of 3 µm, 1 µm, and 0.25 µm, concluding with chemical-mechanical polishing using the colloidal suspension with SiO_2 particles. Before heating, the samples were chemically or color etched to reveal the real structure. Some samples underwent imaging in the SEM using the LOM Zeiss Axio Observer 7 before heating for correlative imaging. In situ heating experiments took place in the SEM Thermofisher Scientific Quattro S, utilizing the Newtec Scientific FurnaSEM 1300 stage for heating up to 1200 °C. The sample was restrained to a 12 mm diameter by a platinum pad, ensuring uniform heating. To enhance thermal conductivity and dissipate charge, samples were affixed to the platinum pad using a carbon suspension. Subsequently, a thermal shield with a 4 mm diameter aperture was installed above the sample to mitigate thermal stress on the microscope chamber components. In addition to the ETD detector, samples were also imaged during heating using the BSE detector Crytur Karmen, equipped for in situ experiments at elevated temperatures. The scintillation crystal of the Karmen detector is coated with a thin layer of aluminum, 100 nm thick, designed to prevent penetration of external light signals into the photomultiplier, such as light emitted by the heated sample [4].
During the melting of the AlMgSi1 alloy, an Al_2O_3 pad was inserted between the sample and the platinum pad. Upon reaching a temperature of 700 °C, microdendrites were observed at the edges of the sample, indicating localized melting. However, this temperature is approximately 150 °C higher than the theoretical melting temperature of the alloy. In the case of TRIP steel, reaching a heating temperature of 900 °C made the boundaries of primary austenite grains visible. With prolonged

exposure at this temperature, secondary phases began to dissolve, gradually increasing the contrast of the grains. Further experiments were carried out using a carbon suspension, and it was verified with an optical pyrometer that the heating temperature and the sample surface temperature could differ by approximately 50 °C. For the AlSi9Cu3(Fe) alloy, at a heating temperature of 550 °C, the dissolution of $CuAl_2$ was observed. During exposure at a heating temperature of 900 °C for the Ti6Al4V alloy, it was possible to observe the transformation of the globular α phase with an HCP lattice to the β phase with a BCC lattice. While a transformation to the α phase was expected during cooling, there was no observed change in morphology. Artificial aging of the CuBe2 alloy occurred at a temperature of 315 °C (Fig. 1). Precipitation of the γ phase likely began before reaching the selected temperature. During exposure, the precipitated particles slightly increased in size. Apart from precipitation, the contrast at the boundaries of some grains began to increase, resulting in their expansion. In the case of artificial aging of the AlMgSi0.5 alloy at a heating temperature of 180 °C, no structural changes were observed. The feasibility of in situ thermal etching was confirmed on ZrO_2 ceramic. The sample was imaged at room temperature and then continuously during exposure to heat. During heating, unstable behavior was observed due to sample charging, the evaporation of water from the carbon suspension used to adhere it to the platinum pad, and thermal expansion. Upon reaching a heating temperature of 750 °C, the contrast of grains in both detectors began to increase slightly. There was no sample charging. Already at a heating temperature of 900 °C, the contrast of grains substantially increased, remaining largely unchanged throughout the exposure period for both detectors.

The in situ SEM experiments at elevated temperatures were successfully conducted, demonstrating the potential applications of this method in materials science. During the experiments, partial insights were gained, and practical procedures were developed, leading to greater validity of the results. The window for pyrometer measurements allowed for further refinement of surface temperature measurements. Direct temperature measurement on the sample may lead to further precision. The carbon suspension for high temperatures improved heat conduction and charge dissipation from the sample. Under specific conditions, samples can also be melted. Thanks to special metallographic preparation, it was possible to observe the real structure already at room temperature; however, further experiments are needed to verify the introduction of artifacts from the preparation process.

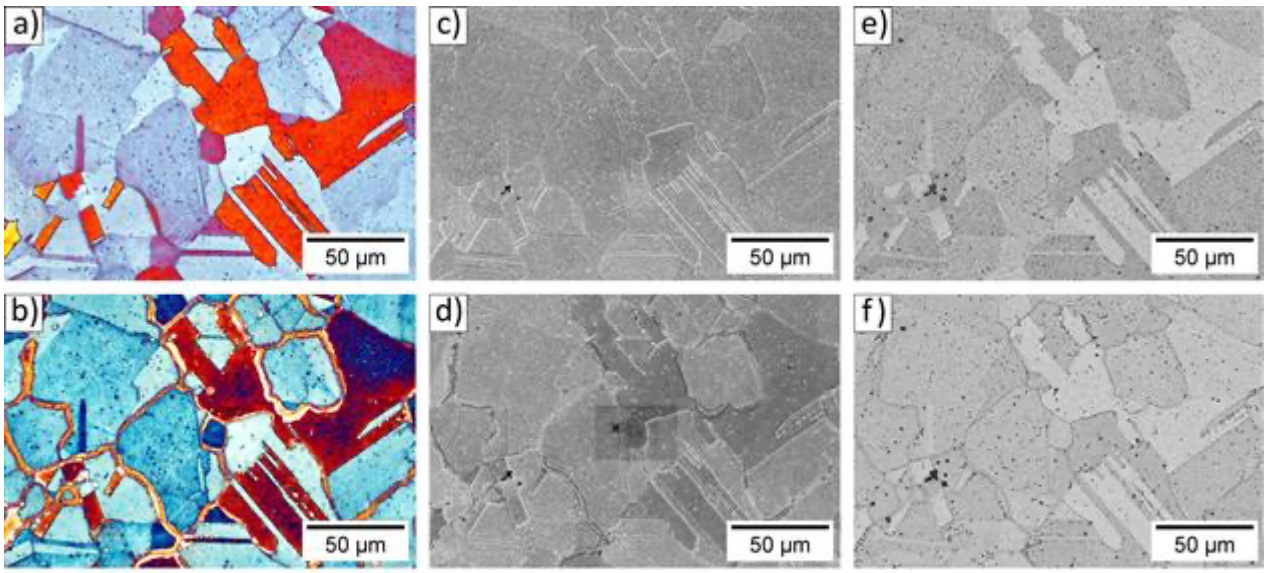

Fig. 1 CuBe2 alloy artificial aging at 315 °C; a) LOM before aging; b) LOM after aging; LOM 500× (croped); c) SEM SE ETD before aging; d) SEM SE ETD, 315 °C, 2.7 h; e) SEM BSE Karmen before aging; f) SEM BSE Karmen, 315 °C, 2.7 h; SEM 1000×, 0,09 nA, 10 kV, WD 18 mm; color etched Klemm I.

Keywords:

in-situ SEM, correlative-microscopy, heat-treatment, thermal-etching

Reference:

[1] G. H. Michler. In Situ Microscopy. In: Electron Microscopy of Polymers, 2008, pp. 145-159.
[2] E. A. Torres, A. J. Ramírez. Sci. Technol. Weld. Join., 2011, 16, 1, pp. 68-78.
[3] R. E. Chinn. Ceramography: Preparation and Analysis of Ceramic Microstructures, 2002.
[4] R. Podor et al. J. Microsc., 2021, 282, 1, pp. 45-59.

885

Characterization of a multiphase nucleus of spheroidal graphite cast irons by transmission electron microscopy techniques

PhD Alessandro Pugliara[1,2], PhD Lydia Laffont[1], PhD Claudie Josse[2], PhD Teresa Hungria[2], PhD Jacques Lacaze[1]
[1]CIRIMAT, Toulouse INP, Université Toulouse 3 Paul Sabatier, CNRS, Université de Toulouse, 4 allée Emile Monso, 31030, Toulouse, France, [2]Centre de microcaractérisation CASTAING, Université Toulouse 3 Paul Sabatier, Toulouse INP, INSA Toulouse, CNRS, Université de Toulouse, Espace Clément Ader, 3 Rue Caroline Aigle, 31400, Toulouse, France

Poster Group 2

Background incl. aims
Spheroidal graphite cast irons are obtained by submitting a cast iron melt to a spheroidizing treatment with a Fe-Si-Mg alloy, followed by so-called post inoculation with a Fe-Si alloy. These additions contain other elements which are mainly strong deoxidizers and/or desulfurizers. It is well established that these two treatments interact to give the final particles acting as graphite nuclei [1]. Accordingly, many of the observations made on graphite nuclei reported the presence of oxides, sulfides and/or oxysulfides [1], though nitrides have been reported from times to times [2]. The fact that the nuclei appear multiphase in most of the reported examples complicates the analysis of the sequence of phase transformations leading to the nuclei. Microstructural, chemical and crystallographic characterization on a multiphase nucleus of a spheroidal graphite in a cast iron manufactured by thin-wall casting is the aim of this study. To describe many phases constituting it, scanning transmission electron microscopy (STEM) coupled with energy dispersive X-ray spectroscopy (EDS) and electron diffraction analyses are carried out. The nucleus contains two parts, one multi-phase rounded "head" encapsulated in an Al-Mg-Si nitride and an elongated "tail" consisting of the same nitride. The central part of the head seems to be related to the inoculant added to the cast iron melt. From this, the precipitation process leading to the final graphite nucleus is inferred.

Methods
A cast iron, i.e. mainly a Fe-C-Si alloy (final composition: 3.8 C, 1.9 Si, bal. Fe, wt.%) was spheroidized with a Fe-Si-Mg alloy. A commercial Fe-Si inoculant was added to the melt at the time of pouring in a thin-wall casting. Because of the high cooling rate, the material contained metastable carbides which were eliminated by a heat-treatment at 950 °C for 15 minutes.
A sample cut perpendicularly to the casting surface was prepared by standard metallographic methods. The microstructure consisted in graphite nodules within an iron-rich matrix. Focused ion beam (FIB)-lift out technique was used to prepare a thin foil of a selected nodule in a FEI NanoLab HELIOS 600i FIB/SEM. A transmission electron microscope JEOL cold-FEG JEM-ARM200F equipped with a probe Cs corrector and a SDD CENTURIO-X EDS detector was used for characterization. Selected area electron diffraction (SAED) and nano-beam diffraction (NBD) were employed to record diffraction patterns.

Results
Bright field (BF) STEM image of a thin diametric section of a graphite nodule prepared by FIB shows the presence of a nucleus in the middle of the nodule. This nucleus appears composed of two parts: a round head loosely connected to an elongated tail. High-angle annular dark-field (HAADF) STEM images evidence a grey contrast of both parts, with bright areas in the head which are indicative of the presence of at least one element much heavier than carbon in the nucleus. Also, the head presents different grey contrasts indicating a multi-phase nature with a fan-like faceted precipitate.

To determine the chemical nature associated with these various contrasts, STEM-EDS mapping was carried out. The elongated tail having an almost uniform grey contrast appears mostly composed of Al, Mg, Si and N, with however a few isolated small bright spots rich in iron. In contrast, the rounded head exhibited at least four different phases: 1) an inner facetted center rich in Fe; 2) a shell rich in S and Mg surrounding the center; 3) the fan-like precipitate mainly composed of Ti and developing outwards from this shell; and 4) a structure having the same composition as the elongated tail.
Finally, SAED and NBD were performed on different parts of the nucleus after appropriate rotation of the sample for each of the phases. The Al-Mg-Si-N phase present in both the elongated tail and the outer area of the head has been indexed as trigonal nitride $A_2Mg_5Si_5N_{12}$ according to Solberg and Onsoien [3]. Concerning the other phases in the rounded head, the center could be indexed as bcc-Fe [4] and the fan-like precipitate as cubic carbo-nitride $Ti_2(C,N)$ [5]. Unfortunately, the shell rich in S and Mg could hardly be characterized.
Observing the spatial distribution of the phases and considering their chemical composition and crystallographic structures, we may suppose a formation sequence of the nucleus as follows: bcc-Fe is the center of nucleus on which a shell rich in S and Mg precipitates; then, the Ti carbo-nitride fan-like structure develops from this shell; and finally (Al,Mg,Si) nitride precipitates from all around this carbo-nitride and appears to be the actual substrate for graphite nucleation. It is conceivable that the tail developed together with the graphite nodule during the graphitizing heat-treatment.

Conclusion

Transmission and analytical electron microscopy allowed determining the multi-phase nature of a graphite nucleus in a spheroidal graphite cast irons. This nucleus was composed of two different parts:

- A rounded multi-phase head organized as follows: 1) an inner facetted center rich in bcc-Fe; 2) a shell rich in S and Mg surrounding this center; 3) then a fan-like fcc Ti carbo-nitride developing from this shell; and finally 4) an external trigonal nitride rich in Al, Mg and Si around the aggregate.
- An elongated tail having the same composition as the outer nitride in the head.

In the literature, it is generally considered that the inoculant fully dissolves in the cast iron melt to lead to precipitation of oxides, sulfides and nitrides. In contrast to previous studies, this study shows that the center of the rounded head which was indexed as bcc-Fe could be a remaining of the Fe-Si inoculant.

Keywords:

Electron-diffraction spheroidal-graphite cast-iron nucleus STEM-EDS

Reference:

[1] T Skaland, O Grong and T Grong, Metall Trans A 24A (1993) p. 2321
[2] H Nakae and Y Igarashi, Mater Trans 43 (2002) p.2826.
[3] JK Solberg and MI Onsoien, Mater. Sci. Tech. 17 (2001) p.1238
[4] ME Straumanis and DC Kim, Zeitschrift fur Metallkunde 60 (1969) p.272.
[5] SI Alyamovskii, BV Mitrofanov, YuG Zainulin and GP Shveikin, High Temperature 11 (1973) p. 616.

897

Surface tension of Au-catalysed GaAs-nanowires

Mr. Christopher Røhl Yskes Andersen[1,2], Mr. Marcus Tornberg[3,4,5], Mr. Daniel Jacobsson[3,4], Prof. Jonas Johansson[4,5], Prof. Kimberly A. Dick[3,4,5], Prof. Kristian S. Mølhave[2]
[1]Quantum DTU, Tech. Uni. of Denmark, Kgs. Lyngby, Denmark, [2]DTU Nanolab, Tech. Uni. of Denmark, Kgs. Lyngby, Denmark, [3]nCHREM, Lund Uni., Lund, Sweden, [4]NanoLund, Lund Uni., Lund, Sweden, [5]Solid State Physics, Lund Uni., Lund, Sweden

Poster Group 2

Droplets are held together by the surface tension, which is the force from the surface molecules attracting each other. It is not only the phenomenon explaining droplet formation, but it is also an important factor, when studying vapor-liquid-solid growth, which is a commonly used growth mechanism for nanowires. Today however, growth models and predictions are based on approximate values of the surface tension, lacking in reports of empirical values e.g., for Au-catalyzed GaAs-nanowires.
An external electric field has previously been used to deform the catalyst droplet on AuSi eutectic droplets on silicon nanowires and the balance of field and surface tension can be used to measure the surface tension. Here, we use a similar procedure growing Au-catalyzed GaAs nanowires on microfabricated Si-cantilevers, which opens up for many types of in-situ experiments, deforming the catalyst in an arsine atmosphere using a unique ETEM with a purpose-built gas injection system. Image analysis and 3D simulations (Fig. 1a) using COMSOL Multiphysics are used to compare the droplet shape e.g., the aspect ratio of the droplet at various fields and temperatures (Fig. 1b) reporting an empirical value of the surface tension for the first time and with improved analysis also an updated value on the AuSi surface tension reported earlier.
In conclusion, an empirical value of the surface tension of the AuGa eutectic of GaAs nanowires is reported using locally heated Si-cantilevers in an ETEM. This will be compared with theoretical predictions.

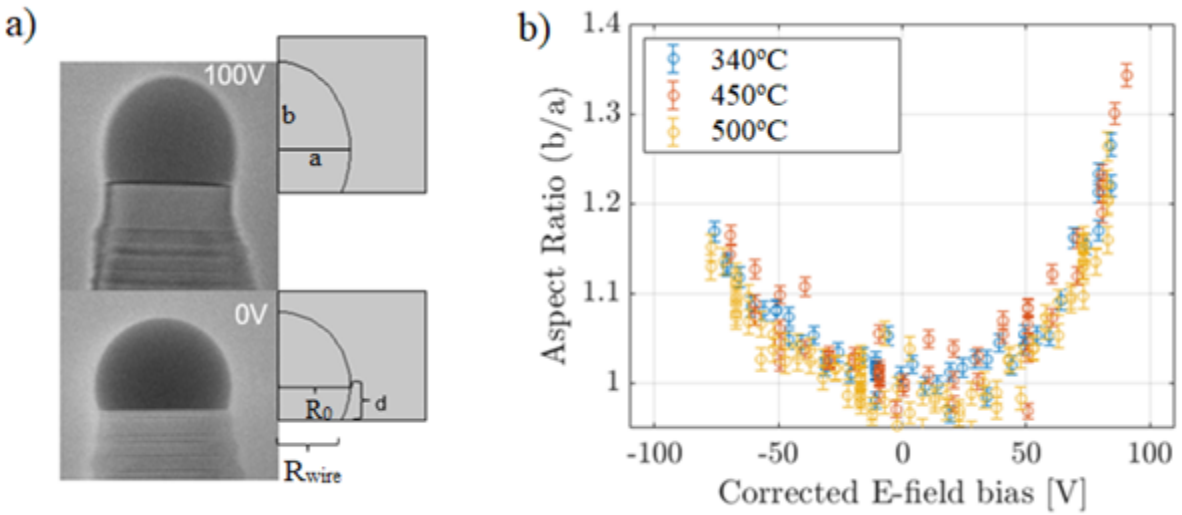

Keywords:

GaAs-nanowires, catalyst, surface tension, MEMS

Reference:

[1] R. S. Wagner & W. C. Ellis, Appl. Phys. Lett. 4, 89 (1964)
[2] E. K. Mårtensson, et al, Nano Lett. 19, 1197 (2019)
[3] F. Panciera et al, Nat. Commun. 7, 12271 (2016)

[4] K.S. Mølhave, Small, 4: 1741, (2008).
[5] M. Tornberg, et al, Microsc. Microanal. 28, 1484 (2022)

901

Microstructural Characterization of Electron Beam Welded Joints between EHEA and Austenitic Stainless Steel

M.Sc. Patrik Jozefovič[1], M.Sc. Jan Ronček[1], M.Sc. Ondřej Ambrož[1], M.Sc. Jan Čermák[1], Ph.D. Šárka Mikmeková[1]
[1]Institute of Scientific Instruments of the Czech Academy of Sciences, Brno, Czech Republic

Poster Group 2

Background incl. aims
Eutectic high-entropy alloys (EHEAs) have been around for a decade but only recently has become a hot topic in a field of metal alloys . As a subclass of high-entropy alloys (HEAs) enriched with a variety of advantages of eutectic alloys, EHEAs possess superior mechanical properties opening a broad spectrum of possible applications in industry [1]. These alloys are best characterized by the absence of the conventional „strength ductility trade-off“ and remarkable stability over a wide temperature range due to their high-entropy state. Combined with excellent castability, mitigating segregation and shrinkage, they appear to be an ideal candidate for demanding design scenarios such as exposure to elevated temperatures or mechanical stresses commonly encountered in the energy industry [2]. Therefore, they can be seen as a possible competitor for austenitic stainless steels, which possess high ductility with lower tensile strength values and are used for such applications nowadays [3,4]. In this regard , examining the behavior of these specific materials when welded together is prudent, as it can provide valuable insights into their compatibility and suitability for coexistence in industrial applications or utilization in tandem within various industrial sectors. Motivated by the imperative to harness the full potential of advanced materials, our study focuses on the characterization of heterogeneous weld joints between AlCoCrFeNi2.1 EHEA and austenitic steel EN 1.4571, achieved through electron beam welding. The primary objectives of this study are to conduct a comprehensive investigation into the microstructural characteristics of the weld interface and constituent materials. Through a multifaceted approach encompassing various analytical techniques, tests, and image analysis methodologies, our aim is to elucidate as much information as possible, thereby enhancing our understanding of the welding process and the resultant material properties.
Methods
The electron beam welding process was employed to fabricate weld joints between EHEA (AlCoCrFeNi2.1) and austenitic stainless steel (EN 1.4571). Three sets of samples were prepared, each subjected to different welding parameters: beam currents of 13 mA, 17 mA, and 25 mA, with corresponding welding speeds of 10 mm/s, 20 mm/s, 30 mm/s respectively. Prior to welding, samples underwent traditional metallographic procedure. The final preparation step involved electro polishing with parameters meticulously adjusted for optimal results. The microstructure of the weld joints and base materials was examined using multiple microscopy techniques. Light optical microscopy provided a macroscopic view of the weld interface, while confocal scanning laser microscopy offered high-resolution imaging of surface features. Additionally, scanning electron microscopy (SEM) was employed to investigate microstructural details at higher magnifications. On the SEM, Energy Dispersive X-ray Spectroscopy (EDS) was employed for elemental analysis of the weld zones. EDS mapping was conducted to assess the spatial distribution of alloying elements and identify any potential elemental segregation. Furthermore, Electron Backscatter Diffraction (EBSD) was utilized for phase identification and crystallographic analysis of the welds and base materials. Apart from microscopic analysis, mechanical properties of the weld joints were assessed through tensile testing and nanoindentation for hardness evaluation. Tensile tests were conducted to measure the mechanical strength and ductility of the weld joints. On top of that, convolutional neural

networks (CNNs) were employed for image analysis to estimate the fractions of BCC and FCC phases present in the microstructure.

Results

All observations were conducted in the same manner to achieve comparable results. The fusion area was examined at three levels: top, middle, and bottom. The top area was defined as 1 mm below the surface of the weld, while the bottom area was 1 mm above the root of the weld, with the middle area positioned equidistantly between these top and bottom regions. Summarizing the results, in all scenarios, EDX line scans along the axis of the weld showed minimal fluctuations in chemical composition. Conversely, significant chemical composition changes were observed when examining lines across the weld, particularly at the fusion zone boundaries, while the elemental levels remained stable after the transition. This phenomenon was consistent at every level of observation, with increasing fluctuations in the middle and bottom areas. It is also noteworthy that carbon nitrides from EN 1.4571 were observed across various regions of the fusion zone, contributing to the complexity of the microstructure and hindering the diffusion of chromium due to carbon and nitrogen binding. From a phase perspective, the entire fusion area exhibited a face-centered cubic (FCC) dendritic structure with interdendritic space formed by body-centered cubic (BCC) precipitates, resembling the EHEA-like phase map, which consists of FCC and BCC lamellas, while EN 1.4571, consistent with its inherent properties, maintained an FCC phase. Moreover, BCC stripes were predominantly observed at the interface between EHEA and the fusion zone, likely as a product of segregation. Conversely, the transition between EN 1.4571 and the fusion zone primarily consisted of an FCC phase with smaller BCC precipitates appearing deeper into the fusion zone. This observation is further supported by the grain orientation map, where grains adjacent to EN 1.4571 maintained larger sizes comparable to the base material matrix on this side of the weld, while also exhibiting almost identical orientation to the nearest grains of the base material.

As one delves deeper into the fusion zone, the relative grain size diminishes, and their orientation becomes more random, coinciding with the appearance of precipitates. These precipitates, besides exhibiting a BCC phase, displayed an inner structure that was analyzed, albeit yielding no further discoveries.

Conclusion

Optimal parameters for welding EHEA together with EN1.4571, as well as metallographic preparation of such welds, were established. The microstructure was subsequently observed and analyzed using a spectrum of different techniques, offering profound insights into both the welding process and the resultant structure. Our observations unveiled a finely nuanced and complex microstructure within the fusion zone, adorned with small BCC precipitates ranging from a few to tens of micrometres. Additionally, EBSD analysis underscored the pivotal role of the weld interface in shaping the evolution of the microstructure. Continued analysis, including the exploration of AI-powered image analysis techniques for fusion zone estimation, is warranted to deepen our understanding and uncover further intricacies.

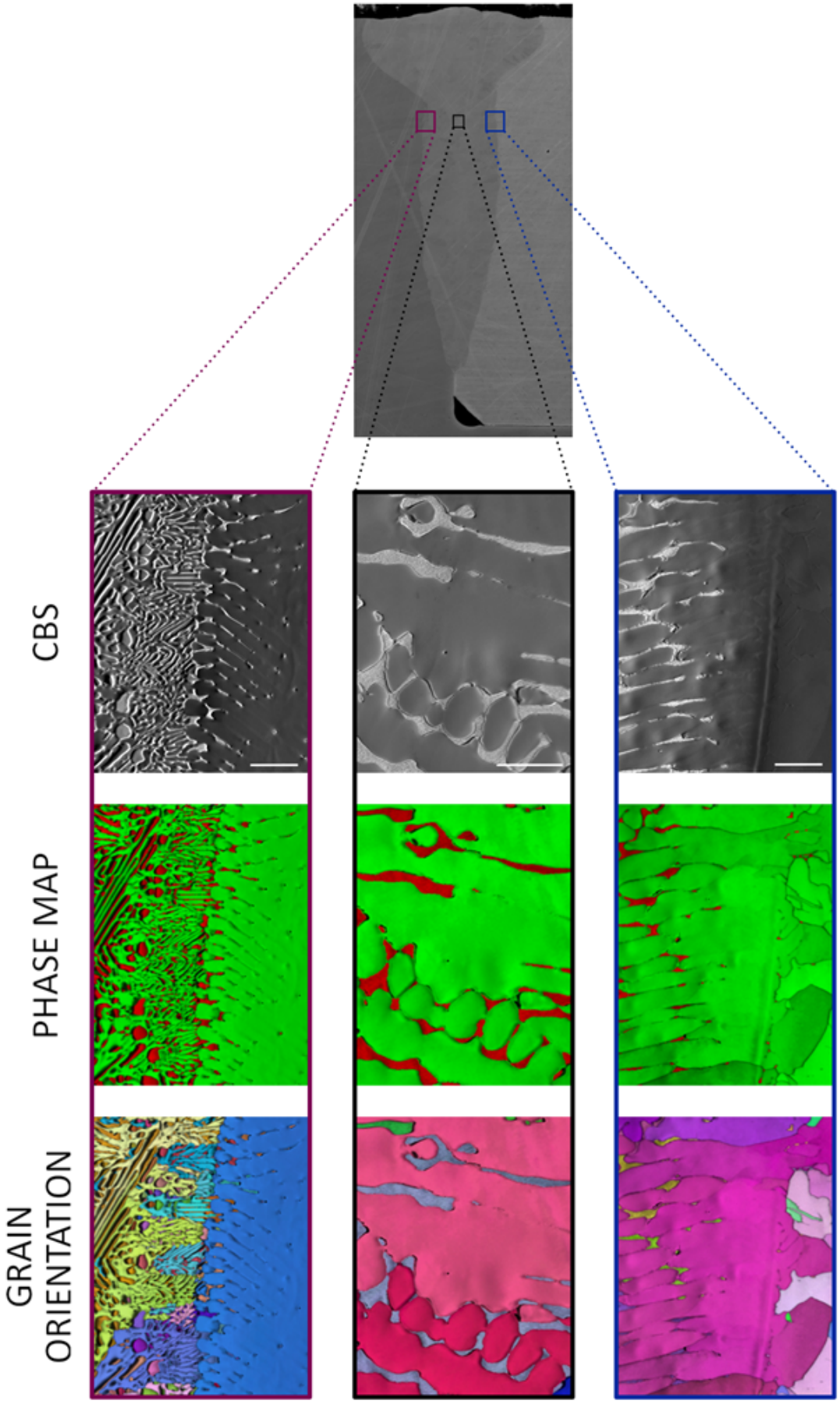

Fig. 1 Micrographs of different areas with corresponding phase and grain orientation maps

Keywords:

EHEA, austenitic-stainless-steel, electron-beam-welding, microstructure-analysis, ML

Reference:

[1] Shafiei, A. Design of Eutectic High Entropy Alloys. Metall Mater Trans A 53, 4349–4361 (2022)
[2] Jiao, W., Wang, Z., Guo, S., Lu, Y.. Eutectic High-Entropy Alloys (2022)
[3] Su, K., Nong, ZS., Gu, ZH. et al. Microstructural and Mechanical Properties of AlCoCrFeNi2.1 Alloy Welded Joint by Vacuum EBW. JOM 75, 2721–2730 (2023).
[4] Zhang, X., Liu, L., Yao, K. et al. The evolution of eutectic microstructure and mechanical properties of AlxCoCrFeNi2.1 high-entropy alloys. Journal of Materials Research 37, 2082–2092 (2022)
The authors acknowledge that the reserch was funded from the Lumina Quaeruntur fellowship established by the Academy Council of the Czech Academy of Sciences, award for prospective researchers recieved by Dr. Mikmeková.

923

SEM Insights: Sample Temperature Evolution during EBSD

Christina Koenig[1], Yi-Chieh Yang[1], Senior Researcher Alice Bastos S. Fanta[1], Professor Joerg Jinschek[1]
[1]National Center for Nanofabrication and Characterisation (DTU Nanolab), Kgs. Lyngby, Denmark

Poster Group 2

Background incl. aims
Electron Backscatter Diffraction (EBSD), with application in geology, ceramics, semiconductor, and metals research, enables a comprehensive analysis of the microstructure in materials. By mapping crystallographic orientation it aids in understanding phenomena, such as character of grain boundaries, etc., for the investigation of crystal/grain growth, phase transformations, as well as the detailed analysis of material deformations and strain.
Despite its widespread use, still many challenges remain, such as the effect of sample surface roughness, sample preparation artifacts, sample drift during data acquisition, image distortions due to the sample positioning and drift, effect of surface contaminations, as well as simply the complexities in EBSD data interpretation. This is stimulating ongoing research and requests further improvements.
Furthermore, potential effects of the electron beam itself, particularly beam-induced heating, remain an unexplored concern . Such effects could affect the microstructure of examined samples or lead to inaccuracies in assumed temperature conditions during experiments, in particular in in-situ heating experiments. Here, we aim to investigate these effects to better understand their impact on samples and discuss potential associated drawbacks.

Methods
In-situ heating holders based on micro-electro-mechanical systems (MEMS) were initially developed for stable and accurate transmission electron microscopy (TEM) investigations, but have since also found application in in-situ SEM experiments. Equipped with a four-point measurement system on their heating spiral, these holders provide real-time temperature feedback based on the measured resistivity of the heating spiral material, enabling precise temperature control during experiments as well as a direct feedback on additional sample heating effects.
With this approach, in our study we want to investigate the effects of beam exposure on sample temperature of various materials, as well as significant data acquisition parameters (i.e. SEM acceleration voltage, beam current, dwell times) as they occur during EBSD measurements of bulk-like samples. By utilizing COMSOL, a finite element analysis tool, we simulate the Joule Heating of the MEMS device to predict the temperature distribution in our sample caused by the Electron Beam, thereby improving our understanding of the complex electron beam-sample interaction.

Results
Our study provides insights into the evolution of sample temperature under EBSD-relevant microscope conditions. We observed an increase in the sample temperature of approximately 40K in dependency of the acceleration voltage used for an Iron Sample. These findings we compare with our COMSOL modeling results.
Thereby, we will emphasize the significance of temperature effects, particularly in critical cases like beam-sensitive samples, where beam-induced sample heating could affect interpretation of microstructural analysis results.
Additionally, we highlight the effects of beam-induced heat during in-situ heating experiments in SEM as well as the importance of incorporating an active temperature control feedback loop in such setups.

Conclusion

Here we present a novel approach to real-time temperature monitoring of samples, particularly under EBSD-relevant measurement conditions. This will provide important insights into the dynamic thermal behavior of specimens during examination in a scanning electron microscope

Keywords:

SEM, EBSD, Beam Heating

971

Atomic-scale structure and defect evolution in Σ5 [001] tilt grain boundaries in copper

Dr. Rer. Nat Hui Ding[1], Anoosheh Akbari[2], Dr Esakkiraja Neelamegan[2], Prof. Sergiy Divinski[2], Prof. Gerhard Wilde[2], Prof. Christian H. Liebscher[1,3]
[1]Structure and Nano- / Micromechanics of Materials, Max-Planck-Institut für Eisenforschung GmbH, Düsseldorf, Germany, [2]Institutre of Materials Physics, University of Münster, Münster, Germany, [3]Faculty of Physics and Astronomy and RC FEMS, Ruhr University Bochum, Bochum, Germany

Poster Group 2

Background: Grain boundaries (GBs) are material imperfections that have a strong influence on material properties. They can act as preferred diffusion pathways for solutes and hence impact the transport properties of polycrystalline materials. In many cases, it is assumed that the GB adopts an idealized structure that can be described by the structural unit model in high-angle tilt boundaries that is often used to establish structure-property correlations. However, the relation between the atomic structure of GBs, and possible deviations from the ideal structure, and their transport properties often remains unexplored.

Methods: We fabricated a Cu bicrystal via a modified Bridgman method. The seed single crystals are aligned with their [001] axes being parallel, corresponding to the growth direction, and are misoriented by an angle of 36.9° to form a symmetric tilt grain boundary. Electron backscattered diffraction is then used to characterize the global GB structure, followed by aberration-corrected scanning transmission electron microscopy to study the atomic structure of a series of near-Σ5 (310) [001] symmetric tilt GB segments of the bicrystal.

Results: In the near Σ 5(310)[001] symmetric tilt grain boundaries, the kite-type structural unit is frequently observed throughout the GB regardless of the deviation from the desired misorientation. However, various GB defects are formed at the GB to accommodate deviations from the exact GB misorientation or inclination. We observe disconnections, asymmetric nanofacet segments and an array of secondary edge dislocations that appear periodically between the normal kite-type structural units. Furthermore, a beam-induced GB phase transformation is observed, characterized by the change of the structural unit as well as the re-shuffling of the atoms at the GB.

Conclusions: The variations in GB structure and the formation of GB defects present an intriguing picture, particularly when considering their potential influence on how solutes diffuse along the interface. These aspects are rarely explored and our atomic scale investigation of the evolution of GB structure lays out the stepping stone towards understanding their role on the kinetic properties of interfaces.

Keywords:

Grain boundary, STEM, fcc, copper

984

Characterization of casting inclusions in superalloys by BSE and EDS

Prof. Dr. Dragan Rajnović[1]
[1]Faculty of Technical Sciences, University of Novi Sad, Novi Sad, Serbia

Poster Group 2

Background incl. aims
Superalloys exhibit remarkable properties such as exceptional mechanical strength, resistance to thermal creep deformation, and robustness against corrosion and oxidation, allowing them to operate efficiently in extreme environments. Their compositions primarily include nickel, cobalt, iron and chromium, whit addition of tungsten, molybdenum, tantalum, niobium, titanium, and aluminum. Innovations in the chemical development of superalloys have enabled the precise tailoring of their properties, ensuring they meet the specific demands of their applications. These materials are crucial in applications demanding high performance at elevated temperatures, such as in aerospace turbine engines and marine engineering.
Superalloys are typically processed by investment casting (also known as lost-wax casting) under vacuum conditions to ensure the highest quality of the casting. During casting, different ceramic materials are used for crucible in which an alloy is melted, for cup in which a molten material is transported, for shell in which casting is performed, or for ceramic slurry used for coating a wax model. All of this is made of different size ceramic particles which during operation could chip and make inclusion in the cast part. For that reason, this work is performed to identify inclusions, and thus identify critical place in casting procedure.

Methods
The casting inclusion are observed at different cross sections of superalloy casted parts which were metallographically prepared and afterwards preliminary examined on Light Microscope Leitz Orthoplan, and further studied in backscatter electrons (BSE) mode on scanning electron microscope JOEL JSM-6460LV equipped with EDS system INCA Oxford Instruments, at 20 kV.

Results
It is found that ceramics inclusions are primarily present in the surface of cast part, thus making a critical place for fracture in operation. In backscatter electron imaging mode it is straightforward to distinguish between the most common inclusions, like: ZrO_2 from crucible, with distinctive white appearance (Fig. 1); Al_2O_3 from cup, with dark gray appearance (Fig. 2); or $ZrSiO_4$ inclusion, originating from ceramic slurry, which could be also simply identified due to the gray shade (Fig. 3). On figure 4, the presence of multiple different inclusions could be observed, also. All observed inclusions are also positively identified by quantitative EDS point or area analysis.

Conclusion
At the end, it could be summarized that backscatter electron (BSE) analysis is a fast and convenient method to identify casting inclusions in superalloys, and thus to identify an origin of inclusion and casting error. Further EDS analysis positively confirms identification of inclusions, and gives additional data about oxidation or other impurities present.

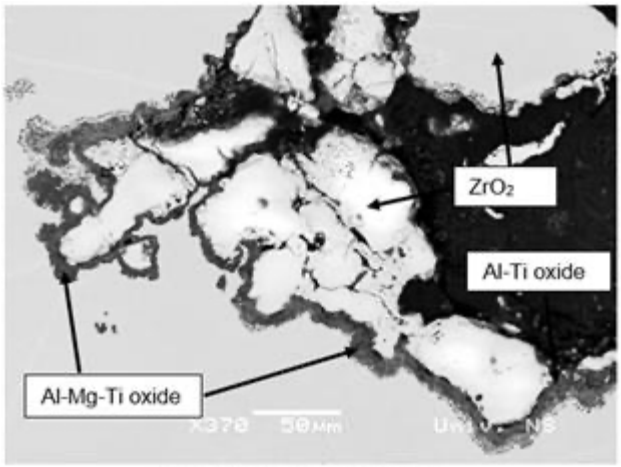

Fig 1. ZrO_2 inclusion (white)

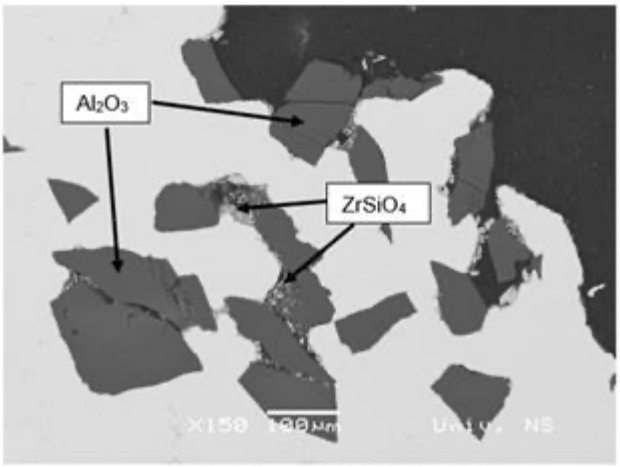

Fig 2. Al_2O_3 inclusion (dark grey)

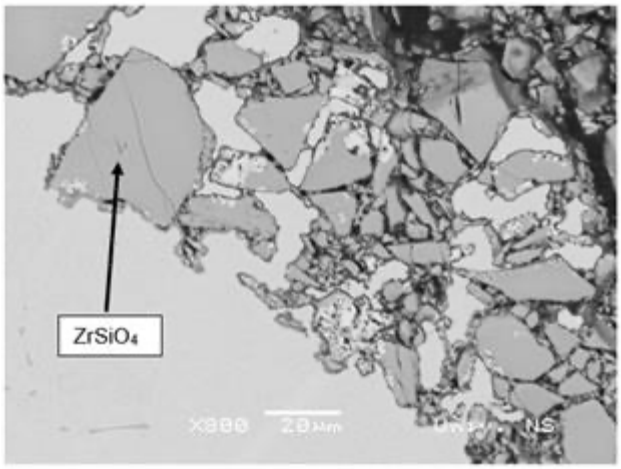

Fig 3. $ZrSiO_4$ inclusion (grey)

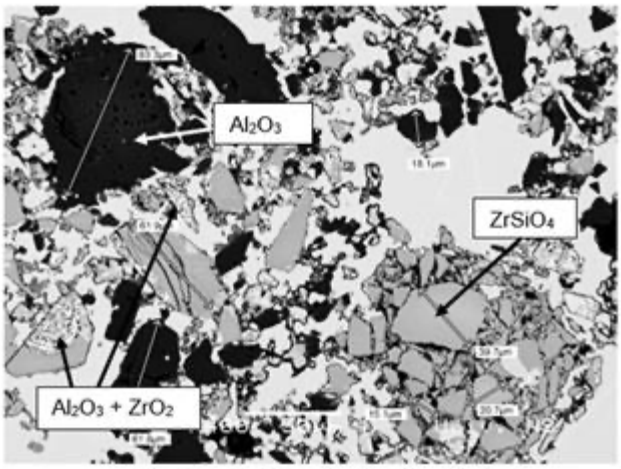

Fig 4. Complex inclusion distribution

Keywords:

Superalloys, casting inclusions, BSE, EDS

988

Deformation of steel chips due to machining

Dr. Sabine Schwarz[1], Univ.Ass. Dipl.-Ing. Christian Baumann[2]
[1]University Service Centre for Transmission Electron Microscopy (USTEM), TU Wien, Vienna, Austria,
[2]Institute of Production Engineering and Photonic Technologies, Vienna, Austria

Poster Group 2

Background incl. aims
During machining of materials, high temperatures and high pressures can occur. So, the materials are exposed to high plastic strain, high strain rates as well as high temperatures and heating rates. In order to be able to describe this, materials are examined to see how they change.
Chips that were removed by turning are very small in contrast to the remaining workpiece. They heat up so quickly that they reach more than half their melting temperature in just a few milliseconds. This in turn can significantly change the strength of the metal [1] and its resistance to the formation of chips. That´s why chips were chosen to be characterized concerning their microstructure.
Precise predictions through simulations are desired and the material model for the simulations must be examined [2]. Therefore, it is essential to compare simulations with experiments and observe actual changes in the microstructure of the chips and gain knowledge of the material behavior. To this end, microstructural investigations on chips were carried out using transmission electron microscopy (TEM).

Methods
For investigating the microstructure in TEM, electron transparent Focused Ion Beam (FIB) lamellae were prepared (Fig. 1). Chemical analyses were carried out by EDX mapping. Information for determining the grain size depending on the distance to the surface (depth) was obtained by bright field and corresponding dark field images.

Results
Several chips were investigated regarding the change of the microstructure from the surface into the depth of the material. Different cutting speeds and different final cooling rates led to a change in grain size over the depth from the surface. The EDX mappings showed an oxide layer on the surface of each sample of the chip.

Conclusion
Microstructure characterizations are important for investigating materials and improving the associated simulations. The present investigations on the steel chips pointed out a clear diffence between the change in microstructure caused by different cutting speeds and different cooling rates.

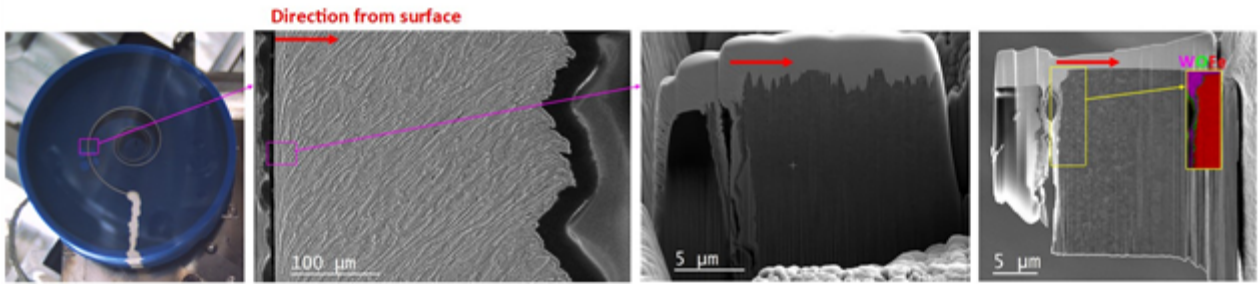

Keywords:

steel chips, microstructure, TEM, simulation

Reference:

[1] Mates, S., Vax, E., Rhorer, R. and Stoudt, M. (2020), Dynamic Flow Stress Behavior of Hypo-Eutectoid Ferrite-Pearlite Steels Under Rapid Heating, Mechanics of Materials, https://doi.org/10.1007/s40870-020-00241-z
[2] Bleicher, F., Baumann, C., Krall, S., Mates, S., Herzig, S., Alder, T. and Herzig, N. (2021), Considering the influence of heating rate, complex hardening and dynamic strain agingin AISI 1045 machining: experiments and simulations, CIRP Annals-ManufacturingTechnology, https://doi.org/10.1016/j.cirp.2021.04.083

993

HR-EBSD Analysis of High-Entropy Alloys: Understanding the Role of Alloying Elements in Mechanical Performance

Mr Pedro Henrique Fernandes Oliveira[1,2], Mr Julio Spadotto[2,3], Mr Edward Pickering[2,3], Mr Francisco Coury[1], Mr Claudemiro Bolfarini[1]
[1]Federal University of Sao Carlos, Sao Carlos, Brazil, [2]The University of Manchester, Manchester, United Kingdom, [3]Henry Royce Institute, Manchester, United Kingdom

Poster Group 2

High-entropy alloys, like $Cr_{33}Co_{33}Ni_{33}$, boast remarkable mechanical strength attributed to solid solution strengthening. Research underscores the pivotal role of plastic deformation in these alloys, governed by the interplay of slip and twinning mechanisms, alongside the emergence of nanometric lamellas of HCP phase during advanced deformation stages. Grasping these deformation intricacies is imperative for elucidating the alloys' mechanical and microstructural characteristics. Yet, in-depth investigations into $Cr_{30}Co_{30}Ni_{30}Pd_{10}$, $Cr_{30}Co_{30}Ni_{30}V_{10}$ alloys remain limited. A meticulous characterization of these materials holds promise for unlocking valuable insights pertinent to their engineering applications.

Methods

Samples of $Cr_{30}Co_{30}Ni_{30}Pd_{10}$, $Cr_{30}Co_{30}Ni_{30}V_{10}$ alloys underwent interrupted tensile tests at various deformation levels, employing a deformation rate of $1X10^{-3}s^{-1}$. Following each deformation stage, high-resolution Electron Backscatter Diffraction (HR-EBSD) analyses were conducted using a FEG-SEM ThermoScientific Apreo 2 high-performance, equipped with an Instruments Symmetry 2 EBSD detector. This detector boasts indexing speeds exceeding 5700 patterns per second, coupled with a high-sensitivity CMOS camera. Data analysis was performed using CrossCourt software, enabling comprehensive assessments including simple orientation measurements, quantitative evaluations of elastic strain fields and stress, and precise measurement of residual stress within the sample. These analyses were conducted with a remarkable sensitivity of 1 part in 10000 and a spatial resolution of 100 nm.

Results

EBSD analyses facilitated the comprehensive mapping of microstructural evolution in both the $Cr_{30}Co_{30}Ni_{30}Pd_{10}$, $Cr_{30}Co_{30}Ni_{30}V_{10}$ alloys during tensile testing. Through the utilization of KAM (Kernel Average Misorientation) and GOS (Grain Orientation Spread) mapping techniques, the distribution of deformation across the microstructure was effectively delineated, alongside the discernment of deformation twin formations during the deformation step. Furthermore, it was discerned that the introduction of V facilitated mechanical deformation through twinning mechanisms, while the incorporation of Pd tended to increase alloy brittleness. This brittleness was notably evidenced by low KAM and GOS indices immediately preceding fracture in the Pd-containing alloy.

Conclusions

The employment of HR-EBSD emerged as pivotal in thoroughly scrutinizing these findings. Its capacity to furnish intricate microstructural insights empowered a profound comprehension of deformation mechanisms and the nuanced impact of alloy constituents on mechanical performance. This underscores the indispensable role of advanced characterization methodologies in unraveling the

intricate behaviors exhibited by materials under mechanical stress, thereby enriching our understanding of material science and engineering.

Keywords:

HR-EBSD, Microstructural Characterization, Mechanical Twinning,

Reference:

[1] B. Gludovatz, A. Hohenwarter, K.V.S. Thurston, H. Bei, Z. Wu, E.P. George, R.O. Ritchie, Exceptional damage-tolerance of a medium-entropy alloy CrCoNi at cryogenic temperatures, Nature Communications, 7 (2016) 10602
[20] J. Shen, J.G. Lopes, Z. Zeng, Y.T. Choi, E. Maawad, N. Schell, H.S. Kim, R.S. Mishra, J.P. Oliveira, Deformation behavior and strengthening effects of an eutectic AlCoCrFeNi2.1 high entropy alloy probed by in-situ synchrotron X-ray diffraction and post-mortem EBSD, Materials Science and Engineering: A, 872 (2023) 144946.
[21] Z. Ye, C. Li, M. Zheng, X. Zhang, X. Yang, J. Gu, In situ EBSD/DIC-based investigation of deformation and fracture mechanism in FCC- and L12-structured FeCoNiV high-entropy alloys, International Journal of Plasticity, 152 (2022) 103247.

1043

In situ SEM of slip localization and its relation to the onset of ductile fracture

Mr Antoine Ollivier, Dr Antonio Pereira, Dr Nicholas Blanchard, Professor Loic Vanel, Dr Döme Tanguy
[1]Universite Claude Bernard Lyon 1, CNRS, Institut Lumière Matière, Villeurbanne, France

Poster Group 2

We present surface deformation measurements by in situ SEM tensile tests. The surface displacement field is obtained by tracking gold nano-droplets formed by laser dewetting. A thin film of gold of a few nm is deposited on the sample surface. The laser fluence and the thickness of the deposit can be varied to modify the diameter of the droplets and their surface density, enabling a fine-tuning of the spatial resolution of the field measurement. Diameters in the range of 10 to 100 nm, densities up to 2000/µm2 can be obtained. The advantage of tracking the center of mass of the droplets with respect to digital image correlation using a correlation window is to limit the smoothing of the displacement discontinuities. Therefore, it is well adapted to the measurement of slip band thicknesses. The field of view of a typical SEM image is of the order of 3 µm. It is enlarged up to 25 µm by automatically acquiring a series of images and stitching them together (Fig. 1). Thus enabling slip system widths as thin as 50 nm to be measured. The tracking of the center of mass of the droplets along the tensile test is done by a homemade code based on the python libraries scikit-image, scipy and run on a computer cluster. It enables a real time image treatment and the acquisition of high magnification images in the regions of interest. For example, the change of shape of the droplets within the thick slip bands or the shearing of droplets by thin slip bands have been observed in situ.
The method is tested on Eurofer 97, a tempered martensite ferritic steel for nuclear application where slip localization might be important for the initiation of ductile fracture.

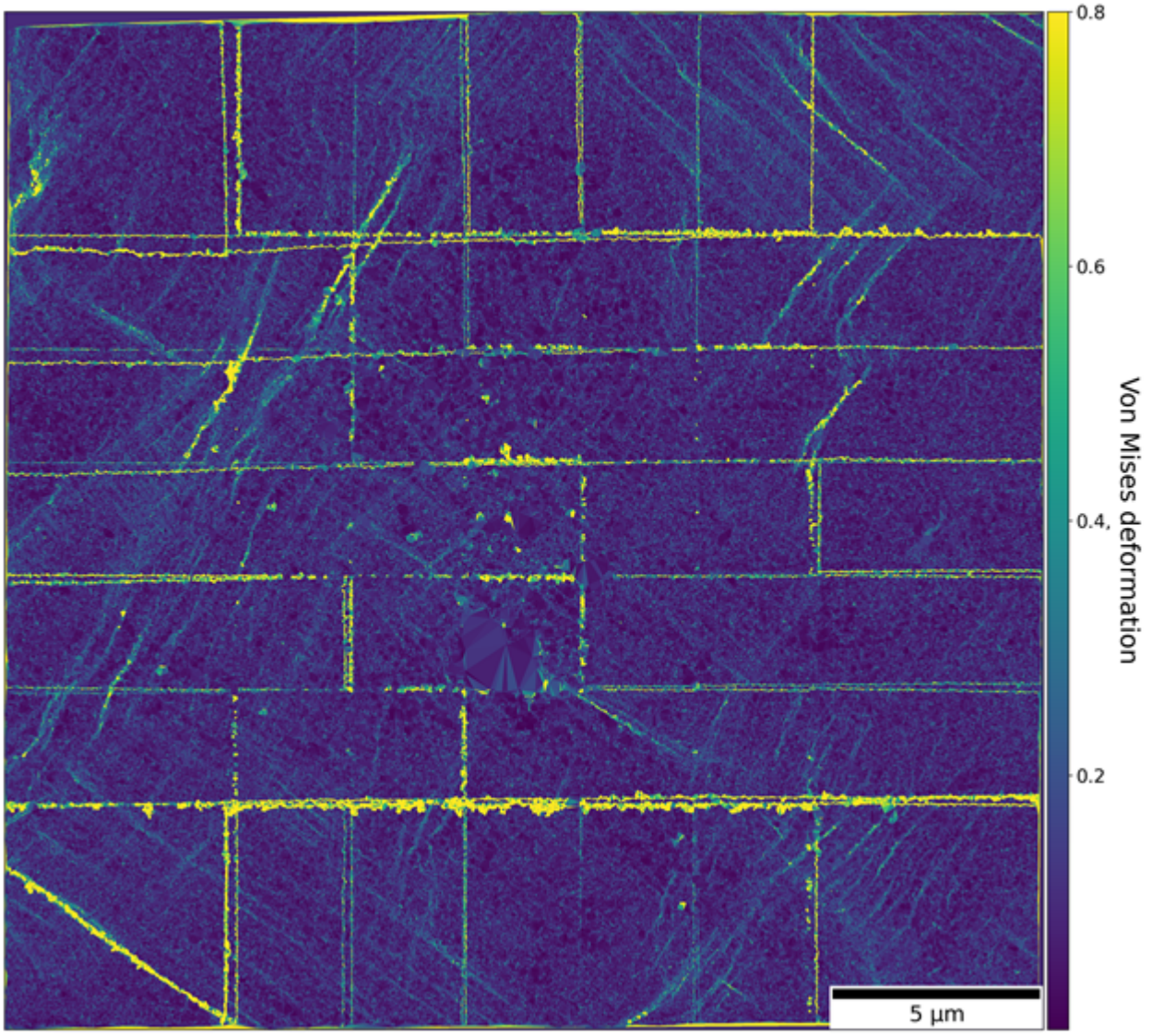

Keywords:

SEM, Python scripting, tensile tests

1061

Fast large-area EDS characterization of additive manufactured steels

Dylan Bailey[1], Christina Nicole König[1], Dr. Joerg Jinschek[1]
[1]National Centre for Nano Fabrication and Characterization (DTU Nanolab),Technical University of Denmark(DTU), Kgs. Lyngby, Denmark

Poster Group 2

Background

Powder Plasma Arc Additive Manufacturing (PLAAM) is a state-of-the-art approach for producing large-scale metallic samples with targeted geometry. One of this technology's defining features is its ability to produce samples with variable chemical composition.

However, further developments in novel additive manufacturing processes, such as PLAAM, require further development in characterization concepts and methodologies. Due to varying alloy composition, unknown process-microstructure-property relations and complex time-temperature-location profiles for each specimen, which result in evaporation, dilution and diffusion, there is a need for a method for time-efficient large-area characterization to become statistically relevant.

Methods

Steel samples were manufactured using the PLAAM process. A layer of steel with the length of 1 meter was welded onto a steel substrate. The chemical composition of the sample was varied gradually from a composition of a low alloyed Carbon Steel to a highly alloyed stainless steel (316L).

Using a Flatquad detector (Bruker®), a detailed energy dispersive spectroscopy (EDS) study was performed to investigate the varying chemical composition in the PLAAM steel samples. Thereby, the SEM electron beam scanning strategy was tested, and has been verified in respect to the results when characterizing the entire sample. In detail, the scanning strategy and parameters were optimized for analyzing for the varying chemical composition along and perpendicular to the PLAAM build direction as well as at the steel substrate interface with HT 20kV, current source 20 nA and dwell time 15µs. Additionally, the effects on diffusion from the thermal history of the build platform were analyzed.

Results

Optimization of the SEM beam scanning strategy and measurement system resulted in findings that were statistically consistent with large-area characterization of the samples using long dwell times (i.e., slow image acquisition).

The use of shorter dwell times, i.e. faster large-sample-area EDS mapping, significantly shortens the experimental time while introducing less significant statistical noise.

Further insights into the effects of local composition control were gained to further optimize the PLAAM process.

Conclusion

Using the Flatquad EDS detector allowed for a higher collection angle compared to normal angled EDS. Combined with an optimized SEM beam scanning strategy, we were able to significantly reduce measurement time required for large-area measurement of PLAAM samples and increased through-put to gain statistically relevant insights into the process-microstructure-property relationship of PLAAM structures.

Keywords:

EDS, Additive Manufacturing, Metals Characterization

Reference:

Casukhela, R., Vijayan, S., Jinschek, J.R. and Niezgoda, S.R.,

A framework for the optimal selection of high-throughput data collection workflows by autonomous experimentation systems. Integrating Materials and Manufacturing Innovation, 11(4), pp.557-567 (2022)

1108

Novel In-situ TKD Nano-tensile Testing: Insights into Nanoscale Crystal Plasticity and Grain Boundary Mechanics

Dr. Tijmen Vermeij[1], Dr. Amit Sharma[1], Dr. Xavier Maeder[1], Prof. Johann Michler[1]
[1]Laboratory for Mechanics of Materials and Nanostructures, Swiss Federal Laboratories for Materials Science and Technology (EMPA), Thun, Switzerland

Poster Group 2

Background

Advancements in nanoscale characterization techniques are crucial for understanding the complex deformation mechanisms of metal alloys, coatings and nanolaminates. Traditional post-mortem Transmission Kikuchi Diffraction (TKD) and Transmission Electron Microscopy (TEM) analyses, although powerful, often fail to capture the complete sequence and nature of deformation mechanisms as they occur [1]. This limitation is due to their inability to observe the initiation, progression, and interaction of deformation features such as dislocations or twins, leading to potential misinterpretations involved in material deformation.
In-situ TEM and in-situ EBSD nano- and micromechanical testing are both well-established techniques that offer detailed characterization of evolving crystal plasticity [2-3]. However, in-situ TEM is technically challenging and is limited in its scale. In contrast, In-situ EBSD is more feasible and allows larger field of views, yet its spatial resolution is typically limited to ~50 nm, which can miss finer structural details critical in nanoscale materials. In-situ TKD, on the other hand, would offer a significantly enhanced spatial resolution down to ~5 nm [4], while still performed inside a relatively accessible SEM.
Given these challenges and opportunities, this study introduces in-situ TKD integrated into nano-tensile testing as a novel methodology designed to provide comprehensive insights into the evolution of twinning, dislocation plasticity, and grain boundary mechanics under applied loading. This method will bridge the gap in understanding the intricate behaviors of complex nanolaminate metal/ceramic structures, while also providing an ideal platform to study phase transformation and twinning in advanced alloys.

Methods

A specialized experimental methodology was devised, combining (i) focused ion beam (FIB) processing for specimen preparation, (ii) a push-to-pull device for in-situ tension application, and (iii) an SEM configured for in-situ TKD with an Alemnis indenter. As proof of concept, we investigate deformations of advanced Cu1-x–Alx (X=0-12 at.%) multi-layers with interlayer interfaces of 2-5 nm amorphous Al2O3 for improved microstructure control and strength. These were synthetized in a novel deposition chamber from Swiss Cluster AG (https://swisscluster.com/), combining physical vapor and atomic layer depositions (PVD and ALD) without breaking the vacuum.
Specimens were prepared through site-specific FIB lift-out, subsequent fixation to the push-to-pull device using Pt deposition [5], a dedicated procedure for thinning to ~150 nm, and creation of a precise gauge section of several µm2. We designed and employed a custom configuration of an Alemnis nanoindenter frame inside a Tescan SEM, configured to fit with an Oxford Instruments Symmetry 2 EBSD detector for in-situ TKD and simultaneous STEM detection. Specimens are loaded with the push-to-pull device under continuous in-situ STEM observation, with intermittent loading pauses for detailed TKD mapping.

Results

In-situ STEM and TKD nano-tensile testing provides detailed and rich insights into the microstructural behavior of nanolaminate CuAl/Al2O3 films. We observe the development of twinning, dislocation

plasticity and interactions at grain boundaries from the undeformed state all the way to the formation of a localized shear band. Thereby, we demonstrate the capability of this methodology to analyze complex mechanical interactions at the nanoscale on a specimen of several micrometers in size.

Conclusions

This study establishes in-situ TKD nano-tensile testing as a valuable approach for analyzing nano- and micromechanical deformation mechanisms of complex metallic specimens. The integration of TKD with nano-tensile testing offers a new perspective for exploring deformation mechanisms, providing insights essential for the design and improvement of nanolaminated metallic materials, as well as advanced alloys that show phase transformation and twinning. The findings emphasize the utility of this method in advancing materials science and engineering.

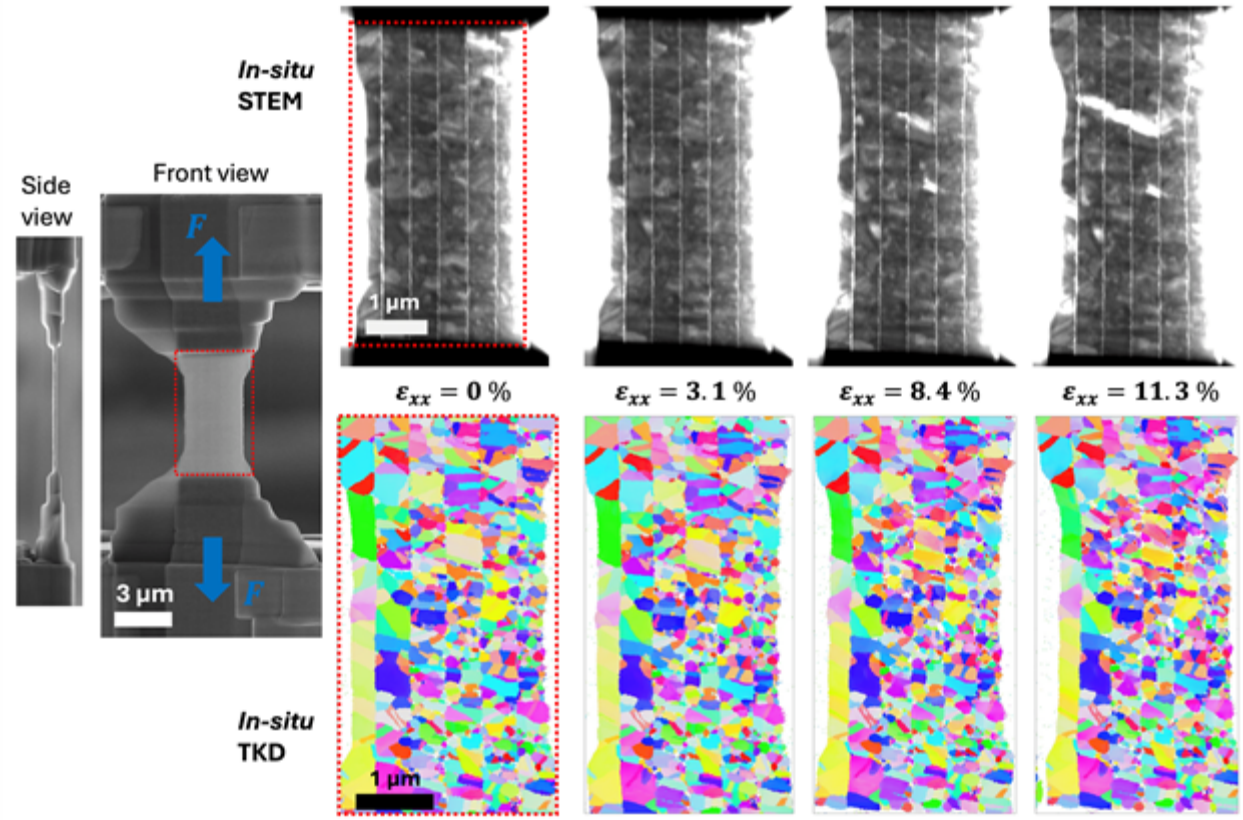

Keywords:

TKD, STEM, twinning, micromechanics, nanolaminates

Reference:

[1] Edwards, T. E. J., Xie, T., della Ventura, N. M., Casari, D., Guerra, C., Huszár, E., ... & Michler, J. (2022). Acta Materialia, 240, 118345.
[2] Yu, Q., Legros, M., & Minor, A. M. (2015). Mrs Bulletin, 40(1), 62-70.
[3] Niederberger, C., Mook, W. M., Maeder, X., & Michler, J. (2010). Materials Science and Engineering: A, 527(16-17), 4306-4311.
[4] Trimby, P. W., Cao, Y., Chen, Z., Han, S., Hemker, K. J., Lian, J., ... & Cairney, J. M. (2014). Acta materialia, 62, 69-80.
[5] Stinville, J. C., Yao, E. R., Callahan, P. G., Shin, J., Wang, F., Echlin, M. P., ... & Gianola, D. S. (2019). Acta Materialia, 168, 152-166.

1112

Structure and stability of core-shell AuTiOx nanoparticles for CO oxidation

Stefan Kei Akazawa[1], Rikke Egeberg Tankard[2], Filippo Romeggio[2], Jakob Kibsgaard[2], Ib Chorkendorff[2], Stig Helveg[1], Christian Danvad Damsgaard[1,2,3]
[1]Center for Visualizing Catalytic Processes (VISION), Department of Physics, Technical University of Denmark, Kgs. Lyngby, Denmark, [2]Surface Physics and Catalysis, Department of Physics, Kgs. Lyngby, Denmark, [3]National Center for Nano Fabrication and Characterization, Kgs. Lyngby, Denmark

Poster Group 2

Background
A catalyst's stability and longevity under operating conditions is key for their long-term application in industrial processes. This calls for an understanding of deactivation mechanisms to advance catalyst design strategies that can counteract such mechanisms.
Here we focus on gold (Au) nanoparticles (NPs) as a catalyst for the CO oxidation reaction (1). Specifically, we demonstrate that NPs formed by titanium (Ti) and Au alloying enables the development of an anchoring shell over the Au NPs, that suppresses sintering during operation. This new design strategy could be generally applicable and offers a higher degree of flexibility in preparing sinter-resistant catalyst nanoparticles.
Here we report the synthesis, structural characterization and stability testing of colloidal core-shell AuTiOx nanoparticles, displaying improved stability under thermal CO oxidation conditions on silicon nitride and TiOx supports (2).

Method
An Au0.5Ti0.5 alloy target was used to synthesize mass-selected nanoparticles of 160k amu under high vacuum conditions onto material supports that were used for the present characterization. Ion Scattering Spectroscopy (ISS), X-ray Photoelectron Spectroscopy (XPS) and High-Resolution Transmission Electron Microscopy (HRTEM) were used to elucidate the structure and chemical composition of the synthesized NPs. The catalytic characteristics of the AuTiOx NPs were then studied by performing comparative studies of the NPs and reference Au NPs under CO oxidation conditions. The NPs deposited on silicon nitride were studied by HRTEM under reactive conditions, by introducing a few mbar CO and O2 at various sample temperatures in a FEI Titan ETEM operated at 300 kV. Precautions were taken to acquire images of areas that were previously unexposed to the electron beam to differentiate beam-induced and environment-induced phenomena. The CO oxidation activity of the NPs deposited on TiOx were studied by running flow reactor experiments with the samples and reactive gasses at various temperatures and measuring gas conversion via a quadrupole mass spectrometer.

Results
ISS of the as-synthesized NPs, produced from the Au0.5Ti0.5 alloy, showed that only a small portion of the outermost layer contained Au atoms. HRTEM imaging of the nanoparticles after air exposure demonstrated that the NPs were composed of a 2.1±2 nm metallic Au core phase surrounded by a lighter ~0.8 nm shell. By XPS measurement the shell layer was identified as primarily consisting of TiOx. Imaging of the NPs in the reactive environment showed that a filament growth mechanism was present in the interface between the Au NPs and silicon nitride support at temperatures ≥200 ℃, mobilizing the Au NPs. The AuTiOx NPs maintained their core-shell shape and size up to at least a temperature of 400 ℃ and did not demonstrate any growth mechanisms. This finding suggests that the TiOx shell acts as a protective layer for the Au NPs in this instance. Comparative activity measurements of the AuTiOx and Au NPs deposited on a TiOx support showed an improved stability of the NP activity for the AuTiOx NPs in comparison to the Au NPs. Furthermore, the AuTiOx NPs

showed a characteristic in which their activity increased over time after the sample temperature was increased. In certain cases, the activity would increase by >2 fold over the span of hours while maintaining a certain temperature. This phenomenon was observed to be reversible when lowering the sample temperature. Nonetheless, the average NP site turnover frequency (TOF) was lower for the AuTiOx NPs than the Au NPs, likely due to a blocking of active sites on the core-shell structure.

Conclusion

Characterization of the AuTiOx alloy nanoparticles revealed an Au core and TiOx dominant shell containing small traces of Au atoms. Supported on silicon nitride, the Au NPs were observed to facilitate a filament growth under CO oxidation conditions while the phenomenon was not observed for the AuTiOx NPS, suggesting that the TiOx shell can act as a protective layer. Activity measurements of the NPs supported on TiOx, showed a time dependent deactivation was observable for the Au NPs and not for the AuTiOx NPs. The average TOF of the core-shell NPs was observed to be lower than the Au NPs, which could be explained by a blocking of NP active sites by the shell layer. Treatment methods to enhance the shell layer porosity could likely improve the activity of the core-shell nanoparticles while maintaining their stability characteristics. Development of such colloidal alloy NPs could lead to significant advances in producing highly stable catalysts for industrial use.

Keywords:

Stability, alloy nanoparticles, electron microscopy

Reference:

1. Haruta M. Chance and necessity: my encounter with gold catalysts. Angew Chem Int Ed Engl. 2014 Jan 3;53(1):52-6. doi: 10.1002/anie.201305987. Epub 2013 Nov 27. PMID: 24285610.
2. Tankard RE, Romeggio F, Akazawa SK, Krabbe A, Sloth OF, Secher NM, Colding-Fagerholt S, Helveg S, Palmer R, Damsgaard CD, Kibsgaard J, Chorkendorff I. Stable mass-selected AuTiOx nanoparticles for CO oxidation. Phys Chem Chem Phys. 2024 Mar 20;26(12):9253-9263. doi: 10.1039/d4cp00211c. PMID: 38445363.
3. The Center for Visualizing Catalytic Processes is sponsored by the Danish National Research Foundation (DNRF146).

1136

Utilization of TEM in archaeology to gain in-depth information on historic artifacts

Lennart Voß[1], Lennart Voss[1], Dr. Ulrich Schürmann[1], Lena Grandin[2], Christian Horn[3], Dr. Khurram Saleem[1], Bruno Vindrola-Padrós[4], Prof. Dr. Lorenz Kienle[1]
[1]Kiel University, Department for Materials Science, Kiel , Germany, [2]The Archaeologists, National Historical Museums, Stockholm/Uppsala, Sweden, [3]University of Gothenburg, , Gothenburg, Sweden, [4]Kiel University, Institute of Prehistory and Early History, Kiel, Germany

Poster Group 2

Background incl. aims
Although inherently dealing with the past, archaeology has profited immensely from the use of modern advanced analysis techniques like electron microscopy [1,2]. Especially TEM can provide inaccessible insights, for example when only miniscule amounts of material are available or faint traces are studied [3,4]. Furthermore, the combination of in situ techniques (like heat treatment) with replicas can lead to vital insights into the exact methods and paramters used for the fabrication of historic artifacts.

In Sweden, two copper axes were found buried in the soil. Both axes were from the late neolithic and comparable to the axe found alongside “Ötzi”. First measurements with X-ray fluorescence spectroscopy (XRF) indicated a silver-rich surface layer next to the obvious strong corrosion. These axes are historic artefacts and therefore a non-destructive sample preparation is necessary. A FIB cut TEM analysis of the surface layers could be carried out adhering to the strict rules of artifact preservation.

The very first settlers in Europe used cow dong as a reinforcement in pottery around 7000 B.C. Mechanical testing measured a higher mechanical strength at certain firing conditions for the reinforced pottery. Apart from the astonishing finding that composite (nano) materials were utilized at this time the exact nature of the strengthening mechanism is not known: is it mechanical (carbon fibres from the grass) or chemical (cow dung ash reacts with clay) in nature? Detailed analysis using TEM can help to better understand the mechanism as well as identify the fabrication procedure of ceramic artifacts.

Methods
The axes were first investigated via XRF and XRD to validate the field measurements. Additionally, the axes were loaded into a FIB-SEM and lamellae were taken out and analyzed via SEM-EDX. The FIB lamellae were subsequently analyzed utilizing a FEI Tecnai F30 G2 and a Jeol JEM-200F NEOARM.
In order to better understand the formation mechanism of silver enrichment and the corrosion layer a replica artifact was produced and artificially aged using suspension in humic acid for multiple weeks.

For the analysis of the reinforced pottery visible grass fibres were extracted with tweezers, ground in a mortar while suspended in butanol and deposited on the TEM substrate via drop coating . The same process was used for the archaeological sample, the unfired replica and several fired replicas. In addition a small amount of material was transferred onto an in situ heating chip (DENS solutions Wildfire) and heat treated up to 1100 °C in order to demonstrate the feasibility of in situ TEM observation of ceramic sintering and give insight into the mechanisms of the reinforced pottery during firing.

Results

XRD Rietveld analysis of the axe material showed a chemical composition in good agreement with XRF analysis . Since both techniques utilise X-rays the penetration depth is similar resulting in the same relative surface sensitivity. Analysis of the FIB-cut reveals the difference between the unoxidized bulk and the oxide layer, where in the CuO layer, precipitations of Ag are identified (see graphic). Additionally, the brittleness of the surface layer can be linked to the high amount of fractures visible in the CuO layer. The bulk material is uniform in contrast and has an Ag content of 0.8 at%.

In situ heating of a non-reinforced ceramic showed that for temperatures below 1000 °C the material showed a decrease in crystallinity as evidenced be loss of contrast in BF TEM and weaker diffraction rings in SAED. Above 1000 °C the material, which initially consisted of numerous crystallites, fused into larger crystals. Sophistaced backround subtraction in rotational averages of the SAED patterns allowed their evaluation even for faint diffraction patterns.

TEM analysis of the plant fiber reinforced ceramics did not reveal the presence of carbon nanofibers in the pristine as well as heated (in situ and ex situ) state. Carbon rich areas in the specimens could be found, yet not unambiguously linked to originate from the plant fibers. During heating no distinct differences to the non-reinforced ceramic were observed.

Conclusion

The investigation of the axes showed that the Ag-rich surface is a result of the corrosion process of the falutype copper, where the oxidization of the Cu reduces the AgO back to pure Ag, which then forms the grains visible in the EDS map. Consequently, the silver spots were not introduced deliberately, and thus, an initially ritualistic origin of the axes is disproven.

The feasibility of in situ TEM observation of ceramic sintering could be successfully shown. Due to the absence of carbon nanofibers for all sintering conditions mechanical reinforcement of the ceramic on the nanoscale can likely be ruled out. Due to the difficulty of unanbigously identifying specimen areas that originated from plant fibers the identification of the strengthening mechanism is the subject of ongoing investigation.

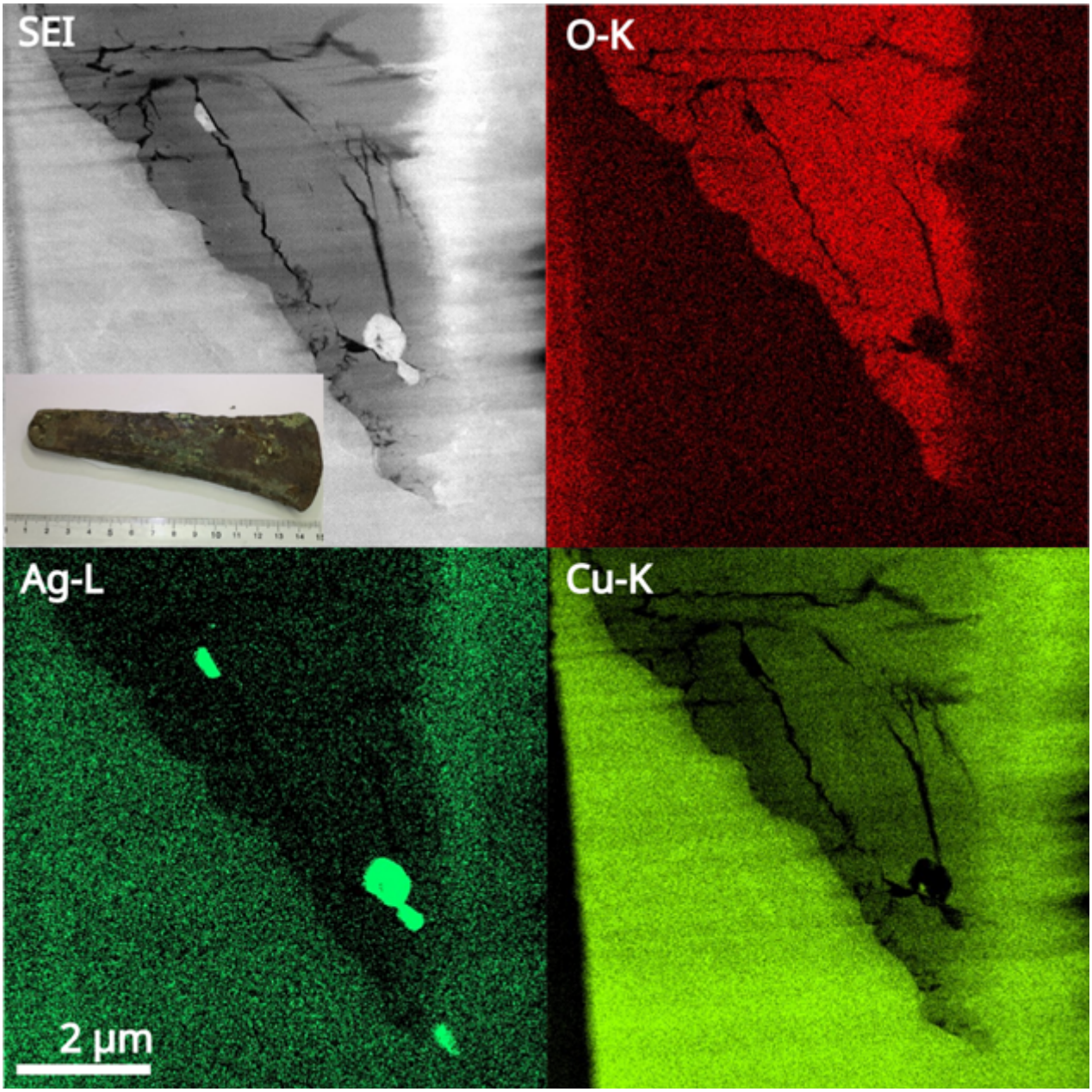

Keywords:

archeology, pottery, traceology, insitu, heating

Reference:

[1] Adriaens, A., and M. G. Dowsett. , Comprehensive Analytical Chemistry, 42:73–128. Non-Destructive Microanalysis of Cultural Heritage Materials. Elsevier, 2004
[2] Saleem et al. , arXiv preprint arXiv:2309.15120 (2023)
[3] Vindel et al. , Archaeometry 60, no. 2 (2018): 342–49.
[4] Yamandú et al. , Paléorient. Revue Pluridisciplinaire de Préhistoire et de Protohistoire de l'Asie Du Sud-Ouest et de l'Asie Centrale, no. 49–1 (June 22, 2023): 133–54.

1142

Correlating microscopy methods: the case of precipitation in lean, bioabsorbable Mg alloys

Dr. Robin Schäublin[1,2], Ms. Tatiana Akhmetshina[1], Dr. Peng Zeng[2], Dr. Stephan Gerstl[1,2], Prof. Jörg Löffler[1]
[1]Department of Materials, ETH Zürich, Zürich, Switzerland, [2]ScopeM, ETH Zürich, Zürich, Switzerland

Poster Group 2

Background incl. aims
Many of the properties of metallic systems are driven by nanoscale precipitation. We present our workflow in the correlative microstructural study of "ZX" lean Mg alloys, which contain zinc and calcium, as a test case. Such alloys are promising candidates for bioabsorbable implants due to their excellent biocompatibility and degradation rate matching tissue regeneration. Because the nanoscale intermetallic precipitates within the alloys drive the mechanical properties and degradation behavior, it is critical to understand their type and role to tailor the alloys for specific applications.

Methods
We are deploying a correlative approach, utilizing mainly atom probe tomography (APT) and transmission electron microscopy (TEM), to cover a wide range of spatial length scales and obtain quantitative information. Despite its power, the correlative approach presents technical hurdles: sample preparation requires meticulous methods, including focused ion beam. Ideally, the same region of interest should be analyzed across all instruments, which can be challenging considering the vastly different size scales involved. Minimizing damage or corrosion during transfer between instruments, which usually occurs in air, is also crucial. Finally, to fully leverage the harvested data, one must apply data-treatment techniques, including AI and simulations to aid data interpretation.

Results
Starting from the solid solution, we were able to elucidate the precipitation sequence via APT at the smallest scales, and, as precipitates matured and grew in size, with STEM imaging and EDS chemical mapping supported by simulations. We revealed that the debated equilibrium phase of the ternary precipitates is based on the Ca2Mg5Zn5 crystal [1]. However, its composition derived from EDS and APT presented a broader range, which we also noted in the correlative nanoscale analysis of Fe–Cr alloys [2, 3]. This showed us that the correlative evaluation of APT- and EDS-derived results is beneficial when assessing a composition. We conclude with an outlook on further correlative approaches, including X-ray nanotomography.

Conclusion
This study showed us that correlating APT and TEM is beneficial for the study of precipitation of metallic systems, starting from the solid solution, and when assessing the composition of nanoscale precipitate. We conclude our presentation with an outlook on further correlative approaches, including X-ray nanotomography, which allows to further bridge the gap between spatial scales.

Keywords:

Mg-alloys, Fe–Cr, correlative-microscopy, APT, TEM

Reference:

[1] R.E. Schäublin, M. Becker, M. Cihova, S.S.A. Gerstl, D. Deiana, C. Hebert, S. Pogatscher, P.J. Uggowitzer, J.F. Löffler, Precipitation in lean Mg-Zn-Ca alloys, Acta Materialia 239, 118223 (2022)

[2] S. Küchler, V. Vojtech, S.S.A. Gerstl, R.E. Schäublin, J.F. Löffler, Thermally Decomposed Binary Fe-Cr Alloys: Toward a Quantitative Relationship Between Strength and Structure, Advanced Engineering Materials 24(3), 2100909 (2022)
[3] V. Vojtech, M. Charilaou, A. Kovacs, A. Firlus, S.S.A. Gerstl, R.E. Dunin-Borkowski, J.F. Löffler, R.E. Schäublin, Macroscopic magnetic hardening due to nanoscale spinodal decomposition in Fe-Cr, Acta Materialia 240, 118265 (2022)

1151

Multiscale characterization of Al-4Fe alloy grown by additive manufactoring

Dr Frédéric Fossard[1], Pauline Stricot[2], Simon Fritz[2], Eric Grevin[1], Maria Tsoutsouva[2], Nicolas Horezan[2], Quentin Barrès[2], Aidar Zakirov[3], Williams Lefebvre[3], Louise Toualbi[2], Yann Le Bouar[1]
[1]Université Paris-Saclay, ONERA, CNRS, LEM, Châtillon, France, [2]Université Paris Saclay, ONERA, Matériaux et Structures, Châtillon, France, [3]Groupe de Physique des Matériaux, Université et INSA de Rouen, UMR CNRS 6634, Rouen, France

Poster Group 2

The advent of Additive Manufacturing (AM) processes in recent years has given us access to parts with complex geometries that are difficult to machine using conventional manufacturing methods. However, Additive Manufacturing leads to microstructures and metallurgical states that differ from those obtained by conventional processes. In this context, it has become necessary to develop new alloy grades dedicated to Additive Manufacturing in order to take full advantage of the specific features of these processes. In the aeronautics sector, there is a strong interest in the study of lightweight titanium- and aluminum-based alloy grades [1,2].

In this work, we are interested in a model Al-Fe alloy, which is not possible to produce using conventional processes due to the precipitation of the embrittling Al13Fe4 phase. The use of the L-PBF (Laser Powder Bed Fusion) additive manufacturing process avoids this pitfall, thanks to a very rapid cooling rate that favors precipitation of the metastable Al6Fe phase. It should also be noted that in the Al-Fe system, due to the very low solubility of Fe in cfc aluminum, it is not possible to carry out post-elaboration homogenization annealing. The aim is therefore to optimize the processing parameters in order to obtain an alloy with the desired mechanical properties at the end of the process. This type of alloy is particularly interesting in the context of repairing parts by AM, since annealing the part is often either not possible or not desirable in order to preserve the mechanical properties of the other parts of the part.
The L-PBF process is an additive manufacturing process involving the successive fusion of layers of powdered material using a laser. This process is characterized by very short interactions between the raw material (powder) and the laser, resulting in very rapid cooling rates (of the order of 106 K/s). The result is a complex microstructure organized on several size scales, which we have characterized in the Al4wt%Fe alloy and which is presented in the figure : At the hundred-micron scale, we observe the melt baths generated by laser melting; Inside the baths, we observe a structure of often columnar grains; Inside the grains, we observe a cellular structure, whose walls are enriched in Fe; Finally, inside the cells, we sometimes observe precipitates, as well as dislocations formed during solidification due to the presence of strong thermal gradients.
We are particularly interested in the hardening mechanisms operating in this microstructure. In addition to a Hall-Pech effect and hardening caused by iron-rich precipitates and cells and by dislocations, hardening due to the presence of iron solute is likely to be significant. Indeed, it is well known that the very rapid cooling rate during the L-PBF process leads to solute trapping in the matrix [3]. Furthermore, it has been shown that the presence of a low concentration of Fe in an aluminum matrix has a significant contribution to yield strength, far greater than that of usual solutes such as copper [4]. For our alloys, it is therefore necessary to measure the Fe composition inside the cells in order to quantify its impact on alloy hardening.
Another point of clarification is the composition of the cell edges, which are also enriched in Fe: this is expected to deviate from the composition of the metastable Al6Fe phase reported in less rapid solidification processes.
A final point that is not stabilized for our samples, as for similar alloys in the literature [5], is the presence of oxygen. Oxygen is present due to the inevitable oxidation of the powders, and may also

originate from the gas present in the preparation chamber. However, its presence and location in Al-Fe alloys produced by L-PBF needs to be investigated. Indeed, the lattice parameters of L-PBF Al-Fe alloys, measured by X-ray diffraction, deviate from the values expected for these alloys, and the explanation put forward in the literature is the presence of oxygen, which would deform the aluminum lattice.

To achieve these goals, detailed characterisation by transmission and scanning electron microscopy (Figure), X-ray diffraction and atomic probe tomography has been carried out on samples produced using different parameters. The impact of manufacturing parameters on microstructure is highlighted, particularly the fact that the size of the solidification cells largely controls the mechanical behaviour. The results also reveals the correlation between the Fe distribution in the microstructure and the material's local hardness. Using transmission electron microscopy enables analysis of the interactions between nanometric precipitates and dislocations resulting from the thermal process, providing a better understanding of the hardening mechanisms. Atomic probe tomography allows to estimate the remaining Fe in the Al matrix in the as-built alloy and local enrichment in iron that lead to precipitation or segregation in the solidification cells.

The results allow the contribution of the different microstructural elements to hardening to be assessed using a phenomenological model. This model, developed based on mechanical tests conducted on various metallurgical states, can be used to propose chemical optimization paths. The purpose is to define an alloy which, in the as-built state, will benefit from a mechanical behaviour combining work and precipitation hardening.

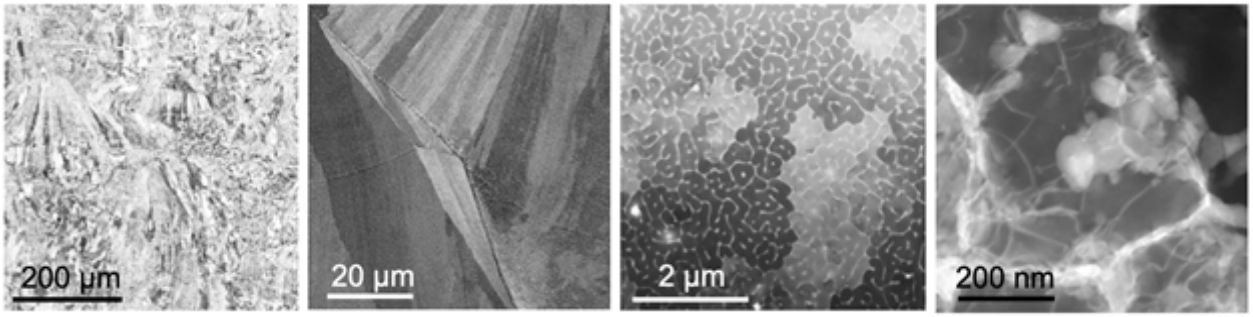

Keywords:

Al alloys, additive manufacturing, solidification

Reference:

1. R. Liu, Z. Wang, T. Sparks, F. Liou, J. Newkirk, 13 - Aerospace applications of laser additive manufacturing, in Laser Additive Manufacturing, Milan Brandt editor, Woodhead Publishing, 2017, 351-371.

2. C. Pauzon, M. Buttard, A. Després, F. Charlot, M. Fivel, B. Chehab, J.J. Blandin, G. Martin, Direct ageing of LPBF Al-1Fe-1Zr for high conductivity and mechanical performance, Acta Materialia 258 (2023) 119199.

3. P. Galenko, S. Sobolev, Local nonequilibrium effect on undercooling in rapid solidification of alloys, Phys. Rev. E 55 (1) (1997) 343.

4. T. Uesugi, K. Higashi, First-principles studies on lattice constants and local lattice distortions in solid solution aluminum alloys, Computational Materials Science 67 (2013) 1–10.

5. X. Qi, N. Takata, A. Suzuki, M. Kobashi, M. Kato, Change in microstructural characteristics of laser powder bed fused Al–Fe binary alloy at elevated temperature, J. Mater. Sci. Technol. 97 (2022) 38–53.

1154

Electron Microscopy of a Gas-Atomized NiSiV Powder

Inga Konow[1], Sigurd Wenner[2], Leander Michels[3], Jan Ove Odden[3], Ursula Ludacka[1], Randi Holmestad[1]
[1]Department of Physics, Norwegian University of Science and Technology (NTNU), Trondheim, Norway, [2]Sintef industry, Department og Materials and Nanotechnology, Trondheim, Norway, [3]Elkem, Kristiansand, Norway

Poster Group 2

Background incl. aims
Gas-atomization is a powder production technique involving rapid solidification of molten metal by high-pressure gas jets. Molten metal is poured through a nozzle into a chamber filled with inert gas where it is rapidly cooled and fragmented into fine, spherical particles by gas jets. The resulting particles are generally spherical with a high degree of uniformity in composition. There is a wide range of applications, from additive manufacturing and as feedstock to thermal spray coatings. In this study, a nickel silicide powder alloyed with vanadium has been investigated, with composition as stated in [1]. Nickel silicides are well-known for their resistance to high temperatures, corrosion, and oxidation, particularly in demanding environments such as in offshore applications. The powders are known to has high brittleness, but the incorporation of transition metals such as vanadium has been shown to improve the ductility. By using electron microscopy, both the surface and the internal structure can be investigated to gain a deeper understanding of the properties of the powder.

Methods
First, the particles surface and polished cross-sections were studied by scanning electron microscopy (SEM). A thin cross-section of a particle was prepared using a focused ion beam (FIB) and then investigated using transmission electron microscopy (TEM) imaging and energy-dispersive X-ray spectrometry (EDS) mapping. Scanning precession electron diffraction (SPED) maps were acquired to obtain high-resolution information on crystal phases and orientation relationships. The data was processed and investigated using the open-source Python libraries Hyperspy [2] and pyxem [3].

Results
SEM imaging reveals spherical particles with diameters from a few hundred microns down to a couple hundred nanometres. The particles are mainly uniform in shape but show signs of irregularities such as helmets and satellites. The surfaces are not smooth, but show signs of parallel stripes, revealing a lamellar dual-phase structure. The same stripes are visible in SEM images of the cross-sections. When looking at TEM bright field images, lamellae with a thickness of around 100 nm can be seen. EDS maps confirm that the lamellae are two distinct phases, alternating between vanadium-rich and silicon-rich, while the nickel is evenly distributed. Vanadium is very soluble in nickel at low quantities, and SPED was used to identify the vanadium-rich areas as the nickel fcc phase, in which vanadium has a high solubility. Equally, the diffraction patterns from the silicon-rich areas suggest a nickel silicide phase. While the crystal structure of nickel is very uniform along the stripes, the nickel silicide phase exhibits signs of misorientations and planar defects.

Conclusion
Gas-atomized nickel silicide powders alloyed with vanadium were studied using electron microscopy. SEM images reveal defects such as helmets and satellites, and structures both on the surface and on the cross-section. TEM methods such as EDS and SPED were used to study this further, and we were able to identify stripes with thicknesses of around 100 nm of alternating nickel solution with vanadium, and nickel silicide. Nickel is shown to have a slightly increased lattice parameter with increasing amount of vanadium [4], which might make it a better lattice match with the nickel silicide

phas and could possibly explain the improved ductility of the material when alloyed with vanadium. Further work includes obtaining a deeper understanding of the variations in the nickel silicide phase along the stripes and what effect this has on the properties, as well as the orientation relationships between the two phases.

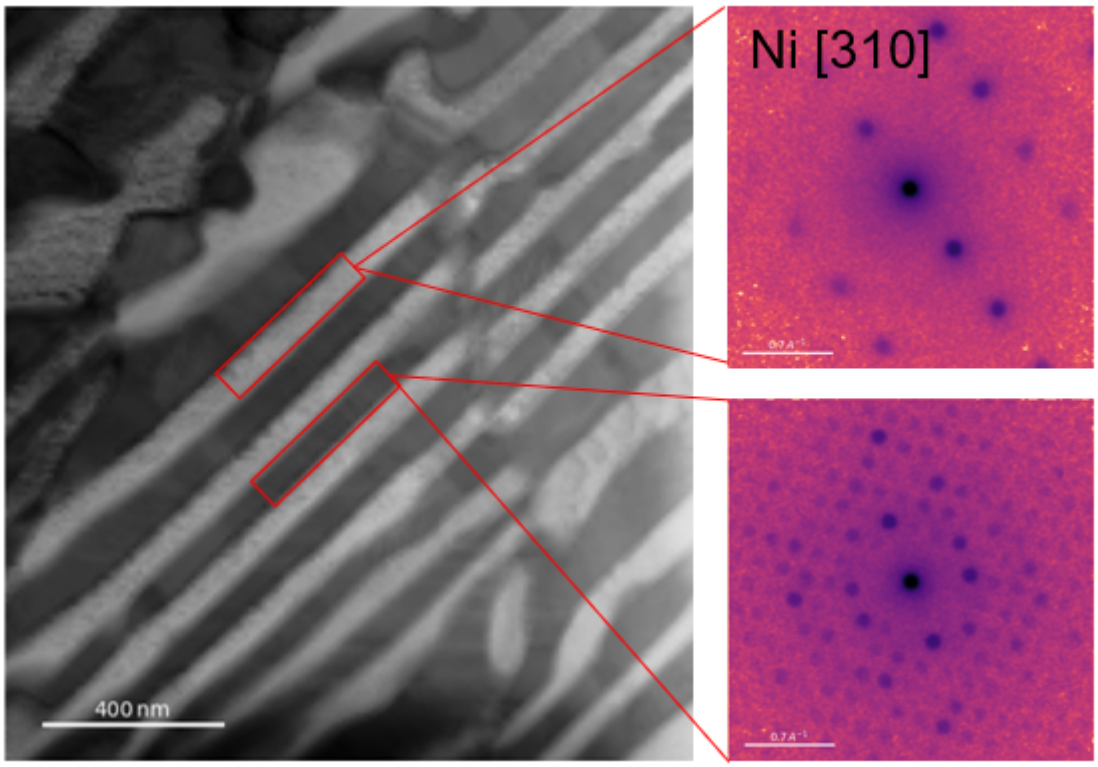

Keywords:

TEM, SEM, SPED, Atomization, NiSiV

Reference:

[1] Mohammad Ibrahim et al., 'Gas-Atomized Nickel Siliced Powders Alloyed with Molybdenum, Cobalt, Titanium, Boron, and Vanadium for Additive Manufacturing', 2023. Publisher: MDPI.

[2] F. de la Peña, E. Prestat, V.T. Fauske, P. Burdet, T. Furnival, P. Jokubauskas, J. Lähnemann, M. Nord, T. Ostasevicius, K.E. MacArthur, et al., Hyperspy/hyperspy: Release v2.0.1, 2024, http://dx.doi.org/10.5281/zenodo.592838.

[3] D.N. Johnstone, P. Crout, M. Nord, J. Laulainen, S. Høgås, E. Opheim, B. Martineau, C. Francis, T. Bergh, E. Prestat, et al., Pyxem/pyxem: pyxem 0.17.0, 2024, http://dx.doi.org/10.5281/zenodo.2649351.

[4] J. F. Smith, O. N. Carlson, P. G. Nash, The Ni-V (Nickel-Vanadium) system, 1982, Bulletin of Alloy Phase Diagrams, Vol. 3.

1169

Direct observation of quadrupolar strain fields forming a shear band in metallic glasses

Dr Sangjun Kang[1], Dr Di Wang[2], Prof Xiaoke Mu[3], Prof Christian Kübel[1]
[1]Tu Darmstadt, Darmstadt, Germany, [2]Karlsruhe Institute of Technology , Karlsruhe , Germany, [3]Lanzhou University, Lanzhou , China

Poster Group 2

The promising application of metallic glasses is limited by their catastrophic failure at low strain due to shear banding [1]. For decades, scanning/transmission electron microscopy (S/TEM) techniques have been employed to analyze shear bands in metallic glasses and understand their formation [2]. However, due to a lack of direct information in reciprocal space, conventional S/TEM cannot characterize structural variation, e.g. local atomic strain, of amorphous materials, which are key to describe the deformation of glasses. With this work [3-4], we solved the longstanding difficulty of experimentally imaging atomic packing structure and local strain of amorphous materials using 4-dimensional scanning transmission electron microscopy (4D-STEM). Figure 1a schematically shows the 4D-STEM setup. A quasi-parallel electron probe is focused to ~5 nm diameter on an electron transparent sample. 4D-STEM records 2D images of local diffraction patterns over a 2D grid of each probe position by stepwise scanning of the probe over the area of interest. As shown in Figure 1b, the local strain is quantified by the elliptical deviation present in each diffraction pattern. We obtain the principal strains from the long and short axes of the ellipse indicated by qmax and qmin. The strain tensor is obtained by algebraic transformation of the principal strains to the loading coordinates. Moreover, a PDF analysis is performed as a structural descriptor based on the 4D-STEM dataset to analyze the local atomic structure of metallic glasses. Thereby, the 4D-STEM approach provides a correlative visualization of the nanoscale strain field and the atomic structure information. We used a Fe85.2Si0.5B9.5P4Cu0.8 (at.%) metallic glass ribbon as an example in this study, which receives attention owing to its soft ferromagnetism. The metallic glass was deformed by scratch testing at ambient conditions using a diamond tip. We observe residual strain fields concentrated at inclusions (Figure 1c). It provides for the first time an experimental visualization of the Eshelby-like inclusions surrounded by quadrupolar strain fields aligned on a shear band in deformed metallic glasses. The results provide direct experimental evidence for a concrete scenario for the initiation of a shear band: the dilatated Eshelby inclusions are the result of local plastic atomic displacements in the glassy matrix, which concentrate a stress field with quadrupolar symmetry. The quadrupolar stress field perturbs the surrounding material in a vortex-like manner and percolates neighboring inclusions. This eventually leads to the formation of a shear band. This provides a new understanding of the formation of shear bands in metallic glass. Our new method is also expected to initiate broad research possibilities for solving questions in amorphous matters.

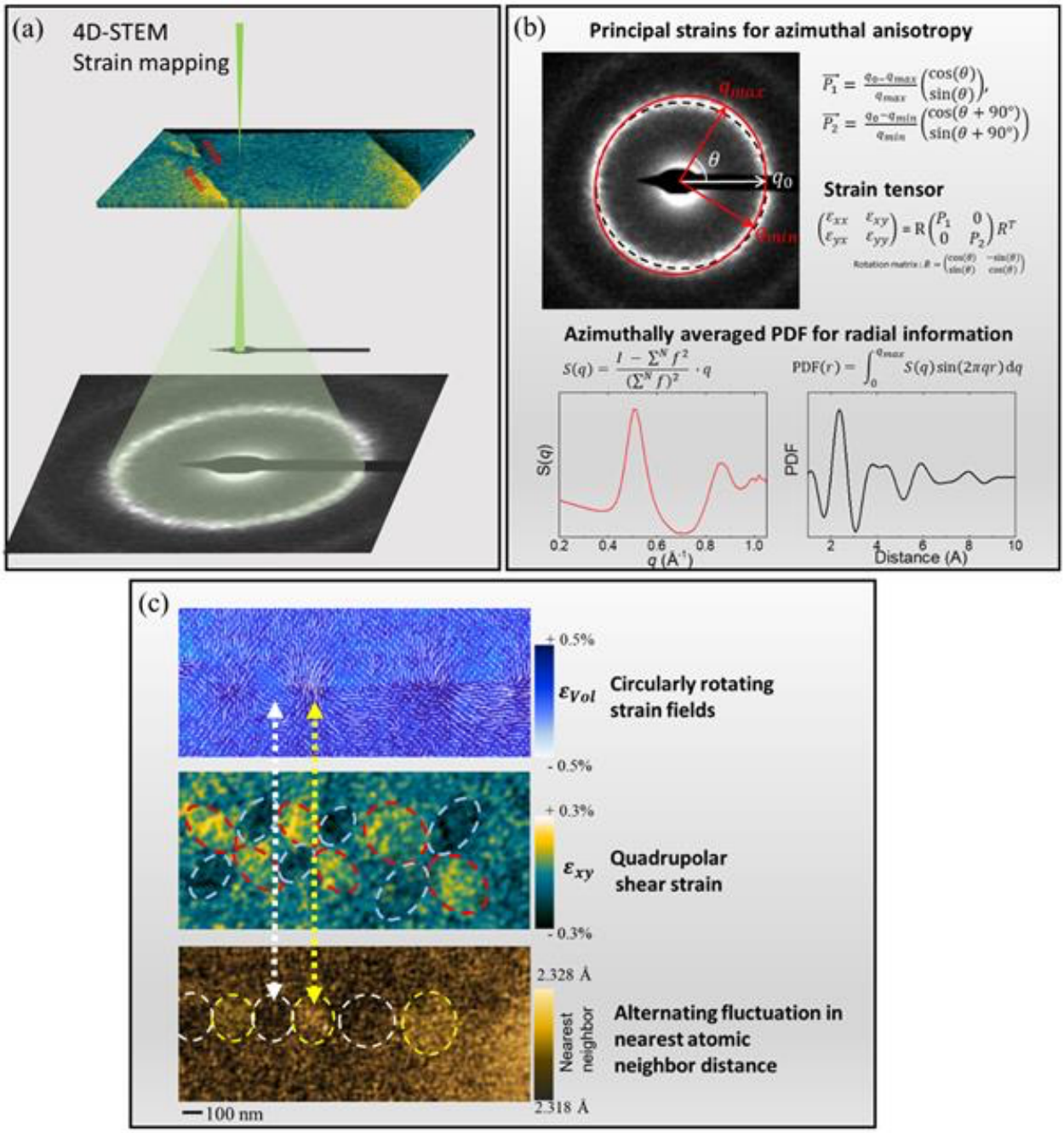

Figure 1: Schematic illustration of 4D-STEM based strain and PDF mapping. (a) The quasi-parallel electron probe is focused on the TEM lamella. Spatially-resolved diffraction patterns are recorded by a camera during stepwise scanning of the probe over the area of interest. (b) Data processing: principal strains ($\overrightarrow{P1}$ and $\overrightarrow{P2}$) are calculated from the elliptic distortion of the diffraction ring. For better visualization, the diffraction pattern is elongated along the principal direction. The strain tensors are algebraically obtained by projecting the principal strains to the reference coordinate system (x- and y-axis). For PDF analysis, the local diffraction patterns are azimuthally integrated into intensity profiles $I(s)$. Structure factors, $S(q)$, are obtained by background subtraction of $I(s)$. The PDFs are obtained by Fourier sine transformation of $S(q)$. (c) Vector field visualization of the maximum shear strain, γ_{max}, overlayed on the map of volumetric strain compared to maps of ε_{xy} and the nearest-neighbor distance from the same region.

Keywords:

Metallic glass, 4D-STEM, Strain field

Reference:

[1] C. Schuh, T. Hufnagel, U. Ramamurty, Mechanical behavior of amorphous alloys, Acta Materialia, 55, 2007, 4067-4109.
[2] C. Liu, V. Roddatis, P. Kenesei, R. Maaß, Acta Materialia 140, 2017, 206.
[3] S. J. Kang, D. Wang, A. Caron, C. Minnert, K. Durst, C. Kübel, X. Mu, Advanced Materials, 2023, 202212086
[4] S. J. Kang, 2, V. Wollersen, C. Minnert, K. Durst, H. S. Kim, C. Kübel, X. Mu, Acta Materialia, 2023, accepted

1222

Nanocrystals with dilated interplanar distances in the carburized surface case of Inconel-718 gas-processed at 570°C

Dr Corneliu Sarbu[1], Phd Student Marian Cosmin Istrate
[1]National Institute for Materials Physics, Magurele, Romania

Poster Group 1

It is utterly important to find appropriate methods of surface processing with the aim of enhancement of the properties of engineering interest of the stainless alloys (SS) and even of superalloys, as are hardness, wear resistance and even corrosion resistance. At Swagelok Co. Ltd. (Solon, OH, USA) it was invented the surface carburization processing at low temperature (LT) in gas-atmosphere (LTC) which matches the engineering requests for many SS alloys and for Inconel-718 (IN-718) Ni-Fe based superalloy [1]. The effect of LT gas-carburization consists in the formation at the alloy's free surface of a so-called carburized case (tens of µm-s thick) which is suggested to consist in crystallographically slightly modified alloy grains having properties that are matching the engineering requests. The theory currently accepted for explanation of the modified crystalline structure is based on a supposed supersaturation with carbon (CSS). It is claimed that carbon diffuses in the interstitial locations of the initial alloy grains (of face centered cubic structure (FCC)), leaving unchanged the initial grain structure and crystallography of the alloy, except for a dilatation of cubic lattice parameter due to the colossal-stuffing with carbon [2]. This theory is currently considered as valid for explanation of the enhancement of all the surface properties of the carburized IN-718 at carburizing temperatures of 843K, 803K and 783K [3]. We report that the low-temperature carbon supersaturation theory (LTCSS) is not valid in the case of IN-718 carburization at 843 K even when a surface carburized case is formed and revealed through chemical etching. We herewith report that the initial micrometer sized grain structure is replaced by a nanostructure located at least in the uppermost layer 1-2 µm thick, generated by the gas-carburization of the surface at LT.
The uppermost layer 1-2 µm thick of the free carburized surface at 843K of IN-718 was investigated by HRTEM by using a JEM-ARM200F aberration corrected (HR)(S)TEM microscope. In view of reaching the highest achievable precision in our measurement of the interplanar distances by using the HRTEM images of the observed nanocrystals, the Fourier transform of the Bragg reflections - mainly of the alloy matrix (111) reflections which have the highest structure factors in transmission electron diffraction (TED) - were analyzed. The usual disk samples of 3 mm diameter were prepared for TEM by following the usual steps: (a) mechanical cutting of a ≈1.5 mm thick sheet along a plane parallel to the free carburized surface of a bulk piece of carburized alloy, (b) mechanical polishing until a ≈80÷100 µm thickness is achieved, (c) ultrasonic punching of Ø=3mm disks, (d) dimpling of the disks until a remaining minimum thickness of ≈20µm is reached at the carburized face and (e) final dual beams milling with Ar+ ions in a Gatan PIPS device. The operations (b), (d) and (e) were done only at the uncarburized face of the disk samples.
A Cu contamination of the free carburized surface was our permanent mark for checking that the observed nanostructure belongs to the uppermost layer of the carburized case, whose entire thickness was reported as ≈20µm [3]. We have investigated the same IN-718 material sample as the one reported in [3], where no mention is made concerning the existence of a surface nanostructure due to the LT gas carburization. We collected a large number of directly measured d(hkl) values from HRTEM images of atomic resolution, regarding mainly the d(111) interplanar distances. We measured d(hkl)-s also for other observed nanocrystalline orientations. Interplanar distances of carbides were also measured, but they are not the object of our interest here. The distribution of the directly measured d(hkl) values revealed that most of the observed matrix (austenite) nanocrystals have enlarged crystallographic interplanar distances in comparison to the uncarburized crystalline FCC structure of the IN-718 austenite matrix. The values measured by us are higher far beyond the errors

that could affect our measurements. A much lower number of IN-718 austenite nanocrystals with non-modified lattice constant was observed. We took as a reference value the IN-718 lattice constant measured via neutron diffraction in a fully aged IN-718 superalloy [4].
Fig-1(a) is a negative inverted photo (used for better visibility of the nanostructure details) and shows the direct HRTEM image of an area located at the rim of a hole resulted by ion milling. It reveals the presence of nanocrystals embedded in an amorphous phase located in the uppermost layer of the carburized case. Fig-1(b) - not allowed by the template of the abstract text - was a reverse Fourier filtered image generated by mask selection of only the (111) reflections in the Fourie transform (FT) of the image shown in Fig-1(a). In many areas similar to the depicted one (Fig-1(a)) we measured several surprising values of the interplanar distance d(111), as for example 2.07, 2.08 , 2.11, 2.18 Å which correspond respectively to the FCC lattice cell parameter of the matrix nanocrystals of 3.58, 3.60, 3.65, 3.77 Å. These are as a rule largely higher than the most precisely measured lattice constant - done by means of neutron diffraction - of 3.5954÷3.6005 Å [4] - in a fully annealed IN-718 alloy.
The image shown in Figure (1a) (the FT of Fig-1a was not allowed by the template of the abstract text) is only an example taken from a wealth of HRTEM recorded images showing similar nanostructures. We got similar d(hkl) values also by measurements done at the recorded transmission electron diffractograms. This large collection of directly measured d(hkl)-s are clearly evidencing that the FCC crystalline cells of the nanosized fragments of the carburized IN-718 matrix are most probably generated via a massive diffusion of carbon in the alloy grains, as claimed by the LTCSS theoretical model, which instead of simply dilating the crystalline cell of the initial alloy grains, is inducing the fragmentation of them. The ultimate evidence concerning the occurrence, the mechanism and the crystallography of this fragmentation process - occuring deeper in the alloy - is obtainable only by means of neutron diffraction or by synchrotron XRD. Furthermore, it should be revisited the original evidence supplied via classical XRD which supports the claimed basic idea of the LTCSS model.

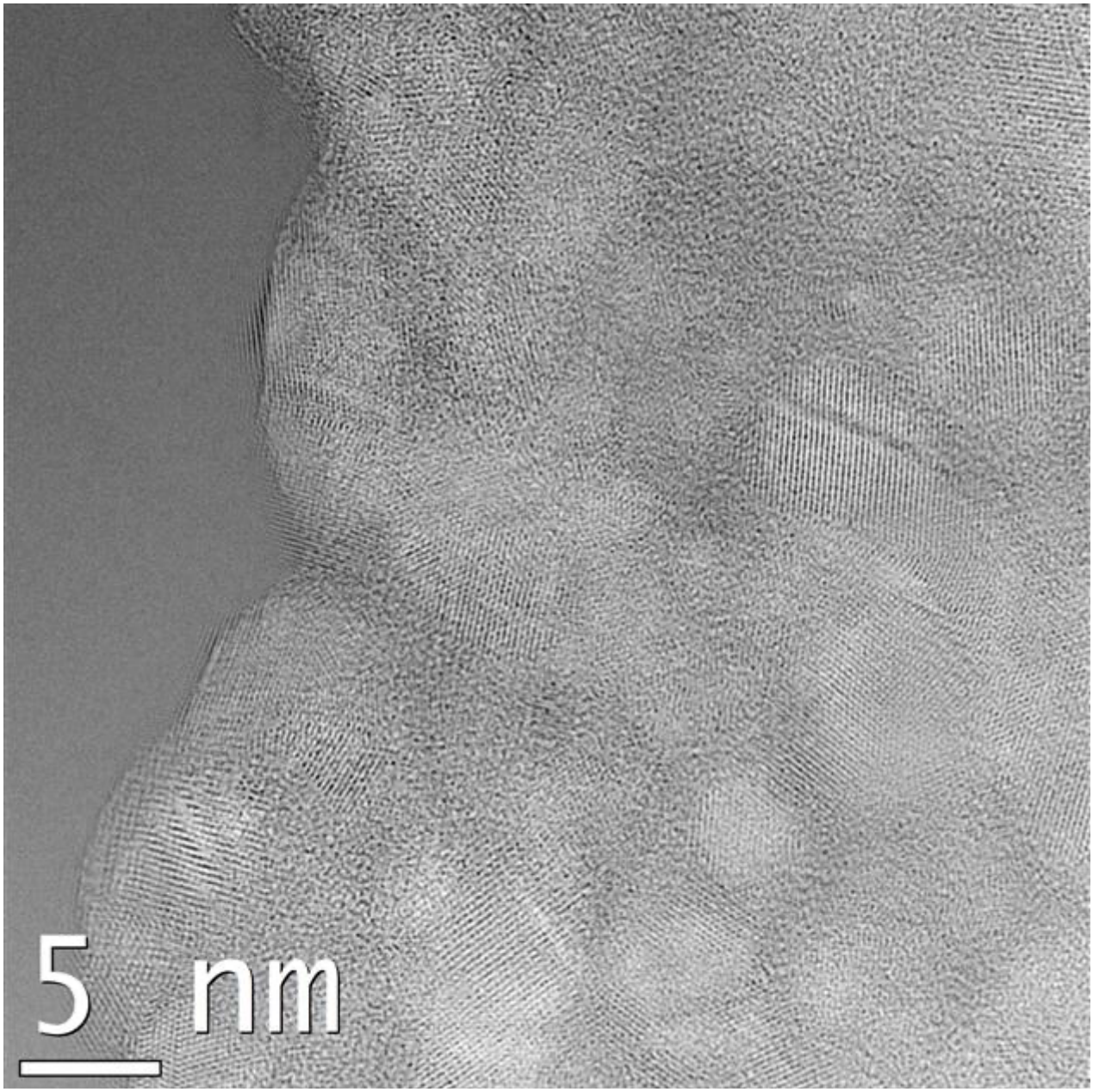

Keywords:

low-temperature gas-carburization, Inconel-718, lattice dilatation, LTCSS model

Reference:

[1] S.R.Collins et al. in J.Dossett & G.E.Totten (Eds.), ASM Handbook, Vol.4D, ASM Int'l (2014)
[2] Y. Cao, F. Ernst and G. Michal, Acta.Mater., vol.51, (2003) 4171
[3] R.Sharghi-Moshtaghin et al, Metall.Mater.Trans.A, 41A, 2022 (2010)
[4] J.Repper, "Einfluss mikroskopischer Eigenspannungen auf die makroskopische Eigenspannungs-analyse mittels Neutronenbeugung", PhD Thesis at Technische Universität München (2010)

1233

Parent grain reconstruction of martensitic microstructures: a comparison of different methods

Dr. Barbara Šetina Batič[1]
[1]Institute of Metals and Technology, Ljubljana, Slovenia

Poster Group 1

Background
Metallographic techniques have traditionally been used for primary austenite grain analysis. In this study, we compare conventional metallography with selective etching to reveal primary austenite grains within the microstructure and two different parent grain reconstruction software packages, which reconstruct the primary austenitic grains based on orientation relationships between (child) martensitic phase and (parent) austenite phase.
Methods
The samples were prepared following standard metallographic procedures. The samples for optical microscopy were etched with different etchants to reveal the primary austenite grain boundaries. For EBSD analysis the samples were finished with 5 min OP-S final polishing.
For light otical microscopy, we used Microphot FXA, Nikon with 3CCD-videocamera Hitachi HV-C20A and analySIS software. For scanning electron microscopy, two different microscope set-ups were considered: Zeiss CrossBeam 550, with EDAX Hikari Super EBSD detector and OIM 8 software for data processing and ThermoFisher Apreo 2, with Oxford Instruments Symmetry 2 EBSD system and Crystal software for data processing was used.
Results
The etching process highlights grain boundaries, facilitating the identification and measurement of primary austenite grains, and providing valuable information about their size, distribution, and orientation. Complementing the metallographic approach, EBSD can also be used to determine primary austenite grains through crystallographic orientation mapping. EBSD data is processed to reconstruct parent grains, offering high spatial resolution and insights into the crystallographic characteristics of the primary austenite phase.
Conclusion
The presented work shows and compares different ways to reconstruct primary austenite grains from martensitic microstructure.
Light microscopy is by all means a much faster technique, while scanning electron microscopy and electron backscatter diffraction require advanced equipment, additional sample preparation and additional post processing of the acquired data; but can give more impartial results that are not as dependent on the skill of metallographer.

Keywords:

steel, martensite, austenite, microstructure

1250

Comparative Analysis of Sample Preparation and Imaging Methods for Metallographic Examination of Archaeological Silver

Dr Alexandra Suvorova[1], Prof Walter Bloom[2]
[1]The University of Western Australia, Perth, Australia, [2]Western Australia Museum, Fremantle, Australia

Poster Group 1

Background
There are two principal considerations for metallographic examination of historical metal artefacts: first, the selected portion of the material must be representative of the object; second, the sample preparation procedure must ensure minimal destruction to the archaeological object. Sample preparation is a critical step in the metallographic analysis of archaeological metals and is a prerequisite for accurately determining the microstructure and elemental composition using SEM, SEM-EDS, EPMA, and EBSD techniques. The quality of the sample surface is crucial for accurate metallographic analysis: surface damage, surface contamination, and limited material availability are key factors that limit the reproducibility and accuracy of structural and analytical results. The sample state (corrosion), area of interest (surface vs. bulk), analytical technique, and intended purpose (information required) play major roles in selecting the optimum sample preparation.
Methods
The 17th century silver coins and artefacts from the Batavia shipwreck of the Dutch East India Company's (VOC) flagship from Western Australian Museum collection have been analysed using STEM and SEM detectors in FEI Verios 460 SEM and FEI Helios FIB-SEM. The samples for SEM examination have been prepared by ultramicrotomy (Leica EMFC7 Ultramicrotome Microsystem equipped with Diatome diamond knife), focused ion beam milling (the FEI Helios Nanolab G3 CX DualBeam FIB), and laser micromachining tool (3D Micromac microPREP).
Results
Various sample preparation methods and their outcomes have been compared to reveal their advantages and limitations for metallographic applications in the archaeological silver artefacts. The outcomes are demonstrated below in Figure(a) 100nm slice prepared from a silver alloy using ultramicrotomy, imaged at 30kV using the TLD detector; Figure(b) sectioned and polished silver alloy sample with the laser micromachining tool, imaged at 20kV using CBS detector; Figure(c) cross-section prepared by focused ion beam milling, imaged at 5kV, 1.4nA, using the ICD detector.
Conclusion
All methods are excellent sample preparation options for archaeological metal samples, such as silver objects and coins when the best surface quality and minimal destruction is required. Additionally, the most suitable protocols for sample preparation, imaging, and analytical studies have been found specifically suitable for historical silver alloys.

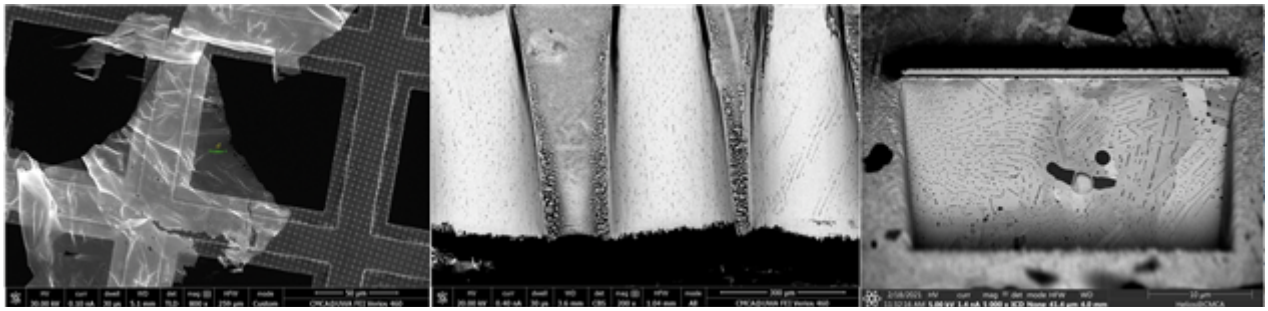

Keywords:

metal alloys, heritage metals, SEM

Reference:

B van Os, A Suvorova, J Pelsdonk, J Woodhead in “Shipwrecks of the Roaring Forties”, ed. J Green and A Paterson,(UWAP) 2020
D.A.Scott, R.Schwab in “ Metallography in Archaeology and Art” Springer 2019

1329

Observation of phase transformation of Sn by transmission electron microscopy

Mr. Yamato Kirii[1], Mr. Tetsuya Kubota[1], Mr. Sotatsu Yanagimoto[1], Mr. Takumi Sannomiya[1]
[1]Tokyo Institute of Technology, Yokohama, Japan

Poster Group 1

Background
Tin (Sn) experiences phase transformation from metallic β phase to semiconductor α phase at 13 °C, and to liquid phase at 232 °C [1]. During the phase transformation from β phase to α phase, the metallic luster is lost [2], and the structure becomes prone to collapse, which is known as tin pests. In recent years, lead-free solder has attracted attention where Sn is often used as a substitute for lead (Pb) in the electronic products. Since the electronic elements become miniaturized down to nanoscales, understanding of the behavior of Sn at nanoscales is important. In this study, we investigated the phase transformations of Sn nanoparticles at low temperatures using transmission electron microscopy (TEM) and also carried out the optical measurement at high temperatures.
Methods
On a TEM grid with a SiN membrane, Sn of 99.9% was deposited with a target thickness of 14 nm for a flat configuration. The Sn-deposited sample was annealed at a temperature of 300 °C for 3 hours to form particles. The prepared sample was measured in TEM after being cooled down to -177 °C using liquid nitrogen. At -177 °C, the sample was held for one hour to allow for a complete phase transformation, and the TEM images and diffraction patterns were acquired. The temperature was then raised to room temperature (20 °C) by the heater and the TEM image and diffraction pattern were acquired.
For the optical measurement, we first deposited Sn nanoparticles of different sizes on borosilicate glass at film thicknesses of 1.5 nm, 3 nm, and 6 nm. The samples for the optical measurement were annealed under the same conditions as before to convert the films into nanoparticles. The particle sizes for each sample were measured to be 21.8 nm, 30.6 nm, and 83.0 nm, respectively. The samples were then coated with a 13.3 nm thick layer of AlN to prevent oxidation. The transmission spectra of the Sn nanoparticles of different sizes were measured while changing the temperature up to the phase transition point.
Results
The obtained TEM images at -177 °C and room temperature are shown in Fig.1(a), and (b), respectively. Although volume change is expected by the phase transformation to the α phase, no clear change in the shape of the nanoparticles was observed in the bright field TEM images. The diffraction patterns at -177 °C and room temperature are shown in Fig.2(a) and (b). The sharp Debye rings are clearly observed in Fig. 2(a) at -177 °C, while the Debye rings at room temperature are broad and vague as shown in Fig. 2(b). This indicates the crystallinity change (from large crystalline to smaller one) during the phase transformation although no clear shape change in the nanoparticles was observed in the bright field TEM image. The low-temperature crystal structure was identified to be the diamond structure, while the crystal structure at the room temperature was unable to be determined.
For the optical measurement at high temperature, the transmission spectrum for the nanoparticle with means diameter of 30.6 nm is shown in Fig. 3. It can be observed that the transmission intensity and the wavelength of the resonance peak change drastically at the phase transition from β phase to liquid. Moreover, the resonance wavelength shifts to the shorter wavelength at the liquid phase together with the decrease in the transmission intensity, and the peak width. The transmission spectra of the samples with other sizes showed similar results.
Conclusions

We have successfully observed the phase transformation of Sn nanoparticles from the β phase to the α phase from the diffraction patterns obtained using TEM. The diffraction pattern at low temperature showed only α-phase rings, indicating a complete transformation of Sn nanoparticles into the α-phase. In the optical measurement at high temperature, we successfully observed the solid-to-liquid phase transition of the Sn nanoparticles in the transmission spectra.

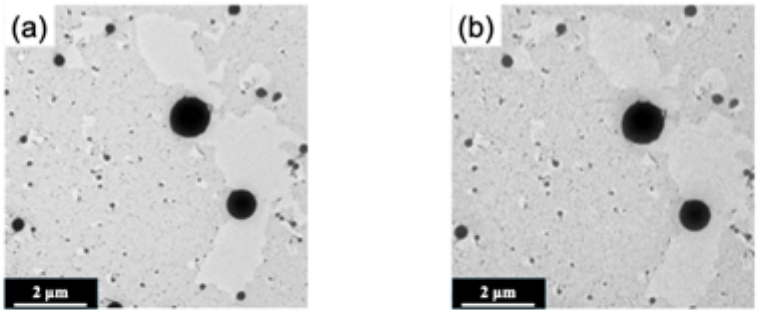

Fig.1 TEM image at (a)-177°C, (b)room temperature. (20 °C)

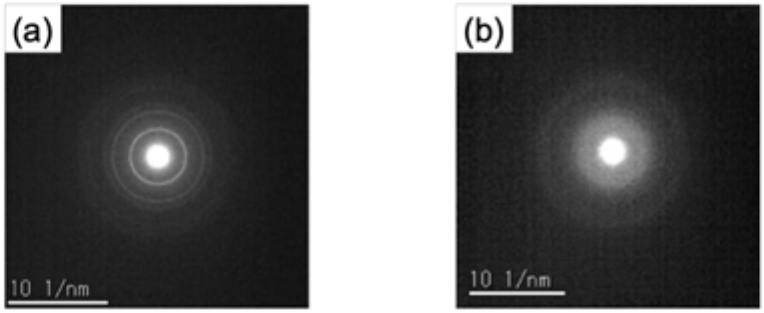

Fig.2 Diffraction image at (a)-177°C, (b)room temperature. (20 °C)

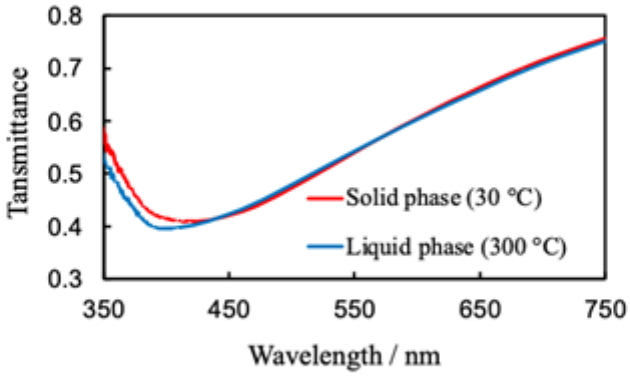

Fig.3 The transmission spectrum for the nanoparticle with means diameter of 30.6 nm. The red and blue lines represent the transmission spectrum of the solid phase and liquid phase, respectively.

Keywords:

Tin(Sn), phase transformation, TEM

Reference:

[1] Cornelius, B., Treivish, S., Rosenthal, Y., & Pecht, M. (2017). The phenomenon of tin pest: A review. Microelectronics Reliability, 79, 175-192.
[2] Barfuss, A., Dudy, L., Scholz, M. R., Roth, H., Höpfner, P., Blumenstein, C., ... & Schäfer, J. (2013). Elemental topological insulator with tunable Fermi level: Strained α-Sn on InSb (001). Physical review letters, 111(15), 157205.